Bacterial infection, immune responses, and autophagy in *lutzomyia longipalpis* sand flies

by

Matthew C. Heerman

B.S., Kansas State University, 2007
B.S., Kansas State University, 2007
M.S., Kansas State University, 2012

AN ABSTRACT OF A DISSERTATION

submitted in partial fulfillment of the requirements for the degree

DOCTOR OF PHILOSOPHY

Department of Entomology
College of Agriculture

KANSAS STATE UNIVERSITY
Manhattan, Kansas

2016

Abstract

Microbial communities residing within the midgut of insect vectors play a critical role in the response to various zoonotic and human pathogens, and can directly alter the development and survival of the insects. Sand flies are the primary vector of *Leishmania*, the causative pathogen of leishmaniasis, a neglected tropical disease. Sand flies acquire many microbes from the soil where immature stages develop until emergence as adults. Gram-negative *Pantoea agglomerans* and gram-positive *Bacillus subtilis* are two bacteria commonly associated with sand fly populations. Here, I demonstrated that an EGFP- and a GFP-expressing version of these two bacteria localize to different compartments of the midgut; a phenomenon that is achieved, in part, to pH differences found across the length of the gut. Additionally, *P. agglomerans* is able to selectively induce midgut epithelial apoptosis while *B. subtilis* does not. This is accompanied by differential immune and homeostasis responses to both bacteria highlighted by immune pathway suppression via the Poor Immune Response upon Knock-in (Pirk) gene. These effects may actually be representative of a broader type of response to bacterial infection that might be present across several insect species. Finally, I demonstrated that during metamorphosis the sand fly relies, at least in part, upon the activation of multiple genes from the autophagy pathway to aid in generating adult tissues. More specifically, I demonstrate, using microscopy, the presence of ATG6 in the cytoplasm of developing midgut epithelial cells of the sand fly pupae.

Bacterial infection, immune responses, and autophagy in *lutzomyia longipalpis* sand flies

by

Matthew C. Heerman

B.S., Kansas State University, 2007
B.S., Kansas State University, 2007
M.S., Kansas State University, 2012

A DISSERTATION

submitted in partial fulfillment of the requirements for the degree

DOCTOR OF PHILOSOPHY

Department of Entomology
College of Agriculture

KANSAS STATE UNIVERSITY
Manhattan, Kansas

2016

Approved by:

Co-Major Professor
Dr. Marcelo Ramalho-Ortigao

Approved by:

Co-Major Professor
Dr. Kun Yan Zhu

Copyright

Abstract

Microbial communities residing within the midgut of insect vectors play a critical role in the response to various zoonotic and human pathogens, and can directly alter the development and survival of the insects. Sand flies are the primary vector of *Leishmania*, the causative pathogen of leishmaniasis, a neglected tropical disease. Sand flies acquire many microbes from the soil where immature stages develop until emergence as adults. Gram-negative *Pantoea agglomerans* and gram-positive *Bacillus subtilis* are two bacteria commonly associated with sand fly populations. Here, I demonstrated that an EGFP- and a GFP-expressing version of these two bacteria localize to different compartments of the midgut; a phenomenon that is achieved, in part, to pH differences found across the length of the gut. Additionally, *P. agglomerans* is able to selectively induce midgut epithelial apoptosis while *B. subtilis* does not. This is accompanied by differential immune and homeostasis responses to both bacteria highlighted by immune pathway suppression via the Poor Immune Response upon Knock-in (Pirk) gene. These effects may actually be representative of a broader type of response to bacterial infection that might be present across several insect species. Finally, I demonstrated that during metamorphosis the sand fly relies, at least in part, upon the activation of multiple genes from the autophagy pathway to aid in generating adult tissues. More specifically, I demonstrate, using microscopy, the presence of ATG6 in the cytoplasm of developing midgut epithelial cells of the sand fly pupae.

Table of Contents

List of Figures ix
List of Tables xiii
Chapter 1 - Literature Review 1
1.1. Paratransgenesis 1
1.2. Commensal Dipteran Microbial Communities and Immunity 1
1.3. Immunity and Autophagy 4
1.4. Autophagy and development 5
1.5. Research Goals and Objectives 7
1.5.1. Determination of distribution and persistence of paratransgenic bacterial candidates in the midgut of sand fly larvae 7
1.5.2. Determination of effects of bacterial infection on midgut epithelium cells and immune responses 7
1.5.3. Investigation of the role of autophagy during larval infection and development to adult stage 8
Chapter 2 - Bacterial Infection and Immune Responses in the Larval Midgut of *Lutzomyia longipalpis* Sand Flies 9
Abstract 9
2.1. Introduction 9
2.2. Materials and Methods 11
2.2.1. Sand fly colony maintenance 11
2.2.2. Culturing and feeding of EGFP-expressing *B. subtilis* and GFP-expressing *P. agglomerans* 11
2.2.3. Immunocytochemistry 13
2.2.4. Larval midgut pH 14
2.2.5. Effect of pH on *in vitro* growth of EGFP-expressing *B subtilis* and GFP-expressing *P. agglomerans* 14
2.2.6. RNA extraction and reverse transcription 15
2.2.7. Quantitative real time PCR 15

2.3. Results 16
2.3.1. Bs and Pa localize to different regions of the sand fly larvae midgut 16
2.3.2. Infection of the sand fly larval midgut by *Pa* or *Bs* leads to differential damage of the larval midgut epithelium 18
2.3.3. Effect of feeding agar on larval development 19
2.3.4. Bacterial feeding leads to differential expression profiles in sand fly larvae 19
2.4. Discussion 20
Chapter 3 - The Role of Autophagy during Metamorphosis of the Sand Fly *Lutzomyia longipalpis* 41
Abstract 41
3.1. Introduction 41
3.2. Material & Methods 43
3.2.1. Sand fly colony maintenance 43
3.2.2. RNA extraction and reverse transcription 44
3.2.3. Real time quantitative PCR 44
3.2.4. Sequence alignments, phylogeny, and putative ecdysone response element prediction 45
3.2.5. Midgut immunocytochemistry & measurements 45
3.3. Results 46
3.3.1. Change in expression profile of ATG1, ATG6, ATG8, and Vein during development 46
3.3.2. Midgut specific autophagy during pupation 48
3.3.3. Evidence linking the role of ecdysone to the activation of autophagy 49
3.4. Discussion 49
Chapter 4 - IMD Recognition, Toll Pathway, and the effect of Pirk Knockdown in Infected *Lutzomyia longipalpis* Larvae 77
Abstract 77
4.1. Introduction 78
4.2. Material & Methods 79
4.2.1. Sand fly colony maintenance 79
4.2.2. Double stranded RNA synthesis and injection 79

4.2.3. RNA extraction and reverse transcription 80
4.2.4. Real time quantitative PCR 80
4.2.5. Predicted amplicon sequences, alignments, and phylogeny 81
4.3. Results 81
4.3.1. Expression of Toll pathways, IMD recognition and signal transduction molecules after infection 81
4.3.2. Comparison of chow fed, agar fed, and infected individuals for autophagy and immunity transcripts 82
4.3.3. RNAi efficiency for Pirk transcript in L3 larvae stage 83
4.3.4. Effect of dsPirk knockdown on transcript levels related to IMD pathway 83
4.3.5. Supplementary sequencing, amplicon, BLAST, and alignment results 84
4.4. Discussion 85
References 102
Appendix A - Bioinformatic and Phylogenetic Data 110

List of Figures

Figure 2.1. Infection of sand fly larva midgut by *B. subtilis* and *P. agglomerans*. 31
Figure 2.2. pH of the sand fly larval gut. 32
Figure 2.3. Effect of pH on in vitro growth of *B. subtilis* and *P. agglomerans*. 33
Figure 2.4. Confocal images of *B. subtilis* and *P. agglomerans* infection of sand fly larvae midguts. 34
Figure 2.5. mRNA expression profiles of 3rd instar *L. longipalpis* larvae post infection with *B. subtilis* and *P. agglomerans*. 35
Figure 2.6. Larval feeding of bacterial lawn. 36
Figure 2.7. Infection of sand fly larval midgut by *B. subtilis* or *P. agglomerans*. 37
Figure 2.8. Paraquat-induced apoptosis in sand fly larval midguts. 38
Figure 2.9. Changes in sand fly larval gut length and width caused by diet. 39
Figure 2.10. Localization of B. subtilis. 40
Figure 2.11. Apical localization of P. agglomerans on midgut epithelia. 40
Figure 3.1. mRNA expression profiles for feeding larvae (L3), non-feeding larvae (L4), early pupae (Pupa), and adult (Adult) sand flies. 57
Figure 3.2. Confocal images for ATG6 showing the anterior midgut of newly formed pupae. 58
Figure 3.3. Confocal images depicting the anterior sand fly midgut at different developmental stages stained with ATG6 antibodies. 59
Figure 3.4. Confocal images depicting the anterior sand fly midgut at larval, pupal, and adult developmental stages stained with ATG8 antibodies. 60
Figure 3.5. Possible promoter sequence of region upstream of *ATG1* 61
Figure 3.6. The midgut morphological changes in the 3rd instar (L3), 4th instar (L4), pupa, and adult developmental stages. 62
Figure 3.7. Axial ratio for the midgut (L/W) for L3, L4, pupa, and adult sand flies. 63
Figure 3.8. Clustal Omega protein alignment of ATG1 sequences from *L. longipalpis, P. papatasi, D. melanogaster, A. aegypti, A. gambiae, C. quinquefasciatus,* and *G. morsitans*. 66
Figure 3.9. Neighbor-joining tree to infer the evolutionary relationship of ATG1 sequences using *T. castaneum* (TcATG1) as an outgroup. 67

Figure 3.10. Clustal Omega protein alignment of ATG6 sequences from *L. longipalpis*, *P. papatasi*, *D. melanogaster*, *A. aegypti*, *A. gambiae*, *C. quinquefasciatus*, and *G. morsitans*. 69
Figure 3.11. Neighbor-joining tree to infer the evolutionary relationship of ATG6 sequences using *A. pisum* (ApATG6) as an outgroup..... 70
Figure 3.12. Clustal Omega protein alignment of ATG8 sequences from *L. longipalpis*, *P. papatasi*, *D. melanogaster*, *A. aegypti*, *A. gambiae*, *C. quinquefasciatus*, and *G. morsitans*. 71
Figure 3.13. Neighbor-joining tree to infer the evolutionary relationship of ATG8 sequences... 72
Figure 3.14. Clustal Omega protein alignment of Vein sequences from *L. longipalpis*, *P. papatasi*, *D. melanogaster*, *A. aegypti*, *A. gambiae*, *C. quinquefasciatus*, and *G. morsitans*. 74
Figure 3.15. Neighbor-joining tree to infer the evolutionary relationship of Vein sequences. 75
Figure 3.16. Clustal Omega protein alignment of ATG8 sequences from *L. longipalpis* and *H. sapiens* depicting *N*-terminal region from human antigen used to make antibodies (Abcam #86479) showing similarity to full length ATG8 from sand fly. 76
Figure 4.1. mRNA expression levels for L3 larvae fed normal diet (chow), control agar (Con), *B. subtilis* agar (Bs), and *P. agglomerans* agar (Pa)..... 93
Figure 4.2. mRNA expression levels for L3 larvae fed normal diet (chow), control agar (Con), *B. subtilis* agar (Bs), and *P. agglomerans* agar (Pa)..... 94
Figure 4.3. mRNA expression levels for L3 larvae that were uninjected, injected with dsGFP, or injected with dsPirk RNA. 95
Figure 4.4. mRNA expression levels for L3 larvae that were uninjected, injected with dsGFP, or injected with dsPirk RNA. 96
Figure 4.5. mRNA expression levels for L3 larvae that were uninjected, injected with dsGFP, or injected with dsPirk RNA. 97
Figure 4.6. mRNA expression levels for L3 larvae that were uninjected, injected with dsGFP, or injected with dsPirk RNA. 98
Figure 4.7. mRNA expression levels for L3 larvae that were uninjected, injected with dsGFP, or injected with dsPirk RNA. 99

Figure 4.8. mRNA expression levels for L3 larvae that were uninjected, injected with dsGFP, or injected with dsPirk RNA. 100
Figure 4.9. mRNA expression levels for L3 larvae that were uninjected, injected with dsGFP, or injected with dsPirk RNA. 101
Figure A.1. Putative CDS for mRNA encoding *L. longipalpis* Vein. 110
Figure A.2. Putative CDS for mRNA encoding *L. longipalpis* Pirk..... 111
Figure A.3. Neighbor-joining tree to infer the evolutionary relationship of Pirk sequences..... 112
Figure A.4. Clustal Omega protein alignment of Pirk sequences from *L. longipalpis*, *P. papatasi*, *D. melanogaster*, *D. buskii, A. albopictus*, *T. castaneum*, *S. oryzae*, and *L. migratoria*. ... 113
Figure A.5. Putative CDS for mRNA encoding *L. longipalpis* ATG6. 114
Figure A.6. Putative CDS for mRNA encoding *L. longipalpis* Attacin. 115
Figure A.7. Neighbor-joining tree to infer the evolutionary relationship of Attacin sequences. 116
Figure A.8. Clustal Omega protein alignment of Attacin sequences from *L. longipalpis*, *P. papatasi*, *D. melanogaster*, *A. aegyti*, and *T. castaneum*. 117
Figure A.9. Putative CDS for mRNA encoding *L. longipalpis* ATG1. 118
Figure A.10. Putative CDS for mRNA encoding *L. longipalpis* ATG8. 119
Figure A.11. Putative CDS for mRNA encoding *L. longipalpis* Duox. 120
Figure A.12. Neighbor-joining tree to infer the evolutionary relationship of Duox sequences. 121
Figure A.13. Clustal Omega protein alignment of Duox sequences from *L. longipalpis*, *P. papatasi*, *D. melanogaster*, *A. gambiae*, *A. aegyti*, and *C. quinquefasciatus*. 127
Figure A.14. Putative CDS for mRNA encoding *L. longipalpis* USP36. 129
Figure A.15. Neighbor-joining tree to infer the evolutionary relationship of USP36 sequences. 130
Figure A.16. Clustal Omega protein alignment of USP36 sequences from *L. longipalpis*, *P. papatasi*, *D. melanogaster*, *A. gambiae*, *A. aegyti*, and *C. quinquefasciatus*. 133
Figure A.17. Putative CDS for mRNA encoding *L. longipalpis* IMD. 134
Figure A.18. Neighbor-joining tree to infer the evolutionary relationship of IMD sequences. . 135
Figure A.19. Clustal Omega protein alignment of IMD sequences from *L. longipalpis*, *P. papatasi*, *D. melanogaster*, *A. gambiae*, *A. aegyti*, *C. quinquefasciatus*, *T. Castaneum*, and *G. morsitans*. 140
Figure A.20. Putative CDS for mRNA encoding *L. longipalpis* Nos. 141

Figure A.21. Neighbor-joining tree to infer the evolutionary relationship of Nos sequences.... 142
Figure A.22. Clustal Omega protein alignment of Nos sequences from *L. longipalpis*, *P. papatasi*, *D. melanogaster*, *A. gambiae*, and *A. aegyti*. 145
Figure A.23. Putative CDS for mRNA encoding *L. longipalpis* Domeless. 147
Figure A.24. Neighbor-joining tree to infer the evolutionary relationship of Domeless sequences. 148
Figure A.25. Clustal Omega protein alignment of Domeless sequences from *L. longipalpis*, *P. papatasi*, *D. melanogaster*, *A. gambiae*, *A. aegyti*, and *C. quinquefasciatus*. 152
Figure A.26. Putative CDS for mRNA encoding *L. longipalpis* IMPer. 154
Figure A.27. Neighbor-joining tree to infer the evolutionary relationship of IMPer sequences. 155
Figure A.28. Clustal Omega protein alignment of IMPer sequences from *L. longipalpis*, *P. papatasi*, *D. melanogaster*, *A. gambiae*, *A. aegyti*, and *C. quinquefasciatus*. 159

List of Tables

Table 2.1. *P. agglomerans* and *B. subtilis* infection rates..... 27
Table 2.2. Persistence of bacterial infection between continuous and non-continuous feedings . 28
Table 2.3. Colony forming units (CFU) from continuous and non-continuous fed larvae..... 29
Table 2.4. List of primer sequence used in this study..... 30
Table 3.1. The accession numbers, identity, score, and expected value for each query protein (*D. melanogaster*) against each subject protein (*L. longipalpis*). 54
Table 3.2. The sequence of RT-qPCR primers used for each transcript measured in this study.. 55
Table 3.3. The species names, gene symbols, accession numbers, and databases for all sequences used for multiple sequence alignment and phylogenetic analysis in this study.*H. sapiens* ATG8 sequence is not derived from a database and may be procured from the company website via that catalog number. 56
Table 4.1. The accession numbers, identity, score, and expected value for each query protein (*D. melanogaster*) against each subject protein (*L. longipalpis*). 89
Table 4.2. The sequence of RT-qPCR primers used for each transcript measured in this study.. 90
Table 4.3. The species name, gene symbol, accession number, and database for all sequences used for multiple sequence alignment and phylogenetic analysis. 91

Chapter 1 - Literature Review

1.1. Paratransgenesis

Current genetic control programs and techniques have been summarized concisely in a recent review [1]. This covers all topics ranging from transgenesis to paratransgenesis. Herein I choose to focus on strategies in place or in development directed towards the use of paratransgenesis as a means for vector and disease control as is currently reviewed [2].

Paratransgenesis is defined as using genetically modified symbiotic bacteria and/or fungi to express molecules that will abrogate the ability of the vector to transmit pathogens. This is a complicated process that involves selecting a microbe that can persist, or be driven into the vector, to diminish the vector competence of the insect without increasing its susceptibility to other pathogens. One example of *Chryseobacterium meningosepticum* showed that the bacteria were able to colonize and become the predominant gut microbe in *Anopheles gambiae* [3]. Furthermore *Escherichia coli* expressing anti *Plasmodium* antibodies were able to block *Plasmodium berghei* progression in *Anopheles stephensi* [4]. *Wolbachia* is a long standing popular intracellular candidate for vector control [5]. However, there is one reported case in *Culex tarsalis* where *Wolbachia* actually increased the susceptibility of the vector for West Nile virus [6]. Taking these things into account we wished to evaluate sand fly commensal bacteria for their ability to be putative paratransgenic platforms as more completely described below.

1.2. Commensal Dipteran Microbial Communities and Immunity

Bacterial symbionts significantly influence many aspects of the physiology of their host. In insects, both pathogenic and non-pathogenic bacteria have been shown to modulate immune response, homeostasis, development, and overall health of midgut physiology for both larval and

adult stages. Both Gram-positive (G+) and Gram-negative (G-) bacteria are commonly associated with the midgut tissue of Diptera, including several disease vectors. Many bacilli and enterobacter such as *Lactobacillus* and *Pantoea* have been identified from the midgut and other tissues of the fruit fly *Drosophila melanogaster* [7]. In field collected *Anopheles stephensi, Anopheles gambiae,* and *Aedes aegypti* from laboratory colonies, a number of G+ and G- bacteria were identified [8-11]. Among the G- bacteria, *Pantoea agglomerans* was also the most common genus identified from all cultivable bacteria in both male and female *Aedes albopictus* collected from two out of four sites in Madagascar [12]. In sand flies, several studies have focused on regional and potential species-specific variability in the microbial community of both *Phlebotomus* and *Lutzomyia* species. *P. agglomerans* and *Bacillus* spp. were commonly found in both natural and laboratory-reared sand fly populations. *Bacillus subtilis* and non-*Pantoea* members of the Enterobacter family were shown to be present in populations of *Phlebotomus papatasi* from, India, Turkey, Tunisia, and Egypt [13, 14]. *Bacillus* spp, *Serratia marcescens,* and *P. agglomerans* were identified in natural and laboratory populations of adult *Lutzomyia longipalpis* [15-18]. In laboratory colonies, Bacilli and Enterobacter were also identified in the larval stages of *L. longipalpis* [19, 20]. However, to date, most studies were focused on microorganisms present in the adult sand fly with little or no attention paid to physiological effects brought about by these microorganisms on developing stages. Here, we investigated the effects of EGFP-expressing *B. subtilis* (*Bs*) or GFP-expressing *P. agglomerans* (*Pa*) on the midgut innate immunity and epithelial homeostasis of 3rd instar larvae of *L. longipalpis*. With particular respect paid toward the ability of the immature vector to undergo metamorphosis and retain the bacteria tested.

The distribution of these bacteria within the midgut of sand fly larvae is likely driven in part by the gut pH gradient [21], and perhaps may display a cytotoxic effect on the midgut epithelium by infection with *Pa* or *Bs* like what is observed in *Drosophila* [22, 23]. These two phenomenon were investigated in these studies. Additionally, we were interested in the activation and regulation of the immune response in the sand fly. It has been previously shown that *Caspar* is involved in negatively regulating the immunodeficiency response in sand flies, and knocking it down via RNAi leads to lower parasite numbers in adult flies [18]. Here, we investigate a differential and suppressive response to infection with respect to G+ and G- bacteria, possibly influenced by the gene encoding another negative regulator of immunity, *"poor immune response upon knock-in*" or *Pirk*. Up-regulation of *Pirk* transcript level would theoretically lead to a significant depletion of the transcripts encoding the antimicrobial peptides.

There is no work conducted in sand flies to measure any phenomenon related to Toll pathway regulation or IMD recognition of foreign organisms and molecules. Additionally, the agar feeding regimens used to determine the effect of Pirk on effector molecule expression are quite different than the natural detritus material that sand flies are generally exposed to in the lab and nature. While there is data on the efficiency of RNAi mediated knockdown in adult sand flies [18, 24], no published data is currently aimed to elucidate the efficiency of RNAi mediated knockdown of sand fly transcripts in the immature larval stages. Here we investigate the negative regulator of Toll signaling, Cactus, as a marker for measuring Toll pathway activity. Although Cactus activity is generally described in hemocyte interactions with gram-positive bacteria and fungal organisms, or dorso-ventral development [25, 26], we wished to see if it may have so effect in the midgut against gram-positive *B. subtilis*. PGRP-LB is a well-studied recognition

molecule for the IMD pathway, known for its ability to protect *W. wigglesworthia* within the bacteriome of the tsetse fly midgut [27].

While a primary focus of these studies is to determine the viability of these bacteria as a paratransgenic platform, we also wanted to gain insights into how these microbes are related to intestinal immunity (explained above), and how they may engage in cross talk with other pathways of interest (explained below) that drive physiological processes and development.

1.3. Immunity and Autophagy

Growing numbers of studies are aimed at teasing out the complex relationships between immune and autophagic processes. The term 'antimicrobial autophagy' was recently used to describe this process and is reviewed thoroughly in Moy et al. 2013 [28], and is categorized as an innate immune response in *D. melanogaster*. It is interesting to see a process typically implicated in development and nutritional status play a role in immunity. Within *D. melanogaster* it is demonstrated to mediate a Toll and IMD independent autophagic response against the intracellular pathogenic bacteria *Listeria* [29]. Combating vesicular stomatitis virus in the fruit fly also occurs through a nutritional sensing phosphatidyl inositol kinase autophagic response (PI3K) [30]. Beyond the realm of insects lays the potential mechanisms and benefits that must be understood for higher animals, specifically mammals. The role of autophagy in immunity, aging, inflammation, and development is reviewed for higher animals in Mizushima et al. 2008 [31].

With respect to our research, we were interested in evaluating the potential of autophagy during immune responses to our putative paratransgenic commensal bacteria. Moreover, we wanted to probe at the putative linkage of autophagy to development of sand flies from immature stages to the adult life cycle (explained below).

1.4. Autophagy and development

Autophagy is a complex process that involves the processing and recycling of cellular macromolecules and larger organelles. This can be associated with a multitude of phenomenon including stresses like starvation, or intriguingly the decision of a cell to undergo programmed cell death or survival. Within higher mammals this process is intimately linked to numerous disease pathologies such as neurological degeneration and cancer. Interestingly, there is mounting evidence to suggest that autophagy is paramount in regulating the varied and finely orchestrated developmental events that occur in various insect life stages. A majority of the work involves the use of the model organism *Drosophila melanogaster*. Here the role of autophagy in recycling tissues and cellular reprogramming is apparent. During fruit fly embryogenesis autophagy plays a role in removing excess sera from developing insects [32]. Additionally, degradation of larval salivary glands during metamorphosis is required to produce the final adult tissues, and is autophagy dependent [33, 34]. Over-proliferation of the neuromuscular junction of larval stages of the fly is prevented via functioning autophagy [35]. Breakdown of fat body during development of not only fruit flies, but *Bombyx mori*, is also a crucial process that has been linked to autophagy [36, 37].

Larval midgut removal and the tissue remodeling and differentiation of the adult gut are a hallmark of metamorphosis. Autophagy plays a center role in nutrient recycling of midgut cells fated to undergo apoptosis and survival of gut cells that will ultimately comprise the adult tissue. A number of more recent studies implicate the function of autophagy in both pro-death and pro-survival in fruit flies and silk worms [38-41].

Within hematophagous insects there are few studies delineating the role of autophagy during development. Studies suggest that autophagy in the fat body of *Aedes aegypti* is important

in maintaining gonadotrophic cycles [42]. Additionally, the presence of electron dense autophagosomes has been detected in the developing midgut of the mosquito during metamorphosis [43].

Ecdysone is the major hormone employed by insects to progress through various developmental stages. Its complex set of interactions with ecdysone receptors and primary response genes is vital in finely tuning spatial and temporal developmental events. Briefly and specifically, E93 and Broad (Br-C) have been identified as 2 primary ecdysone response genes that signal the removal of the larval midgut of *D. melanogaster* before completion of the adult gut via autophagy [44-46]. Further, it is suggested that the action of these molecules may be conserved across holometabolous insects [47]. However, insights into the direct mode of action of ecdysone, primary response genes, and autophagy in affecting successful metamorphosis have only very recently begun to be understood. In *B. mori* it has been shown that autophagy-related 1 (ATG1) is a response gene to ecdysone. E93 is able to bind to ATG1 promoter region and induce its expression [48]. While these finding help in understanding how the larval gut may be removed during pupation, little is known about how the new adult gut is formed. It is suggested that Vein, an epidermal growth factor, may be involved in signaling intestinal stem cells of adult *D. melanogaster* to differentiate into healthy adult epithelial cells [23, 49, 50].

To our knowledge there is no study published on the role of autophagy and its possible response to ecdysone, or the place of epidermal growth factors during metamorphosis of the sand fly *L. longipalpis*. Here we investigate whether the key components of the autophagy pathway are conserved in sand flies and expressed during metamorphosis of the fly. We also take a preliminary glimpse into the midgut specificity for expression of an autophagy component in the cytoplasm of developing epithelial cells. Additionally, we investigate a possible candidate for the

generation of an adult midgut tissue in sand flies. Finally, tenable evidence supportive of a link between ATG1 and ecdysone is provided.

1.5. Research Goals and Objectives

1.5.1. Determination of distribution and persistence of paratransgenic bacterial candidates in the midgut of sand fly larvae

To evaluate the potential of *P. agglomerans* and *B. subtilis* as delivery systems for paratransgeneic microbes, we plan to examine GFP-labeled bacteria in the midgut of the sand fly larvae by using an agar based feeding system. Owing to their GFP or EGFP (respectively) signals, we expect to visualize the distribution of the bacteria within the alimentary canal using confocal microscopy. Additionally, we propose to determine midgut pH gradients, which may influence the localization of bacteria *in vivo* for the entire sand fly larval alimentary canal by using two different pH indicators. We plan to further confirm this via *in vitro* measurements of bacterial growth on selected pH media. The persistence of *P. agglomerans* and *B. subtilis* in the midgut will be determined by confocal microscopy visualization or by counting bacteria colonies on selected media. Our goal is to determine basic physiological traits exhibited within the gut of the fly larvae, and determine their ability to survive therein.

1.5.2. Determination of effects of bacterial infection on midgut epithelium cells and immune responses

To evaluate possible effects of *P. agglomerans* and *B. subtilis* on the midgut of sand fly larvae, we propose to employ qRT-PCR to determine the mRNA levels of immune effector and regulatory molecules within the gut. To visualize the direct effects of microbial presence on the

midgut epithelium we plan to use confocal microscopy to see cells specifically undergoing programmed cell death. We also propose to evaluate the efficiency of RNAi targeting candidate genes by injection in larvae, which have not been explored in sandy fly larvae.. Our goal is to understand basic physiological effects of *P. agglomerans* and *B. subtilis* infection on developing larval gut tissues, and analyze the efficiency of RNAi as a common reverse genetic tool on larval stages.

1.5.3. Investigation of the role of autophagy during larval infection and development to adult stage

To explore the role of autophagy during bacterial infection or metamorphosis of the sand fly larvae we propose to measure relative transcript levels of selected markers of autophagy signaling. We will dissect gut tissues and specifically visualize autophagic expression within the epithelium of the insect undergoing metamorphosis by using confocal microscopy. The goal of these studies is to better understand the role of bacterial infection with respect to immune response and autophagy during the larval developmental stages. Moreover, we expect to gain insights as to how autophagy may play crucial roles in the metamorphosis of the sand flies as a disease vector.

Chapter 2 - Bacterial Infection and Immune Responses in the Larval Midgut of *Lutzomyia longipalpis* Sand Flies

Abstract

The midgut microbial community in insect vectors of disease is crucial for an effective immune response against infection with various human and animal pathogens. Depending on the aspects of their development, insects can acquire microbes present in soil, water, and plants. Sand flies are major vectors of leishmaniasis, and shown to harbor a wide variety of Gram-negative and Gram-positive bacteria. Sand fly larval stages acquire microorganisms from the soil, and the abundance and distribution of these microorganisms may vary depending on the sand fly species or the breeding site. Here, we assess the distribution of two bacteria commonly found within the gut of sand flies, *Pantoea agglomerans* and *Bacillus subtilis*. We demonstrate that these bacteria are able to differentially infect the larval digestive tract, and regulate the immune response in sand fly larvae. Moreover, colonization of the gut is driven, at least in part, a gradient of pH present in the gut.

2.1. Introduction

Bacterial symbionts significantly influence many aspects of the physiology of their host. In insects, both pathogenic and non-pathogenic bacteria have been shown to modulate immune response, homeostasis, development, and overall health of midgut physiology for both larval and adult stages. Both Gram-positive (G+) and Gram-negative (G-) bacteria are commonly associated with the midgut tissue of Diptera, including several disease vectors. Many bacilli and enterobacter such as *Lactobacillus* and *Pantoea* have been identified from the midgut and other tissues of the fruit fly *Drosophila melanogaster* [7]. In field collected *Anopheles stephensi,*

Anopheles gambiae, and *Aedes aegypti* from laboratory colonies, a number of G+ and G- bacteria were identified [8-11]. Among G-, *Pantoea agglomerans* was also the most common genus identified from all cultivable bacteria in both male and female *Aedes albopictus* collected from two out of four sites in Madagascar [12]. In sand flies, several studies have focused on regional and potential species-specific variability in the microbial community of both *Phlebotomus* and *Lutzomyia* species. *P. agglomerans* and *Bacillus* spp. were commonly found in both natural and laboratory-reared sand fly populations. *Bacillus subtilis* and non-*Pantoea* members of the Enterobacter family were shown to be present in populations of *Phlebotomus papatasi* from, India, Turkey, Tunisia, and Egypt [13, 14]. *Bacillus* spp, *Serratia marcescens,* and *P. agglomerans* were identified in natural and laboratory populations of adult *Lutzomyia longipalpis* [15-18]. In laboratory colonies, Bacilli and Enterobacter were also identified in the larval stages of *L. longipalpis* [19, 20]. However, to date, most studies were focused on microorganisms present in the adult sand fly with little or no attention paid to physiological effects brought about by these microorganisms on developing stages. Here, we investigated the effects of EGFP-expressing *B. subtilis* (*Bs*) or GFP-expressing *P. agglomerans* (*Pa*) on the midgut innate immunity and epithelial homeostasis of 3rd instar larvae of *L. longipalpis*. Additionally, we determined that the distribution of these bacteria within the midgut of sand fly larvae is in part driven by the gut pH, and demonstrate a cytotoxic effect on the midgut epithelium by infection with *Pa*. Strikingly, we show evidence suggesting a differential and suppressive response to infection with respect to G+ and G- bacteria, likely influenced by the gene encoding the negative regulator of immunity, *"poor immune response upon knock-in*" or *Pirk*. Up-regulation of *Pirk* transcript level leads to a significant depletion of the transcripts encoding the antimicrobial peptide *Attacin* and the immunomodulatory peroxidase *IMPer*. With

respect to the organization of these microbes across the length and distal spacing of the midgut, G+ *Bs* were distributed throughout the entire alimentary canal in larvae, whereas G- *Pa* were found primarily in the posterior midgut. Our results strongly suggest that the range of pHs present within the sand fly larval gut likely is a driving force defining the ability of certain bacteria such as *P. agglomerans* to infect areas of the gut. The results presented here may have implications beyond the sand fly system and may explain how the distribution (and possibly colonization) of bacteria and other microbes may occur within the guts of insects.

2.2. Materials and Methods

2.2.1. Sand fly colony maintenance

L. longipalpis (Jacobina strain – LLJB) were the colony maintained in the Department of Entomology, Kansas State University. Larvae were maintained in 250 or 500 ml plastic jars (Nalgene) with an approximately 2 cm-thick bed made of dental plaster (Schein), and fed on either larval chow (a mixture of 50 % rabbit droppings and 50 % rabbit food) or on 1.5 % agar in LB, with or without the (E)GFP-expressing bacteria (see below).

2.2.2. Culturing and feeding of EGFP-expressing *B. subtilis* and GFP-expressing *P. agglomerans*

EGFP-expressing *B. subtilis* (strain 1012 transformed with plasmid pAD43-25, obtained from the Bacillus Genetic Stock Center) and GFP-expressing *P. agglomerans* (strain EPA-E325 transformed with plasmid pT-3078-5, a gift from Dr. David Lampe) were cultured at 30 °C overnight in LB medium supplemented with 5 µg/ml chloramphenicol (Alfa Aesar, A Jonson Mattey Co.) or with 50 µg/ml Carbenicillin (Teknova), respectively. Bacterial cultures were

centrifuged at 2500 rpm for 20 minutes at room temperature and the pellets were washed twice with 1X PBS. Bacteria were then suspended in PBS for a final concentration of 10^9 bacteria in 50-to-80 µl that was spread on a plate containing a thin layer (2-3 mm thick) of LB-agar (no antibiotics) and grown overnight. The following day, fluorescence of the bacterial lawn was confirmed and the LB-agar was cut into 3-to-5 mm^2 pieces to be fed to early L3 *L. longipalpis* larvae (depicted in Supporting Figure 2.6.), and lawns were replaced every 48 h. Prior to feeding on the LB-agar with *Bs* or *Pa*, all larvae were starved for 6 to 10 hours to allow for excretion of midgut contents, and rinsed in sterile water. As controls, L3 larvae were fed on LB-agar plus 5 mM paraquat, an herbicide that strongly induces apoptosis [51], and on LB-agar plus kanamycin (50 µg/ml) (we were unable to use plain LB-agar due to contamination). Larvae fed *ad libitum* for up to 48 h at 26 °C and 80 % humidity, with a 12:12 h light-dark cycle. Groups of (n=20) larvae were collected at 12, 24, 36, and 48 h post feeding with three biological replicates. Food intake was determined by examining each larva under a dissecting microscope (10X). All larval feedings were done according to feeding groups using 500 ml Nalgene pots with a 2-3 cm layer of dental cement.

Alternatively, larvae were fed for 12 h on bacteria-containing LB-agar and transferred to pots with plain LB-agar (no bacteria and no antibiotics). Larvae in groups of 3 to 5 were collected every 3 h and assessed for GFP signal using a Zeiss confocal LSM microscope. CFUs were also measured for larvae collected at 12 h and 24 h, by surface sterilizing each larva, dissecting and grinding each whole gut using a hand-held homogenizer in 60 µl 1X PBS, and plating the homogenate on selective media (5 µg/ml chloramphenicol for *B. subtilis* or 50 µg/ml carbenicillin for *P. agglomerans*) and incubating at 28 ºC to 30 ºC.

To assess for any effects of diet on midgut development, the length and width of the larval midgut were measured using the LSM 510 using the software ZEISS LSM Image Browser (Zeiss International). Midgut length was determined by measuring from the beginning of the anterior midgut to the posterior region of the midgut. Width measurements were obtained from three regions of each midgut: the anterior (ant), the middle (mid), and the posterior (pos) regions.

2.2.3. Immunocytochemistry

Whole guts from *L. longipalpis* L3 larvae were dissected (n=3) from three separate treatments of L3 into PBS and fixed for 20 minutes at room temperature with 4 % paraformaldehyde in PBS. Tissues were washed 4 times for 30 minutes with PBS containing 0.3 % Triton X-100 (PBST), then blocked with PBS containing 1 % bovine serum albumin for 30 minutes at room temperature. Tissues were then incubated overnight at 4 °C with primary antibodies for rabbit anti cleaved caspase3 (Cell Signaling Technology) diluted 1:500 in PBST. Tissues were washed 3 times for 30 minutes with PBST, and incubated overnight at 4 °C with Alexa Fluor® 594 goat anti-rabbit (Invitrogen) diluted 1:1000 in PBST. Tissues were washed 3 times for 30 minutes with PBST, and nuclei were stained for 5 minutes with 10 µg/mL of DAPI (Invitrogen). Samples were mounted in Vectashield® (Vector Laboratories) anti-photo bleaching reagent, and images were obtained with a LSM 510 confocal microscope using the software ZEISS LSM Image Browser. In addition, measurements of larval guts length and width were obtained for each feeding treatment using the LSM510 confocal microscope.

2.2.4. Larval midgut pH

We assessed the pH within the midgut by feeding *L. longipalpis* L3 larvae with LB-agar containing 0.4 % of the pH indicators Bromothymol blue and Phenol red. LB-agar medium adjusted to pH 7 added prior to sterilization. Each indicator agar medium was fed to a group to 50 L3 larvae following six hours of food deprivation. Feeding of the larvae was performed by placing the larvae and fragments of approximately 3-5 mm^2 of the dye-containing agar inside a 500 ml Nalgene pot with a 1 cm layer of plaster, maintained at room temperature and with a relative humidity of 80-85 %. Larvae were allowed to feed *ad libitum* for 20 hours. The pH indicator dyes were visualized through the translucent cuticle of the larvae. The pH inside the larval gut was determined by comparing the color and intensity shown within the gut with those from 0.4 % solutions of both dyes made in 8 ml LB medium (with one added drop of chloroform to prevent bacterial growth), and with pH ranging from pH 4 to 10 in 0.5 increments.

2.2.5. Effect of pH on *in vitro* growth of EGFP-expressing *B subtilis* and GFP-expressing *P. agglomerans*

Overnight cultures of fluorescent *Bs* and *Pa* were diluted to OD_{600} = 0.1 and further diluted $1:10^4$ prior to plating onto LB-agar plates supplemented with either 50 µg/ml of carbenicillin (CAR) or 5 µg/ml of chloramphenicol (CAM) for selection of *Pa* or *Bs*, respectively. The pH of plates ranged from pH 6 to 9.5 in 0.5 increments. Plates were incubated overnight at 37 °C for *Bs*, and at room temperature for *Pa*, and each experiment was performed in triplicate, and repeated twice. The following day bacterial colonies were counted, and colonies growing at each pH were observed under fluorescent microscope. One-way ANOVA with a Tukey test was performed to determine differences between pH.

2.2.6. RNA extraction and reverse transcription

Midguts from *L. longipalpis* L3 larvae were dissected under a stereoscope microscope in Hyclone® (Thermo Scientific) phosphate buffered saline (PBS) at 12, 24, and 36 h post feeding in either the *Bs* or *Pa*. Sterile, 1.5 % agar in LB was used as feeding control. Total RNA was isolated from pools of 20 midguts using TRIzol® (Invitrogen). For each group of larval midguts, RNA isolation was done in triplicate. RNA quality was assessed by electrophoresis on 1 % agarose-5 % formaldehyde in 1x MOPS, and stored at -80 °C. First strand cDNA synthesis was conducted using Superscript™ III reverse transcription kit (Invitrogen) as described [24].

2.2.7. Quantitative real time PCR

mRNA levels were quantified with iQ™ SYBER® Green Supermix (Bio-Rad) using 95 ºC melting, 57 ºC annealing, and 72 ºC extension temperature for 40 cycles using a Realplex^4 Master cycler (Eppendorf). Relative fold changes were assessed using the ΔΔCt method [24, 52], and calibrated against the expression observed for same stage larvae fed on the plain LB-agar control. Sequences for *Attacin* (*Att*), *IMPer*, *Vein*, *Domeless*, *IMD*, *Pirk*, *USP36*, and *Duox* were obtained using the tBLASTN algorithm from corresponding annotated sequences found in *D. melanogaster* blasted against *L. longipalpis* contigs. Predicted full-length transcripts were made using GENSCAN (http://genes.mit.edu/GENSCAN.html), and primers sequences were generated using Primer3 (http://biotools.umassmed.edu/bioapps/primer3_www.cgi). Primers for RPS6 were previously described in [16]. Primers for *Def1* were based on the sequences described in an earlier study [17]. All other primers used in this study were designed from gene sequences in the NCBI database and their accession numbers are as follows: IMPer, AJWK01035414.1; DUOX,

AJWK01035414.1; IMD, AJWK01008032.1; Domeless, AJWK01008028.1; Attacin, AJWK01017071.1; Pirk, AJWK01015539.1; USP36, AJWK01027563.1; and Vein, AJWK01005322.1.All primer sequences used in this study are summarized in Table 2.4.

2.3. Results

2.3.1. Bs and Pa localize to different regions of the sand fly larvae midgut

A scheme representing the anatomy of *L. longipalpis* sand fly 3rd instar (L3) gut is depicted in Figure 1.1.A. Following continuous feeding of LB-agar containing EGFP-expressing *Bs* to larvae, a pervasive signal was found across the entire length of the midgut for infected insects as depicted by the fluorescent signal of full length images of the gut (Figure 2.1.B, 2.7.A, and 2.10.). However, when the GFP-expressing *Pa* was fed to larvae in a similar manner the bacteria were mostly localized to a narrow area of the posterior portion of the midgut (Figure 2.1.C and 2.7.B), and were only found on the apical surface of the midgut lumen (Figure 2.11.). Also observed were areas of high intensity GFP signal in *Pa*-infected guts, suggesting the presence of biofilm (Figure 2.1.C). A less pronounced GFP signal in *Pa* fed was also observed in the proventriculus of the gut (Figure 2.1.C). Infection rates as determined by a qualitative assessment of the GFP signal within the midgut of the larvae following continuous feeding are described in Table 2.1.

To further investigate what could be driving such a distinct microbial distribution, we assessed the gut pH range within larvae *in vivo*, and compared it to pH growth assays for the two GFP-expressing bacteria *in vitro*. LB-agar supplemented with pH indicators Bromothymol blue or Phenol red were fed to larvae, and the color gradient generated was visible through the translucent cuticle of larvae using light microscopy. Intensity of colors varied between larvae due

to the initial ingestion time, load size, and bolus movement across the gut. Fifteen larvae of each treatment were compared to the pH references. The bromothymol blue dye has a range of pH from 6 to 7.6, and phenol red has a range of 6.8 to 8.4. Previous results on *L. longipalpis* larval gut pH indicated a basic pH >9 in the anterior portion and an more acidic pH >6.5 in the posterior portion of the midgut [21]. The results shown in Figure 2.2. confirm such a pH gradient in the *L. longipalpis* larvae, clearly pointing to a basic pH for the anterior part of the midgut, including the proventriculus (PV), and an acidic pH in the posterior part of the midgut.

Both *Bs* and *Pa* bacteria were grown on antibiotic supplemented LB-agar plates with pH ranging from 6 to 9.5. CFU counts were obtained in triplicate to assess the viability of the two strains at different pH (Figure 2.3.A). Colonies of EGFP-expressing *Bs* did not show a significant difference in CFU counts at any given pH. Additionally, the colony size for *Bs* fed was smaller at low (6-6.5), and high (9.5) pH. However, *Pa* showed a significant difference in CFU counts at pH ranging from 6-7 with respect to pH 9.5 (Figure 2.3.B). Also, at pH 8-9 colony size and fluorescent intensity began to decrease, and by pH 9.5 there was no visible growth.

Following the continuous feeding experiment described above, we tested whether similar results could be obtained by feeding larvae once with either *Bs* or *Pa*. Larvae were fed for 12 h on LB-agar with the respective bacteria and transferred to pots with fresh LB-agar (no antibiotics). *Pa* bacteria were cleared by 21 h after infection, whereas *Bs* were cleared by 24 h (Table 2.2.). CFU counts (Table 2.3.) were generally in agreement with the results observed for the GFP signals assessed.

2.3.2. Infection of the sand fly larval midgut by *Pa* or *Bs* leads to differential damage of the larval midgut epithelium

Bs and *Pa* were assessed for their ability to infect the sand fly L3 larvae midgut following feeding, and their effect on induction of apoptosis. Monoclonal antibodies targeting the cleaved caspase3 were used as an immunocytochemical marker to identify epithelial cells undergoing caspase-dependent programmed cell death, and to assess the integrity of the midgut. In order to test if this was a viable approach, we fed larvae with LB-agar supplemented with the apoptosis inducer paraquat, and compared its effects to larvae fed on LB-agar alone. The LB-agar fed larvae displayed a well-defined midgut epithelium with little background staining for active caspase3 (Figure 2.8.A). In contrast, larvae fed on LB-agar supplemented with paraquat showed midgut epithelia with significant loss of integrity, that were also severely flattened after mounting on the slide with reduced luminal space detectable by looking at nuclei alone (Figure 2.8.B). The apoptotic effect of the paraquat was further confirmed by the presence of a large population of cells showing heavy cytoplasmic specific staining for caspase3 (Figure 2.8.C and D). After 12h of infection with *Bs* an extensive amount of luminal nucleic material is observed using DAPI staining (Figure 2.4.A), and a massive infection can be seen in Figure 2.4.B. Very little background caspase staining is observed in *Bs*-fed compared to the paraquat treated controls (Figures 2.4.C, 2.4.D, and 2.8.). In contrast, when *Pa* was used for infection, the Gram-negative bacteria induced staining comparable to that of the paraquat control (Figures 2.4.G, H, and 2.8.). However, we did not observe a similar breakdown in midgut superstructure.

2.3.3. Effect of feeding agar on larval development

Effects of feeding agar to the developing sand fly L3 larvae were assessed by comparing the length of the whole midgut and the width of three areas within the midgut to those obtained from larvae raised on regular larvae food (50 % rabbit feces + 50 % rabbit food). The same parameters were also measured from guts of *Pa* and *Bs* infected larvae. A significant difference was found for midgut length when comparing regular sand fly larval food and the agar fed, except at 48 h. For the three measurements of gut width (anterior, middle and posterior), significant differences were only observed between regular food and agar (Supporting Figure 2.9.).

2.3.4. Bacterial feeding leads to differential expression profiles in sand fly larvae

We compared the mRNA expression profiles of nine genes likely involved in various physiological processes ranging from innate immunity, homeostasis, and epithelial regeneration in midguts of *L. longipalpis* L3 larvae fed on *Bs* and *Pa* bacteria. Among the transcripts assessed were *Att*, *Def1*, *Duox*, *IMPer*, *Vein*, *Domeless*, *IMD*, *Pirk*, and *USP36*. Results from qRT-PCR indicate that, compared to control fed, larvae fed on agar containing either *Bs* or *Pa* showed significant difference in expression for a number of genes analyzed.

At 12 h post infection, transcript levels for *Att* were downregulated by nearly 75 % for both *Bs* and *Pa* infected larvae, and *IMPer* was downregulated by 25 % in *Pa* fed (Figure 2.5.A). *Pirk* showed a 2.5-fold change (~150 % increase) in expression following infection with *Pa* (Figure 2.5.B).

At 24 h post infection, *Domeless* and *IMD* followed a similar profile and were upregulated in both infections, albeit *Domeless* was not significantly different between the

control and *Bs* fed. *Pirk* was also upregulated at in both bacterial infections, and with a profile that also was similar to *Domeless* and *IMD* (Figure 2.5.E). *USP36* was downregulated only in *Bs* infection, and *Def1* was upregulated only in *Pa* (Figure 2.5.F).

At 36 h post infection, *Domeless* and *IMD* again displayed similar profiles, however both were downregulated in comparison to control (Figure 2.5.H). For *Pirk*, whereas expression if *Bs* fed returned to control levels, in *Pa* infection it remained significantly higher (nearly 2-fold) (Figure 2.5.H). Finally, *USP36* expression was reduced by roughly 10 % in both infections, but for *Bs* the significance was 0.078 (Figure 2.5.I).

2.4. Discussion

In insects, gut bacteria have been shown to significantly contribute to nutrition, modulation of the immune response, and protection from parasites and other pathogens. The insect gut varies greatly in terms of morphology and physicochemical properties, and these may influence the distribution and structure of the microbial community in the gut. During development, sand fly larvae are exposed to a wide variety of soil bacteria and other microorganisms that are able to colonize the insect gut [13-20, 53]). However, as we are aware, no studies have focused on the mechanisms by which bacteria are able to develop within the sand fly gut, or the types of specific responses induced by the colonization. Here, we assessed the ability of two bacteria previously identified from the guts of insects, including sand flies, to infect the gut of sand fly larvae, and investigated the specific responses (innate immunity, epithelia regeneration, homeostasis) induced by these bacteria.

When fed to *L. longipalpis* larvae, EGFP-expressing *Bs* bacteria were distributed throughout the entirety of the alimentary canal, residing within the peritrophic matrix and along

the lumen. In contrast, GFP-expressing *Pa* bacteria were mostly localized to the posterior midgut, and only at the apical surface (although we did observe GFP signal for *Pa* at the proventriculus of the gut, it is possible that these bacteria had not yet been killed by the alkaline conditions). We speculated that this phenomenon must be driven by pH and/or by specific cell types that line the midgut lumen. A pH driven effect on the colonization of the gut was suggested by the use of pH indicators. It has been previously determined in sand fly larvae that the pH of the midgut is highly alkaline at the anterior portion and decreases towards the posterior region [21]. Our approach allowed us to confirm the location within the larval gut wherein the pH ranges between 6 and 7, which also coincides with the location where Gram-negative *Pa* preferentially infects the larval gut. These results were indirectly confirmed by *in vitro* growth assays obtained for *Pa* in which these bacteria clearly favor a pH in the range of 6-to-7. The ability of *Bs* to sporulate under unfavorable growth conditions may have further contributed to its survival along the gut of the larvae.

In addition, we observed a marked difference between the rates and the persistence of infections of *Pa* and *Bs* in sand fly larvae. Following continuous feeding on bacterial lawn, most of the *Pa* bacteria are cleared within 24 h whereas infection with *Bs* remained for up to 48 h. However, if the bacterial lawn is replaced at 48 h during continuous feeding, larvae do re-infect. In contrast, with the non-continuous feeding on the bacterial lawn led to clearing of *Pa* by 21 h and *Bs* by 24 h. Hence, the data indicate that the sand fly larvae are able to clear bacterial infection if exposure is not maintained. Another possibility if that the loss of *Pa* and *Bs* during non-continuous feeding may also be caused by competition with other microorganisms present in the larval gut. And in spite of differences known to exist in the half-lives of GFP and EGFP

proteins [54, 55], the CFU counts reported support the clearing of *Pa* from the midgut during loss of GFP signal.

Using a caspase3 antibody [22, 23] to detect apoptotic activity in *L. longipalpis*, we also were able to clearly identify differences between *Bs* and *Pa* infection of the sand fly larval gut. The microscopy data strongly suggest that only *Pa* induces caspase activity within the midgut of the sand fly, while *Bs* causes little to no staining.

Quantitative RT-PCR analyses were used to assess changes in the expression profiles of nine selected genes chosen based on their roles in insect midgut immunity and homeostasis. Related to midgut immunity, selected genes included those coding for effector molecules such as the antimicrobial peptides (AMPs) attacin (*Att*) and defensin (*Def1*), as well as *Duox* and *IMPer*. Also included in this category was the immunodeficiency regulatory gene encoding *"poor immune response upon knock-in"* or *Pirk*.

Attacin has long been implicated in bacteria killing from a number of studies pertaining to its role in innate immunity [56]. *Def1* was shown to be upregulated in adult *L. longipalpis* after bacterial challenge [17]. It has been shown that Defensin A, acting in concert with Cecropin A, blocks *Plasmodium* transmission in *A. aegypti* [57]. The effector molecules Duox and IMPer have been demonstrated to have effects on the midgut peritrophic matrix structure and parasite killing in *A. gambiae* mosquitoes [58-60]. For Def1, Att, DUOX, and IMPer, there are multiple studies suggesting that these effector molecules are regulated by the immunodeficiency pathway [59, 61, 62]. Pirk has been previously shown to be a negative regulator of IMD activity [63, 64]. While Pirk acts to suppress IMD at the level of signal transduction, Caspar negatively regulates IMD at the level of transcription. Studies in *A. gambiae* implicate the knockdown of *IMD* in

increased infectivity of mosquitoes [65, 66]. In sand flies, *Caspar* knockdown led to a decrease in *Leishmania mexicana* load in *L. longipalpis* [18].

Domeless, *Vein*, and *USP36* were selected based on their roles in pathways related to innate immunity to midgut regeneration. When the innate immune response is activated in the midgut, there are associated energy costs and damage to healthy epithelial cells that can negatively affect the insect. Artificially activating ROS production in *A. stephensi* led to reduction in infective lifespan, and deleterious effects associated with mitochondria [67]. Domeless is a receptor in the JAK/STAT pathway that is crucial for recognizing damage to healthy epithelial cells. JAK/STAT signaling reaches intestinal stem cells (ISCs) and enteroblasts (EBs) leading to the secretion of an epidermal growth factor (Vein) ending in regeneration of midgut epithelia via proliferation and differentiation of ISCs and EBs [23, 68-70]. Additionally, the deubiquitinating enzyme USP36 is a negative regulator of IMD and provides a route of cross-talk between IMD and JAK/STAT pathways [71, 72]. USP36 is also involved in controlling selective autophagy [72].

Our results suggest that *Pirk* may be acting to suppress *Att* and *IMPer* activity at 12 h post infection for *Pa*-infected insects, however, another still unidentified mechanism likely is involved in the reduction of *Att* levels for *Bs*-infected. Although *Pirk* was significantly upregulated during *Bs* and *Pa* infection at 24 h, there was also an increase for the immune transcription factor *IMD*. Such *IMD* increase can be linked to an associated upregulation of *Def1* in *Pa* infected, but no significant difference was found in *Def1* for *Bs* infected. The upregulation of *IMD* may be explained by the concomitant down regulation of *USP36* in the *Bs* infected larvae, but not *Pa* infected. Additionally, the nearly two-fold increase of *Domeless* in *Pa* fed

larvae suggests the possibility of homeostatic response to damage by the larvae immune response that occurs within the first 12 h of infections as our data have demonstrated.

By 36 h, upregulation of *Pirk* continued in *Pa* infected individuals, but no effect was observed for the expression of the effector molecules. With the downregulation of *USP36*, we expected an upregulation of *IMD*. However, the opposite was detected: *IMD* was downregulated. Interestingly, *Domeless* was also downregulated at 36 h, possibly due to lack (or clearing) of bacteria in the gut as indicated by the non-continuous feeding experiments. It remains to be investigated whether downregulation of *IMD*, when *USP36* levels were also lowered, is associated with increased autophagy during bacterial clearing. The expression analyses data corroborates what was observed with regards to the progress of infection in *Bs* and *Pa*. Of significance, our results indicate that sand fly larvae are able to differentially regulate (or suppress, as the case here) their immune response according to the bacterial challenge they are exposed to.

We have previously shown that feeding different bacteria to *L. longipalpis* larvae affects survival and development [20]. In the current study, we demonstrate a selective localization of bacteria in the larvae driven by gut pH and downstream effects on the larval gut. This provides a link between the type of bacteria colonizing the gut, physicochemical aspects of the gut, and overall insect health. With regards to mechanisms driving the localization of bacteria, it is also likely that different cell types lining the gut epithelia are involved. In support of this hypothesis, concentrated pockets of *Pa* binding to the posterior end of the larval gut were observed, indicating the presence of a biofilm. However, the presence of a preferred cell type or membrane receptor involved in binding of bacteria cannot be discarded. Gram-negative bacteria are known to form biofilm within the gut of vectors [73]. *P. agglomerans* form intestinal biofilms in the

Mediterranean fruit fly *Cerititis capitata* [74] that resemble what we observed in sand fly larvae. Taken together, these data suggest a pH-dependent localization or growth of bacteria within the insect midgut previously reported to be a random event [74].

With regards to cell type, Fernandes et al [43] reported the presence of different cell types in *A. aegypti* during development and metamorphosis, and a precedent for favored microbial binding was previously demonstrated for *Leishmania major* binding to the midgut epithelial cell lining of the sand fly *P. papatasi* [75]. Thus, it is conceivable that at least one of these events may also be involved in dictating the success of bacterial colonization within the sand fly gut. Nevertheless, mechanisms such as autophagy may also play a role in bacterial removal (reviewed in Huang et al. [76]). Further, both *Pa* and *Bs* do not survive metamorphosis.

It is important to note that the agar based feeding system used in our experiments does not replicate the natural conditions faced by sand fly larvae and agar does not provide the necessary nutrition for normal larvae development. As shown by our analyses, the midgut length and width differed significantly between larvae fed on agar versus those fed on regular sands fly larvae chow. However, no differences in such parameters of the midgut morphology were observed between agar fed larvae and the agar plus bacteria fed larvae. Interestingly, differences observed for the midgut parameters tested only lasted until either the agar or the bacterial lawn were replaced. Additionally, larvae were not able to sustain a GFP-positive signal when fed on LB-agar plus bacteria for 12 h and then transferred to plain LB-agar. These data were also supported by CFU counts. Notwithstanding, this method was proven useful for specifically delivering the EGFP- or GFP-expressing bacteria. Similar approaches may be used to deliver selected microbes to sand fly larvae in paratransgenic applications to control sand fly populations [77, 78].

In conclusion, this study demonstrates that bacteria selectively infect the sand fly larval midgut, (possibly) leading to epithelial damage. In addition, the data also point to a modulation of the innate immune response likely controlled by expression of *Pirk*. We also show for the first time that the insect midgut pH is a factor driving microbial organization of the gut. Our results contribute towards understanding of midgut responses to infections and provide new insights for development of vector control approaches using paratransgenesis.

Table 2.1. *P. agglomerans* and *B. subtilis* infection rates

	GFP positive signal	
Time post infection	***P. agglomerans***	***B. subtilis***
12 h	9 of 14 (64%)	14 of 15 (93%)
24 h	0 of 9	15 of 15 (100%)
36 h	1 of 9 (11%)	7 of 7 (100%)
48 h	0 of 9	3 of 8 (37.5%)

P. *agglomerans* and *B*. *subtilis* were continuously fed to sand fly larvae. At time points indicated (left column), the infection rates in sand fly larvae were determined by a qualitative assessment (presence or absence) of GFP signal using a Zeiss 510 confocal microscope.

doi:10.1371/journal.pntd.0003923.t001

Table 2.2. Persistence of bacterial infection between continuous and non-continuous feedings

	GFP positive signal			
	Continuous feeding		Non-continuous feeding	
Time	*P. agglomerans*	*B. subtilis*	*P. agglomerans*	*B. subtilis*
12 h	8 of 10*	10 of 10*	-*	*-
15 h	-	-	1 of 5	4 of 5
18 h	-	-	1 of 5	1 of 5
21 h	-	-	0 of 5	3 of 5
24 h	1 of 5	5 of 5	0 of 4	0 of 5
27 h	-	-	0 of 5	0 of 5
30 h	-	-	0 of 5	0 of 5
36 h	1 of 5	4 of 4	0 of 3	0 of 2
42 h	-	-	0 of 5	0 of 5
48 h	0 of 5	3 of 5	0 of 5	0 of 5

Persistence of bacterial infection in sand fly larvae was determined by a qualitative assessment (presence or absence) of GFP signal using a Zeiss 510 confocal microscope. GFP positive signal observed for larvae fed for up to 48 h on bacterial lawns (continuous feeding), of for larvae fed 12 h on bacterial lawn of each bacteria, and transferred to plain LB-agar (non-continuous feeding). Larvae were collected at different time points and the midguts were dissected and prepared for confocal analyses as indicated. Results observed for the continuous and non-continuous feeding are shown as number of larvae displaying a GFP signal per total larval guts.

*As larvae in both groups fed for 12h, there is no difference between continuous and non-continuous for that time point; all larvae were grouped into the continuous feeding group.

doi:10.1371/journal.pntd.0003923.t002

Table 2.3. Colony forming units (CFU) from continuous and non-continuous fed larvae

	Continuous feeding		Non-continuous feeding	
Time	***P. agglomerans***	***B. subtilis***	***P. agglomerans***	***B. subtilis***
12 h	0–48 (n = 5) (10.8 ± 20.9)	30–2600 (n = 5) (647.6 ± 1095.6)	-	-
24 h	4–6 (n = 3) (6.0 ± 2.0)	0–480 (n = 3) (330.2 ± 286.2)	0–190† (n = 3) (63.3 ± 109.7)	0 (n = 3)

Range (AVG±Stdev) distribution of CFUs present in gut larva at 12 h (n = 5) and 24 h (n = 3) after continuous or non-continuous feeding. In continuous feeding, larvae were fed on LB-agar plus bacteria for 24 h; for non-continuous feeding, larvae were fed on LB-agar plus bacteria for 12 h and transferred to LB-agar. Guts were dissected from surface sterilized larvae and homogenized in 60 μl of 1X PBS followed by plating on selective LB media. After overnight incubation at 37°C plates were scored for the presence of colonies assessed according to morphology and GFP signal. Results shown are representative of three experiments.

†CFUs present in *Pa*-fed larva at 24 h were likely due to cannibalism observed in this group.

doi:10.1371/journal.pntd.0003923.t003

Table 2.4. List of primer sequence used in this study

Gene Name	Symbol	Sequence
Dual Oxidase F	DUOX	5'-GGCAAGACGGAAGACAAG-3'
Dual Oxidase R	DUOX	5'-TCAACAAGGGAACGACATC-3'
Immuno-Modulatory Peroxidase F	IMPer	5'-CTGTGTGCGTGATAAATGTC-3'
Immuno-Modulatory Peroxidase R	IMPer	5'-GTGGTAGGTGCTGGTGAAG-3'
Immunodeficiency F	IMD	5'-GGTGAACAACACTCAAGCAT-3'
Immunodeficiency R	IMD	5'-GTTACTCTGGGTCTGGGAGA-3'
Domeless F	Dome	5'-TCAAACACACCCCAAAATAC-3'
Domeless R	Dome	5'-ACGCCTCTCAATCACCATA-3'
AttacinA F	AttA	5'-ATGGAATGACCTCTGTGGAT-3'
AttacinA R	AttA	5'-AGCGATGAGAAAGACCAAGT-3'
Pirk F	Pirk	5'-AAGATGAGTGGGAGTGAGAAG-3'
Pirk R	Pirk	5'-CCAACAATACGCAAATGG-3'
USP36 F	USP36	5'-CTACGAACTGGAAGATGGTG-3'
USP36 R	USP36	5'-GATTTTGTCTCTGGCTGATG-3'
Vein F	Vein	5'-CGCAATGGATGAGAACAC-3'
Vein R	Vein	5'-TGAGCAATACCTACGCTGAC-3'
Defensin1 F	Def1	5'-GCCTGTGTGTTGTAGTTCT-3'
Defensin1 R	Def1	5'-GCATCTCCCCATCCTGTT-3'
Ribosomal Protein s6	LIS6	5'-TCCCCTGGGTGATGAGTGG-3'
Ribosomal Protein s6	LIS6	5'-CCTTTGTGCGTGGCTTCTTCC-3'

Supporting Table S1 – Primer list

Primers were based on sequence information obtained from various databases. F and R in each primer indicate the forward and reverse primers used, respectively.

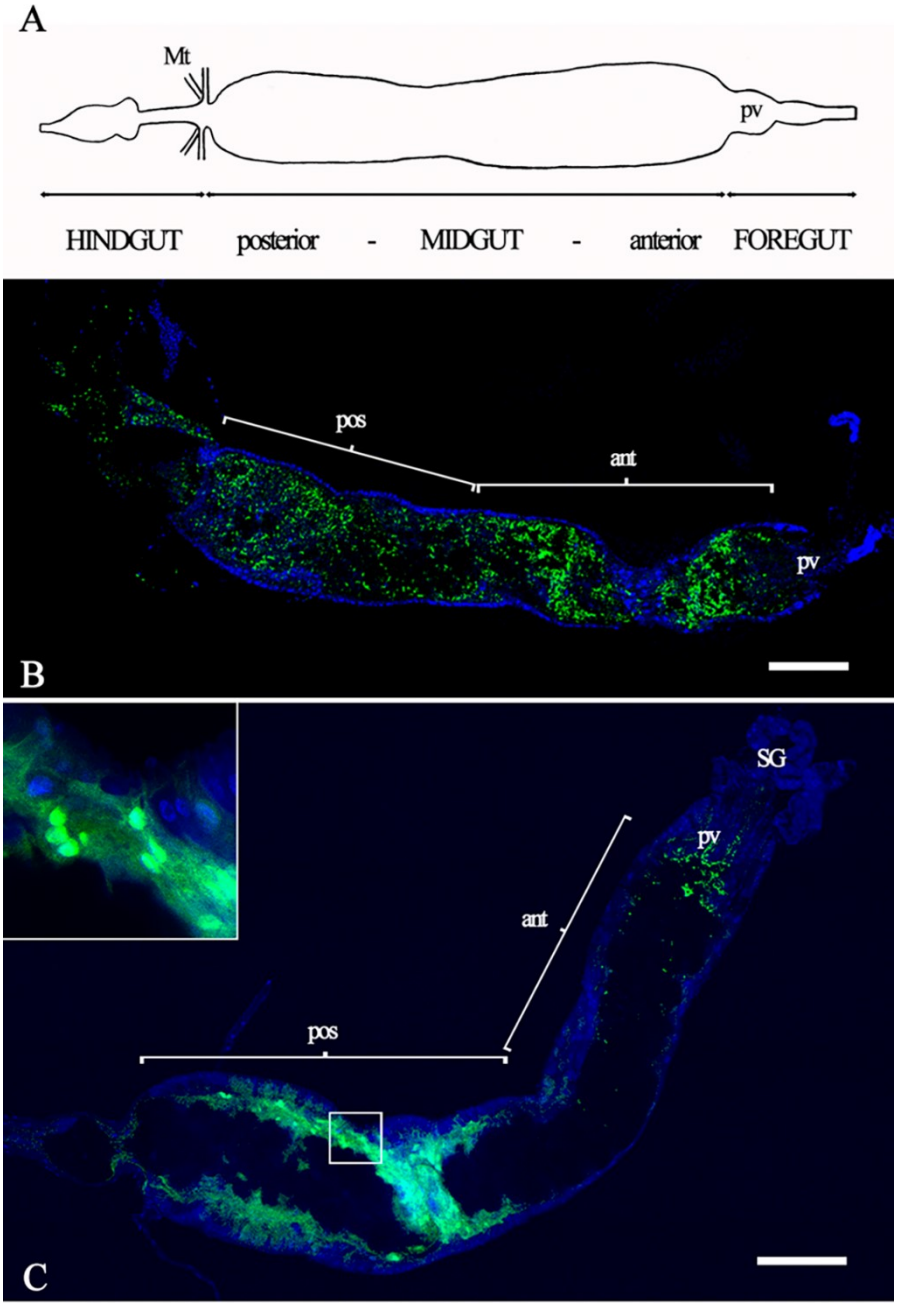

Figure 2.1. Infection of sand fly larva midgut by *B. subtilis* and *P. agglomerans*.

EGFP- or GFP-expressing Bs and Pa were grown on LB-agar plates with selective media and fed to 3rd instar sand fly larvae. Larvae guts were dissected and assessed for the distribution of each bacterium. In A, a schematic representation of the sand fly larval gut. Ingested food is moved from right (proventriculus – pv) to left, towards to posterior midgut and hindgut. Confocal images (1024x1024 per tile pixel resolution) of the distribution of EGFP-expressing Bs-infected and GFP-expressing Pa-infected midguts are shown in panels B and C. Posterior (pos) and anterior (ant) portions of midguts are indicated. SG, salivary glands. Inset in 1C: blow up of area of gut delineated by a rectangle (asterisk) showing biofilm formed in Pa infection. Bars = 100 μm.

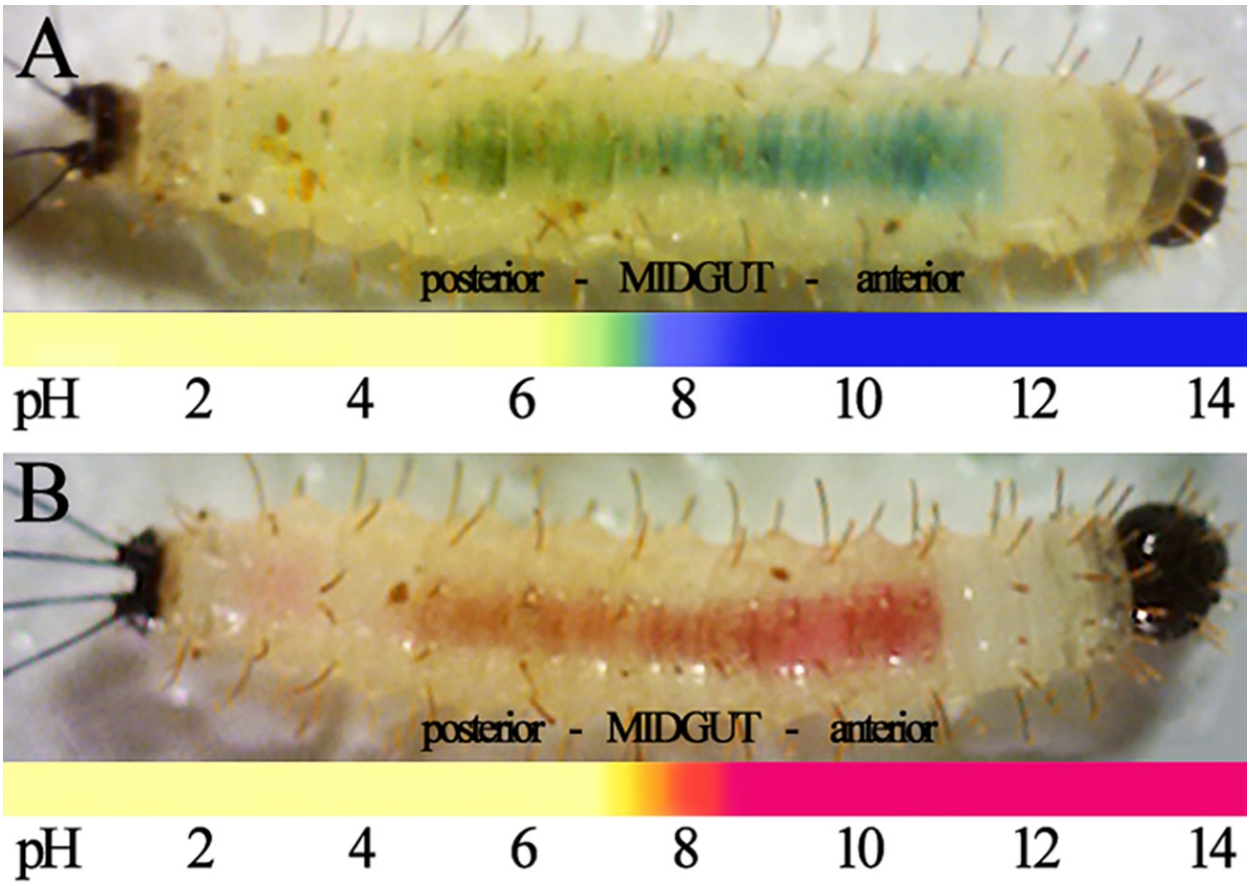

Figure 2.2. pH of the sand fly larval gut.

Third instar sand fly larvae were fed with pH indicators bromothymol blue (A) and phenol red (B). Shown is the distribution of each indicator within live sand fly larval guts, with the predicted pH for each area of the gut indicated. Live 3rd instar sand fly larvae are shown from left (posterior or caudal setae) to right (anterior or head).

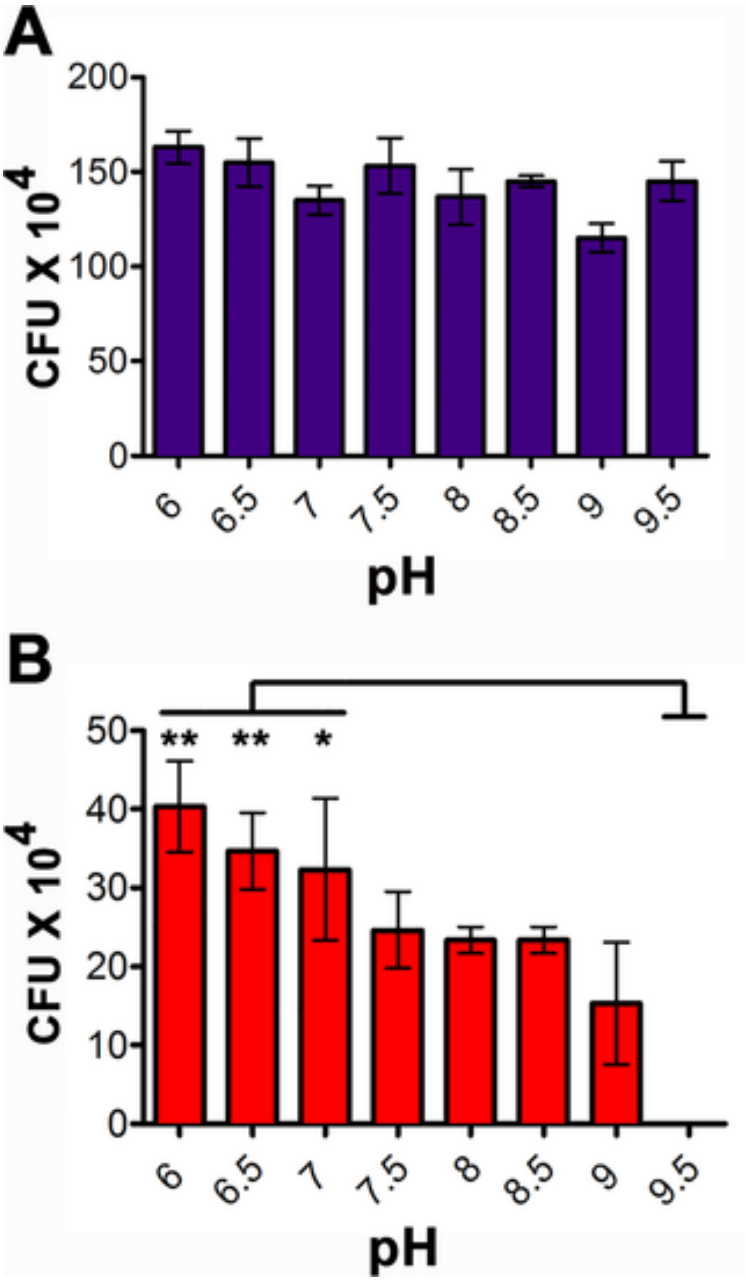

Figure 2.3. Effect of pH on in vitro growth of *B. subtilis* and *P. agglomerans*.

Cultured bacteria were grown on LB-agar plates of pH varying from 6-9.5. The colony forming units are measured for Bs (A) and Pa (B). One way ANOVA, with a post hoc Tukey test, was performed to assess significance. pHs 6, 6.5, and 7 were statistically different than pH 9.5 ($P<0.01$ for pH 6 and 6.6; and $P<0.05$ for pH 7).

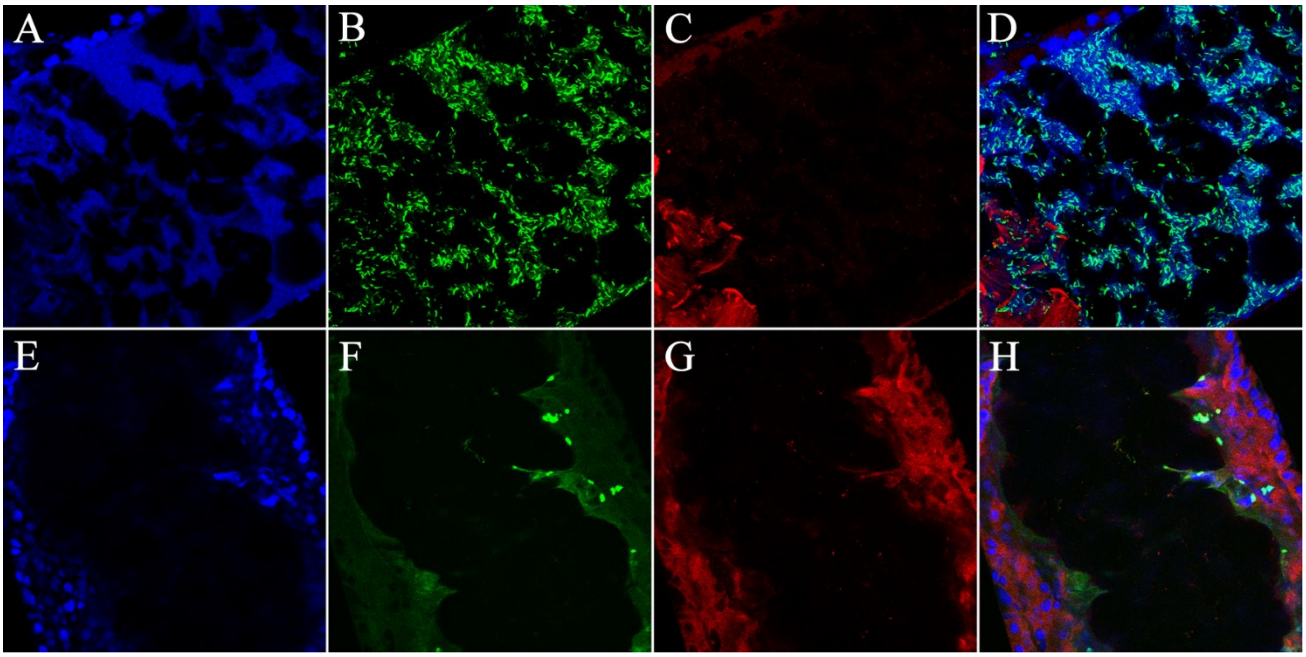

Figure 2.4**. Confocal images of *B. subtilis* and *P. agglomerans* infection of sand fly larvae midguts.**

Anterior midgut image 12h post feeding depicting differential distribution of bacteria and apoptotic responses. A) DAPI staining; B) Shows Bs distributed throughout the anterior larval gut; C) Immuno-staining for cleaved caspase3 along the lumen of the midgut. D) Merge. 12h post infection with GFP-expressing Pa localized to the posterior region of the midgut epithelium and induces apoptotic activity. E) DAPI staining depicting the midgut epithelium. F) Shows Pa localized on the apical portion of the lumen of the midgut. G) Immuno-staining for cleaved caspase3 along the lumen of the midgut depicting high levels of caspase3 activity. H) Merge. Bars = 50 μm.

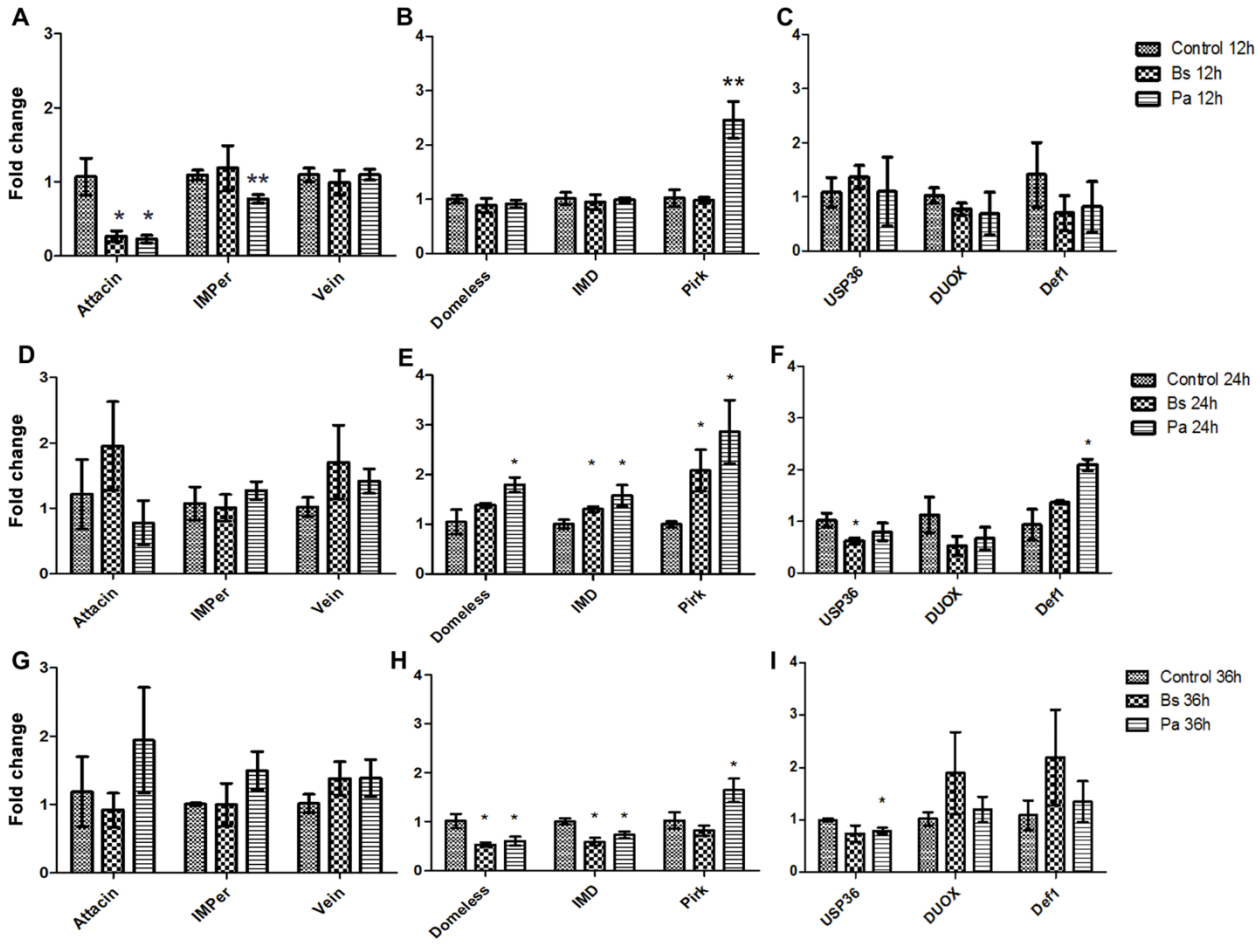

Figure 2.5**. mRNA expression profiles of 3rd instar *L. longipalpis* larvae post infection with *B. subtilis* and *P. agglomerans*.**

B. subtilis (Bs) or *P. agglomerans* (Pa) bacteria were fed to larvae and the expression of selected transcripts relative to agar fed control larvae was assessed. Expression profiles were obtained for the effector molecules Att and IMPer, in addition to the epithelial growth factor Vein are shown in A. D, and G, Expression profiles for the JAK/STAT receptor Domeless, the transcription factor for immunodeficiency IMD, and the negative regulator of IMD pathway Pirk are shown in are shown in B.G, and H. Expression profiles for the E3 Ubiquitin ligase associated with IMD, and the effector molecules dual oxidase DUOX and Def1are shown in C, F, and I. Following bacterial feeding, total RNA was obtained at 12 h (A, B, and C), at 24 h (D, E, and F), and at 36 h (G, H, and I) post infection (PI). All Ct values were normalized to the ribosomal protein S6 (RPS6). Error bars are represented as the standard deviation determined from three biological replicates each with n=20 midguts. Significance was determined using student t-tests. * denotes $P<0.05$ and ** denotes $P<0.01$. Y-axis, fold change.

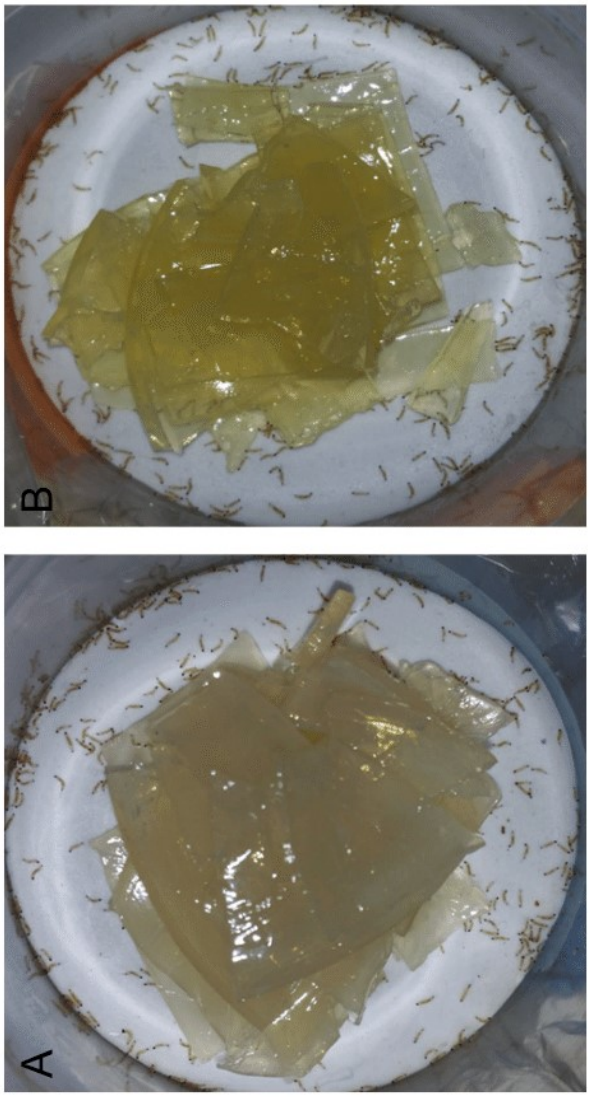

Figure 2.6**. Larval feeding of bacterial lawn.**

After overnight incubation on LB-agar plus antibiotics, each bacterial lawn was cut and fed to 3rd instar larvae. On the left (A) the larvae are feeding on EGFP-expressing *Bs*, while on the right (B) the larvae are feeding on GFP-expressing *Pa*.

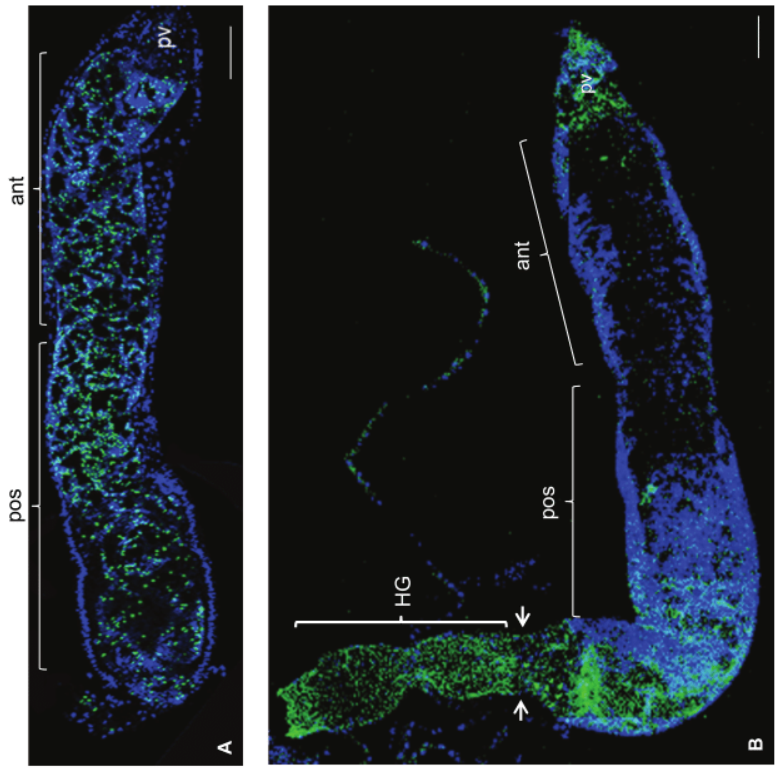

Figure 2.7. Infection of sand fly larval midgut by *B. subtilis* or *P. agglomerans*.

Larval guts were imaged using a resolution of 512 x 512 (number of pixels per tile). Ingested food is moved from right (proventriculus – pv) to left, towards to posterior midgut and hindgut. EGFP-expressing *Bs*-infected (A) and GFP-expressing *Pa*-infected (B) midguts are shown. Posterior (pos) and anterior (ant) midgut are marked. Arrowheads indicate the separation between midgut and hindgut. Bars = 100 µm.

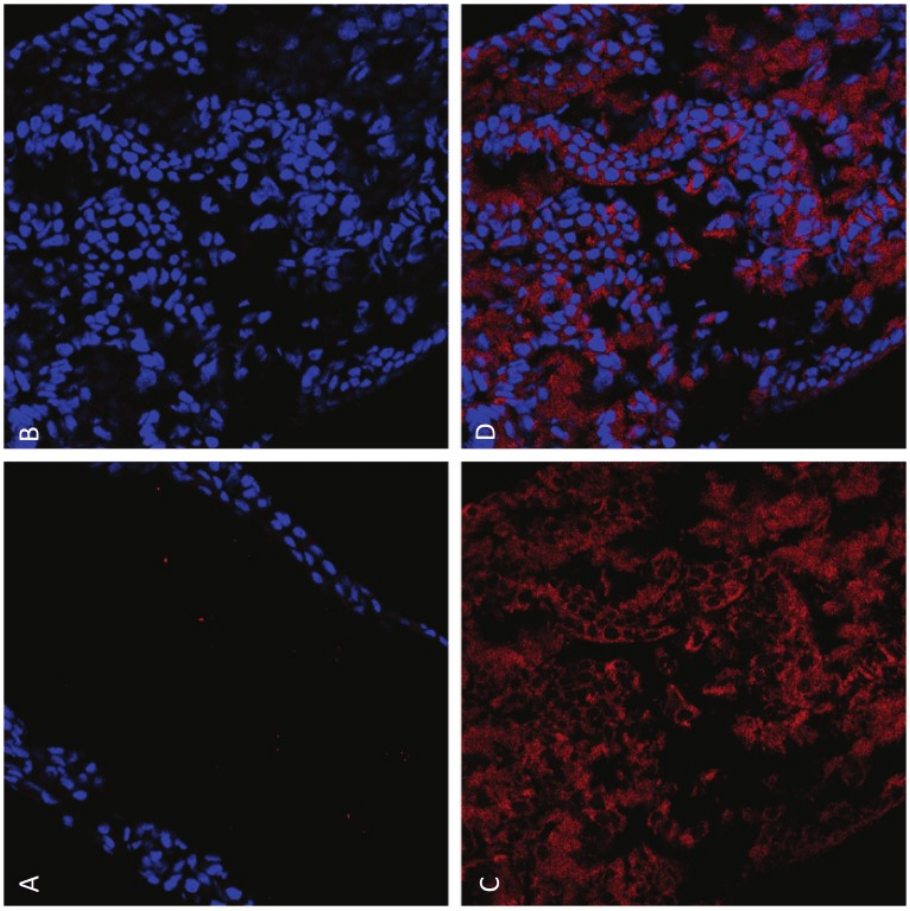

Figure 2.8. Paraquat-induced apoptosis in sand fly larval midguts.

Ingestion of paraquat induces a detectable and systemic apoptotic response in the cytoplasm of midgut epithelial cells 12h post feeding. A) Merge of caspase3 and DAPI stained nuclei for larvae fed only LB-agar medium in the anterior midgut versus B) larvae with LB-agar supplemented with paraquat visualized with DAPI 12h post infection (anterior midgut). C) Immuno-staining for cleaved caspase3 in paraquat fed larvae. D) Merge of B and C. Bars = 50 μm.

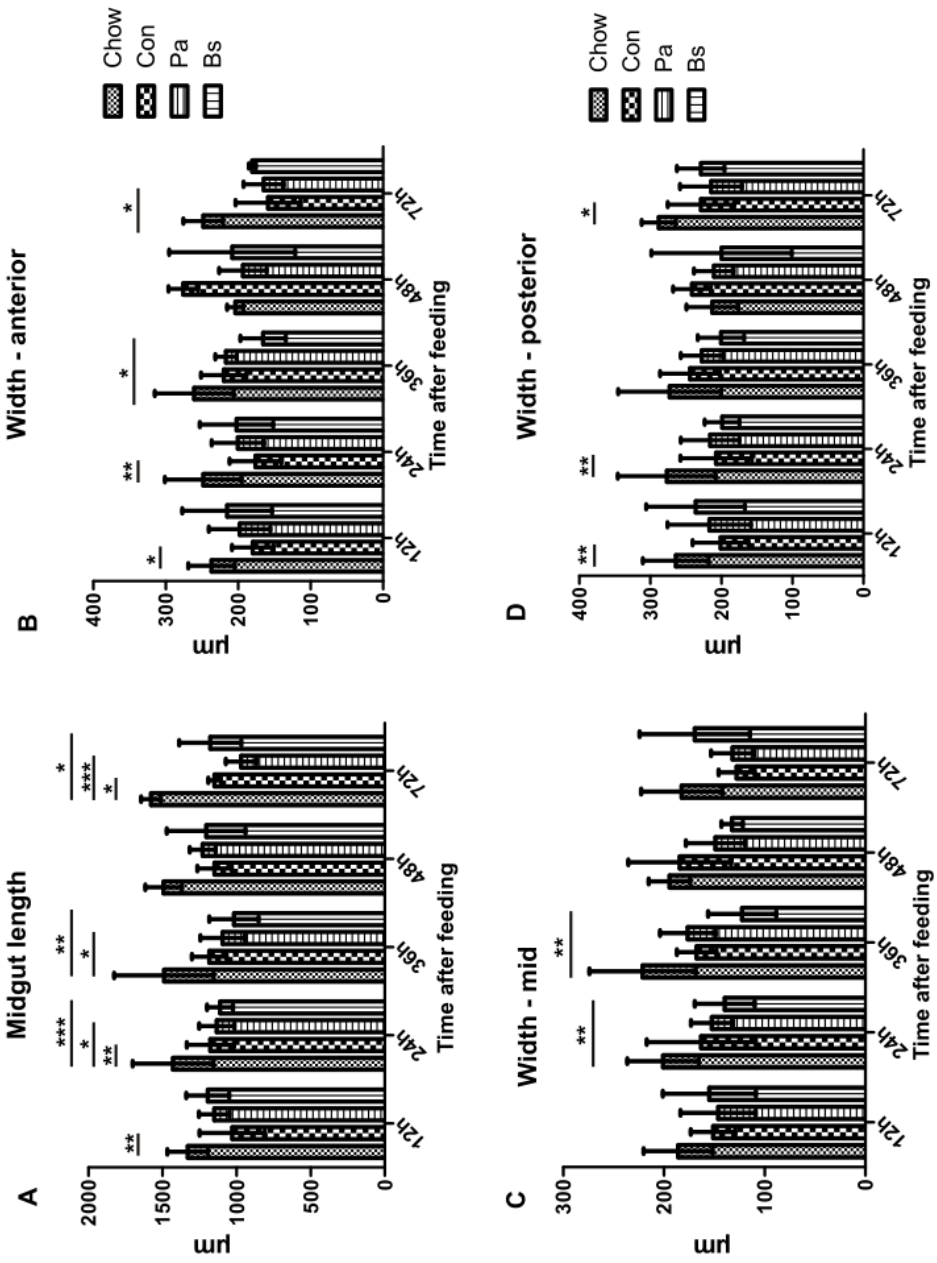

Figure 2.9**. Changes in sand fly larval gut length and width caused by diet.**

L. longipalpis 3rd instar larvae were fed on either regular sand fly larval food (50 % rabbit feces + 50 % rabbit food), or on LB-agar with or without bacteria, for up to 72 hours. Larval midguts were dissected and measured for length, and width in the anterior, middle, and posterior regions of the gut.

Figure 2.10. Localization of B. subtilis.

Refer to Supporting Information Figure S1 Video found at
http://journals.plos.org/plosntds/article?id=10.1371%2Fjournal.pntd.0003923

Figure 2.11. Apical localization of P. agglomerans on midgut epithelia.

Refer to Supporting Information Figure S2 Video found at
http://journals.plos.org/plosntds/article?id=10.1371%2Fjournal.pntd.0003923

Chapter 3 - The Role of Autophagy during Metamorphosis of the Sand Fly *Lutzomyia longipalpis*

Abstract

The development of holometabolous insects is a complex process, especially with respect to the stages where the organism does not acquire nutrients from the environment. Undergoing the metamorphosis from larvae to adult requires the insect to manage and recycle its own available resources to develop fully. Autophagy is crucial for non-feeding larvae to undergo successful pupation and metamorphosis into the adult form. Here, we were able to measure 3 genes related to the pre-autophagesome, nucleation, and sequestration involved in successful autophagy. We found that during pupation and metamorphosis that these transcripts were significantly upregulated. Additionally, we provide evidence for one candidate epidermal growth factor *Vein* for production of adult tissues within the pupae of sand flies. We were also able to visualize autophagasomes residing within the cytoplasmic compartment of pupal stages using confocal microscopy. Finally, we present preliminary evidence from the sand fly genome that ecdysone secretion during metamorphosis may be directly linked to the activation of autophagy. Understanding the underlying mechanisms of this process will provide invaluable data in the future management of this neglected tropical vector.

3.1. Introduction

Autophagy is a complex process that involves the processing and recycling of cellular macromolecules and larger organelles. This can be associated with a multitude of phenomenon including stresses like starvation, or intriguingly the decision of a cell to undergo programmed cell death or survival. Within higher mammals this process is intimately linked to numerous disease pathologies such as neurological degeneration and cancer. Interestingly, there is

mounting evidence to suggest that autophagy is paramount in regulating the varied and finely orchestrated developmental events that occur in various insect life stages. A majority of the work involves the use of the model organism *Drosophila melanogaster*. Here the role of autophagy in recycling tissues and cellular reprogramming is apparent. During fruit fly embryogenesis autophagy plays a role in removing excess sera from developing insects [32]. Additionally, degradation of larval salivary glands during metamorphosis is required to produce the final adult tissues, and is autophagy dependent [33, 34]. Over-proliferation of the neuromuscular junction of larval stages of the fly is prevented via functioning autophagy [35]. Breakdown of fat body during development of not only fruit flies, but *Bombyx mori*, is also a crucial process that has been linked to autophagy [36, 37].

Larval midgut removal and the tissue remodeling and differentiation of the adult gut are a hallmark of metamorphosis. Autophagy plays a center role in nutrient recycling of midgut cells fated to undergo apoptosis and survival of gut cells that will ultimately comprise the adult tissue. A number of more recent studies implicate the function of autophagy in both pro-death and pro-survival in fruit flies and silk worms [38-41].

Within hematophagous insects there are few studies delineating the role of autophagy during development. Studies suggest that autophagy in the fat body of *Aedes aegypti* is important in maintaining gonadotrophic cycles [42]. Additionally, the presence of electron dense autophagosomes has been detected in the developing midgut of the mosquito during metamorphosis [43].

Ecdysone is the major hormone employed by insects to progress through various developmental stages. Its complex set of interactions with ecdysone receptors and primary response genes is vital in finely tuning spatial and temporal developmental events. Briefly and

specifically, E93 and Broad (Br-C) have been identified as 2 primary ecdysone response genes that signal the removal of the larval midgut of *D. melanogaster* before completion of the adult gut via autophagy [44-46]. Further, it is suggested that the action of these molecules may be conserved across holometabolous insects [47]. However, insights into the direct mode of action of ecdysone, primary response genes, and autophagy in affecting successful metamorphosis have only very recently begun to be understood. In *B. mori* it has been shown that autophagy-related 1 (ATG1) is a response gene to ecdysone. E93 is able to bind to ATG1 promoter region and induce its expression [48]. While these finding help in understanding how the larval gut may be removed during pupation, little is known about how the new adult gut is formed. It is suggested that Vein, an epidermal growth factor, may be involved in signaling intestinal stem cells of adult *D. melanogaster* to differentiate into healthy adult epithelial cells [23, 49, 50].

To our knowledge there is no study published on the role of autophagy and its possible response to ecdysone, or the place of epidermal growth factors during metamorphosis of the sand fly *L. longipalpis*. Here we present evidence that key components of the autophagy pathway are conserved in sand flies and expressed during metamorphosis of the fly. We also demonstrate the midgut specificity for expression of an autophagy component in the cytoplasm of developing epithelial cells. Additionally, we provide a possible candidate for the generation of an adult midgut tissue in sand flies. Finally, we provide a preliminary link that suggests that the promoter region of ATG1 may contain the necessary elements for interaction with primary response genes associated with ecdysone.

3.2. Material & Methods

3.2.1. Sand fly colony maintenance

L. longipalpis (Jacobina strain – LLJB) colonies were reared in the Department of Entomology, Kansas State University. Larvae were maintained in 250 or 500 ml plastic jars (Nalgene) with an approximately 2 cm-thick bed made of dental plaster (Schein), and fed on larval chow (a mixture of 50% rabbit droppings and 50% rabbit food).

3.2.2. RNA extraction and reverse transcription

Whole insects from *L. longipalpis* L3, wandering L4, pupae, or adult insects were dissected under a stereoscope microscope in Hyclone (Thermo Scientific) phosphate buffered saline (PBS). Total RNA was isolated from pools of 5 insects using TRIzol (Invitrogen). For each group of midguts, RNA was isolated in triplicate. RNA quality was assessed by electrophoresis on 1% agarose-5% formaldehyde in 1x MOPS gel, and stored at -80 °C. First strand cDNA synthesis was conducted using Superscript™ III reverse transcription kit (Invitrogen) as described [24].

3.2.3. Real time quantitative PCR

mRNA levels for different developmental stages were quantified with iQ SYBER Green Supermix (Bio-Rad) using 95º C melting, 57º C annealing, and 72º C extension temperature for 40 cycles using a Realplex^4 Master cycler (Eppendorf). Relative fold changes were assessed using the ΔΔCt method [24, 52, 79]. Sequences for *ATG1*, *ATG6*, and *ATG8* were obtained by taking sequences from *D. melanogaster* and using tBlastn and/or Blastp against *L. longipalpis* sequences found at VectorBase (https://www.vectorbase.org/blast). Primer sequences were generated using Primer3 software (http://biotools.umassmed.edu/bioapps/primer3_www.cgi). Primers for *Vein* were based on the sequences used in a previous study [79]. PCR amplicon

sequence was verified using direct sequencing at Kansas State University. All Blastp data and primer sequences used in this study are summarized in Table 3.1. & 3.2.

3.2.4. Sequence alignments, phylogeny, and putative ecdysone response element prediction

Sequences for ATG1, ATG6, ATG8, and Vein were obtained for various dipterans and humans using Blastp at NCBI or VectorBase (summary of organisms, accession numbers, and databases are provided in supplementary table 3.3.). In the case of Homo sapiens GABARALP1 (ATG8) the sequence was provided by the manufacturer (Abcam). Multiple sequence alignments at the protein level were conducted using Clustal Omega software (http://www.ebi.ac.uk/Tools/msa/clustalo/). Alignments were then visualized using BoxShade (http://www.ch.embnet.org/software/BOX_form.html). To determine phylogeny, neighbor joining trees were generated with 1000 bootstrap replicates using Mega7 (www.megasoftware.net). To determine putative ecdysone response element regions upstream of ATG1, genomic sequence (AJWK01026160.1) was obtained from the European Nucleotide Archive (http://www.ebi.ac.uk/ENA/). This sequence was searched for the canonical and non-canonical ecdysone responsive sequence elements described previously [80-82].

3.2.5. Midgut immunocytochemistry & measurements

Whole guts from *L. longipalpis* larvae (n=5) were dissected from three separate treatments of L3, wandering L4, pupae, or adult into PBS and fixed for 20 minutes at room temperature with 4% paraformaldehyde in PBS. Tissues were washed 4 times for 30 minutes with PBS containing 0.3% Triton X-100 (PBST), then blocked with PBS containing 1% bovine

serum albumin for 30 minutes at room temperature. Tissues were then incubated overnight at 4 °C with primary antibodies for rabbit anti-*Drosophila melanogaster* Beclin1 (ATG6) rabbit anti-Human GABARAPL (ATG8) from Abcam diluted 1:500 in PBST. Tissues were washed 3 times for 30 minutes with PBST, and incubated overnight at 4 °C with Alexa Fluor® 594 goat anti-rabbit (Invitrogen) diluted 1:1000 in PBST. Tissues were washed 3 times for 30 minutes with PBST, and nuclei were stained for 5 minutes with 10 µg/mL DAPI (Invitrogen). Samples were mounted in FluorSave (CalBiochem) anti-photo bleaching reagent, and images were obtained with a LSM 700 confocal microscope (Zeiss). In addition, images were manipulated and midgut length, width, and axial ratios [83] were measured using the Zen confocal microscope software (Zeiss).

3.3. Results

3.3.1. Change in expression profile of ATG1, ATG6, ATG8, and Vein during development

There are multiple stages associated with autophagy including the early autophagasome kinase activity, membrane trafficking, and elongation. We sought to quantify elements of these stages by measuring transcript markers for each. Additionally, there is little known about how the formation of the midgut is signaled, so we measured a putative epidermal growth factor (EGF). We began by selecting feeding 3rd instar (L3) larvae, non-feeding 4th instar (L4) larvae, newly formed pupae, and adult sand flies for performing qRT-PCR to measuring fold changes for the transcripts *ATG1* (serine/threonine kinase), *ATG6* (vesicle trafficking), *ATG8* (elongation), and *Vein* (putative EGF) calibrated against the L3 stage. We found 1 to 1 orthology for all of these transcripts against other dipterans and designed primers accordingly (summarized

in Figures 3.8.-3.16. and Tables 3.1.-3.3.). For *ATG1* we observed a greater than 10 fold increase in transcript abundance for pupae compared to all other developmental stages (Figure 3.1.A). We saw a modest but non-significant increase for *ATG6* at L4, and a significant 200 plus fold change for the transcript at the pupal stage versus all other stages (Figure 3.1.A). The significant peak stage for *ATG8* expression occurred during L4 versus L3 and adult. Pupa showed a mean upregulation of expression but not significantly different using one way ANOVA with Tukey multiple comparisons to any other stage due to the high degree of variability in L4 (Figure 3.1.B). If the same statistical method is repeated sans L4 data, pupae is indeed significantly ($P<0.05$) different from L3 and adult samples. In the case of *Vein* an increase of ~30 fold is observed for both L4 and pupa versus L3 and adult (Figure 3.1.B. However, this change is again insignificant ($P<0.06$) using one way ANOVA with Tukey multiple comparisons due to, again, the large degree of variability in the L4 samples obtained. When conducting this same statistical test using only L3, Pupa, and adult we observe a significant ($P<0.001$) difference with respect to pupa versus L3 and adult. For both *ATG8* and *Vein* it is of importance to note that there was a high degree of variability in biological replicates obtained from L4 larvae.

We also measured via confocal microscopy the differences in midgut dimensions and axial ratios (L/W) at all four stages as a means to identify developmental timing. There is no significant difference in length between L3, pupa, and adult sand fly guts. However, the L4 gut is significantly ~200 microns longer than pupa and adult on average (Figure 3.6.A). In addition to length, the average width of the L4 midgut is ~100 microns wider than any other stage observed (Figure 3.6.B). This correlates to a significantly lower value for the axial ratio observed in L4 larvae in comparison to pupae (Figure 3.7.). These observations allow us to see specific midgut morphologies as the insect approaches, proceeds through, and exits metamorphosis.

3.3.2. Midgut specific autophagy during pupation

Since our differences in RT-qPCR were generated from the entire insect undergoing development, we wished to further probe the midgut in order to visualize using immunocytochemistry specifically what was occurring in that tissue. To do so we applied antibodies targeting c-terminal end of *D. melanogaster ATG6* and n-terminal end of *Homo sapiens ATG8*. The n-terminal antigen sequence used to generate antibodies against *HsATG8* is similar to that of *L. longipalpis* as shown by multiple sequence alignment (Figure 3.11.), and we expected cross-reaction between species.

We processed tissues and looked for fluorescent signal using confocal microscopy. We observed that the anterior midgut region of pupae showed staining within only the epithelial cells (Ec) for *ATG6* while no staining was observed in the midgut lumen (Lu) (Figure 3.2.A). More specifically the staining was limited to the cytoplasmic compartment of positively stained cells where one would expect autophagasomes to be present (Figure 3.2.B and C). This indicates that the midgut epithelial cells of pupae forming adult midgut tissues are expressing *ATG6*. The other stages, L3, L4, and adult, probed for *ATG6* staining showed little to no red signal for the presence of antibodies and shown again by anterior region (Figure 3.3.A-C). We did see a non-significant upregulation for the *ATG6* transcript in L4 larvae, but we were unable to see staining in the midgut for this protein.

According to qRT-PCR, we expected to see staining for *ATG8* in the midgut epithelial cells of both L4 and pupae. However, in the case of this particular antibody we were unable to see any signal. Not only did L4 and pupae lack staining, but also L3 and adults (Figure 3.4.A-D). It is possible that the antibodies derived from the human sequence simply did not cross react with

sand fly tissues, or tissues other than the midgut at these developmental stages were expressing the *ATG8* protein.

3.3.3. Evidence linking the role of ecdysone to the activation of autophagy

We previously mentioned that there is growing evidence to support the idea that ecdysone hormone action may be directly linked to autophagy through the promoter of response genes, specifically the *ATG1*. So we procured the promoter region for *L. longipalpis ATG1* from VectorBase and searched the sequence upstream of the start codon for possible candidate sequences. These sequence elements are formed from imperfect palindromic sequences comprising two half sites separated by n nucleotides (-/n/+). One of the original and canonical negative (-) ecdysone responsive element sequence half sites identified as 5'-GTTTCA-3'[80] was found twice upstream of the start codon (Figure 3.4.). Another possible positive (+) half site, 5'-TGACAT-3', is seen downstream of the negative sites (Figure 3.4.). Additionally, the GAGA motif previously described [82] as binding to primary response gene E93 is conserved in *L. longipalpis* (Figure 3.4.). There is a non-canonical difference in these results, as these half-sites contain a large number of nucleotides (>5) between them. While containing the correct sequence, this fact, makes them poor candidates for a canonical primary ecdysone response. These datas will require rigorous scientific confirmation of these sequences role in activating *ATG1* expression in response to ecdysone. However, there is observable preliminary evidence to suggest that *ATG1* in *L. longipalpis* may be directly linked to ecdysone at the level of promoter activation and expression.

3.4. Discussion

Growing evidence in multiple orders of insects suggests an intimate link between developmental transitions and autophagy. This finely tuned interplay between death of the larvae

stages cells and tissues and survival of progenitor cells destined to become adult tissues during metamorphosis is only partially understood. On one hand autophagy has been roundly demonstrated to remove immature tissues. However, there is suggested a likely role of autophagy in pro survival for certain subsets of cells. Additionally, there is little published data demonstrating what types of signals are produced to guide these progenitor cells into differentiating into adult tissues. Moreover, traditional theory dictates that autophagy is a downstream event of target of rapamycin (TOR) regulation [33, 36, 37] in the presence of ecdysone. However, recent work in *B. mori* demonstrates a direct link between the molting hormone and the onset of autophagy that may skip the need for TOR signaling [48].

To date there are few studies within hematophagous insects dedicated to understanding the potential roles of autophagy during metamorphosis, and how the adult midgut may be signaled to form. Here we show preliminary evidence showing a conserved autophagy primary network genes present in the sand fly *L. longipalpis* and present a possible candidate for midgut formation. Additionally, we are the first within blood feeding insects to provide a putative direct genetic link between the ecdysone hormone and the expression of autophagy molecules.

When we measured the transcripts *ATG1*, *ATG6*, *ATG8*, and *Vein* during metamorphosis we saw that they were all up-regulated during the pupal stage. These three target transcripts have been demonstrated from yeast to mammalian systems to be markers for the various stages of autophagy. *ATG1* is a crucial gene in establishing successful autophagy. The kinase activity of *ATG1* allows for the phosphorylation of downstream targets leading to the formation of autophagasomes (reviewed in [84]). The n-terminal kinase domain in sand flies bears striking resemblance to that of other dipteras (Figure 3.8. and 3.9.), and likely serves a conserved function with respect to autophagy. Ubiquitin like protein *ATG8* is extremely conserved from

insects to higher organisms (Figures 3.12. & 3.13. as its n-terminal region in *H. sapiens* almost exactly matches that of *L. longipalpis* (Figure 3.16.). It is anchored to the membrane of the autophagasome via a phosphatidylethanolamine addition and serves to extend the size of the isolation vesicle [85, 86]. It has also been noted in mammals for its ability to remove insoluble ubiquitinated proteins leading to survival [87]. The role of *ATG6* in autophagasome formation is quite interesting as it interacts with a number of different proteins, which can lead to programmed cell death or cell survival depending on its binding partners. In insects its function is best understood in *D. melanogaster*. It has a role in vesicle trafficking and leads to the degradation of cellular components and apoptosis when paired with vacuolar protein sorter (Vps34) [88]. However, it is also required for hematopoiesis and cellular differentiation in the fruit fly [89]. This pro-survival mode of action for *ATG6* is likely due to its association with the anti-apoptotic protein Bcl-2 [90]. It would be interesting to further probe what protein complex *ATG6* is involved in during metamorphosis within the sand fly to determine if it is playing a pro-survival or pro-apoptotic role or both and in what tissues, or specifically cells, is this role being carried out. *Vein* was our putative epidermal growth factor that may be signaling adult tissues to develop within the puparium. It contains conserved epidermal growth factor and immunoglobulin domains for EGFR signaling in vertebrates [91]. There are studies that pinpoint *Vein*'s action in the development of the adult fruit fly midgut [49, 50]. Additionally, it plays a role in the repair of adult midguts after infection [23]. We have previously describe *L. longipalpis Vein* in response to infection from *Bacillus subtilis* and *Pantoea agglomerans* in the sand fly larvae [79]. It's presence in both L4 larvae and pupae suggests the beginning of adult tissue formation in sand fly puparium. We have also seen an up-regulation for the putative *Vein* in the Dengue fever mosquito *Aedes aegypti* (data not shown here). It would be interesting to see

if *Vein* up-regulation was being localized to intestinal stem cells lining the midgut, however, we did not have suitable antibodies to probe at this possibility.

While we saw an increase in autophagy and EGF expression in the whole insect during metamorphosis, we wanted to visualize their localization spatially in dissected midguts of sand flies. We used antibodies against *ATG6* and *ATG8* to determine localization within the guts. It was extremely interesting to note that we saw *ATG6* staining within the epithelial cells of developing adults within the puparium. To date, most studies implicate its role in the removal of the larval gut, or a pro-apoptotic response [38-41]. However, our results may be indicating a pro-survival and differentiation of newly formed epithelial cells. As mentioned before it would be interesting to see which proteins are interacting with *ATG6* in this particular situation to gain further insights into the mode of action of this protein within this context. It was unfortunate to not see similar staining for the *ATG8* antibodies in the pupal midgut. It is possible that *H. sapiens ATG8* antigen used to create these antibodies is different enough from that of *L. longipalpis* to prevent cross-reaction, however this is unlikely (Figure 3.16.). It is more likely that the concentration of antibodies (1:500) used to probe the gut was not sufficient to generate a signal. A previous paper in *A. aegypti* used *ATG8* primary antibodies at a 10-fold higher concentration and were able to very clearly observe autophagasomes with anchored *ATG8* molecules [42]. Another possibility remains that the increased *ATG8* expression seen in RT-qPCR was occurring in other tissue types within the puparium, and not within the midgut.

It is exciting to provide preliminary evidence to further the idea that ecdysone may be able to directly activate *ATG1*'s expression leading to its kinase activity and autophagasome assembly through the promoter directly. There are many studies that demonstrate *ATG1* response to ecdysone, but the mechanism is only now beginning to be unraveled. A very recent paper

delves into the biochemistry of ecdysone response genes and the activation of the *ATG1* promoter for expression [48]. While sharing the canonical sequences demonstrated in multiple systems for decades, they do not share same distance between half-sites or putative secondary structure elements. It is likely that they are not the same imperfect palindromes sequences describe in previous work. However, this does not disqualify them as having structural proclivities as other elements previously described above. Here we are able to show that the primary response ecdysone responsive element and GAGA sequences are conserved within the promoter of *L. longipalpis*. Of course further experimentation would be required to determine if this region of the *ATG1* gene is indeed responsive to ecdysone treatment *in vivo*. However, these preliminary results show promise that autophagy may be hardwired into the process of metamorphosis across different insect orders.

Table 3.1. The accession numbers, identity, score, and expected value for each query protein (*D. melanogaster*) against each subject protein (*L. longipalpis*).

Gene Symbol	Accesion # *D. melanogaster*	Accession # *L. longipalpis*	Identity	Score	E-value
ATG1	NP_648601.1	LLOJ007855	79.70%	1431	4.00E-157
ATG6	NP_651209.1	LLOJ007047	59.30%	1907	0
ATG8	NP_727447.1	LLOJ007649	96.60%	814	3.00E-80
Vein	NP_523942.2	LLOJ001534	61%	933	1.00E-84

Table 3.2. The sequence of RT-qPCR primers used for each transcript measured in this study.

Gene Symbol	Primer 5' - 3' Forward	Primer 5'-3' Reverse
ATG1	GGTGATTTGGCGGACTAC	ATTCTGTGGCTTGAGGTC
ATG6	GCTCCTGTTGATTGGTCA	CGTAAGGGACGAGTTTGTAG
ATG8	GAAGTACCTTGTGCCGTCT	CAGAGATCCCATTGATGC
Vein	CGCAATGGATGAGAACAC	TGAGCAATACCTACGCTGAC

Table 3.3. The species names, gene symbols, accession numbers, and databases for all sequences used for multiple sequence alignment and phylogenetic analysis in this study.*H. sapiens* ATG8 sequence is not derived from a database and may be procured from the company website via that catalog number.

Organism	Gene Symbol	Accession Number	Database
L. longipalpis	ATG1	LLOJ007855	VectorBase
	ATG6	LLOJ007047	VectorBase
	ATG8	LLOJ007649	VectorBase
	Vein	LLOJ001534	VectorBase
P. papatasi	ATG1	PPAI003929	VectorBase
	ATG6	FG117924.1	VectorBase
	ATG8	PPAI007833	VectorBase
	Vein	PPAI005726	VectorBase
D. melanogaster	ATG1	NP_648601.1	NCBI
	ATG6	NP_651209.1	NCBI
	ATG8	NP_727447.1	NCBI
	Vein	NP_523942.2	NCBI
A. aegypti	ATG1	XP_001657286.1	NCBI
	ATG6	XP_001654535.1	NCBI
	ATG8	XP_001652571.1	NCBI
	Vein	XP_001662637.1	NCBI
A. gambiae	ATG1	XP_309350.4	NCBI
	ATG6	XP_310418.5	NCBI
	ATG8	XP_312238.3	NCBI
	Vein	XP_001237118.2	NCBI
C. quinquefasciatus	ATG1	XP_001842942.1	NCBI
	ATG6	XP_001861442.1	NCBI
	ATG8	XP_001844428.1	NCBI
	Vein	XP_001846605.1	NCBI
G. morsitans	ATG1	GMOY006001	VectorBase
	ATG6	GMOY009498	VectorBase
	ATG8	GMOY001732	VectorBase
	Vein	GMOY004977	VectorBase
H. Sapiens	ATG8	See Abcam #86497	NA

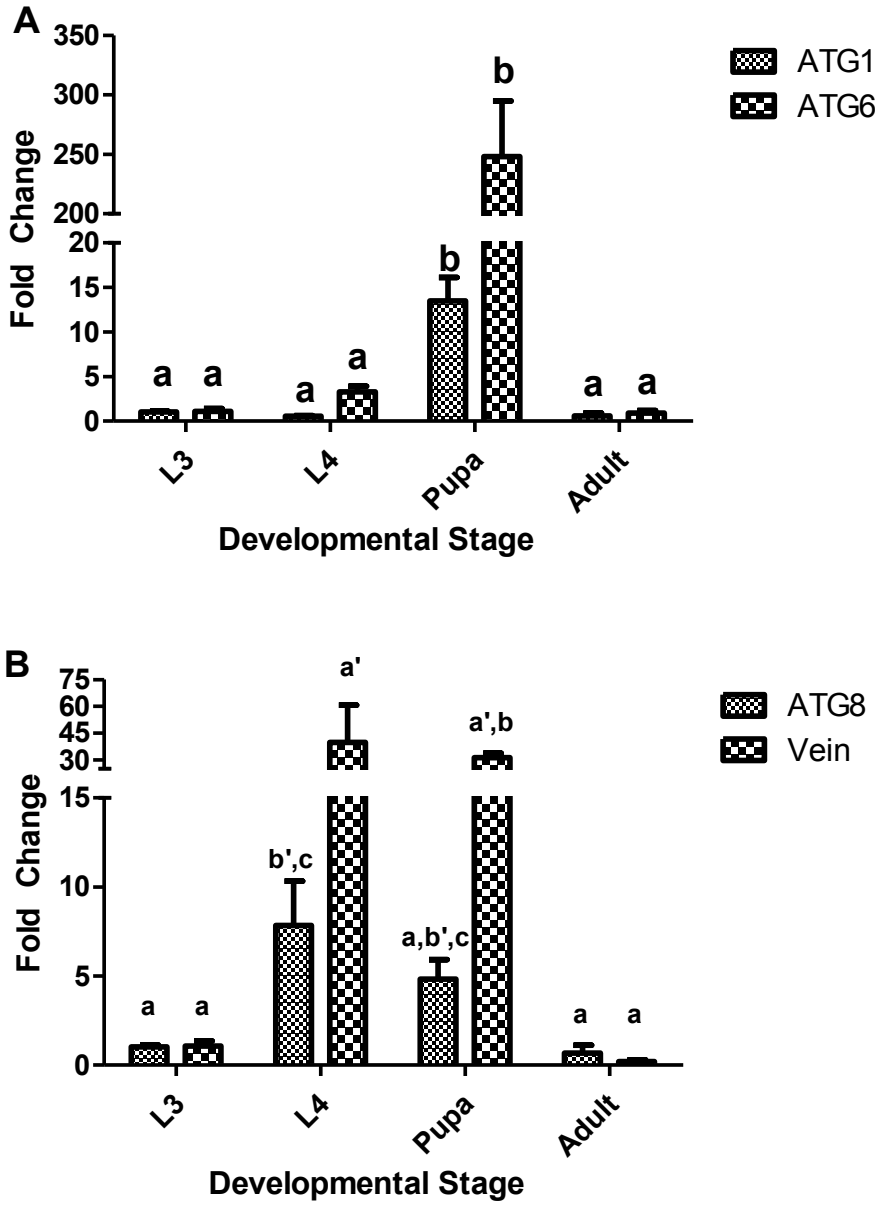

Figure 3.1. mRNA expression profiles for feeding larvae (L3), non-feeding larvae (L4), early pupae (Pupa), and adult (Adult) sand flies.

(A) The fold change and standard errors for the transcripts encoding ATG1 and ATG6 while. (B) The fold measurements and errors for ATG8 and Vein transcripts. One way ANOVA was performed with a Tukey posttest for multiple comparisons to measure statistical significance ($P<0.05$, a' = ns $P<0.06$) [a' & b', represent ANOVA with Tukey test data taken without the biological replicate explained in the results section].

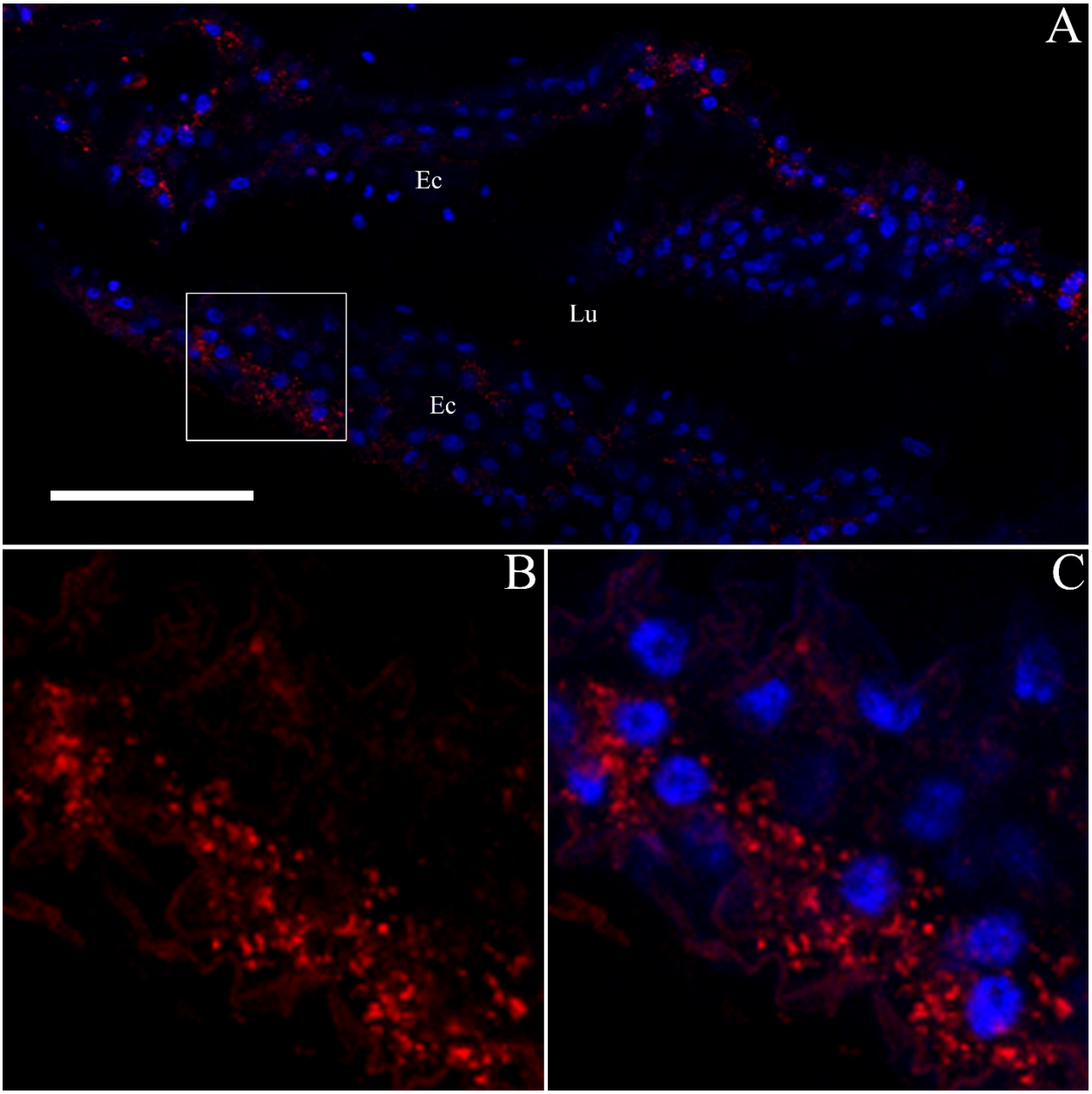

Figure 3.2. Confocal images for ATG6 showing the anterior midgut of newly formed pupae.

The empty lumen (Lu) space of the midgut, DAPI stained nuclei of epithelial cells (Ec), and red staining for ATG6 are shown in (A). The insets show red staining for ATG6 in the cytoplasmic compartments of epithelial cells (B), while a merge of the nuclei and cytoplasm can also be seen (C). Bar indicates 100 microns

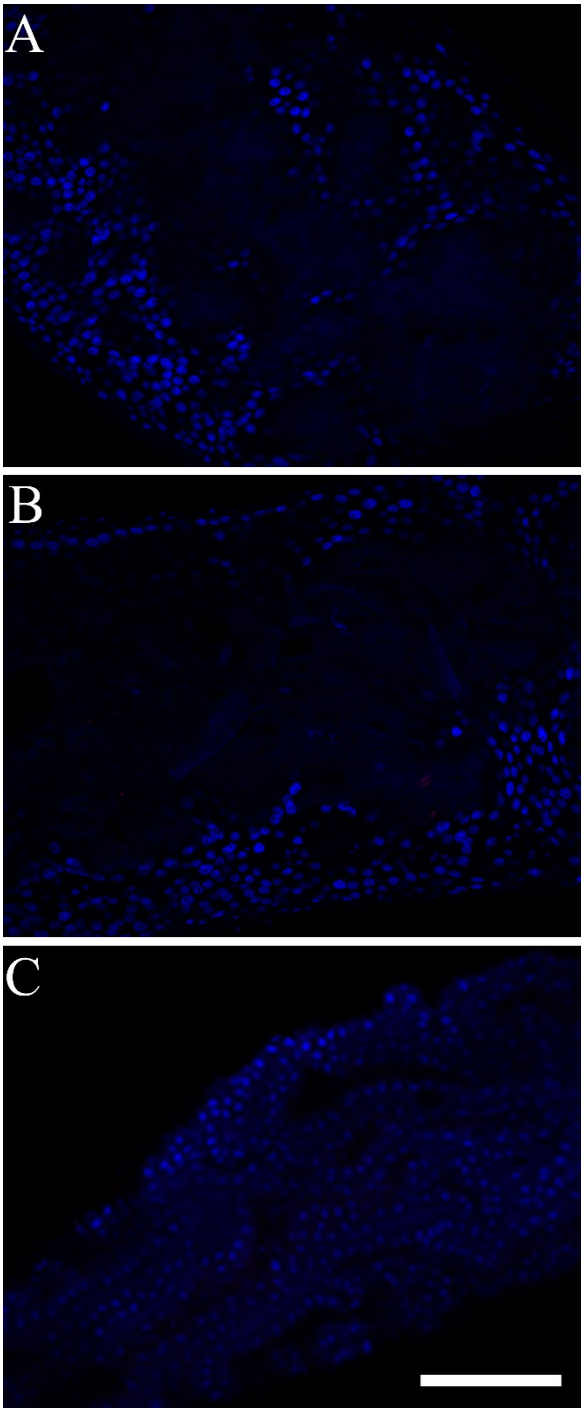

Figure 3.3. Confocal images depicting the anterior sand fly midgut at different developmental stages stained with ATG6 antibodies.

The nuclei of cells are visualized via DAPI staining while ATG6 is in red. The anterior portion of 3rd instar (L3) larvae (A), 4th instar (L4) larvae (B), and adult (C) midguts are shown. Bar indicates 100 microns.

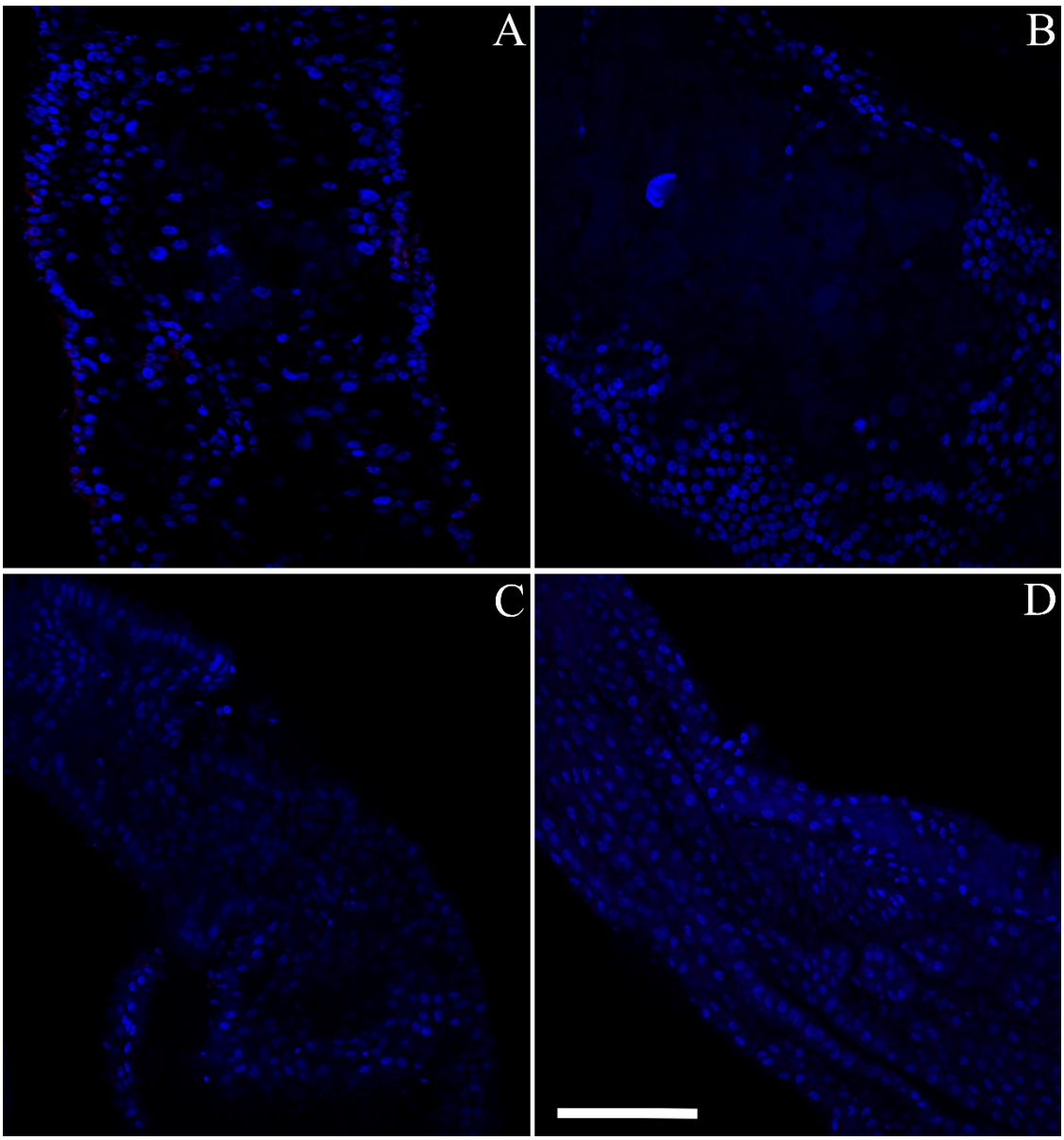

Figure 3.4. Confocal images depicting the anterior sand fly midgut at larval, pupal, and adult developmental stages stained with ATG8 antibodies.

The nuclei of cells are visualized using DAPI while *ATG8* is in red. L3 (A), L4 (B), Pupae (C), and adult (D) are shown. Bar indicates 100 microns.

ACTCGCTACGTAAACTGCATGACAATCAATGGGAATTCCACCATTATTGCATCCGGA
TCGAATGATCGTAGTGTAATTGTGTGGGATTTAAATGGGGAATTAAGTTTGAATTCT
CATGTGTCTGAAATGAGGAGCCTCTTGTTTCGCCTTGTGGCTGATAGT**GGTTCA**GAT
ATGCCACTTGAATTTATTTGTCCAATTACACATGAGCTTATGCGGAATCCAGTTATGC
TGGAAGATGGTTTTTCCTATGAAGAAGCAGCAATTGATGAGT**GGTTCA**AAATGGGC
AAGGGAACGTCTCCAATGACAAATCT**TGAACT**CACATCGATGGAAACAATCCCAAA
TACTTATCTTAAGAGTTGTATTGATAAATATCTTAAATCATTGGATTACGATGCAGTA
GACACTGGATTTTAAAAGGATTTATCTAAATCGACCTACAACATTATACAATTTCAC
TCTACTCCACGTGATTTTTATATTTCATAAACTTTGTGATTTTTACACAGAAATAAAA
TTATAAAATGCCCGCCAAAGTTTATTTTTTCATTGATTTCAATGAAATTTATTTTTTC
GTGTGGAAAATTGAAATTTTCACAACACAAAGAAACTTTCCAATAGTGTCTGGAAA
GGAATGTTTCTTCTGCGCTCATTTCCTCTTTCCATTGGAAATGTATGTTTCATTGGTG
CCATTTTGATTGCCCATCATTTCCTGCAAGCTCCATGAATCAATGGCGTTGAAAAAA
TAATTGCGTTTCAATGAAAGTTTAGTGAAAATTGAGGAAAAAAGTGCAATAAATGTT
ATGAATTGAGTGCTACTAGTT**GAGACTTTGTAGAGATAGTGCAGGAGAAGGAG**TA
GGTGTAAGTTAGATTAAGAAAAATGTGATAGATGTGGGAGAAAAGTTGAAAGTGTG
ATTAAGGAAAAAATCGATTGCTTTGTGCAAGAATTTCCGGACATCTTTCTTTTTTTC
TTCATCACAATGATGGAGATTGTGGGTGACT**ATG**

Figure 3.5. Possible promoter sequence of region upstream of *ATG1*

A 1000 nucleotide sequence before the start codon (green) contains a 3 putative ecdysone response elements (red) and a putative GAGA binding sequence (blue). GGTTCA and TGAACT are canonical EcRE sequences reported in earlier work.

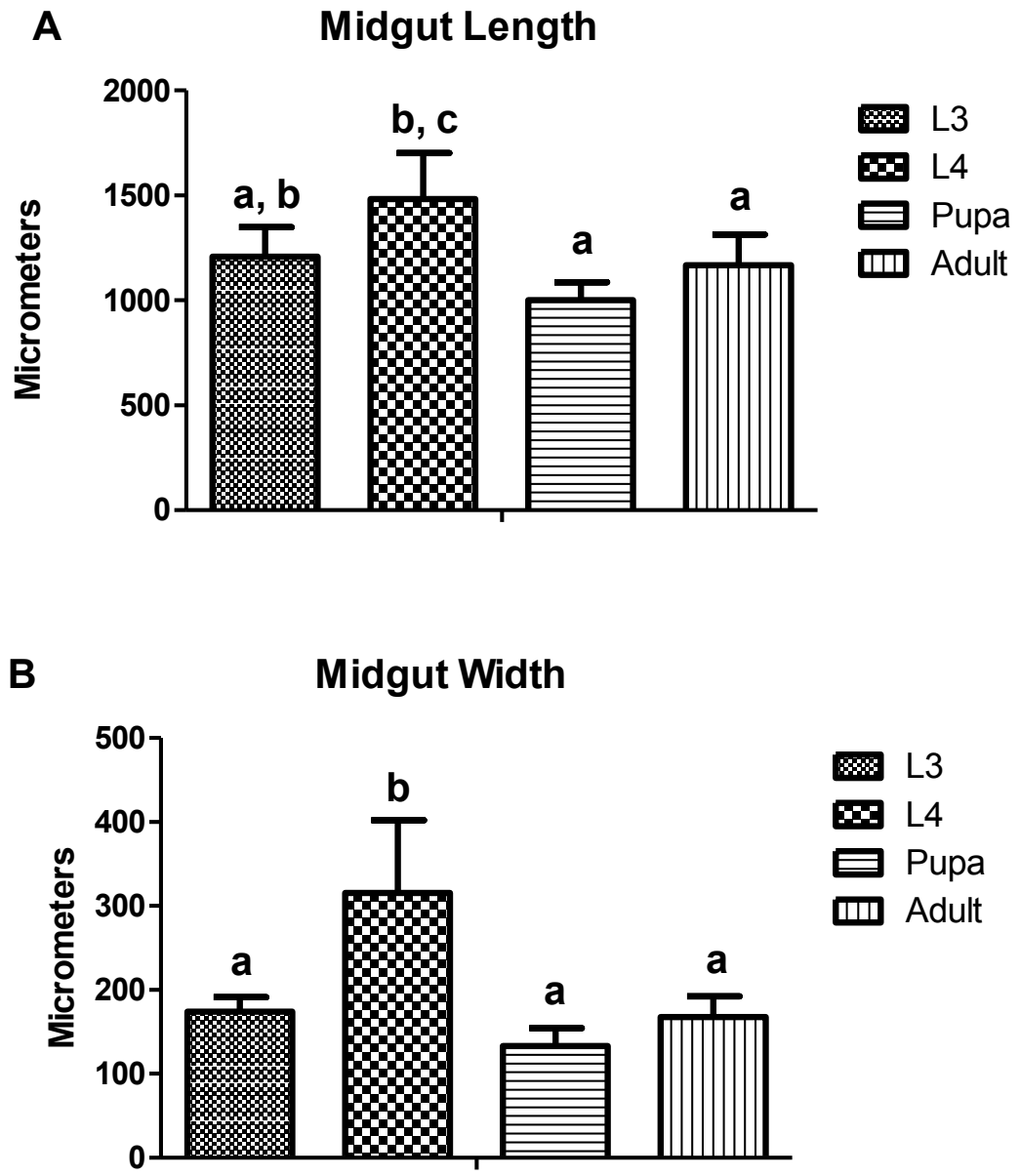

Figure 3.6. The midgut morphological changes in the 3rd instar (L3), 4th instar (L4), pupa, and adult developmental stages.

(A) The average length and standard deviation of insects in each stage. (B) The change in average width across stages. One way ANOVA was performed with a Tukey posttest for multiple comparisons to measure statistical significance ($P<0.05$).

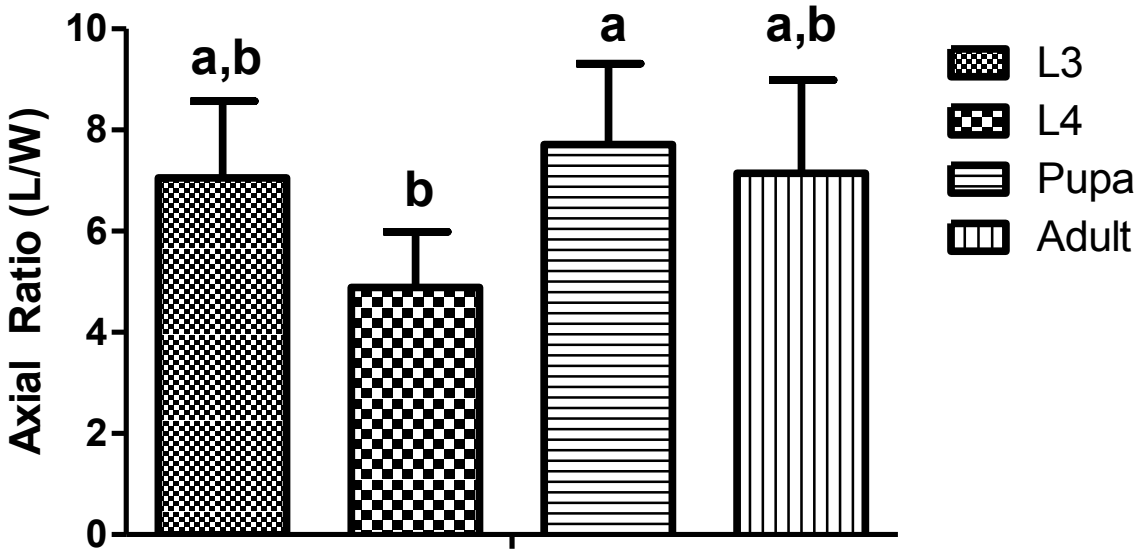

Figure 3.7. Axial ratio for the midgut (L/W) for L3, L4, pupa, and adult sand flies.

This calculation is based on the length of the midgut divided by the average width of the midgut across its length. One way ANOVA was performed with a Tukey posttest for multiple comparisons for significance ($P<0.05$).

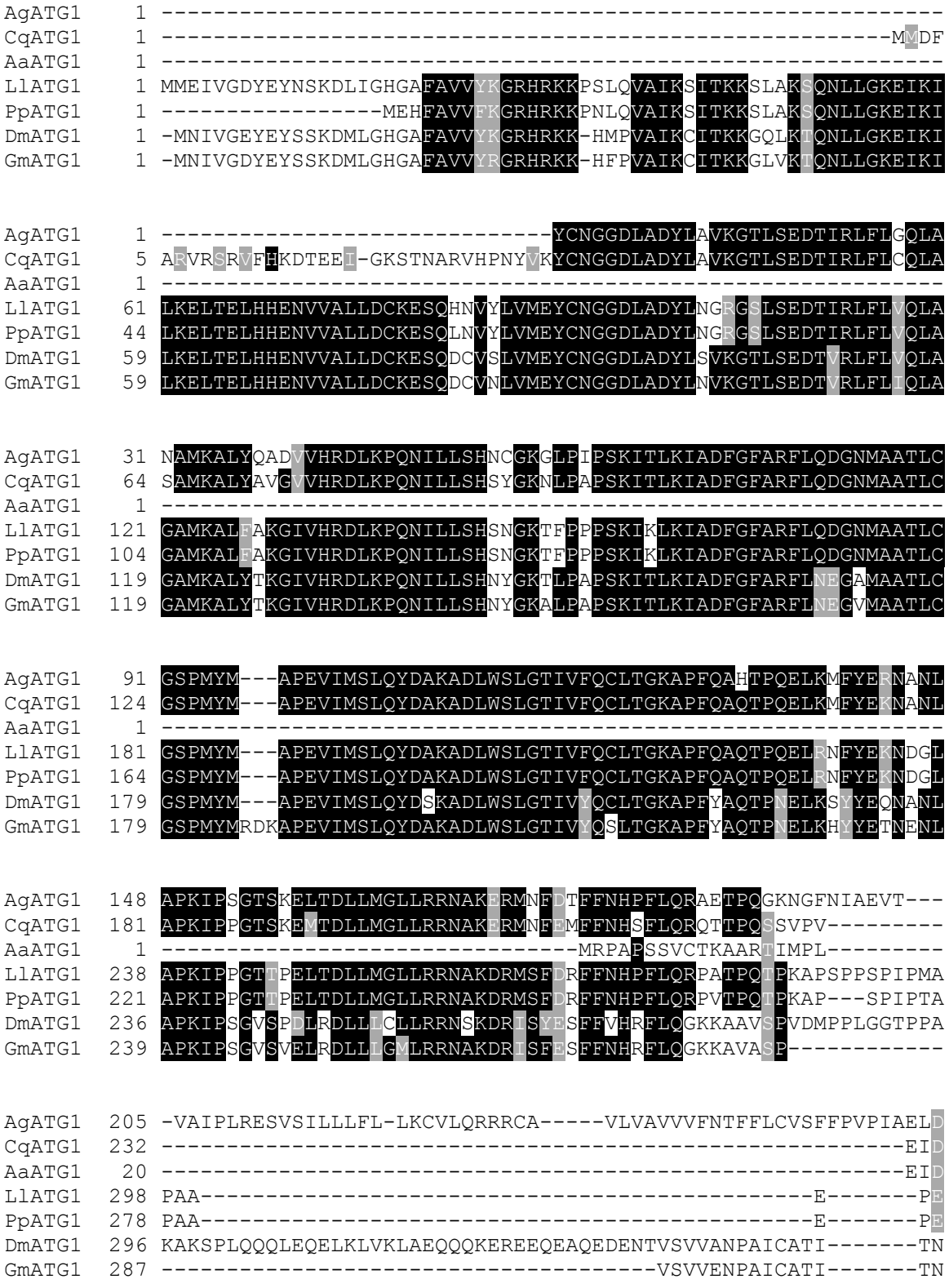
AgATG1 1
CqATG1 1
AaATG1 1
LlATG1 1 MMEIVGDYEYNSKDLIGHGAFAVVYKGRHRKKPSLQVAIKSITKKSLAKSQNLLGKEIKI
PpATG1 1
DmATG1 1 -MNIVGEYEYSSKDMLGHGAFAVVYKGRHRKK-HMPVAIKCITKKGQLKTQNLLGKEIKI
GmATG1 1 -MNIVGDYEYSSKDMLGHGAFAVVYRGRHRKK-HFPVAIKCITKKGLVKTQNLLGKEIKI
AgATG1 1
CqATG1 5
AaATG1 1
LlATG1 61 LKELTELHHENVVALLDCKESQHNVYLVMEYCNGGDLADYLNGRGSLSEDTIRLFLVQLA
PpATG1 44 LKELTELHHENVVALLDCKESQLNVYLVMEYCNGGDLADYLNGRGSLSEDTIRLFLVQLA
DmATG1 59 LKELTELHHENVVALLDCKESQDCVSLVMEYCNGGDLADYLSVKGTLSEDTVRLFLVQLA
GmATG1 59 LKELTELHHENVVALLDCKESQDCVNLVMEYCNGGDLADYLNVKGTLSEDTVRLFLIQLA
AgATG1 31
CqATG1 64
AaATG1 1
LlATG1 121 GAMKALFAKGIVHRDLKPQNILLSHSNGKTFPPPSKIKLKIADFGFARFLQDGNMAATLC
PpATG1 104 GAMKALFAKGIVHRDLKPQNILLSHSNGKTFPPPSKIKLKIADFGFARFLQDGNMAATLC
DmATG1 119 GAMKALYTKGIVHRDLKPQNILLSHNYGKTLPAPSKITLKIADFGFARFLNEGAMAATLC
GmATG1 119 GAMKALYTKGIVHRDLKPQNILLSHNYGKALPAPSKITLKIADFGFARFLNEGVMAATLC
AgATG1 91 GSPMYM---APEVIMSLQYDAKADLWSLGTIVFQCLTGKAPFQAHTPQELKMFYERNANL
CqATG1 124 GSPMYM---APEVIMSLQYDAKADLWSLGTIVFQCLTGKAPFQAQTPQELKMFYEKNANL
AaATG1 1
LlATG1 181 GSPMYM---APEVIMSLQYDAKADLWSLGTIVFQCLTGKAPFQAQTPQELRNFYEKNDGL
PpATG1 164 GSPMYM---APEVIMSLQYDAKADLWSLGTIVFQCLTGKAPFQAQTPQELRNFYEKNDGL
DmATG1 179 GSPMYM---APEVIMSLQYDSKADLWSLGTIVYQCLTGKAPFYAQTPNELKSYYEQNANL
GmATG1 179 GSPMYMRDKAPEVIMSLQYDAKADLWSLGTIVYQSLTGKAPFYAQTPNELKHYYETNENL
AgATG1 148 APKIPSGTSKELTDLLMGLLRRNAKERMNFDTFFNHPFLQRAETPQGKNGFNIAEVT---
CqATG1 181 APKIPPGTSKEMTDLLMGLLRRNAKERMNFEMFFNHSFLQRQTTPQSSVPV---------
AaATG1 1 ----------MRPAPSSVCTKAARTIMPL---------
LlATG1 238 APKIPPGTTPELTDLLMGLLRRNAKDRMSFDRFFNHPFLQRPATPQTPKAPSPPSPIPMA
PpATG1 221 APKIPPGTTPELTDLLMGLLRRNAKDRMSFDRFFNHPFLQRPVTPQTPKAP---SPIPTA
DmATG1 236 APKIPSGVSPDLRDLLLCLLRRNSKDRISYESFFVHRFLQGKKAAVSPVDMPPLGGTPPA
GmATG1 239 APKIPSGVSVELRDLLLGMLRRNAKDRISFESFFNHRFLQGKKAVASP------------
AgATG1 205 -VAIPLRESVSILLLFL-LKCVLQRRRCA-----VLVAVVVFNTFFLCVSFFPVPIAELD
CqATG1 232 ----------EID
AaATG1 20 ----------EID
LlATG1 298 PAA----------E-------PE
PpATG1 278 PAA----------E-------PE
DmATG1 296 KAKSPLQQQLEQELKLVKLAEQQQKEREEQEAQEDENTVSVVANPAICATI-------TN
GmATG1 287 ----------VSVVENPAICATI-------TN

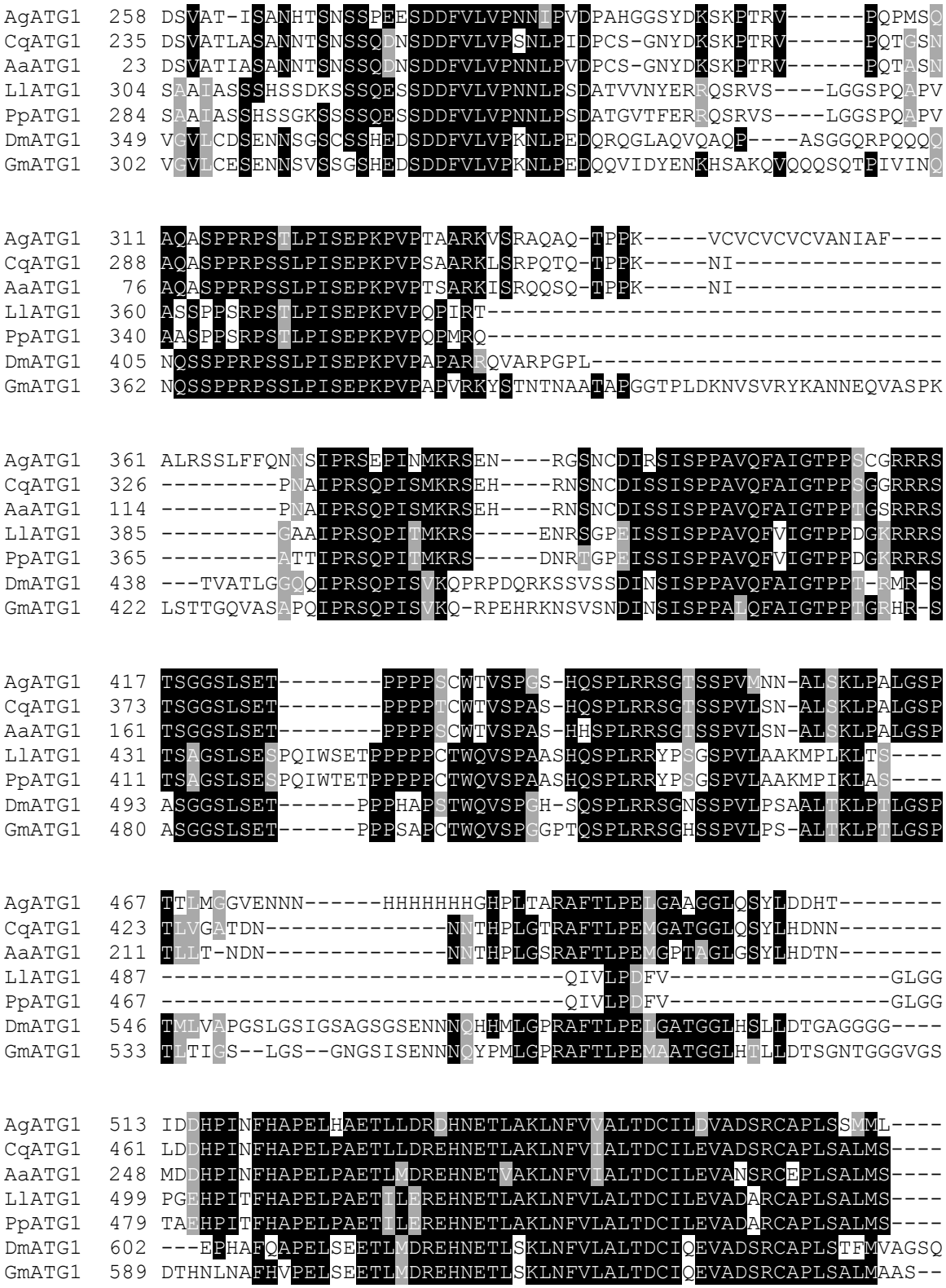
AgATG1 258 DSVAT-ISANHTSNSSPEESDDFVLVPNNIPVDPAHGGSYDKSKPTRV------PQPMSQ
CqATG1 235 DSVATLASANNTSNSSQDNSDDFVLVPSNLPIDPCS-GNYDKSKPTRV------PQTGSN
AaATG1 23 DSVATIASANNTSNSSQDNSDDFVLVPNNLPVDPCS-GNYDKSKPTRV------PQTASN
LlATG1 304 SAAIASSSHSSDKSSSQESSDDFVLVPNNLPSDATVVNYERRQSRVS----LGGSPQAPV
PpATG1 284 SAAIASSHSSGKSSSSQESSDDFVLVPNNLPSDATGVTFERRQSRVS----LGGSPQAPV
DmATG1 349 VGVLCDSENNSGSCSSHEDSDDFVLVPKNLPEDQRQGLAQVQAQP----ASGGQRPQQQQ
GmATG1 302 VGVLCESENNSVSSGSHEDSDDFVLVPKNLPEDQQVIDYENKHSAKQVQQQSQTPIVINQ
AgATG1 311 AQASPPRPSILPISEPKPVPTAARKVSRAQAQ-TPPK-----VCVCVCVCVANIAF----
CqATG1 288 AQASPPRPSSLPISEPKPVPSAARKLSRPQTQ-TPPK-----NI----------------
AaATG1 76 AQASPPRPSSLPISEPKPVPTSARKISRQQSQ-TPPK-----NI----------------
LlATG1 360 ASSPPSRPSTLPISEPKPVPQPIRT-----------------------------------
PpATG1 340 AASPPSRPSTLPISEPKPVPQPMRQ-----------------------------------
DmATG1 405 NQSSPPRPSSLPISEPKPVPAPARRQVARPGPL---------------------------
GmATG1 362 NQSSPPRPSSLPISEPKPVPAPVRKYSTNTNAATAPGGTPLDKNVSVRYKANNEQVASPK
AgATG1 361 ALRSSLFFQNNSIPRSEPINMKRSEN----RGSNCDIRSISPPAVQFAIGTPPSCGRRRS
CqATG1 326 ---------PNAIPRSQPISMKRSEH----RNSNCDISSISPPAVQFAIGTPPSGGRRRS
AaATG1 114 ---------PNAIPRSQPISMKRSEH----RNSNCDISSISPPAVQFAIGTPPTGSRRRS
LlATG1 385 ---------GAAIPRSQPITMKRS-----ENRSGPEISSISPPAVQFVIGTPPDGKRRRS
PpATG1 365 ---------ATTIPRSQPITMKRS-----DNRTGPEISSISPPAVQFVIGTPPDGKRRRS
DmATG1 438 ---TVATLGGQQIPRSQPISVKQPRPDQRKSSVSSDINSISPPAVQFAIGTPPT-RMR-S
GmATG1 422 LSTTGQVASAPQIPRSQPISVKQ-RPEHRKNSVSNDINSISPPALQFAIGTPPTGRHR-S
AgATG1 417 TSGGSLSET--------PPPPSCWTVSPGS-HQSPLRRSGTSSPVMNN-ALSKLPALGSP
CqATG1 373 TSGGSLSET--------PPPPTCWTVSPAS-HQSPLRRSGTSSPVLSN-ALSKLPALGSP
AaATG1 161 TSGGSLSET--------PPPPSCWTVSPAS-HHSPLRRSGTSSPVLSN-ALSKLPALGSP
LlATG1 431 TSAGSLSESPQIWSETPPPPPCTWQVSPAASHQSPLRRYPSGSPVLAAKMPLKLTS----
PpATG1 411 TSAGSLSESPQIWTETPPPPPCTWQVSPAASHQSPLRRYPSGSPVLAAKMPIKLAS----
DmATG1 493 ASGGSLSET------PPPHAPSTWQVSPGH-SQSPLRRSGNSSPVLPSAALTKLPTLGSP
GmATG1 480 ASGGSLSET------PPPSAPCTWQVSPGGPTQSPLRRSGHSSPVLPS-ALTKLPTLGSP
AgATG1 467 TTLMGGVENNN------HHHHHHHGHPLTARAFTLPELGAAGGLQSYLDDHT--------
CqATG1 423 TLVGATDN--------------NNTHPLGTRAFTLPEMGATGGLQSYLHDNN--------
AaATG1 211 TLLT-NDN--------------NNTHPLGSRAFTLPEMGPTAGLGSYLHDTN--------
LlATG1 487 --------------------------------QIVLPDFV-----------------GLGG
PpATG1 467 --------------------------------QIVLPDFV-----------------GLGG
DmATG1 546 TMLVAPGSLGSIGSAGSGSENNNQHHMLGPRAFTLPELGATGGLHSLLDTGAGGGG----
GmATG1 533 TLTIGS--LGS--GNGSISENNNQYPMLGPRAFTLPEMAATGGLHTLLDTSGNTGGGVGS
AgATG1 513 IDDHPINFHAPELHAETLLDRDHNETLAKLNFVVALTDCILDVADSRCAPLSSMML----
CqATG1 461 LDDHPINFHAPELPAETLLDREHNETLAKLNFVIALTDCILEVADSRCAPLSALMS----
AaATG1 248 MDDHPINFHAPELPAETLMDREHNETVAKLNFVIALTDCILEVANSRCEPLSALMS----
LlATG1 499 PGEHPITFHAPELPAETILEREHNETLAKLNFVLALTDCILEVADARCAPLSALMS----
PpATG1 479 TAEHPITFHAPELPAETILEREHNETLAKLNFVLALTDCILEVADARCAPLSALMS----
DmATG1 602 ---EPHAFQAPELSEETLMDREHNETLSKLNFVLALTDCIQEVADSRCAPLSTFMVAGSQ
GmATG1 589 DTHNLNAFHVPELSEETLMDREHNETLSKLNFVLALTDCIQEVADSRCAPLSALMAAS--

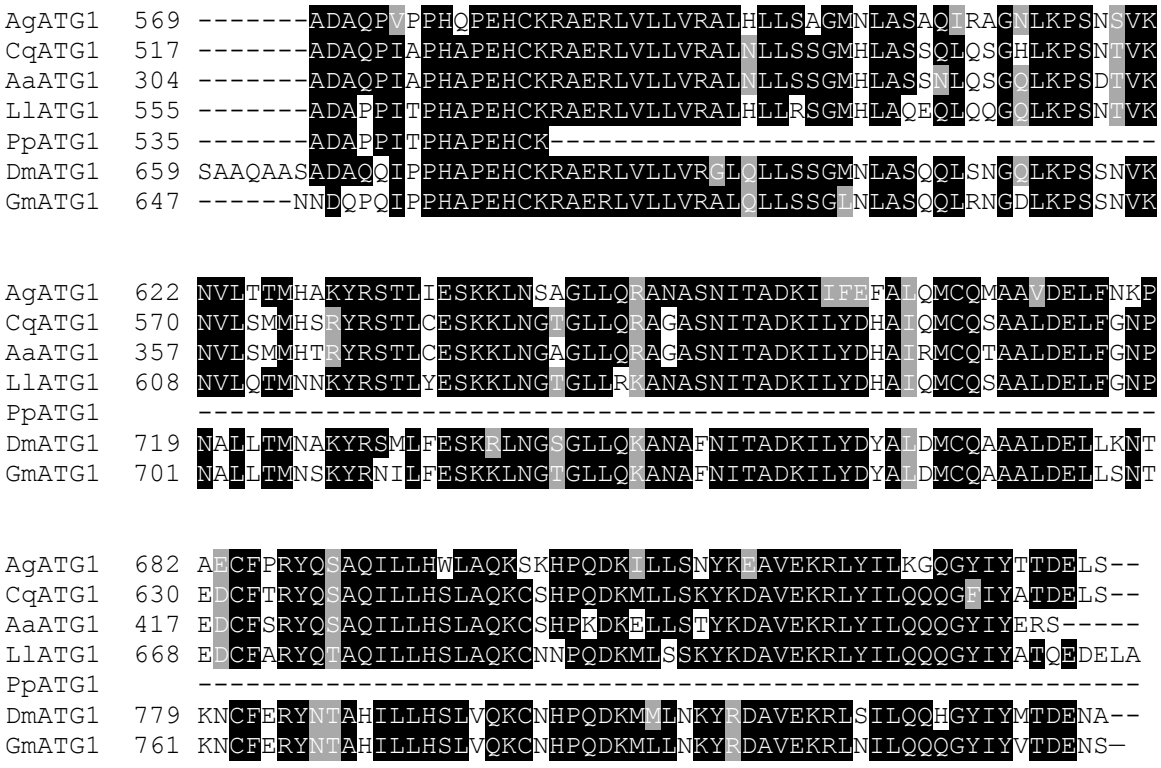

Figure 3.8. Clustal Omega protein alignment of ATG1 sequences from *L. longipalpis, P. papatasi, D. melanogaster, A. aegypti, A. gambiae, C. quinquefasciatus,* and *G. morsitans*.

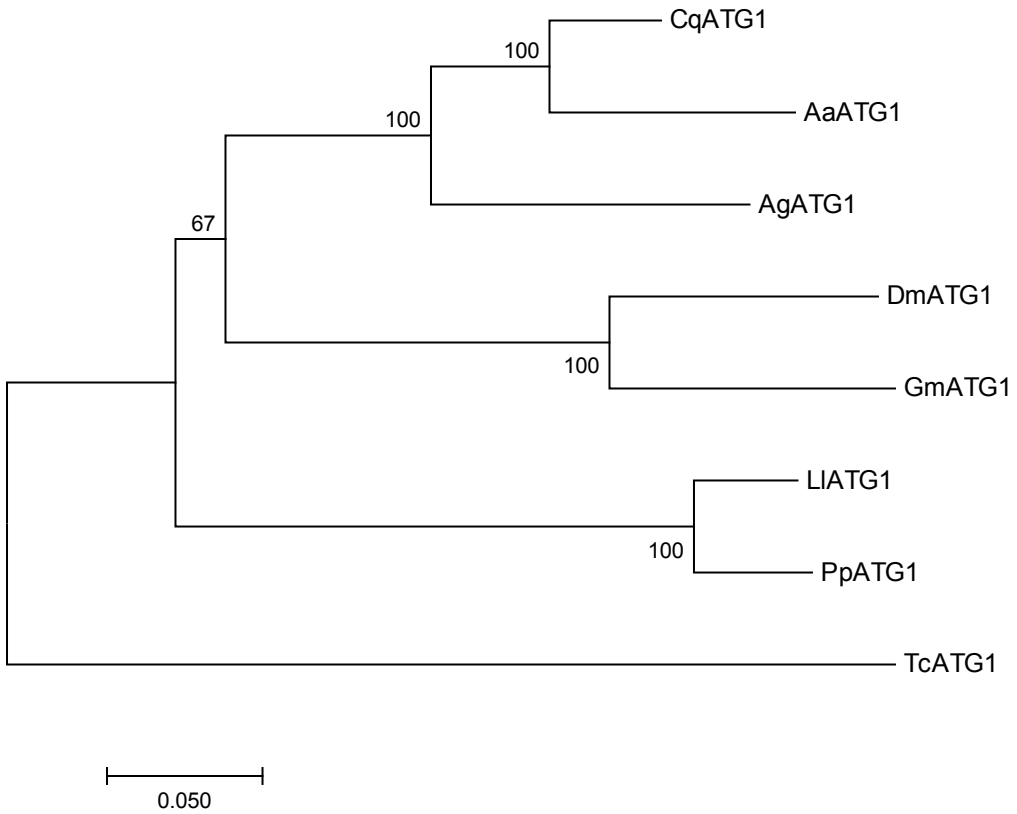

Figure 3.9. Neighbor-joining tree to infer the evolutionary relationship of ATG1 sequences using *T. castaneum* (TcATG1) as an outgroup.

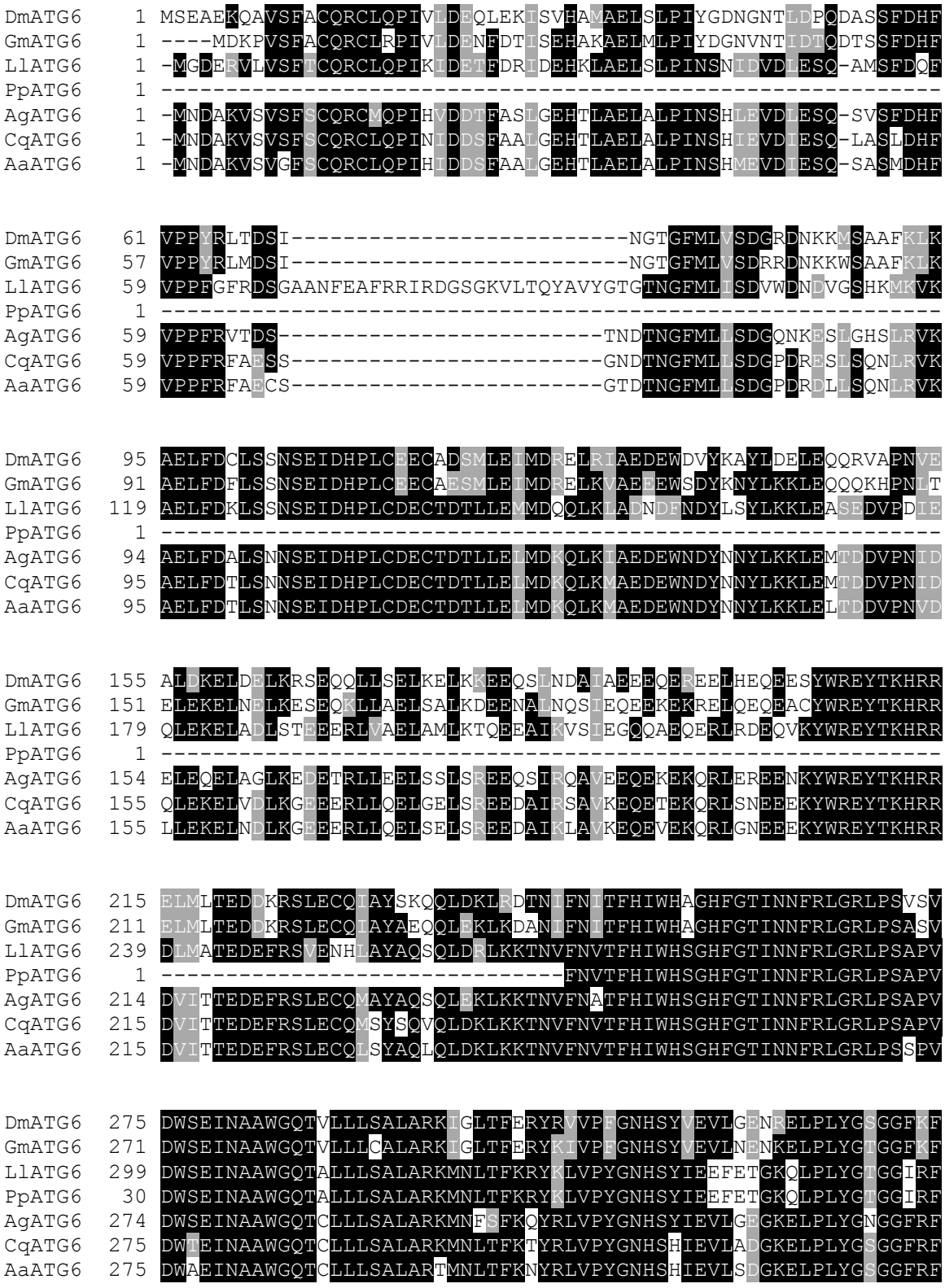
DmATG6 1 MSEAEKQAVSFACQRCLQPIVLDEQLEKISVHAMAELSLPIYGDNGNTLDPQDASSFDHF
GmATG6 1 ----MDKPVSFACQRCLRPIVLDENFDTISEHAKAELMLPIYDGNVNTIDTQDTSSFDHF
LlATG6 1 -MGDERVLVSFTCQRCLQPIKIDETFDRIDEHKLAELSLPINSNIDVDIESQ-AMSFDQF
PpATG6 1 ----------
AgATG6 1 -MNDAKVSVSFSCQRCMQPIHVDDTFASLGEHTLAELALPINSHLEVDIESQ-SVSFDHF
CqATG6 1 -MNDAKVSVSFSCQRCLQPINIDDSFAALGEHTLAELALPINSHIEVDIESQ-LASLDHF
AaATG6 1 -MNDAKVSVGFSCQRCLQPIHIDDSFAALGEHTLAELALPINSHMEVDIESQ-SASMDHF
DmATG6 61 VPPYRLTDSI----------NGTGFMLVSDGRDNKKMSAAFKLK
GmATG6 57 VPPYRLMDSI----------NGTGFMLVSDRRDNKKWSAAFKLK
LlATG6 59 VPPFGFRDSGAANFEAFRRIRDGSGKVLTQYAVYGTGTNGFMLISDVWDNDVGSHKMKVK
PpATG6 1 ----------
AgATG6 59 VPPFRVTDS----------TNDTNGFMLLSDGQNKESLGHSLRVK
CqATG6 59 VPPFRFAES----------GNDTNGFMLLSDGPDRESLSQNLRVK
AaATG6 59 VPPFRFAEC----------GTDTNGFMLLSDGPDRDLLSQNLRVK
DmATG6 95 AELFDCLSSNSEIDHPLCEECADSMLEIMDRELRIAEDEWDVYKAYLDELEQQRVAPNVE
GmATG6 91 AELFDFLSSNSEIDHPLCEECAESMLEIMDRELKVAEEEWSDYKNYLKKLEQQQKHPNLT
LlATG6 119 AELFDKLSSNSEIDHPLCDECTDTLLEMMDQQLKIADNDFNDYLSYLKKLEASEDVPDIE
PpATG6 1 ----------
AgATG6 94 AELFDALSNNSEIDHPLCDECTDTLLELMDKQLKIAEDEWNDYNNYLKKLEMTDDVPNID
CqATG6 95 AELFDTLSNNSEIDHPLCDECTDTLLELMDKQLKMAEDEWNDYNNYLKKLEMTDDVPNID
AaATG6 95 AELFDTLSNNSEIDHPLCDECTDTLLELMDKQLKMAEDEWNDYNNYLKKLELTDDVPNVD
DmATG6 155 ALDKELDELKRSEQQLLSELKELKKEEQSLNDAIAEEEQEREELHEQEESYWREYTKHRR
GmATG6 151 ELEKELNELKESEQKLLAELSALKDEENALNQSIEQEEKEKRELQEQEACYWREYTKHRR
LlATG6 179 QLEKELADLSTEEERLVAELAMLKTQEEAIKVSIEGQQAEQERLRDEQVKYWREYTKHRR
PpATG6 1 ----------
AgATG6 154 ELEQELAGLKEDETRLLEELSSLSREEQSIRQAVEEQEKEKQRLEREENKYWREYTKHRR
CqATG6 155 QLEKELVDLKGEEERLLQELGELSREEDAIRSAVKEQETEKQRLSNEEEKYWREYTKHRR
AaATG6 155 LLEKELNDLKGEEERLLQELSELSREEDAIKLAVKEQEVEKQRLGNEEEKYWREYTKHRR
DmATG6 215 ELMLTEDDKRSLECQLAYSKQQLDKLRDTNIFNITFHIWHAGHFGTINNFRLGRLPSVSV
GmATG6 211 ELMLTEDDKRSLECQLAYAEQQLEKLKDANIFNITFHIWHAGHFGTINNFRLGRLPSASV
LlATG6 239 DLMATEDEFRSVENHLAYAQSQLDRLKKTNVFNVTFHIWHSGHFGTINNFRLGRLPSAPV
PpATG6 1 ----------FNVTFHIWHSGHFGTINNFRLGRLPSAPV
AgATG6 214 DVITTEDEFRSLECQMAYAQSQLEKLKKTNVFNATFHIWHSGHFGTINNFRLGRLPSAPV
CqATG6 215 DVITTEDEFRSLECQMSYSQVQLDKLKKTNVFNVTFHIWHSGHFGTINNFRLGRLPSAPV
AaATG6 215 DVITTEDEFRSLECQLSYAQLQLDKLKKTNVFNVTFHIWHSGHFGTINNFRLGRLPSSPV
DmATG6 275 DWSEINAAWGQTVLLLSALARKIGLTFERYRVVPFGNHSYVEVLGENRELPLYGSGGFKF
GmATG6 271 DWSEINAAWGQTVLLLCALARKIGLTFERYKIVPFGNHSYVEVLNENKELPLYGTGGFKF
LlATG6 299 DWSEINAAWGQTALLLSALARKMNLTFKRYKLVPYGNHSYIEEFETGKQLPLYGTGGIRF
PpATG6 30 DWSEINAAWGQTALLLSALARKMNLTFKRYKLVPYGNHSYIEEFETGKQLPLYGTGGIRF
AgATG6 274 DWSEINAAWGQTCLLLSALARKMNFSFKQYRLVPYGNHSYIEVLGEGKELPLYGNGGFRF
CqATG6 275 DWTEINAAWGQTCLLLSALARKMNLTFKTYRLVPYGNHSHIEVLADGKELPLYGSGGFRF
AaATG6 275 DWAEINAAWGQTCLLLSALARTMNLTFKNYRLVPYGNHSHIEVLSDGKELPLYGSGGFRF

Figure 3.10. Clustal Omega protein alignment of ATG6 sequences from *L. longipalpis*, *P. papatasi*, *D. melanogaster*, *A. aegypti*, *A. gambiae*, *C. quinquefasciatus*, and *G. morsitans*.

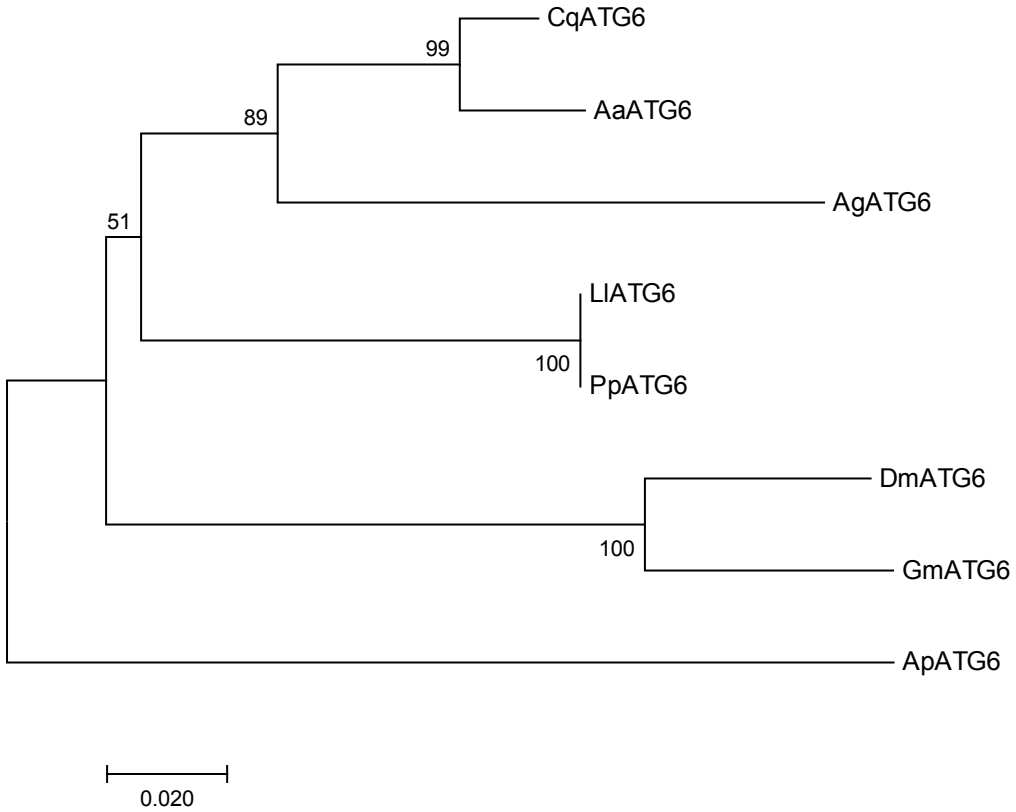

Figure 3.11. Neighbor-joining tree to infer the evolutionary relationship of ATG6 sequences using *A. pisum* (ApATG6) as an outgroup.

Figure 3.12. Clustal Omega protein alignment of ATG8 sequences from *L. longipalpis*, *P. papatasi*, *D. melanogaster*, *A. aegypti*, *A. gambiae*, *C. quinquefasciatus*, and *G. morsitans*.

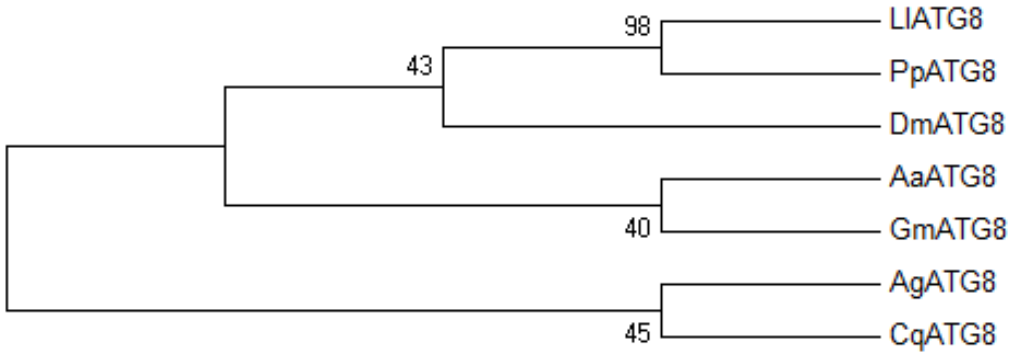

Figure 3.13. Neighbor-joining tree to infer the evolutionary relationship of ATG8 sequences.

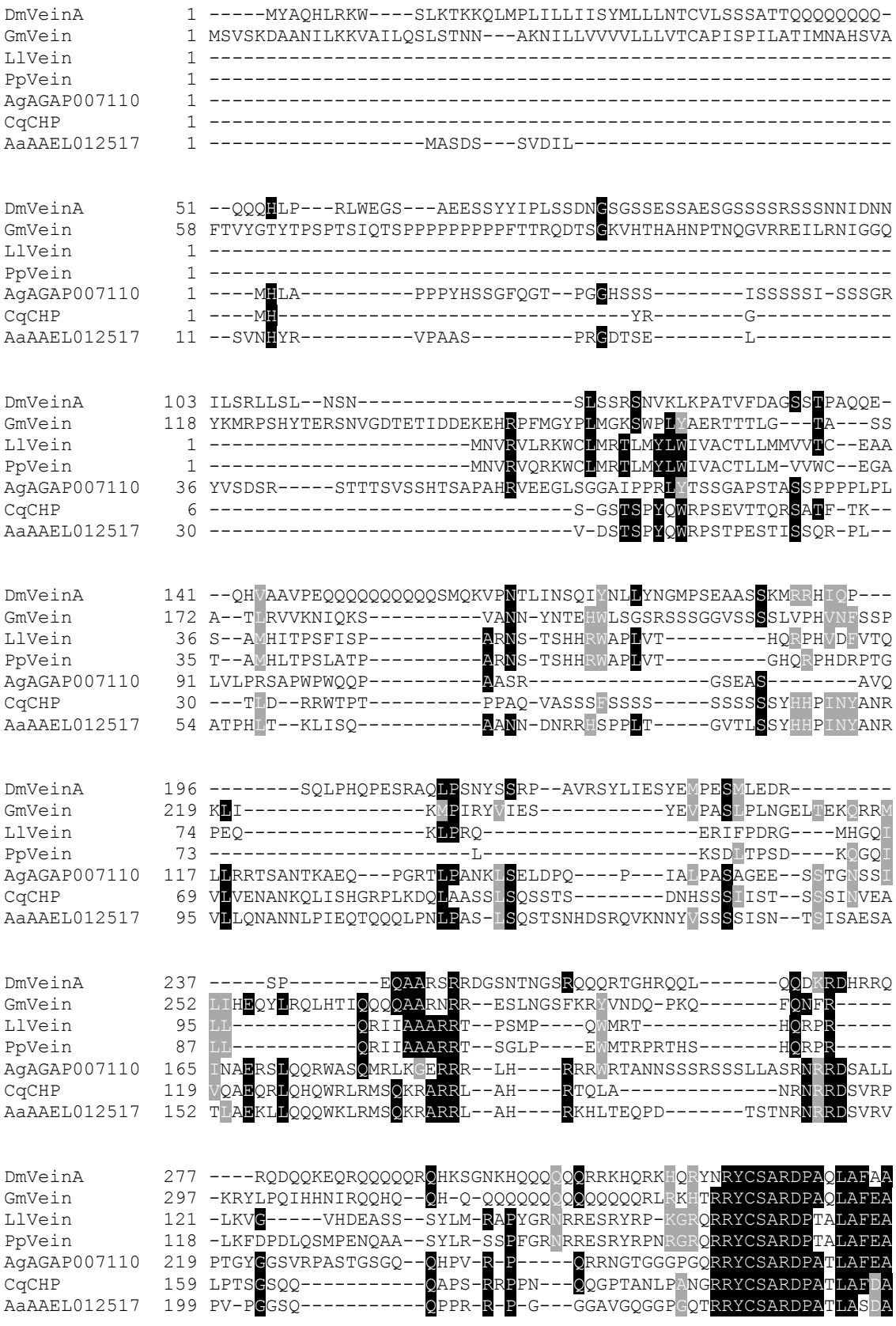

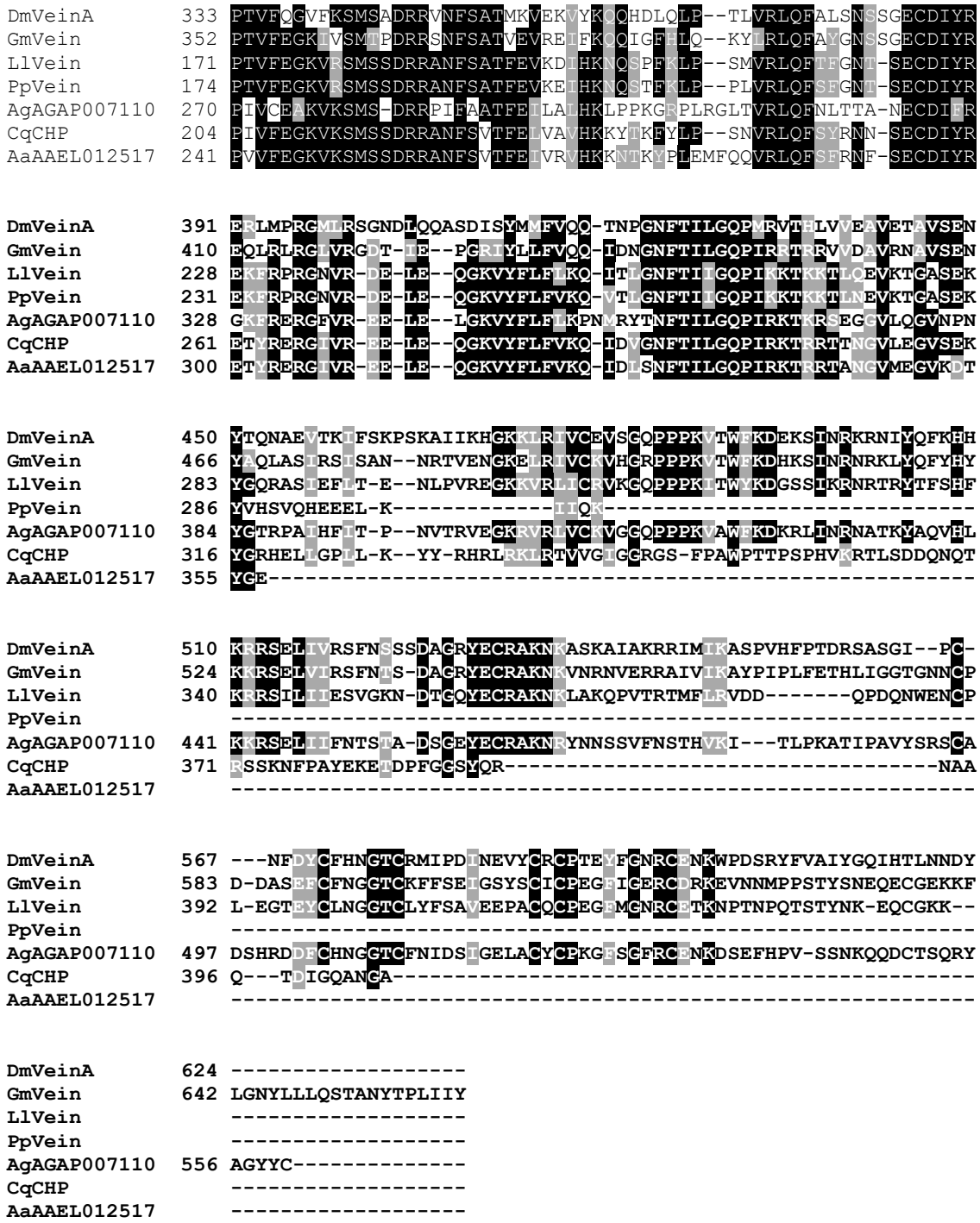

Figure 3.14. Clustal Omega protein alignment of Vein sequences from *L. longipalpis*, *P. papatasi*, *D. melanogaster*, *A. aegypti*, *A. gambiae*, *C. quinquefasciatus*, and *G. morsitans*.

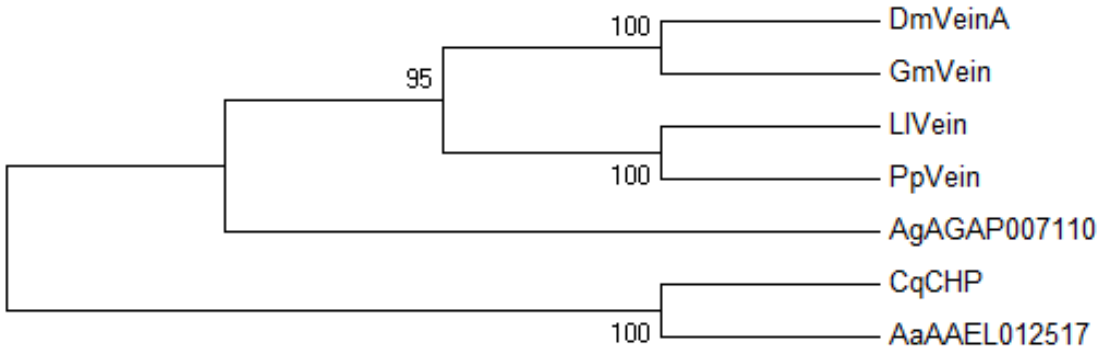

Figure 3.15. Neighbor-joining tree to infer the evolutionary relationship of Vein sequences.

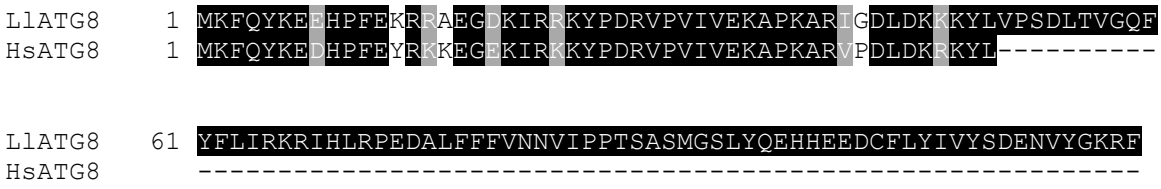

Figure 3.16. Clustal Omega protein alignment of ATG8 sequences from *L. longipalpis* and *H. sapiens* depicting *N*-terminal region from human antigen used to make antibodies (Abcam #86479) showing similarity to full length ATG8 from sand fly.

Chapter 4 - IMD Recognition, Toll Pathway, and the Effect of Pirk Knockdown in Infected *Lutzomyia longipalpis* Larvae

Abstract

Our previous efforts have elucidated a number of physiological mechanisms occurring within the sand fly with respect to immunity, homeostasis, and autophagy. We have sought to build on these observations in regards to the areas of IMD recognition of foreign particles and possible effects of the Toll pathway during infection with *P agglomerans* and *B. subtilis*. We also sought provide additional observations pertaining to the agar based feeding system compared to the normal laboratory chow that insect typically receive with respect to the expression of autophagic and immune molecules. Importantly, our lab was the first to demonstrate that RNAi can be applied to adult sand flies, and subsequently other studies have confirmed this phenomenon. Here I present evidence to suggest that RNAi mediated knockdown of 'poor immune response upon knockin' is achievable in the immature larval stage. We show that there is no change in Cactus levels suggesting that Toll pathway may not be playing any significant role in the midgut response to *P. agglomerans* or *B. subtilis*. Also, autophagy transcript levels do not significantly change, further encouraging the idea that agar based feeding methods may be comparable to normal dietary chow on the basis of nutritional value. Most importantly we show for the first time that it is possible to achieve almost 50% RNAi efficiency in the L3 larval stage of the sand fly. This has implications for controlling this vector of blood borne pathogens at the immature stages.

4.1. Introduction

IMD and Toll pathway are both crucial in the ability of insects to fight off microbial insults. Previous results in sand flies have suggested that the immature larval stages may suppress their IMD response via *Pirk* expression to allow *B. subtilis* and *P. agglomerans* to reside within the midgut of sand flies [79]. However, there is no work conducted in sand flies to measure any phenomenon related to Toll pathway or IMD recognition of foreign organisms and molecules. Additionally, the agar feeding regimens used to determine the effect of *Pirk* on effector molecule expression are quite different than the natural detritus material that sand flies are generally exposed to in the lab and nature. While there are data on the efficiency of RNAi mediated knockdown in adult sand flies [18, 24], no published data are currently aimed to elucidate the efficiency of RNAi mediated knockdown of sand fly transcripts in the immature larval stages. Here we investigate the negative regulator of Toll signaling, Cactus, as a marker for measuring Toll pathway activity. Although Cactus activity is generally described in hemocyte interactions with gram-positive bacterial and fungal organisms or dorso-ventral development [25, 26], we wished to see if it may have so effect in the midgut against gram-positive *B. subtilis*. PGRP-LB is a well-studied recognition molecule for the IMD pathway, known for its ability to protect *W. wigglesworthia* within the bacteriome of the tsetse fly midgut [27]. Here we measure the sand fly ortholog after infection to see any changes in expression level. With respect to chow versus agar fed insects we assess changes in the autophagic markers ATG1, 6, & 8; in addition to the immune regulators USP36 and IMD. Using Pirk as a target for injection mediated dsRNA delivery we measure its efficiency and effect on other immune transcripts of interest.

4.2. Material & Methods

4.2.1. Sand fly colony maintenance

L. longipalpis (Jacobina strain – LLJB) colonies were reared in the Department of Entomology, Kansas State University. Larvae were maintained in 250 or 500 ml plastic jars (Nalgene) with an approximately 2 cm-thick bed made of dental plaster (Schein), and fed on larval chow (a mixture of 50% rabbit droppings and 50% rabbit food).

4.2.2. Double stranded RNA synthesis and injection

Double stranded RNA targeting *Pirk* or *GFP* transcripts were synthesized using the primer sequences described to generate a 269 bp fragment for dsPirk and 300 bp fragment for dsGFP (Table 4.2., Figure A.2.). Templates for dsRNA synthesis were generated via GoTaq Green mastermix (Promega) PCR using 95º C for 2 min followed by 30 cycles of: 95º for 30s melting, 58º C annealing, and 72º C extension, with a final 10 min extension time at 72º C. One ug of template DNA was used to synthesize dsRNA overnight at 37º C. dsRNA molecules were column purified per the manufacturers instruction and eluted in 2 rounds of Hyclone (Thermo Scientific) water and concentrated to 3 µg/µL using the YM-100 filter columns (Millipore).

Third instar larvae were place in a cold dish, then injected between the head and 1st thoracic segment with 23 nL of dsRNA using a Nanojet II microinjector (Drummond). Larvae were then transferred to a humid Nalgene plaster container for approximately 12h to recover before being exposed to their respective diet treatments. Feeding post injection was taken hours after recovery from injection and being placed on diet.

4.2.3. RNA extraction and reverse transcription

Whole insects from *L. longipalpis* feeding on different treatments at 12, 24, and 36h post injection were selected under a stereoscope microscope in Hyclone (Thermo Scientific) phosphate buffered saline (PBS). Total RNA was isolated from pools of 5 midguts in the case of expression profile analysis, and 5 whole insects in the case of dsRNA injections using TRIzol (Invitrogen). For each group of midguts or insects, RNA isolation was conducted in triplicate. RNA quality was assessed by electrophoresis on 1% agarose-5% formaldehyde in 1x MOPS gel, and stored at -80 °C. First strand cDNA synthesis was conducted using Superscript™ III reverse transcription kit (Invitrogen) as described [24].

4.2.4. Real time quantitative PCR

mRNA levels for different developmental stages were quantified with iQ SYBER Green Supermix (Bio-Rad) using 95º C melting, 57º C annealing, and 72º C extension temperature for 40 cycles using a Realplex^4 Master cycler (Eppendorf). Relative fold changes were assessed using the ΔΔCt method [24, 52, 79], and calibrated against the expression of each transcript for the control fed and/or uninjected L3 larvae [52]. Sequences for obtained by taking sequences from *D. melanogaster* and using tBlastn and/or Blastp against *L. longipalpis* sequences found at VectorBase (https://www.vectorbase.org/blast). Primer sequences were generated using Primer3 software (http://biotools.umassmed.edu/bioapps/primer3_www.cgi). PCR amplicon sequence was verified using direct sequencing at Kansas State University. All Blastp data and primer sequences used in this study are summarized in Tables 3.1., 3.2., 4.1., and 4.2.

4.2.5. Predicted amplicon sequences, alignments, and phylogeny

Sequences were obtained for various orders of insects using Blastp at NCBI or VectorBase (summary of organisms, accesion numbers, and databases are provided in supplementary Tables 3.3. and 4.3.). Multiple sequence alignments at the protein level were conducted using Clustal Omega software (http://www.ebi.ac.uk/Tools/msa/clustalo/). Alignments were then visualized using BoxShade (http://www.ch.embnet.org/software/BOX_form.html). To determine phylogeny, neighbor joining trees were generated with 1000 bootstrap replicates using Mega7 (www.megasoftware.net).

4.3. Results

4.3.1. Expression of Toll pathways, IMD recognition and signal transduction molecules after infection

To build on our previous studies concerning the effect of Bs and Pa infection on midgut immune molecule expression we assessed the transcript levels of a negative regulator of Toll signaling (Cactus), a negative regulator of IMD pathway (Caudal), and a putative enzymatically active IMD recognition protein (PGRP-LB) 12 and 24h post infection. Although Bs is classified as gram-positive bacteria, it produces DAP-type peptidoglycans on its surface and may be better recognized by gram-negative IMD pathway instead of Toll. Additionally, we wanted to compare our previous agar based feeding method to traditional dietary chow lab larvae are accustomed to. At both 12 and 24h post infection it is observed that the level of Cactus remains unchanged no matter what feeding regimen is employed (Figure 4.1.), suggestive of at least no change in the regulation of the Toll pathway during infection experiments. Caudal levels do increase in Bs and

Pa more than 2 fold 12h post infection, but not significantly (Figure 4.1.A), and continue this increase for all feeding regimen at 24h (Figure 4.1.B). We also observe a non-significant increase in PGRP-LB levels for Agar fed insects for control and Bs at 12h, and for all 3 agar feeding regimens at 24h (Figure 4.1.).

4.3.2. Comparison of chow fed, agar fed, and infected individuals for autophagy and immunity transcripts

In continuing to assess differences between the laboratory chow diet and agar based feeding methods we measured transcript levels of ATG1, 6, and 8 to see if there were any changes between feeding conditions that maybe related to nutrition and stress. Additionally, we measured the levels of USP36 and IMD transcripts to see if there may be differences associated with immunity when larvae were fed chow, with its own associate microbial community, as opposed to agar based diets that contain controlled microbial communities. We matched the time points from the first study to see if any significance was observed [79] . With respect to the autophagy transcripts surveyed there were no significantly different changes observed across feeding treatments. However, there is a variable increase in the mean for agar fed regimens versus chow fed for ATG8 at all time points (Figure 4.2.A, C, E). Interestingly, we see a decrease in the expression level of immune transcripts USP36 and IMD that increase with time. At 12h post infection this difference is not significantly noticeable, but at 24h ($P<0.001$) and 36h ($P<0.01$) post infection the expression of both USP36 and IMD is diminished significantly for agar fed versus chow fed (Figure 4.2.B, D, F).

4.3.3. RNAi efficiency for Pirk transcript in L3 larvae stage

Our previous study demonstrated that Pirk may play a significant role in suppressing IMD effector molecule production after infection with microbes [79]. Here we injected dsRNA for *GFP*, *Pirk*, or the larvae remained uninjected. We allowed larvae to recover for 12h and then placed them on their respective chow or agar based feeding regimens and measured *Pirk* transcript level for individually injected insects at 12 and 24h post injection. Our initial measurements for efficiency of knockdown for insects fed on chow indicated a >50% non-significant reduction for the *Pirk* transcript when compared to uninjected or dsGFP injected individuals (Figure 4.3.A & B). However, this particular experiment only included n=5 individuals per time point per treatment. Combining this knockdown efficiency data with later knockdowns including all individuals placed on all feeding regimens, n=20 per time point per treatment, yielded a significant 40% knockdown efficiency of dsPirk individuals compared to uninjected and dsGFP injected individuals by 24h post injection, but not 12h post injection (Figure 4.3.C & D). This evidence suggests a partial knockdown of *Pirk* transcripts in feeding L3 larvae is achievable and can be further investigated.

4.3.4. Effect of dsPirk knockdown on transcript levels related to IMD pathway

Observing that RNAi mediated knockdown of *Pirk* transcript levels was at least partially effective, we moved on to see what effect *Pirk* transcript knockdown may have on other immune related molecules. Following the previously mentioned injection procedure, we expanded our studies to include treated insects fed on control agar, Bs agar, or Pa agar 12 and 24h post injection. Our previous study suggested that Pirk may be suppressing the anti-microbial peptide attacin, and modulating changes in IMPer and USP36 levels [79]. However, at no observed time

point or treatment was any significant difference seen between uninjected, dsGFP, and dsPirk injected individuals fed on control versus infected agar. There was a very high degree of variability associated with a number of samples that is discussed further, and IMPer levels for Pa fed 12h post injection were not determine. The data for *Pirk* expression respresented for each time point and feeding regimen is, however, more stable and is included in the previous injection reports (Figures 4.4.-4.9.).

4.3.5. Supplementary sequencing, amplicon, BLAST, and alignment results

In order to further explain the studies presented here and in chapters 2 & 3 additional information is provided now and discussed hereafter. While specific alignments and phylogenetic trees are provided in chapter 2 to support the sequences of Vein, ATG1, ATG6, and ATG8 further information is provided here for the putative sequence of the transcript, sequence of the amplicons used, and the position of the primers to generate said amplicons (Figures A.1., A.2., A.5., A.6., A.9.-11., A.14., A.17., A.20., A.23., & A.26.). For the sequences used here and in Chapter 2 similar data are also provided, and when appropriate discussed further. All BLAST data used to obtain these sequences unless otherwise stated is summarized (Table 4.3.), and additional PCR primers used are also provided (Tables 2.4., 3.2., and 4.2.). With regard to the position of the *Pirk* amplicon and dsRNA primer positions data showing a non-overlap of probe and dsRNA targeting region are provided (Figure A.2.). Also, accession numbers are provided (Table 4.3.) for the sequences found in the multiple sequence alignments (Figures A.4., A.8., A.13., A.16., A.19., A.22., A.25., & A.28.), and neighbor joining phylogenetic trees (A.3., A.7., A.12., A.15., A.18., A.21., A.24., A.27.,). Specific details about Blast data and sequence similarity are discussed below.

4.4. Discussion

We had previously sought to understand effector molecule production and IMD regulation in our previous work [79]. Here we further explore other possible transcripts that may play a role in Toll and IMD pathways.

During conditions where fungal and/or Gram-positive microbes are not detected by an insect Cactus generally remains stably bound to dorsal preventing its entry into the nucleus and downstream transcription of Toll immune effector molecules, and also plays a role in early dorso-ventral development [25, 26]. However, when recognition of these organisms and their associated molecules occurs phosphorylation and degradation of Cactus occurs and the transcription factors may enter the nucleus [92]. *B. subtilis* is an interesting microbe to study in this scenario. While it is characterized as a gram-positive bacteria, it presents DAP type peptidoglycans on its surface, making it more putatively recognizable by PGRPs associated with IMD pathway. However, we did not detect any noticeable decrease in Cactus transcript level at any time point or treatment suggesting that there is no change in expression for this negative regulator of immunity and midgut immunity in this case may be dictated by the regulation of IMD pathway.

Caudal is typically associated with developing *D. melanogaster* at the embryonic stage [93]. In the case of immunity, caudal is known for its prohibitory action in allowing Relish to enter the nucleus and initiate transcription of immune effector molecules [94]. While we had previously shown that *Pirk* was capable of providing negative feedback to the IMD pathway we wanted to observe what effect caudal might have in the midguts of sand flies infected with *B. subtilis* or *P. agglomerans*. Although the increase was not statistically significant, it was apparent that infected midguts had a greater mean expression of this molecule. While this is not

conclusive, it does not rule out the role of caudal in inhibiting IMD pathway responses in the midgut when infection with commensal bacteria occurs.

IMD pathway recognition is a very complex process that includes numerous peptidoglycan recognition proteins that may be secreted or retain; enzymatically active or inactive. For the sake of our experiment we chose PGRP-LB, a protein that has been demonstrated in protecting the obligate symbiont of tsetse flies, *W. glossinidae*. Interestingly, we see an increase for PGRP-LB in all agar feeding treatments used by 24h. While this increase is not statistically significant it does point a possible role of this molecule for both *B. subtilis* and *P. agglomerans* recognition. It is again important to note that recognition of DAP type peptidoglycans associated with gram-negative bacteria is extremely complex and includes a number of: short, long, enzymatically active, and enzymatically inactive PGRPs as discussed in chapter 1 and the introduction herein. It would require much more extensive analysis of expression patterns (RNA-SEQ or microarray) of infected individuals to more readily acquire the data necessary for delineating these associated complexities.

Our previous studies also involved measuring USP36 and IMD transcript levels during the hours post infection, and the levels of ATG1, 6, and 8 during metamorphosis. We sought to investigate how our agar based feeding system may compare to the normal day to day chow diet the insects were acclimated to. While autophagy plays a role in the rearrangement of cells and tissues, it is predominately linked to its role in TOR signaling and nutrient level sensing. Since the agar based feeding method is starkly different than the detritus materials that sand fly larvae are accustomed to, we measured the levels of autophagic transcripts to gain insights into how this pathway may be behaving. Surprisingly, we did not see any significant change between chow and agar fed insects, although there was a mean increase in autophagy markers suggesting that

the agar diet may be less than a sufficient source of nutrients. One important take away from these two feeding methods is the change in expression of immune molecules. USP36 and IMD were both significantly down regulated in the hours post agar feeding. This points to a possible global down regulation immune molecules in the midgut of insects fed a more simplified and directed microbial community.

Understanding the RNAi effect at all life stages of insect development is important in developing putative and practical strategies for controlling insect populations and competence for pathogens. Previously demonstrated by our group was a highly efficient knockdown the transcript encoding chitinase 1 in *P. papatasi* [24]. Also, effective knockdown of the transcript encoding Caspar, a negative regulator of immunity, was achieved by another group in *L. longipalpis* [18]. However, these studies focused on the adult stage of the sand fly and its competence for *Leishmania* parasites. Here we investigated the possibility of suppressing a midgut immune suppressor *Pirk* in an attempt to understand the fundamental basics of sand fly larvae gut immunity. The larval stage was difficult to inject do to the inherent thickness of its integument, and a suitable spot for injection of L3 larvae was only found in the inter-segmental region between the head capsule and the first thoracic segment. We were able to achieve significant suppression of *Pirk* transcripts approaching 50% by 24h post injection when considering all injected insects. This is a promising result for the possible control of larval sand fly populations via RNAi, especially considering its possible use as a 'platform' of paratransgenesis [78].

Using this injection method we attempted to see what effects knockdown might have on other immune related transcripts during infection situations. However, this experiment proved to

extremely laborious and expensive, and it its current form produced highly variable results that did not provide much valuable expression data.

The discovery, at times, and analysis of putative transcripts within the *L. longipalpis* genome was a very time intensive process. Although there are numerous EST libraries available for *L. longipalpis*, only a few of the genes predicted and RT-qPCR amplicons synthesized for were supported by EST data. I will discuss the implication of the few that were indeed supported. ATG1 and 6 are both transcripts involved in autophagy, and are often associated with nutritional sensing. ATG6 ESTs (AM092571.1, AM092621.1) were found in total EST libraries. Interestingly, an ATG1 EST (EX991142.1) was found during adult female blood digestion, which coincides with the requirement of ATG1 in *A. aegyti* for digestion and egg production [42, 95]. Also, a USP36 EST (AM108362.1) was found in the total EST library, and more interestingly, ESTs for Attacin (EX211749.1) and IMPer (EX211579.2, EX212073.1) were found in adult females infected with *Leishmania* parasites. These evidences further the possibility of these transcripts studied in larvae being of importance in the adult form of the sand fly *L. longipalpis*.

Table 4.1. The accession numbers, identity, score, and expected value for each query protein (*D. melanogaster*) against each subject protein (*L. longipalpis*).

Gene Symbol	Accesion # D. melangogaster	Accession # L. longipalpis	Identity	Score	E-value
Attacin	AAL23662.1	LLOJ005408	40.50%	220	1.00E-14
Domeless	NP_523412.1	LLOJ002449	27.75	987	3.00E-81
Duox	NP_608715.2	LLOJ010494	94.30%	4361	0
IMD	NP_573394.1	LLOJ010482	40.40%	422	2.00E-34
Pirk	NP_611598.1	LLOJ004926	40%	329	3.00E-26
USP36	NP_001246639.1	LLOJ008157	53%	1968	0
NOS	AAF25682.1	LLOJ005465	59.70%	2081	0
IMPer	NP_996223.1	LLOJO10504	36.30%	1153	1.00E-103

Table 4.2. The sequence of RT-qPCR primers used for each transcript measured in this study.

Gene Symbol	Primer 5' - 3' Forward	Primer 5'-3' Reverse
Nos	CAACTACGAGCCAAATGTTC	AGCCAGCATAGAGGATAAGC
dsPirk	TAATACGACTCACTATAGGGTTAAGGTGGCTCAGAATGC	TAATACGACTCACTATAGGGGATATTGGCGGAATTGGT
dsGFP	TAATACGACTCACTATAGGGATGGTGAGCAAGGGCGAGGA	TAATACGACTCACTATAGGGTAGTGGTTGTCGGGCAGCAG
Caudal	ATCGCAGAGTCATTCAAGTG	GTGATGGTGGAGGGTATGT
Cactus	NA	NA
PGRP-LB	NA	NA

Table 4.3. The species name, gene symbol, accession number, and database for all sequences used for multiple sequence alignment and phylogenetic analysis.

	Gene	Accession Number
L. longipalpis	**Pirk**	**LLOJ004926**
P. papatasi	**Pirk**	**AJVK01084806.1**
T. castaneum	**Pirk**	**XP_008193927.1**
A. albopictus	**Pirk**	**KXJ77933.1**
L. migratoria	**Pirk**	**AJF38200.1**
D. busckii	**Pirk**	**ALC41356.1**
D. melanogaster	**Pirk**	**NP_611598.1**
L. longipalpis	**Attacin**	**LLOJ005408**
P. papatasi	**Attacin**	**PPAI003791**
D. melanogaster	**Attacin**	**AAL23662.1**
A. aegyti	**Attacin**	**XP_001656768.1**
T. castaneum	**Attacin**	**XP_001809216.1**
M. domestica	**Attacin**	**XP_011296538.1**
L. longipalpis	**Duox**	**LLOJ010494**
P. papatasi	**Duox**	**PPAI003114**
C. quinquefasciatus	**Duox**	**XP_001844503.1**
D. melanogaster	**Duox**	**NP_608715.2**
A. gambiae	**Duox**	**XP_319115.4**
A. aegyti	**Duox**	**XP_001658452.2**
L. longipalpis	**USP36**	**LLOJ008157**
P. papatasi	**USP36**	**PPAI006417**
A. aegyti	**USP36**	**XP_001662174.1**
A. gambiae	**USP36**	**XP_001237068.2**
D. melanogaster	**USP36**	**NP_001246639.1**
C. quinquefasciatus	**USP36**	**XP_001848432.1**
L. longipalpis	**IMD**	**LLOJ010482**
P. papatasi	**IMD**	**PPAI001062**
T. castaneum	**IMD**	**XP_008199405.1**
D. melanogaster	**IMD**	**NP_573394.1**
A. gambiae	**IMD**	**XP_001688608.1**
A. aegyti	**IMD**	**XP_001660624.1**
C. quinquefasciatus	**IMD**	**XP_001861391.1**

G. morsitans	**IMD**	**GMOY013006**
L. longipalpis	**Nos**	**LLOJ005465**
P. papatasi	**Nos**	**PPAI005982**
A. gambiae	**Nos**	**XP_555207.2**
A. gambiae	**Nos**	**XP_317213.1**
D. melanogaster	**Nos**	**AAF25682.1**
A. aegyti	**Nos**	**XP_001660328.1**
L. longipalpis	**Domeless**	**LLOJ002449**
P. papatasi	**Domeless**	**PPAI001065**
D. melanogaster	**Domeless**	**NP_523412.1**
A. gambiae	**Domeless**	**XP_319240.5**
A. aegyti	**Domeless**	**XP_001662596.1**
A. pisum	**Domeless**	**XP_003245751.1**
C. quinquefasciatus	**Domeless**	**XP_001867486.1**
L. longipalpis	**IMPer**	**LLOJO10504**
P. papatasi	**HPX1**	**PPAI009674**
A. gambiae	**HPX4**	**AGAP007237**
A. aegyti	**HPX4**	**AAEL018292**
A. gambiae	**HPX15IMPER**	**XP_003436891.1**
C. quinquefasciatus	**peroxidase**	**PPAI009674**
D. melanogaster	**peroxidase**	**NP_996223.1**

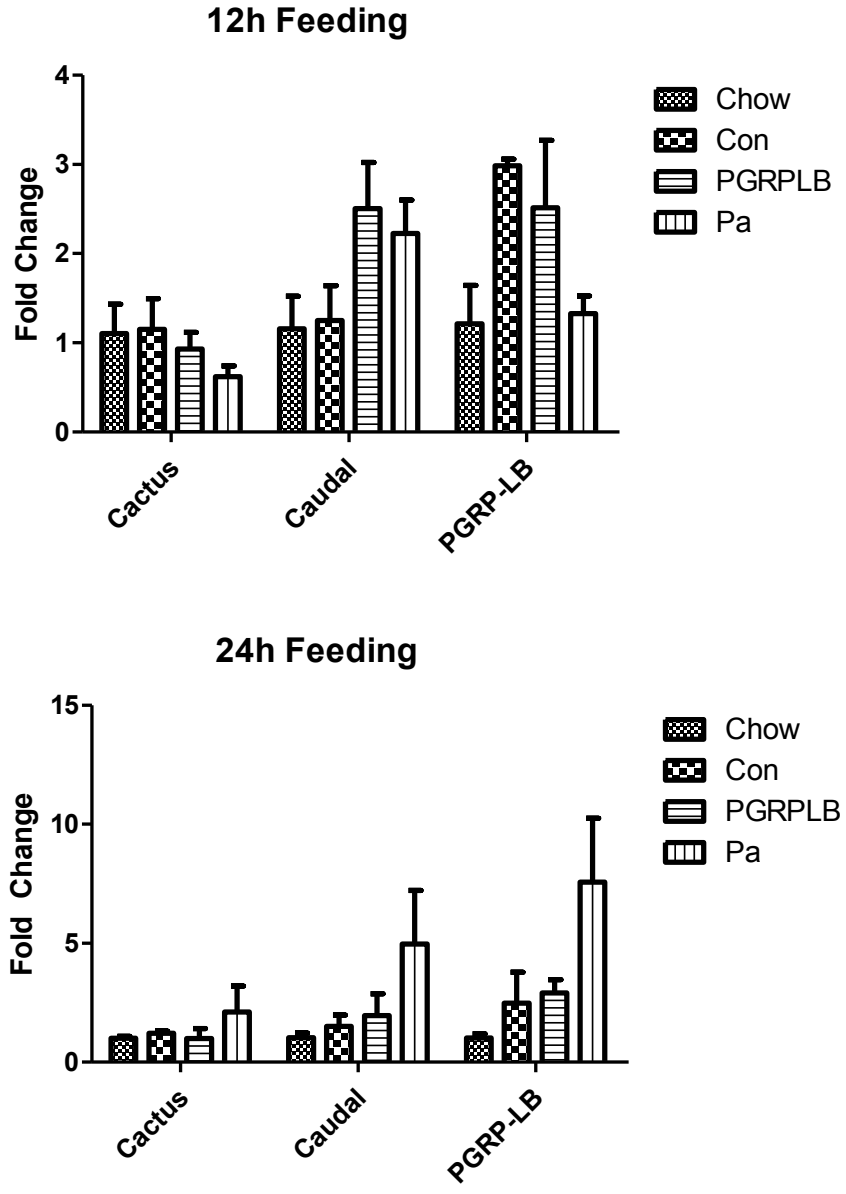

Figure 4.1. mRNA expression levels for L3 larvae fed normal diet (chow), control agar (Con), *B. subtilis* agar (Bs), and *P. agglomerans* agar (Pa).

(A) The fold change with standard errors for the transcripts negative regulator of Toll pathway (Cactus), Caudal, and PGRP-LB after 12h of feeding on their respective substrates. (B) The same measurements after 24h feeding. One way ANOVA was performed with a Tukey posttest for multiple comparisons to measure statistical significance.

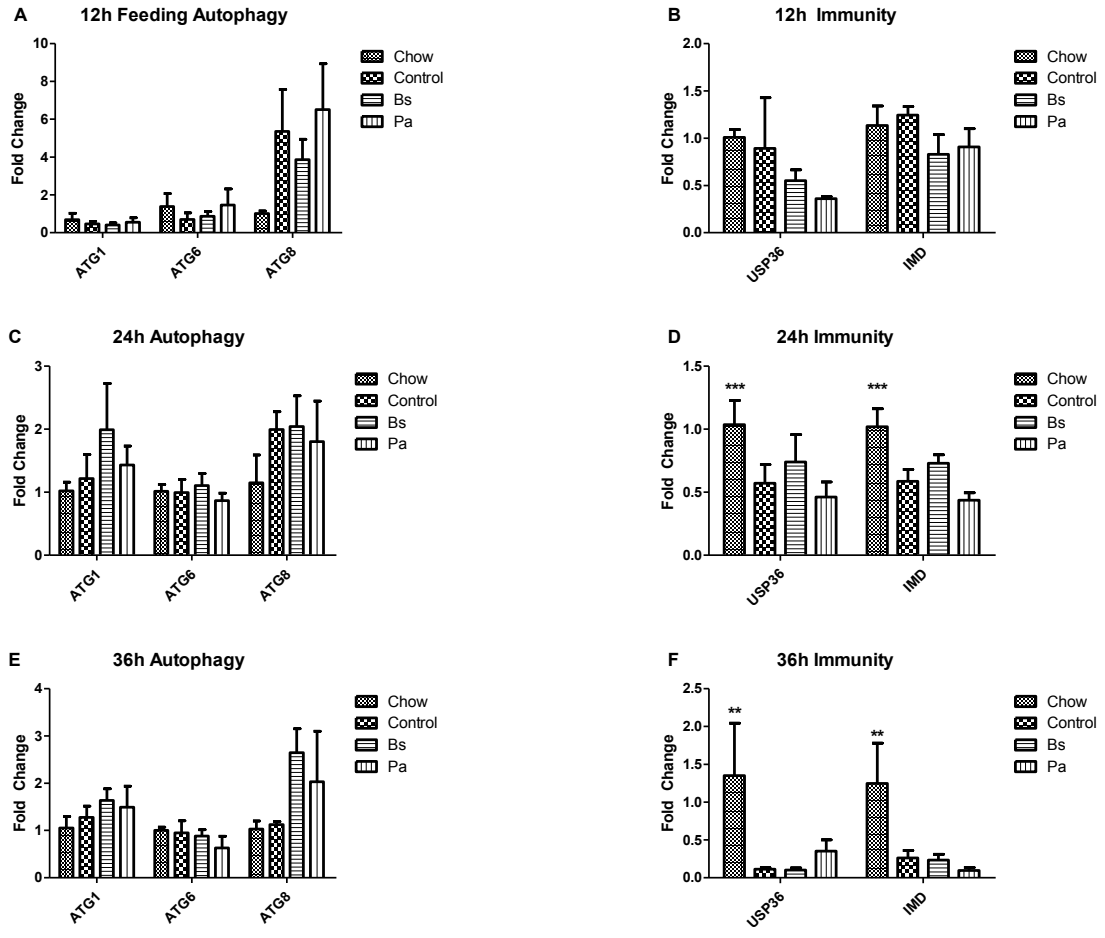

Figure 4.2. mRNA expression levels for L3 larvae fed normal diet (chow), control agar (Con), *B. subtilis* agar (Bs), and *P. agglomerans* agar (Pa).

(A, C, & E) The fold change with standard errors for the autophagy transcripts: 1, 6, & 8 after: 12, 24, & 36h of feeding on their respective substrates. (B, D, F) The same measurements the immune transcripts USP36 and IMD. One way ANOVA was performed with a Tukey posttest for multiple comparisons to measure statistical significance (** $P<0.01$ & *** $P<0.001$).

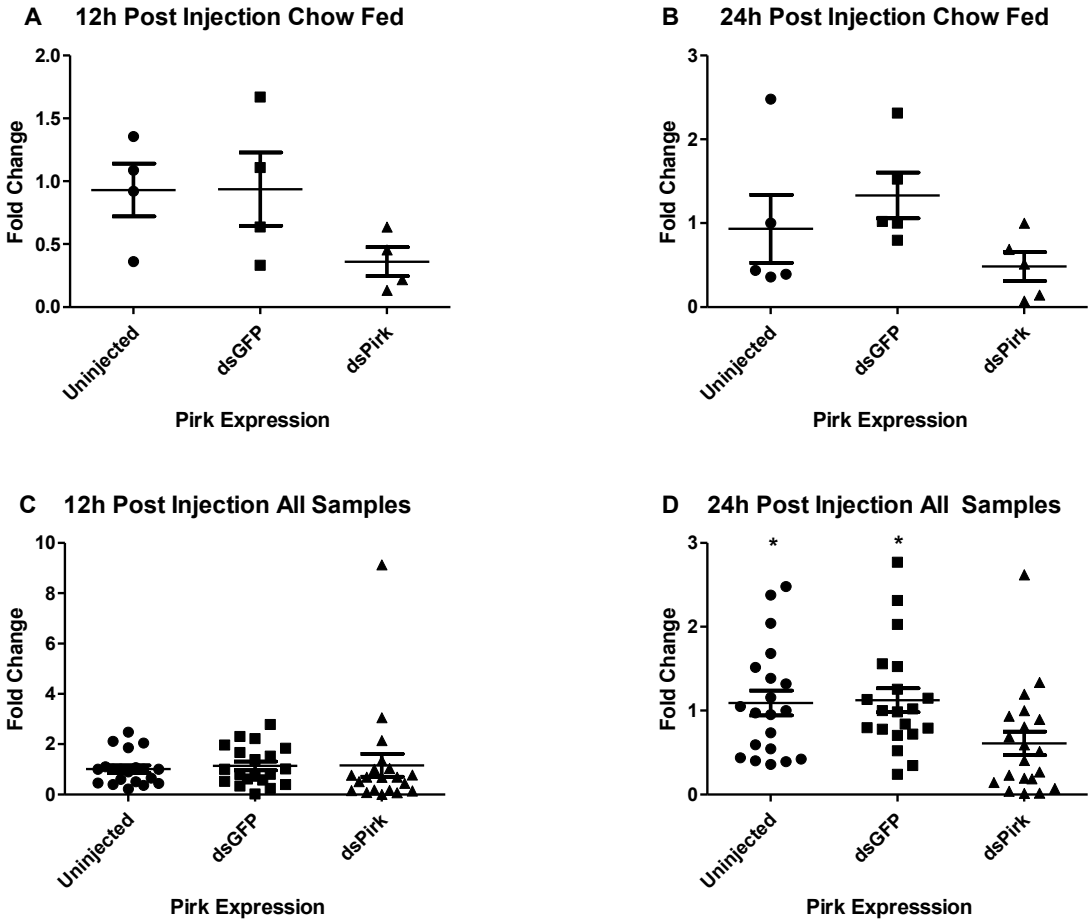

Figure 4.3. mRNA expression levels for L3 larvae that were uninjected, injected with dsGFP, or injected with dsPirk RNA.

Larvae were fed on chow, control agar, *B. subtilis* or *P. agglomerans* agar. (A) The fold change with standard errors for *Pirk* expression at 12h post injections feeding on chow, (B) 24h post injection for samples feeding on chow alone. (C) *Pirk* expression levels 12h post injection for all treated insects feeding on their respective substrates combined, and (D) 24h post injection. One way ANOVA was performed with a Tukey posttest for multiple comparisons to measure statistical significance (* $P<0.05$).

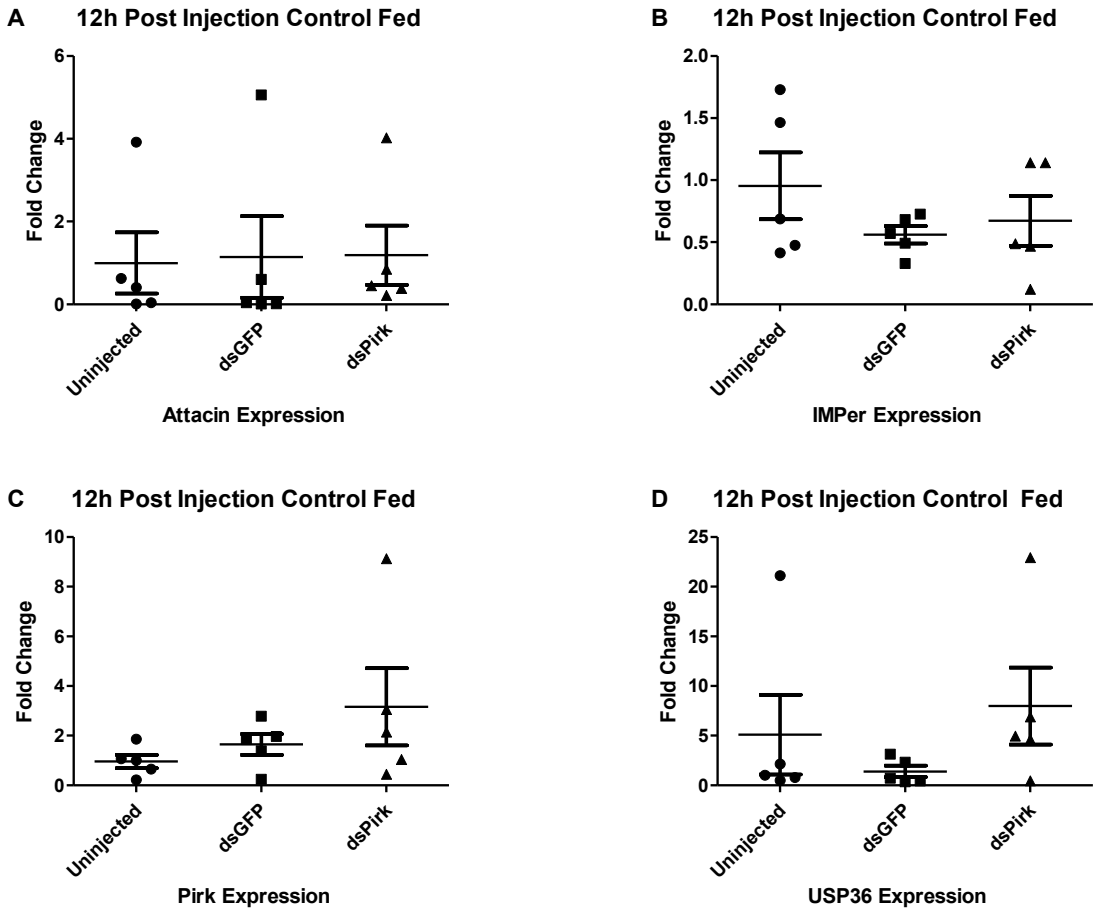

Figure 4.4. mRNA expression levels for L3 larvae that were uninjected, injected with dsGFP, or injected with dsPirk RNA.

Larvae were fed on control agar. (A) The fold change with standard errors for Attacin expression at 12h post injections, and (B, C, & D) 12h post injection for transcripts IMPer, Pirk, and USP36 respectively. One way ANOVA was performed with a Tukey posttest for multiple comparisons to measure statistical significance (* $P<0.05$).

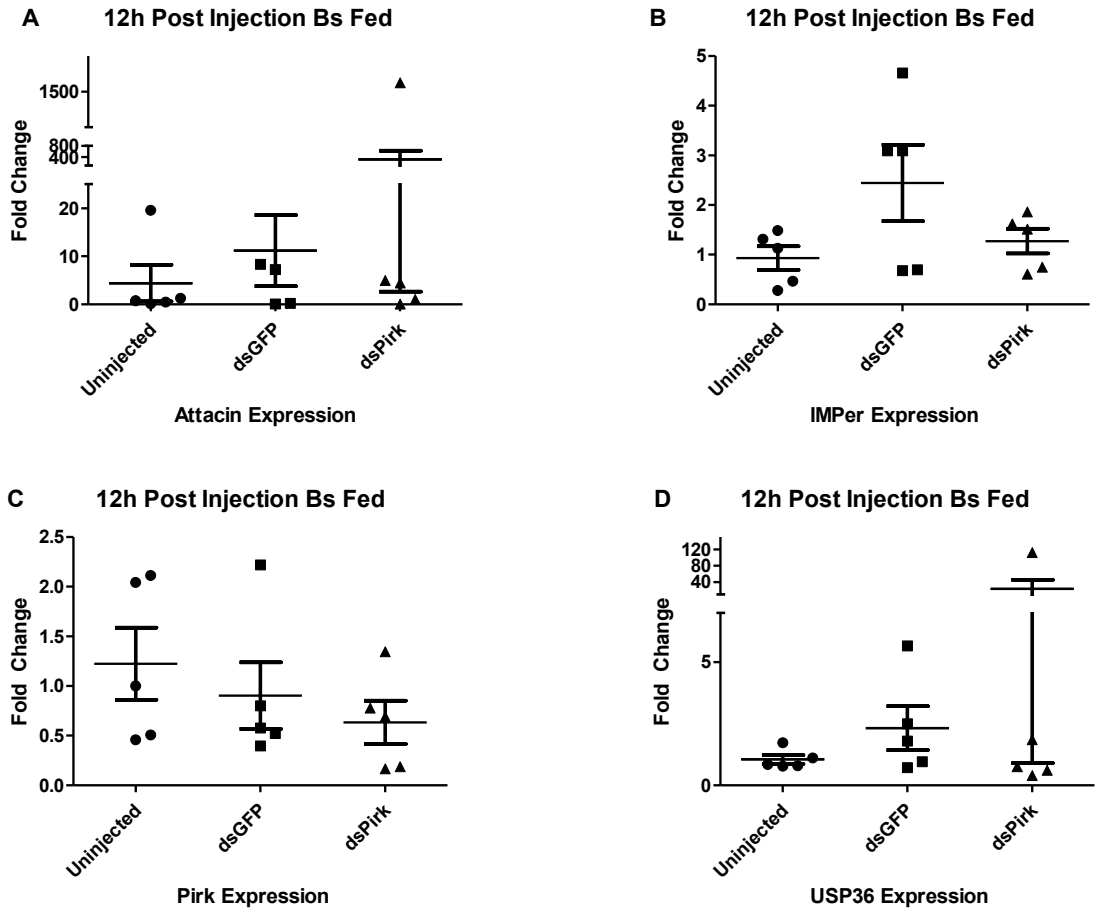

Figure 4.5. mRNA expression levels for L3 larvae that were uninjected, injected with dsGFP, or injected with dsPirk RNA.

Larvae were fed on *B. subtilis* agar. (A) The fold change with standard errors for Attacin expression at 12h post injections, and (B, C, & D) 12h post injection for transcripts IMPer, Pirk, and USP36 respectively. One way ANOVA was performed with a Tukey posttest for multiple comparisons to measure statistical significance.

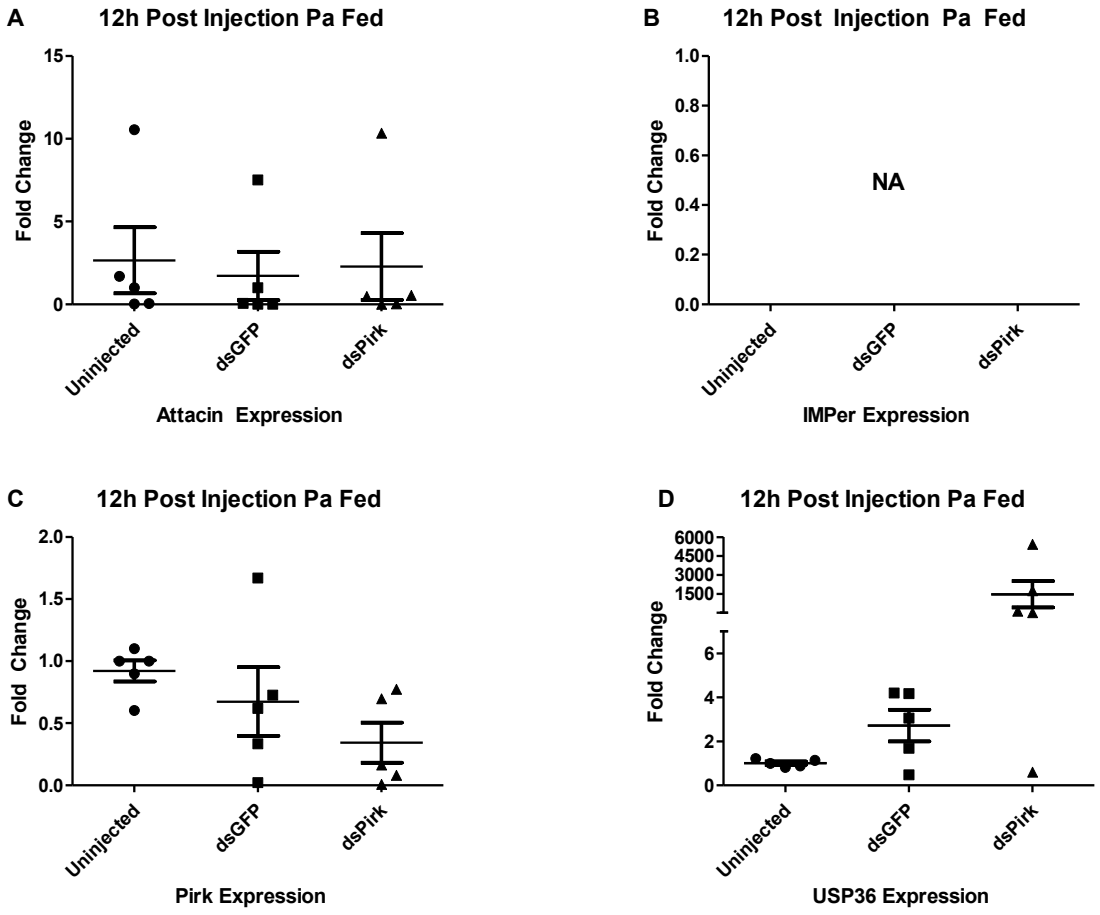

Figure 4.6. mRNA expression levels for L3 larvae that were uninjected, injected with dsGFP, or injected with dsPirk RNA.

Larvae were fed on P. agglomerans agar. (A) The fold change with standard errors for Attacin expression at 12h post injections, and (B, C, & D) 12h post injection for transcripts IMPer (NA = not available), Pirk, and USP36 respectively. One way ANOVA was performed with a Tukey posttest for multiple comparisons to measure statistical significance.

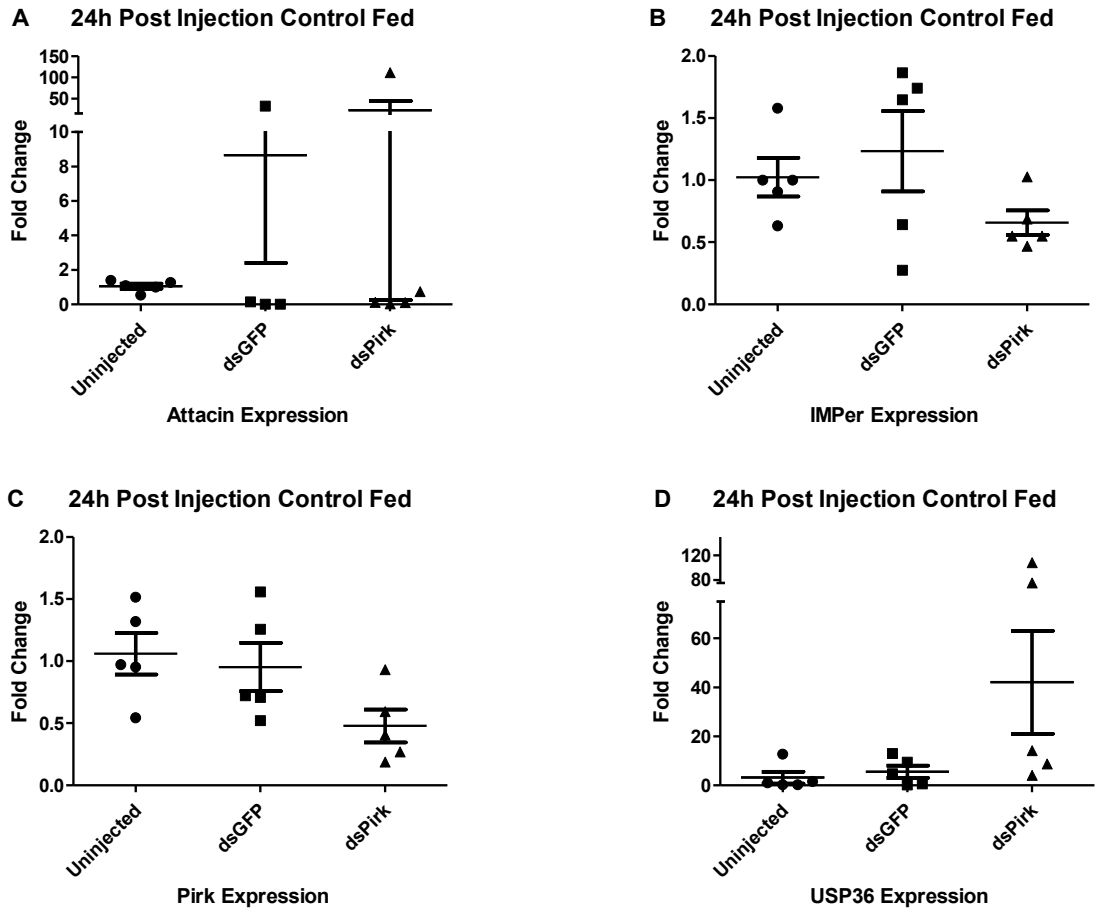

Figure 4.7. mRNA expression levels for L3 larvae that were uninjected, injected with dsGFP, or injected with dsPirk RNA.

Larvae were fed on control agar. (A) The fold change with standard errors for Attacin expression at 24h post injections, and (B, C, & D) 24h post injection for transcripts IMPer, Pirk, and USP36 respectively. One way ANOVA was performed with a Tukey posttest for multiple comparisons to measure statistical significance.

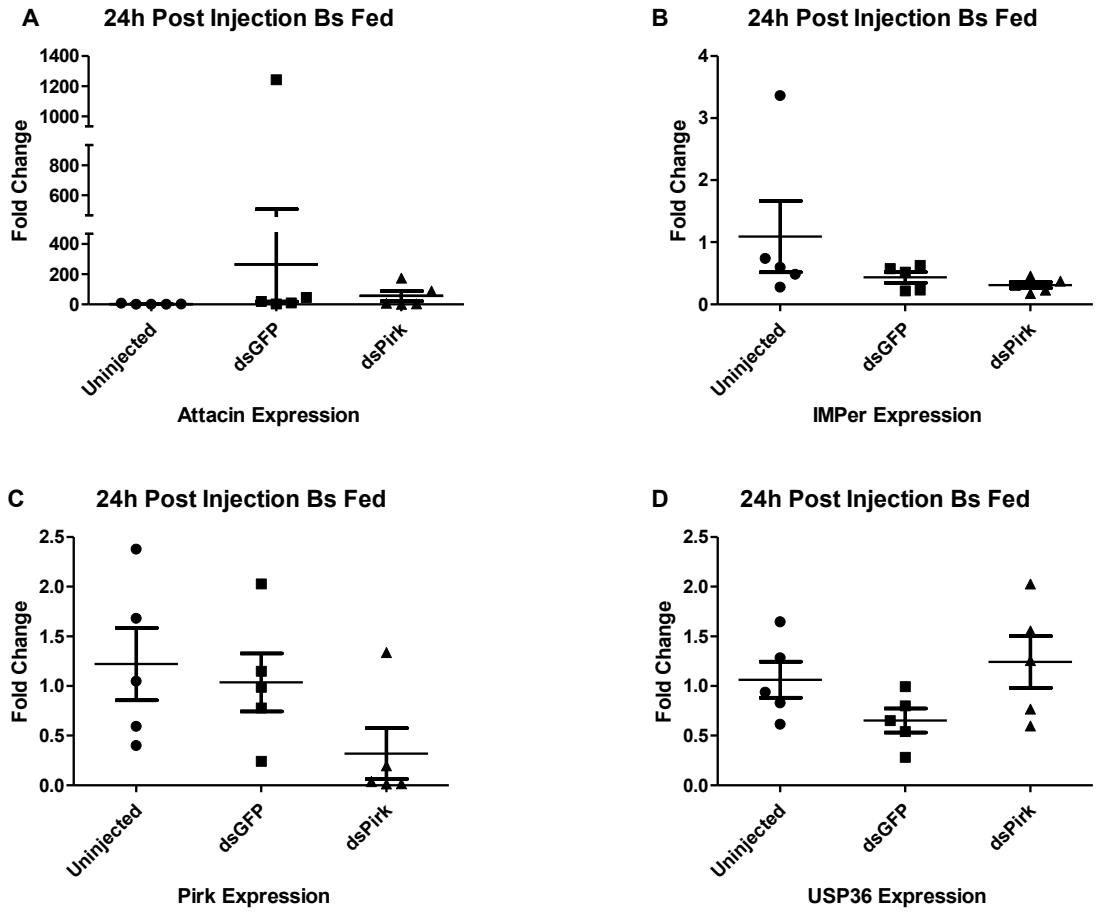

Figure 4.8. mRNA expression levels for L3 larvae that were uninjected, injected with dsGFP, or injected with dsPirk RNA.

Larvae were fed on *B. subtilis* agar. (A) The fold change with standard errors for Attacin expression at 24h post injections, and (B, C, & D) 24h post injection for transcripts IMPer, Pirk, and USP36 respectively. One way ANOVA was performed with a Tukey posttest for multiple comparisons to measure statistical significance.

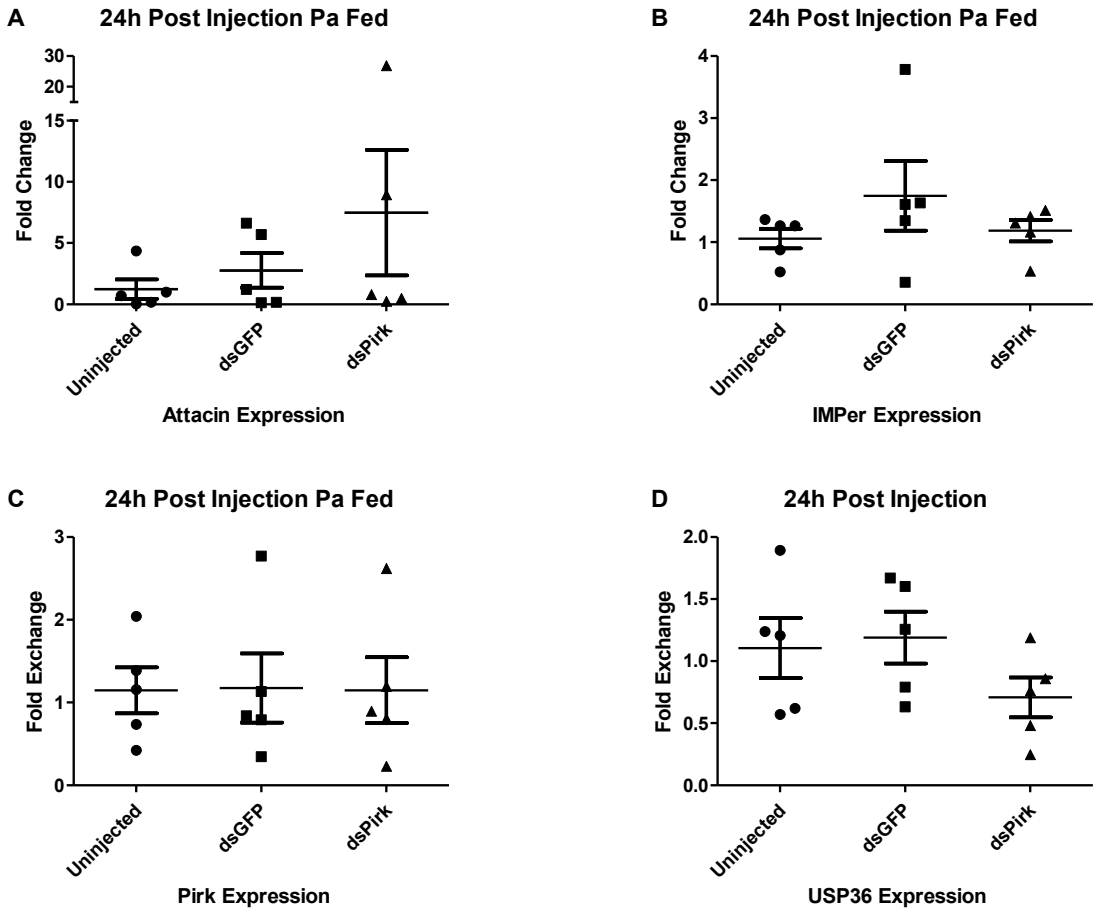

Figure 4.9. mRNA expression levels for L3 larvae that were uninjected, injected with dsGFP, or injected with dsPirk RNA.

Larvae were fed on *P. agglomerans* agar. (A) The fold change with standard errors for Attacin expression at 24h post injections, and (B, C, & D) 24h post injection for transcripts IMPer, Pirk, and USP36 respectively. One way ANOVA was performed with a Tukey posttest for multiple comparisons to measure statistical significance.

References

1. Alphey L, Genetic control of mosquitoes. Annu Rev Entomol, 2015. **59**: p. 205-24.

2. Wilke ABB and Marrelli MT, Paratransgenesis: a promising new strategy for mosquito vector control. Parasit Vectors, 2015. **8**(1): p. 1-9.

3. Dong Y, Manfredini F, Dimopoulos G, Implication of the mosquito midgut microbiota in the defense against malaria parasites. PLoS Pathog, 2009. **5**(5): p. e1000423.

4. Yoshida S, Ioka D, Matsuoka H, Endo HIshii A, Bacteria expressing single-chain immunotoxin inhibit malaria parasite development in mosquitoes. Mol Biochem Parasitol, 2001. **113**(1): p. 89-96.

5. Laven H, Eradication of Culex pipiens fatigans through cyioplasmic incompatibility. Nature, London, 1967. **216**(5113): p. 383-384.

6. Richins RD, Kaneva I, Mulchandani A, Chen W, Biodegradation of organophosphorus pesticides by surface-expressed. Nat. Biotechnol, 1997. **15**.

7. Chandler JA, Lang JM, Bhatnagar S, Eisen JA, Kopp A, Bacterial communities of diverse *Drosophila* species: ecological context of a host-microbe model system. PLoS Genet, 2011. **7**(9): p. e1002272.

8. Boissiere A, Tchioffo MT, Bachar D, Abate L, Marie A, Nsango SE, et al., Midgut microbiota of the malaria mosquito vector *Anopheles gambiae* and interactions with *Plasmodium falciparum* infection. PLoS Pathog, 2012. **8**(5): p. e1002742.

9. Rani A, Sharma A, Rajagopal R, Adak TB, hatnagar RK, Bacterial diversity analysis of larvae and adult midgut microflora using culture-dependent and culture-independent methods in lab-reared and field-collected *Anopheles stephensi*-an Asian malarial vector. BMC Microbiol, 2009. **9**: p. 96.

10. Terenius O, Lindh JM, Eriksson-Gonzales K, Bussiere L, Laugen AT, Bergquist H, et al., Midgut bacterial dynamics in *Aedes aegypti.* FEMS Microbiol Ecol, 2012. **80**(3): p. 556-65.

11. Wang Y, Gilbreath TM, Kukutla P, Yan G, Xu J, Dynamic gut microbiome across life history of the malaria mosquito *Anopheles gambiae* in Kenya. PLoS One, 2011. **6**(9): p. e24767.

12. Valiente Moro C, Tran FH, Raharimalala FN, Ravelonandro PM, avingui P, Diversity of culturable bacteria including *Pantoea* in wild mosquito *Aedes albopictus.* BMC Microbiol, 2013. **13**: p. 70.

13. Hillesland H, Read A, Subhadra B, Hurwitz I, McKelvey R, Ghosh K, et al., Identification of aerobic gut bacteria from the kala azar vector, *Phlebotomus argentipes*:

a platform for potential paratransgenic manipulation of sand flies. Am J Trop Med Hyg, 2008. **79**(6): p. 881-6.

14. Mukhopadhyay J, Braig HR, Rowton ED, Ghosh K, Naturally occurring culturable aerobic gut flora of adult *Phlebotomus papatasi*, vector of *Leishmania major* in the Old World. PLoS One, 2012. **7**(5): p. e35748.

15. Diaz-Albiter H, Sant'Anna MR, Genta FA, Dillon RJ, Reactive oxygen species-mediated immunity against *Leishmania mexicana* and *Serratia marcescens* in the sand phlebotomine fly *Lutzomyia longipalpis.* J Biol Chem, 2012. **287**(28): p. 23995-4003.

16. Gouveia C, Asensi MD, Zahner V, Rangel EF, Oliveira SM, Study on the bacterial midgut microbiota associated to different Brazilian populations of *Lutzomyia longipalpis* (Lutz & Neiva) (Diptera: Psychodidae). Neotrop Entomol, 2008. **37**(5): p. 597-601.

17. Telleria EL, Sant'Anna MR, Alkurbi MO, Pitaluga AN, Dillon RJ, Traub-Cseko YM, Bacterial feeding, *Leishmania* infection and distinct infection routes induce differential defensin expression in *Lutzomyia longipalpis.* Parasit Vectors, 2013. **6**: p. 12.

18. Telleria EL, Sant'Anna MR, Ortigao-Farias JR, Pitaluga AN, Dillon VM, Bates PA, et al., Caspar-like gene depletion reduces *Leishmania* infection in sand fly host *Lutzomyia longipalpis.* J Biol Chem, 2012. **287**(16): p. 12985-93.

19. Maleki-Ravasan N, Oshaghi MA, Hajikhani S, Saeidi Z, Akhavan AA, Gerami-Shoar M, et al., Aerobic microbial community of insectary population of *Phlebotomus papatasi.* Iran J of Arthropod Borne Dis, 2014. **8**(1): p. 69-81.

20. Peterkova-Koci K, Robles-Murguia M, Ramalho-Ortigao M, Zurek L, Significance of bacteria in oviposition and larval development of the sand fly *Lutzomyia longipalpis.* Parasit Vectors, 2012. **5**: p. 145.

21. Fazito do Vale V, Pereira MHc, Gontijo NF, Midgut pH profile and protein digestion in the larvae of *Lutzomyia longipalpis* (Diptera: Psychodidae). J Insect Physiol, 2007. **53**(11): p. 1151-1159.

22. Buchon N, Broderick NA, Chakrabarti S, Lemaitre B, Invasive and indigenous microbiota impact intestinal stem cell activity through multiple pathways in *Drosophila.* Genes Dev, 2009. **23**(19): p. 2333-44.

23. Buchon N, Broderick NA, Kuraishi T, Lemaitre B, *Drosophila* EGFR pathway coordinates stem cell proliferation and gut remodeling following infection. BMC Biol, 2010. **8**: p. 152.

24. Coutinho-Abreu IV, Sharma NK, Robles-Murguia M, Ramalho-Ortigao M, Targeting the midgut secreted PpChit1 reduces *Leishmania major* development in its natural vector, the sand fly *Phlebotomus papatasi.* PLoS Negl Trop Dis, 2010. **4**(11): p. e901.

25. Lemaitre B, Nicolas E, Michaut L, Reichhart J-M, Hoffmann JA, The Dorsoventral Regulatory Gene Cassette spaetzle/Toll/cactus Controls the Potent Antifungal Response in Drosophila Adults. Cell, 1996. **86**(6): p. 973-983.

26. Steward R, Dorsal, an embryonic polarity gene in Drosophila, is homologous to the vertebrate proto-oncogene, c-rel. Science, 1987. **238**(4827): p. 692-694.

27. Wang J, Wu Y, Yang G, Aksoy S, Interactions between mutualist Wigglesworthia and tsetse peptidoglycan recognition protein (PGRP-LB) influence trypanosome transmission. Proc. Natl. Acad. Sci. U.S.A., 2009. **106**(29): p. 12133-12138.

28. Moy RH and Cherry S, Antimicrobial autophagy: a conserved innate immune response in *Drosophila.* J Innate Immun, 2013. **5**(5): p. 444-455.

29. Yano T, Mita S, Ohmori H, Oshima Y, Fujimoto Y, Ueda R, et al., Autophagic control of listeria through intracellular innate immune recognition in drosophila. Nat Immunol, 2008. **9**(8): p. 908-916.

30. Shelly S, Lukinova N, Bambina S, Berman A, Cherry S, Autophagy is an essential component of Drosophila immunity against vesicular stomatitis virus. Immunity, 2009. **30**(4): p. 588-598.

31. Mizushima N, Levine B, Cuervo AM, Klionsky DJ, Autophagy fights disease through cellular self-digestion. Nature, 2008. **451**(7182): p. 1069-1075.

32. Mohseni N, McMillan SC, Chaudhary R, Mok J, Reed BH, Autophagy promotes caspase-dependent cell death during Drosophila development. Autophagy, 2009. **5**(3): p. 329-338.

33. Berry DL and Baehrecke EH, Growth arrest and autophagy are required for salivary gland cell degradation in Drosophila. Cell, 2007. **131**(6): p. 1137-1148.

34. McPhee CK, Balgley BM, Nelson C, Hill JH, Batlevi Y, Fang X, et al., Identification of factors that function in Drosophila salivary gland cell death during development using proteomics. Cell Death Differ, 2013. **20**(2): p. 218-225.

35. Shen W and Ganetzky B, Autophagy promotes synapse development in Drosophila. The J Cell Biol, 2009. **187**(1): p. 71-79.

36. Rusten TE, Lindmo K, JuhÃ¡sz Gb, Sass Ms, Seglen PO, Brech A, et al., Programmed autophagy in the Drosophila fat body is induced by ecdysone through regulation of the PI3K pathway. Dev Cell, 2004. **7**(2): p. 179-192.

37. Tian L, Ma L, Guo E, Deng X, Ma S, Xia Q, et al., 20-hydroxyecdysone upregulates Atg genes to induce autophagy in the Bombyx fat body. Autophagy, 2013. **9**(8): p. 1172-1187.

38. Denton D, Shravage B, Simin R, Mills K, Berry DL, Baehrecke EH, et al., Autophagy, not apoptosis, is essential for midgut cell death in drosophila. Curr Biol, 2009. **19**(20): p. 1741-1746.

39. Denton D, Chang TK, Nicolson S, Shravage B, Simin R, Baehrecke EH, et al., Relationship between growth arrest and autophagy in midgut programmed cell death in Drosophila. Cell Death Differ, 2012. **19**(8): p. 1299-1307.

40. Franzetti E, Huang Z-J, Shi Y-X, Xie K, Deng X-J, Li J-P, et al., Autophagy precedes apoptosis during the remodeling of silkworm larval midgut. Apoptosis, 2012. **17**(3): p. 305-324.

41. Xu T, Nicolson S, Denton D, Kumar S, Distinct requirements of Autophagy-related genes in programmed cell death. Cell Death Differ, 2015. **22**(11): p. 1792-1802.

42. Bryant B and Raikhel AS, Programmed autophagy in the fat body of *Aedes aegypti* is required to maintain egg maturation cycles. PLoS One, 2011. **6**(11): p. e25502.

43. Fernandes KM, Neves CvA, Serralo JE, Martins GF, *Aedes aegypti* midgut remodeling during metamorphosis. Parasitol Int, 2014. **63**(3): p. 506-512.

44. Lee C-Y, Wendel DP, Reid P, Lam G, Thummel CS, Baehrecke EH, E93 directs steroid-triggered programmed cell death in Drosophila. Molecular Cell, 2000. **6**(2): p. 433-443.

45. Lee C-Y, Cooksey BAK, Baehrecke EH, steroid regulation of midgut cell death during Drosophila development. Dev Biol, 2002. **250**(1): p. 101-111.

46. Jiang C, Lamblin A-FoJ, Steller H, Thummel CS, A steroid-triggered transcriptional hierarchy controls salivary gland cell death during Drosophila metamorphosis. Molecular Cell, 2000. **5**(3): p. 445-455.

47. Ureña E, Chafino S, Manjón C, Franch-Marro X, Martín D, The occurrence of the holometabolous pupal stage requires the interaction between E93, Krüppel-Homolog 1 and Broad-Complex. PLoS Genet, 2016. **12**(5): p. e1006020.

48. Liu X, Dai F, Guo E, Li K, Ma L, Tian L, et al., 20-Hydroxyecdysone (20E) primary-response gene E93 modulates 20E signaling to promote bombyx larval-pupal metamorphosis. J Biol Chem, 2015.

49. Jiang H and Edgar BA, EGFR signaling regulates the proliferation of Drosophila adult midgut progenitors. Development, 2009. **136**(3): p. 483-493.

50. Biteau Bt and Jasper H, EGF signaling regulates the proliferation of intestinal stem cells in Drosophila. Development, 2011. **138**(6): p. 1045-1055.

51. Buchon N, Broderick NA, Poidevin M, Pradervand S, Lemaitre B, *Drosophila* intestinal response to bacterial infection: activation of host defense and stem cell proliferation. Cell Host Microbe, 2009. **5**(2): p. 200-11.

52. Schmittgen TD and Livak KJ, Analyzing real-time PCR data by the comparative CT method. Nat. Protocols, 2008. **3**(6): p. 1101-1108.

53. Akhoundi M, Bakhtiari R, Guillard T, Baghaei A, Tolouei R, Sereno D, et al., Diversity of the bacterial and fungal microflora from the midgut and cuticle of phlebotomine sand flies collected in North-Western Iran. PLoS One, 2012. **7**(11): p. e50259.

54. Corish P and Tyler-Smith C, Attenuation of green fluorescent protein half-life in mammalian cells. Protein Eng, 1999. **12**(12): p. 1035-1040.

55. Mazzola PG, Ishii M, Chau E, Cholewa O, Penna TCV, Stability of green fluorescent protein (GFP) in chlorine solutions of varying pH. Biotechnol Prog, 2006. **22**(6): p. 1702-1707.

56. Hultmark D, Engstrom A, Andersson K, Steiner H, Bennich H, Boman HG, Insect immunity. Attacins, a family of antibacterial proteins from Hyalophora cecropia. EMBO J, 1983. **2**(4): p. 571-6.

57. Kokoza V, Ahmed A, Woon Shin S, Okafor N, Zou Z, Raikhel AS, Blocking of *Plasmodium* transmission by cooperative action of Cecropin A and Defensin A in transgenic *Aedes aegypti* mosquitoes. Proc. Natl. Acad. Sci U.S.A., 2010. **107**(18): p. 8111-6.

58. Goncalves RL, Oliveira JH, Oliveira GA, Andersen JF, Oliveira MF, Oliveira PL, et al., Mitochondrial reactive oxygen species modulate mosquito susceptibility to *Plasmodium* infection. PLoS One, 2012. **7**(7): p. e41083.

59. Kumar S, Molina-Cruz A, Gupta L, Rodrigues J, Barillas-Mury C, A peroxidase/dual oxidase system modulates midgut epithelial immunity in *Anopheles gambiae.* Science, 2010. **327**(5973): p. 1644-1648.

60. Oliveira GdA, Lieberman J,Barillas-Mury C, Epithelial nitration by a peroxidase/NOX5 system mediates mosquito antiplasmodial immunity. Science, 2012. **335**(6070): p. 856-859.

61. Lemaitre B, Kromer-Metzger E, Michaut L, Nicolas E, Meister M, Georgel P, et al., A recessive mutation, immune deficiency (*imd*), defines two distinct control pathways in the *Drosophila* host defense. Proc. Natl. Acad. Sci. U.S.A., 1995. **92**(21): p. 9465-9.

62. Lemaitre B, Reichhart JM, Hoffmann JA, *Drosophila* host defense: differential induction of antimicrobial peptide genes after infection by various classes of microorganisms. Proc. Natl. Acad. Sci. U.S.A., 1997. **94**(26): p. 14614-9.

63. Kleino A, Myllymaki H, Kallio J, Vanha-aho LM, Oksanen K, Ulvila J, et al., Pirk is a negative regulator of the *Drosophila* Imd pathway. J Immunol, 2008. **180**(8): p. 5413-22.

64. Lhocine N, Ribeiro PS, Buchon N, Wepf A, Wilson R, Tenev T, et al., PIMS modulates immune tolerance by negatively regulating *Drosophila* innate immune signaling. Cell Host Microbe, 2008. **4**(2): p. 147-58.

65. Garver LS, Dong Y, Dimopoulos G, Caspar controls resistance to *Plasmodium falciparum* in diverse anopheline species. PLoS Pathog, 2009. **5**(3): p. e1000335.

66. Gupta L, Molina-Cruz A, Kumar S, Rodrigues J, Dixit R, Zamora RE, et al., The STAT pathway mediates late-phase immunity against *Plasmodium* in the mosquito *Anopheles gambiae.* Cell Host Microbe, 2009. **5**(5): p. 498-507.

67. Luckhart S, Giulivi C, Drexler AL, Antonova-Koch Y, Sakaguchi D, Napoli E, et al., Sustained activation of Akt elicits mitochondrial dysfunction to block *Plasmodium falciparum* infection in the mosquito host. PLoS Pathog, 2013. **9**(2): p. e1003180.

68. Chakrabarti S, Liehl P, Buchon N, Lemaitre B, Infection-induced host translational blockage inhibits immune responses and epithelial renewal in the *Drosophila* gut. Cell Host Microbe, 2012. **12**(1): p. 60-70.

69. Jiang H, Patel PH, Kohlmaier A, Grenley MO, McEwen DG, Edgar BA, Cytokine/Jak/Stat signaling mediates regeneration and homeostasis in the *Drosophila* midgut. Cell, 2009. **137**(7): p. 1343-55.

70. Liu W, Singh SR, Hou SX, JAK-STAT is restrained by Notch to control cell proliferation of the *Drosophila* intestinal stem cells. J Cell Biochem, 2010. **109**(5): p. 992-9.

71. Paquette N, Broemer M, Aggarwal K, Chen L, Husson M, Erturk-Hasdemir D, et al., Caspase-mediated cleavage, IAP binding, and ubiquitination: linking three mechanisms crucial for *Drosophila* NF-kappaB signaling. Mol Cell, 2010. **37**(2): p. 172-82.

72. Taillebourg E, Gregoire I, Viargues P, Jacomin AC, Thevenon D, Faure M, et al., The deubiquitinating enzyme USP36 controls selective autophagy activation by ubiquitinated proteins. Autophagy, 2012. **8**(5): p. 767-79.

73. Maltz MA, Weiss BL, O'Neill M, Wu Y, Aksoy S, OmpA-mediated biofilm formation is essential for the commensal bacterium *Sodalis glossinidius* to colonize the tsetse fly gut. Appl Environ Microbiol, 2012. **78**(21): p. 7760-8.

74. Lauzon CR, McCombs SD, Potter SE, Peabody NC, Establishment and vertical passage of Enterobacter (*Pantoea*) *Agglomerans* and *Klebsiella pneumoniae* through all life stages of the Mediterranean fruit fly (Diptera: Tephritidae). Ann Entomol Soc Am, 2009. **102**(1): p. 85-95.

75. Kamhawi S, Ramalho-Ortigao M, Van MP, Kumar S, Lawyer PG, Turco SJ, et al., A Role for Insect Galectins in Parasite Survival. Cell, 2004. **119**(3): p. 329-341.

76. Huang J and Brumell JH, Bacteria-autophagy interplay: a battle for survival. Nat Rev Micro, 2014. **12**(2): p. 101-114.

77. Hurwitz I, Forshaw A, Yacisin K, Ramalho-Ortigao JM, Satoskar A, Durvasula R, *Paratransgenic Control of Leishmaniasis: New Developments*, in *Pathogenesis of Leishmaniasis: New Developments in Research*, S. A and D. R, Editors. 2014: New York.

78. Hurwitz I, Hillesland H, Fieck A, Das P, Durvasula R, The paratransgenic sand fly: a platform for control of *Leishmania* transmission. Parasit Vectors, 2011. **4**: p. 82.

79. Heerman M, Weng J-L, Hurwitz I, Durvasula R, Ramalho-Ortigao M, Bacterial infection and immune responses in *Lutzomyia longipalpis* sand fly larvae midgut. PLoS Negl Trop Dis, 2015. **9**(7): p. e0003923.

80. Cherbas L, Lee K, Cherbas P, Identification of ecdysone response elements by analysis of the Drosophila Eip28/29 gene. Genes Dev, 1991. **5**(1): p. 120-131.

81. Antoniewski C, Laval M, Lepesant J-A, Structural features critical to the activity of an ecdysone receptor binding site. Insect Biochem Mol Biol, 1993. **23**(1): p. 105-114.

82. Nishita Y, Identification of a DNA sequence critical for ecdysone receptor binding to the distal promoter of the Bombyx Broad-Complex gene. J Insect Biotechnol Sericology, 2013. **82**(3): p. 3_071-3_078.

83. Letsou A, Alexander S, Orth K, Wasserman SA, Genetic and molecular characterization of tube, a Drosophila gene maternally required for embryonic dorsoventral polarity. Proc. Natl. Acad. Sci. U.S.A., 1991. **88**(3): p. 810-4.

84. Mizushima N, The role of the Atg1/ULK1 complex in autophagy regulation. Cur Opin Cell Biol, 2010. **22**(2): p. 132-139.

85. Ichimura Y, Kirisako T, Takao T, Satomi Y, Shimonishi Y, Ishihara N, et al., A ubiquitin-like system mediates protein lipidation. Nature, 2000. **408**(6811): p. 488-492.

86. Nakatogawa H, Ichimura Y, Ohsumi Y, Atg8, a ubiquitin-like protein required for autophagosome formation, mediates membrane tethering and hemifusion. Cell, 2007. **130**(1): p. 165-178.

87. Simonsen A, Cumming RC, Brech A, Isakson P, Schubert DR, Finley KD, Promoting basal levels of autophagy in the nervous system enhances longevity and oxidant resistance in adult Drosophila. Autophagy, 2008. **4**(2): p. 176-184.

88. Lorincz P, Lakatos Z, Maruzs T, Szatmari Z, Kis V, Sass M, Atg6/UVRAG/Vps34-containing lipid kinase complex is required for receptor downregulation through endolysosomal degradation and epithelial polarity during Drosophila wing development. BioMed Research Int, 2014. **2014**: p. 19.

89. Shravage BV, Hill JH, Powers CM, Wu L, Baehrecke EH, Atg6 is required for multiple vesicle trafficking pathways and hematopoiesis in Drosophila. Development, 2013. **140**(6): p. 1321-1329.

90. Pattingre S, Tassa A, Qu X, Garuti R, Liang XH, Mizushima N, et al., Bcl-2 antiapoptotic proteins inhibit Beclin 1-dependent autophagy. Cell, 2005. **122**(6): p. 927-939.

91. Schnepp B, Grumbling G, Donaldson T, Simcox A, Vein is a novel component in the Drosophila epidermal growth factor receptor pathway with similarity to the neuregulins. Genes Dev, 1996. **10**(18): p. 2302-2313.

92. Belvin MP, Jin Y, Anderson KV, Cactus protein degradation mediates Drosophila dorsal-ventral signaling. Gene Dev, 1995. **9**(7): p. 783-793.

93. Mlodzik M and Gehring WJ, Expression of the caudal gene in the germ line of Drosophila: Formation of an RNA and protein gradient during early embryogenesis. Cell, 1987. **48**(3): p. 465-478.

94. Ryu J-H, Kim S-H, Lee H-Y, Bai JY, Nam Y-D, Bae J-W, et al., Innate immune homeostasis by the homeobox gene Caudal and commensal-gut mutualism in Drosophila. Science, 2008. **319**(5864): p. 777-782.

95. Bryant B, Macdonald W, Raikhel AS, microRNA miR-275 is indispensable for blood digestion and egg development in the mosquito Aedes aegypti. Proc. Nat. Acad. Sci. U.S.A., 2010. **107**(52): p. 22391-22398.

Appendix A - Bioinformatic and Phylogenetic Data

>Ll_Vein_LLOJ001534

ATGAATGTGCGCGTCCTGCGCAAATGGTGTCTCATGAGAACTCTAATGTACCTGTGGATTGTGGCCTGCA
CACTACTAATGATGGTTGTTACGTGTGAGGCTGCTTCCGCCATGCACATCACACCGAGTTTCATTAGTCC
TGCAAGGAATTCCACATCCCACCACCGGTGGGCGCCACTAGTCACCCACCAGCGCCCCCATGTTGATTTT
GTCACACAACCAGAGCAGAAACTTCCACGCCAGGAACGCATTTTTCCCGATAGGGGGATGCATGGGCAAA
TACTGCTGCAACGCATCATTGCAGCAGCACGAAGAACACCGAGTATGC**CGCAATGGATGAGAACAC**ATCA
GCGGCCAAGACTGAAAGTCGGCGTCCATGATGAGGCGTCATCTAGTTACCTCATGCGTGCCCCCTATGGG
CGAAATAGGCGCGAGTCACGCTACAGGCCCAAAGGGCGTCAGCGTAGGTATTGCTCAGCTCGCGACCCAA
CGGCCTTAGCATTTGAGGCACCCACAGTATTTGAGGGTAAAGTGCGTTCCATGAGCTCCGATAGGCGCGC
CAACTTCTCAGCCACGTTCGAAGTCAAGGATATCCACAAGAATCAGTCGCCCTTTAAGTTGCCATCAATG
GTACGGCTGCAATTCACATTCGGGAATACCAGTGAGTGTGACATCTATAGGGAAAAATTTCGTCCGCGTG
GCAATGTGCGCGATGAACTGGAGCAGGGGAAGGTGTACTTTCTTTTTCTCAAGCAAATCACCTTGGGGAA
TTTCACAATCATCGGACAGCCCATCAAGAAGACCAAGAAGACACTCCAAGAGGTCAAAACTGGAGCTAGC
GAAAAATATGGACAGCGCGCCTCCATTGAATTTCTCACGGAAAATCTTCCCGTGCGAGAGGGCAAGAAAG
TCCGTTTGATATGCAGAGTGAAAGGTCAACCGCCACCGAAAATCACATGGTACAAAGATGGGAGTTCCAT
TAAAAGAAATCGTACCAGATATACTTTTTCTCACTTTAAGAGAAGATCAATCCTAATCATTGAGTCGGTA
GGAAAGAACGACACGGGACAATATGAATGTCGCGCTAAGAATAAATTGGCGAAACAACCTGTTACACGAA
CAATGTTCTTGAGAGTCGATGACCAGCCAGATCAAAATTGGGAGAATTGCCCATTGGAGGGTACGGAGTA
TTGCTTAAATGGTGGCACCTGTCTGTACTTTAGTGCTGTGGAAGAGCCAGCTTGTCAATGTCCTGAAGGC
TTTATGGGGAATCGCTGTGAGACGAAAAACCCAACAAATCCCCAAACGAGTACGTACAACAAAGAACAAT
GTGGCAAAAAATAATCATGGCGGTTATTATTGCTAAAATAAGGCATTCTCTAGCACCAATTGCTGCAAAG
TTATTTTTTTTACCAAAAAAGCCATGCGAGAAAATCAAAGAGCATTCATTTTTTCTTAAAACATTTTTGC
AAAAATCTAATATAATATATTGCTCTATCATATATAGTTTTTCTCACAATAAATAAATGAGAAAATCAAG
CAAGATTTTTTTATAGTACAAATTTGTATATATTTATTTTAAAAGGAAATGAGAATTTACAGTAATTTTG
CTTTATGTAAGACTAAAGAAAATTTCATTTAATTCGCAATGAGAAAAATATGTAATAACTATTTTTTTTA
ATTTAAAAACATTGAGCGTTAGAGAATGTAAAAAAAGATATTCATAA

Figure A.1. Putative CDS for mRNA encoding *L. longipalpis* Vein.

Full length predicted mRNA is depicted in black, while the primers used for RT-qPCR amplicon measurement are shown in pink. Sequences in blue denote agreement between prediction and sequenced amplicons, while nucleotides in red depict a difference at that base pair.

>Ll_Pirk_LLOJ004926

ATGGTGATTAAGATGAGTGGGAGTGAGAAGATGCAGCAGCGTCGTGAACTAATTGGGAATCGCAAGGAGT

TCCGAATTGAGAAGAATGATGCCCATTTGCGTATTGTTGGGAACGATAATCGCATCCTGGTGCACCACAA

CAATGGCTCCGTGGACATTGTTGGGAATTCCTCAACTGTTAAGGTGGCTCAGAATGCAGGAAGTATCCAA

TACACGGGAAATTGTGGACGCATCAGTCTCGGTGCAGGGAGTTCAAATACCAACGTCAACTACACCGGAA

GTGGCGGACGGATGAAGCTGATTGATGGCACAAATGCGCTGTGGAAGAAAAAATCCCCGAATGATAAGAA

AGAGCATCGTAAGACGTCGGAGCAAGCACGTGGGAGCAGCCCCAAGATCTTCCCTGATGCCACTAATGTT

CACATCAACACCAATTCCGCCAATATCGTCATCAACAATACAATAATTAGATGA

Figure A.2. Putative CDS for mRNA encoding *L. longipalpis* Pirk.

Full length predicted mRNA is depicted in black, while the primers used for RT-qPCR amplicon measurement are shown in pink, while primers used for the synthesis of dsPirk RNA molecules are shown in violet. Sequences in blue denote agreement between prediction and sequenced amplicons, while nucleotides in red depict a difference at that base pair.

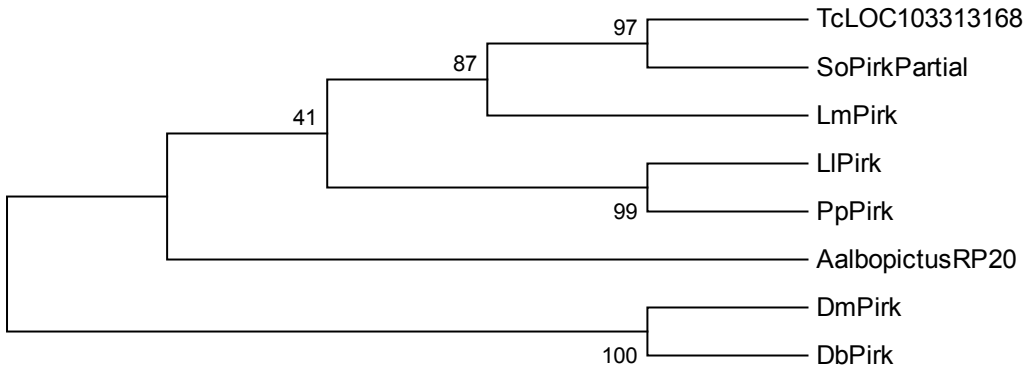

Figure A.3. Neighbor-joining tree to infer the evolutionary relationship of Pirk sequences.

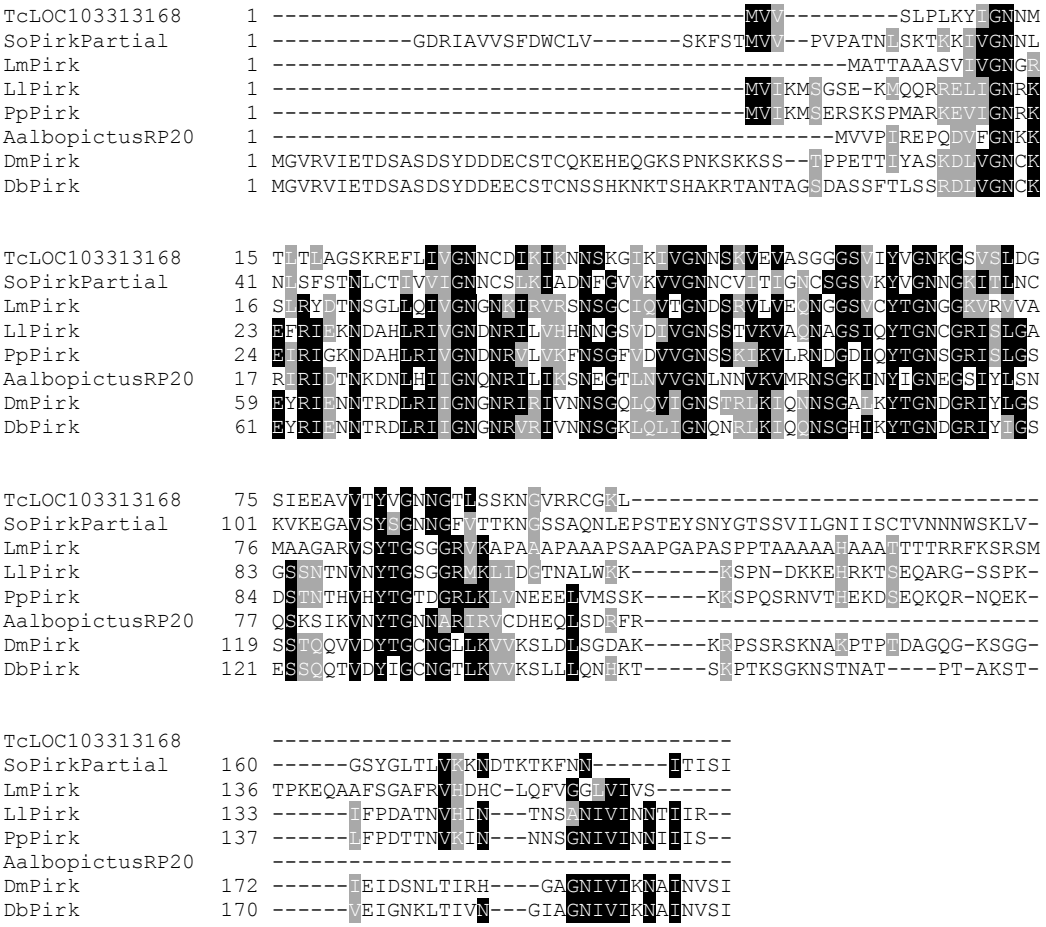

Figure A.4. Clustal Omega protein alignment of Pirk sequences from *L. longipalpis*, *P. papatasi*, *D. melanogaster*, *D. buskii*, *A. albopictus*, *T. castaneum*, *S. oryzae*, and *L. migratoria*.

>Ll_ATG6_LLOJ007047

ATGGGAGATGAGAGAGTCCTCGTAAGTTTTACGTGCCAGAGATGCCTTCAGCCCATA
AAGATTGATGAAACTTTCGATAGAATTGACGAGCATAAATTGGCTGAACTTTCTCTG
CCAATTAATTCTAATATAGATGTAGATTTGGAGTCTCAGGCAATGAGTTTTGATCAA
TTTGTCCCTCCGTTTGGTTTCCGGGACTCCGGAGCTGCGAATTTTGAGGCATTCCGTC
GCATTAGAGATGGTTCCGGGAAGGTTCTCACACAGTATGCTGTCTATGGGACTGGAA
CGAATGGCTTTATGCTCATTTCTGACGTCTGGGACAACGATGTGGGGAGCCACAAGA
TGAAAGTCAAAGCGGAATTGTTTGATAAGCTCTCATCCAATTCCGAAATTGATCATC
CACTGTGTGATGAGTGCACAGACACCTTGCTGGAGATGATGGATCAGCAGCTAAAG
TTGGCAGATAATGACTTCAATGACTATCTGAGTTATCTCAAGAAGTTGGAAGCTTCG
GAGGATGTTCCGGACATCGAGCAGCTGGAGAAGGAATTGGCAGATTTGAGTACGGA
GGAGGAACGCTTGGTGGCTGAGTTGGCTATGCTCAAGACACAGGAGGAAGCAATTA
AGGTTTCCATTGAGGGACAACAGGCTGAGCAGGAACGTCTCCGGGATGAACAAGTA
AAATACTGGCGAGAGTACACAAAGCACCGACGTGATCTCATGGCAACAGAGGATGA
ATTTAGAAGTGTGGAGAATCATTTGGCCTACGCTCAATCCCAGCTGGATCGTCTCAA
GAAGACAAATGTCTTCAATGTGACCTTCCACATCTGGCATTCCGGACACTTTGGCAC
CATTAACAATTTCCGCCTCGGGCGCCTTCCATCC**GCTCCTGTTGATTGGTCA**GAAA
TCAATGCAGCCTGGGGCCAGACAGCTCTTCTCCTTTCCGCCCTGGCACGAAAG
ATGAATCTCACCTTCAAGCGCTACAAACTCGTCCCTTACGGCAATCATTCCTACA
TTGAGGAATTTGAGACCGGGAAGCAGCTTCCGCTCTACGGCACAGGAGGCATTCGA
TTCTACTGGGATACCAAATTTGATGCAGCCATGGTGGCTTTCCTGGATTGTCTGCAG
CAATTCAAAGATGAGGTTGAGAAGGGTGATTCCGGCTTCTGTCTACCCTACAAGATG
GACAAGGGGAAGATTGAGGATTCAGCCACGGGGAATTCCTATTCCATCAAGATTCA
ATTTAATTCCGAAGAACAATGGACGAAGGCTCTCAAATTCCTGCTGACTAACCTCAA
ATGGGGACTTGCGTGGGTGTCGTCTCAATTTGCAGATGATAAGCTTGATGATTAG

Figure A.5. Putative CDS for mRNA encoding *L. longipalpis* ATG6.

Full length predicted mRNA is depicted in black, while the primers used for RT-qPCR amplicon measurement are shown in pink. Sequences in blue denote agreement between prediction and sequenced amplicons, while nucleotides in red depict a difference at that base pair.

>Ll_Attacin_LLOJ005408

ATGATCTCATCAGTGAAAGTTGCAATCCTGTTGGCCTGTGTGGCTGTATCCTGTGCTTACTCTTTTGAGTATCCTTC

CGAACTGGAGGATGCCGTTGAGGAACTCTCTCCGTGGGACGTTGCCGTGGAGCCCATGTACATTCTGCCTCTGCCAT

TGGCCAAACAACGCGTCAGGCGTCAGACAATCTTCGGTGGGGTAACTCCTGGAAATCCTGGAGGTGTTCAGGGAACC

GTTGGAGCTCGTGGTACACTGTTTGAGAACAATGGACATCGTCTCGATGGGCATGGCAGCGTCTCTCGCAATTGGCA

CCCAACTGGACCTACATCTATTGGTGGTGGGCTCGACTACACAGGACCCAGAGGATCAGCCTCAGTCAGTGCTCAGC

ATCAGCATCGTTTTGGAACAACAATTGGTGCTGAAGGACGCGCCAATCTCTACAGGAGCCCCA**ATGGAATGACCTCT**

GTGGATGCCCATGGATCCTACCAGCGCCACTTTGGAGGACCCTTCGGGACATCAAGGCCCAACTACAACGTTGGACT

TGGTCTTTCTCATCGCTTCTAA

Figure A.6. Putative CDS for mRNA encoding *L. longipalpis* Attacin.

Full length predicted mRNA is depicted in black, while the primers used for RT-qPCR amplicon measurement are shown in pink. Sequences in blue denote agreement between prediction and sequenced amplicons, while nucleotides in red depict a difference at that base pair.

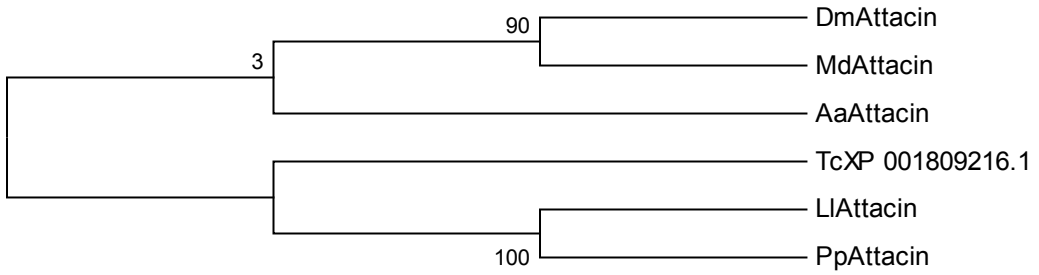

Figure A.7. Neighbor-joining tree to infer the evolutionary relationship of Attacin sequences.

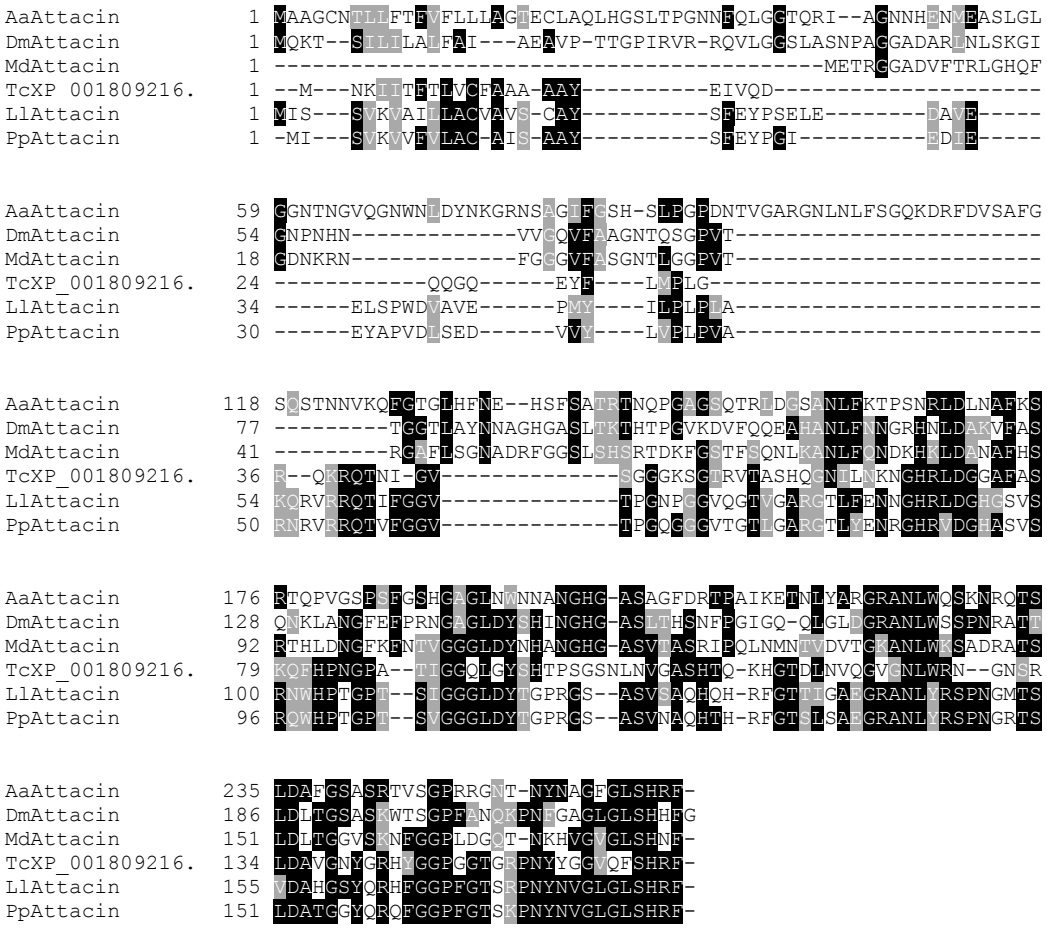

Figure A.8. Clustal Omega protein alignment of Attacin sequences from *L. longipalpis*, *P. papatasi*, *D. melanogaster*, *A. aegyti*, and *T. castaneum*.

>Ll_ATG1_LLOJ007855

ATGATGGAGATTGTGGGTGACTATGAGTACAACAGCAAAGATCTCATTGGGCACGGGGCATTTGCTGTTGTGTACAA

GGGACGCCACAGGAAGAAGCCAAGCCTGCAAGTGGCCATAAAGAGTATAACAAAGAAGAGTCTCGCTAAGAGTCAAA

ATCTCCTTGGGAAGGAGATAAAAATACTCAAAGAGCTCACTGAGCTGCACCATGAGAACGTCGTGGCTCTGCTGGAC

TGCAAGGAGTCCCAGCACAATGTGTACCTTGTGATGGAGTACTGCAATGGA**GGTGATTTGGCGGACTAC**TTAAATGG

GAGGGGCTCCCTCAGTGAGGACACCATTAGGCTCTTCCTCGTGCAGCTGGCTGGTGCCATGAAGGCACTTTTCGCCA

AGGGGATCGTCCATCGGGACCTCAAGCCACAGAATATTCTATTATCACACTCAAATGGAAAAACCTTTCCGCCCCCG

TCGAAGATTAAGCTGAAAATTGCGGACTTTGGCTTTGCACGCTTCCTCCAAGATGGGAATATGGCGGCCACGCTATG

TGGTTCACCCATGTACATGGCGCCCGAGGTGATAATGTCCCTTCAGTACGACGCCAAGGCGGACCTGTGGTCATTGG

GAACAATTGTATTTCAATGCCTGACGGGAAAGGCACCATTCCAGGCCCAAACGCCGCAGGAATTGAGGAATTTCTAT

GAGAAGAATGATGGGTTAGCACCGAAAATTCCACCAGGTACCACGCCCGAGTTAACAGACCTCCTAATGGGACTTCT

CAGGCGCAATGCAAAGGATCGCATGAGTTTCGACAGATTCTTCAATCATCCCTTCCTGCAGCGTCCGGCTACGCCAC

AAACACCCAAAGCCCCCTCACCCCCATCACCCATTCCCATGGCACCGGCAGCAGAACCCGAAAGTGCCGCCATTGCG

TCCAGCAGTCACAGCTCCGATAAGTCATCGAGTCAAGAGAGTTCCGATGATTTTGTCCTGGTACCAAATAATTTACC

CAGTGACGCCACAGTGGTGAACTACGAGCGTCGTCAGAGTCGCGTCTCACTGGGTGGCTCCCCGCAGGCTCCTGTTG

CATCGAGTCCACCCTCCCGACCGAGTACGTTGCCCATTTCAGAGCCAAAACCCGTACCACAACCCATCCGTACGGGA

GCAGCAATCCCGCGAAGTCAGCCCATCACGATGAAGCGTTCGGAGAATCGCTCAGGCCCGGAGATTAGTTCCATTTC

CCCGCCAGCTGTGCAGTTTGTCATTGGAACACCACCAGATGGGAAACGGCGACGTTCCACATCAGCGGGATCCTTGT

CTGAATCACCGCAGATATGGAGTGAAACACCCCCTCCGCCACCGTGTACGTGGCAAGTTAGCCCCGCGGCATCCCAC

CAGTCACCATTGCGACGCTACCCCTCAGGATCACCCGTCCTGGCGGCAAAGATGCCCCTCAAGCTCACAAGTCAGAT

TGTTTTGCCTGATTTTGTGGGGCTCGGTGGCCCTGGGGAGCATCCAATTACTTTCCACGCACCCGAATTACCGGCAG

AGACAATTCTCGAAAGGGAACACAATGAAACGTTGGCAAAGTTGAATTTTGTCCTCGCACTCACGGATTGTATTCTC

GAAGTTGCGGACGCCAGATGTGCCCCATTGTCTGCTCTCATGTCTGCCGATGCGCCCCCCATTACGCCCCATGCACC

GGAACACTGCAAGCGTGCTGAACGTCTCGTGCTCCTTGTCAGAGCGCTGCACCTTCTTCGCTCGGGAATGCATTTGG

CCCAGGAGCAATTGCAACAAGGTCAACTAAAACCATCCAATACTGTGAAGAATGTTTTGCAGACGATGAACAATAAG

TATCGCTCAACGCTGTACGAAAGCAAGAAACTCAATGGAACGGGTTTGCTGAGGAAGGCAAATGCCAGCAATATAAC

AGCCGATAAAATTCTCTACGATCACGCCATTCAGATGTGCCAATCAGCGGCACTTGATGAGCTCTTTGGCAATCCCG

AGGATTGTTTTGCGCGATACCAAACGGCACAGATTCTCCTGCATTCGTTGGCGCAGAAATGCAACAATCCCCAGGAT

AAGATGCTCTCGTCCAAGTACAAGGATGCCGTGGAGAAGAGATTGTACATTCTGCAGCAGCAGGGTTACATCTATGC

AACGCAGGAGGATGAATTGGCGTAA

Figure A.9. Putative CDS for mRNA encoding *L. longipalpis* ATG1.

Full length predicted mRNA is depicted in black, while the primers used for RT-qPCR amplicon measurement are shown in pink. Sequences in blue denote agreement between prediction and sequenced amplicons, while nucleotides in red depict a difference at that base pair.

>ATG8

ATGAAGTTCCAATACAAGGAGGAGCATCCCTTTGAGAAGAGACGTGCCGAGGGTGACAAAATCCGCAGGAAATATCC

GGATCGTGTTCCTGTGATTGTGGAGAAGGCACCAAAGGCGAGAATTGGGGATTTGGACAAGAA**GAAGTACCTTGTGC**

CGTCTGATTTGACTGTTGGCCAATTCTACTTTCTCATCCGCAAGCGAATTCACTTGCGCCCTGAGGATGCTCTCTTC

TTCTTTGTCAACAATGTGATTCCGCCCACATCCGCATCAATGGGATCTCTGTACCAGGAGCATCACGAAGAAGACTG

TTTCCTCTACATTGTCTACTCCGATGAGAATGTCTACGGCAAGAGGTTCTAA

Figure A.10. Putative CDS for mRNA encoding *L. longipalpis* ATG8.

Full length predicted mRNA is depicted in black, while the primers used for RT-qPCR amplicon measurement are shown in pink. Sequences in blue denote agreement between prediction and sequenced amplicons, while nucleotides in red depict a difference at that base pair.

>Duox

ATGACTGTGATGAGAACAAGCTTGTCAAAGGCTGAATTTGCATCGGCTCTGGGAATGAAATCGGACGATATGTTTGT

GCGGAAAATGTTCAATATCGTCGACAAGGATCAGGATGGTCGAATCTCCTTTCAGGAATTTCTCGAAACAGTGGTGT

TATTCTCGCGC**GGCAAGACGGAAGACAAG**CTGCGGATTATCTTTGATATGTGCGACAACGATAGGAATGGTGTGATT

GATAAGGGGGAACTGAGCGAGATGATGCGTTCCCTTGTTGAGATTGCGCGCACAACAAGCCTGGGGGATGATCAGGT

GACGGAACTAATTGATGGGATGTTCCAAGATGTTGGCCTGGAGCACAAGAATCATCTCACCTATCAGGATTTCAAGT

TGATGATGAAGGAGTACAAGGGGGAGTTTGTGGCCATTGGGCTGGATTGCAAGGGGGCCAAGCAGAACTTCCTCGAT

ACATCGACAAATGTTGCGCGCATGACGTCATTCCACATTGAGCCAATGATGGACTCAAGACGCCACTGGATGCTCGA

GAAGTGGGACAGCTACACGACATTCCTTGAGGAGAATCGCCAAAATATCTTCTACCTGTTCTTGTTCTACGTCGTAA

CCATTGTGCTGTTCGTTGAGCGATTCATTCACTATTCCTTCATGGCGGAACATACGGATCTGAGGCATATCATGGGT

GTTGGCATAGCCATTACACGTGGCTCAGCAGCATCGTTGTCCTTCTGCTATTCCTTGCTGCTGCTAACAATGTCACG

GAATCTCCTGACGAAGCTCAAAGAATTCCCCATACAGCAGTATATTCCACTGGATTCGCACATTCAATTCCACAAAA

TTGCTGCCTGTACTGCTTTATTCTTCTCCCTGCTGCACACAGTGGGGCACATTGTGAACTTCTATCATGTCTCCACG

CAGAGTATTGAGAACCTTCGTTGCCTCACGCGTGAAGTTCACTTTACCTCAGACTACAAGCCAGACATCAGTTTTTG

GCTCTTCCAGACCGTCACGGGAGTCACGGGGGTGATTCTCTTCATCACCATGTGCATAATTTTTGTCTTTGCCCATC

CCACAATCCGGAAGAAGGCCTACAAGTTCTTCTGGAATATGCATTCACTCTTCATCCTACTCTACATTCTCTGTCTC

ATCCACGGACTGGCCAGACTGACGGGACCACCGCGGTTTTGGCTCTTCTTCATTGGACCCGGAATTATCTACACGCT

GATTGTCTCTCTGCGTACAAAGTACATGGCTCTGGATGTGATGGAAACGGATCTCCTCCCGTCTGATGTGATTAAAA

TTAAATTCTATCGCCCGCCGAATCTCAAATATCTCTCCGGGCAGTGGGTGAGGTTGTCGTGTACGGCCTTCCGCCCG

CAGGAGATGCACAGCTTCACACTCACCTCGGCGCCACATGAGAACTTCCTGAGTTGCCACATAAAGGCACAGGGACC

GTGGACGTGGAAGTTGCGCAACTATTTCGATCCGTGCAACTACAACCCCGAAGATCAGCCAAAGATTCGCATCGAGG

GGCCCTTTGGGGGTGGCAATCAGGATTGGTATAAGTTTGAGGTGGCCGTAATGGTGGGCGGTGGTATTGGGGTGACG

CCCTATGCGTCCATCCTCAATGACTTAGTCTTCGGTACCAGTACAAATCGCTACTCAGGTGTGGCGTGCAAGAAAGT

CTACTTCCTCTGGATATGCCCGTCGCACAAGCACTTTGAATGGTTCATTGATGTGCTGCGCGATGTGGAGAAGAAGG

ATGTAACGAATGTCCTCGAGATTCATATTTTCATCACACAATTCTTCCATAAGTTCGATCTACGAACGACAATGTTG

Figure A.11. Putative CDS for mRNA encoding *L. longipalpis* Duox.

Full length predicted mRNA is depicted in black, while the primers used for RT-qPCR amplicon measurement are shown in pink. Sequences in blue denote agreement between prediction and sequenced amplicons, while nucleotides in red depict a difference at that base pair.

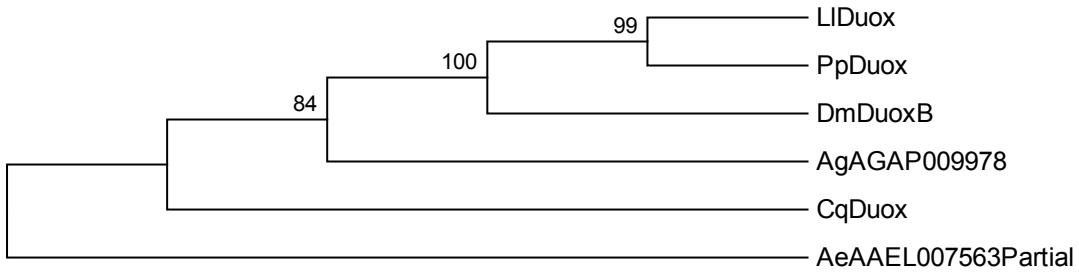

Figure A.12. Neighbor-joining tree to infer the evolutionary relationship of Duox sequences.

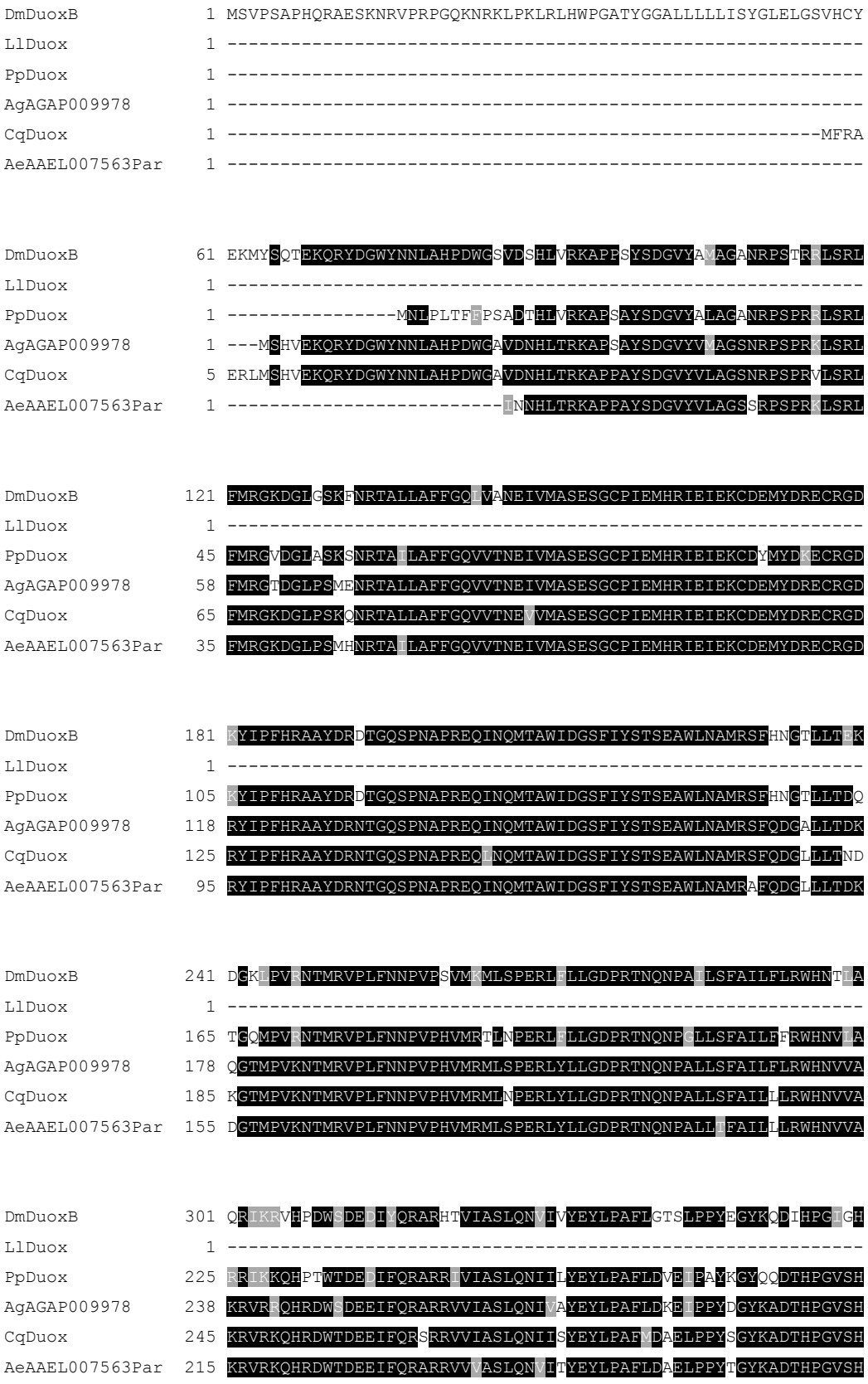
DmDuoxB 1 MSVPSAPHQRAESKNRVPRPGQKNRKLPKLRLHWPGATYGGALLLLLISYGLELGSVHCY
LlDuox 1
PpDuox 1
AgAGAP009978 1
CqDuox 1 MFRA
AeAAEL007563Par 1
DmDuoxB 61 EKMYSQTEKQRYDGWYNNLAHPDWGSVDSHLVRKAPPSYSDGVYAMAGANRPSTRRLSRL
LlDuox 1
PpDuox 1 MNLPLTFFPSADTHLVRKAPSAYSDGVYALAGANRPSPRRLSRL
AgAGAP009978 1 MSHVEKQRYDGWYNNLAHPDWGAVDNHLTRKAPSAYSDGVYVMAGSNRPSPRKLSRL
CqDuox 5 ERLMSHVEKQRYDGWYNNLAHPDWGAVDNHLTRKAPPAYSDGVYVLAGSNRPSPRVLSRL
AeAAEL007563Par 1 INNHLTRKAPPAYSDGVYVLAGSSRPSPRKLSRL
DmDuoxB 121 FMRGKDGLGSKFNRTALLAFFGQLVANEIVMASESGCPIEMHRIEIEKCDEMYDRECRGD
LlDuox 1
PpDuox 45 FMRGVDGLASKSNRTALLAFFGQVVTNEIVMASESGCPIEMHRIEIEKCDYMYDKECRGD
AgAGAP009978 58 FMRGTDGLPSMENRTALLAFFGQVVTNEIVMASESGCPIEMHRIEIEKCDEMYDRECRGD
CqDuox 65 FMRGKDGLPSKQNRTALLAFFGQVVTNEVVMASESGCPIEMHRIEIEKCDEMYDRECRGD
AeAAEL007563Par 35 FMRGKDGLPSMHNRTALLAFFGQVVTNEIVMASESGCPIEMHRIEIEKCDEMYDRECRGD
DmDuoxB 181 KYIPFHRAAYDRDTGQSPNAPREQINQMTAWIDGSFIYSTSEAWLNAMRSFHNGTLLTEK
LlDuox 1
PpDuox 105 KYIPFHRAAYDRDTGQSPNAPREQINQMTAWIDGSFIYSTSEAWLNAMRSFHNGTLLTDQ
AgAGAP009978 118 RYIPFHRAAYDRNTGQSPNAPREQINQMTAWIDGSFIYSTSEAWLNAMRSFQDGALLTDK
CqDuox 125 RYIPFHRAAYDRNTGQSPNAPREQLNQMTAWIDGSFIYSTSEAWLNAMRSFQDGLLLTND
AeAAEL007563Par 95 RYIPFHRAAYDRNTGQSPNAPREQINQMTAWIDGSFIYSTSEAWLNAMRAFQDGLLLTDK
DmDuoxB 241 DGKLPVFNTMRVPLFNNPVPSVMKMLSPERLFLLGDPRTNQNPAILSFAILFLRWHNTLA
LlDuox 1
PpDuox 165 TGQMPVFNTMRVPLFNNPVPHVMRTLNPERLFLLGDPRTNQNPGLLSFAILFFRWHNVLA
AgAGAP009978 178 QGTMPVKNTMRVPLFNNPVPHVMRMLSPERLYLLGDPRTNQNPALLSFAILFLRWHNVVA
CqDuox 185 KGTMPVKNTMRVPLFNNPVPHVMRMLNPERLYLLGDPRTNQNPALLSFAILLLRWHNVVA
AeAAEL007563Par 155 DGTMPVKNTMRVPLFNNPVPHVMRMLSPERLYLLGDPRTNQNPALLTFAILLLRWHNVVA
DmDuoxB 301 QRIKRVEPDWSDEDIYQRARHTVIASLQNVIVYEYLPAFLGTSLPPYEGYKQDIHPGIGH
LlDuox 1
PpDuox 225 RRIKKQHPTWTDEDIFQRARRIVIASLQNIILYEYLPAFLDVEIPAYKGYQQDTHPGVSH
AgAGAP009978 238 KRVRKQHRDWSDEEIFQRARRVVIASLQNIVAYEYLPAFLDKEIPPYDGYKADTHPGVSH
CqDuox 245 KRVRKQHRDWTDEEIFQRSRRVVIASLQNIISYEYLPAFVDAELPPYSGYKADTHPGVSH
AeAAEL007563Par 215 KRVRKQHRDWTDEEIFQRARRVVVASLQNVITYEYLPAFLDAELPPYTGYKADTHPGVSH

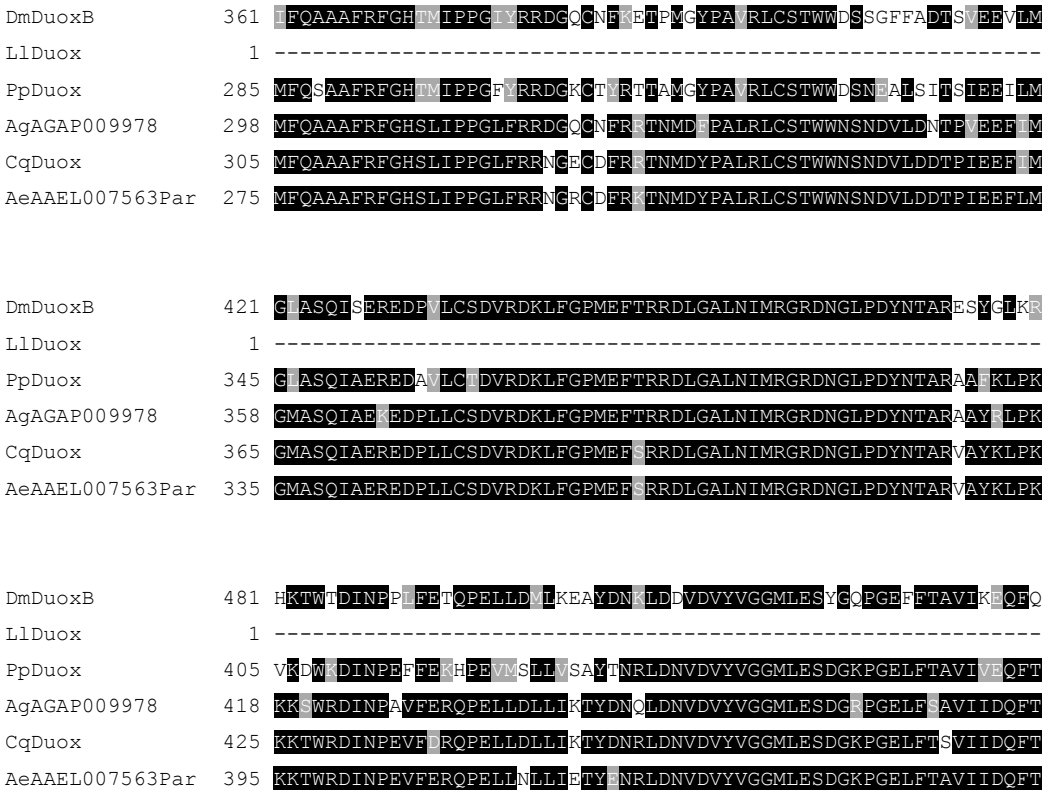
DmDuoxB 361
LlDuox 1
PpDuox 285
AgAGAP009978 298
CqDuox 305
AeAAEL007563Par 275
DmDuoxB 421
LlDuox 1
PpDuox 345
AgAGAP009978 358
CqDuox 365
AeAAEL007563Par 335
DmDuoxB 481
LlDuox 1
PpDuox 405
AgAGAP009978 418
CqDuox 425
AeAAEL007563Par 395

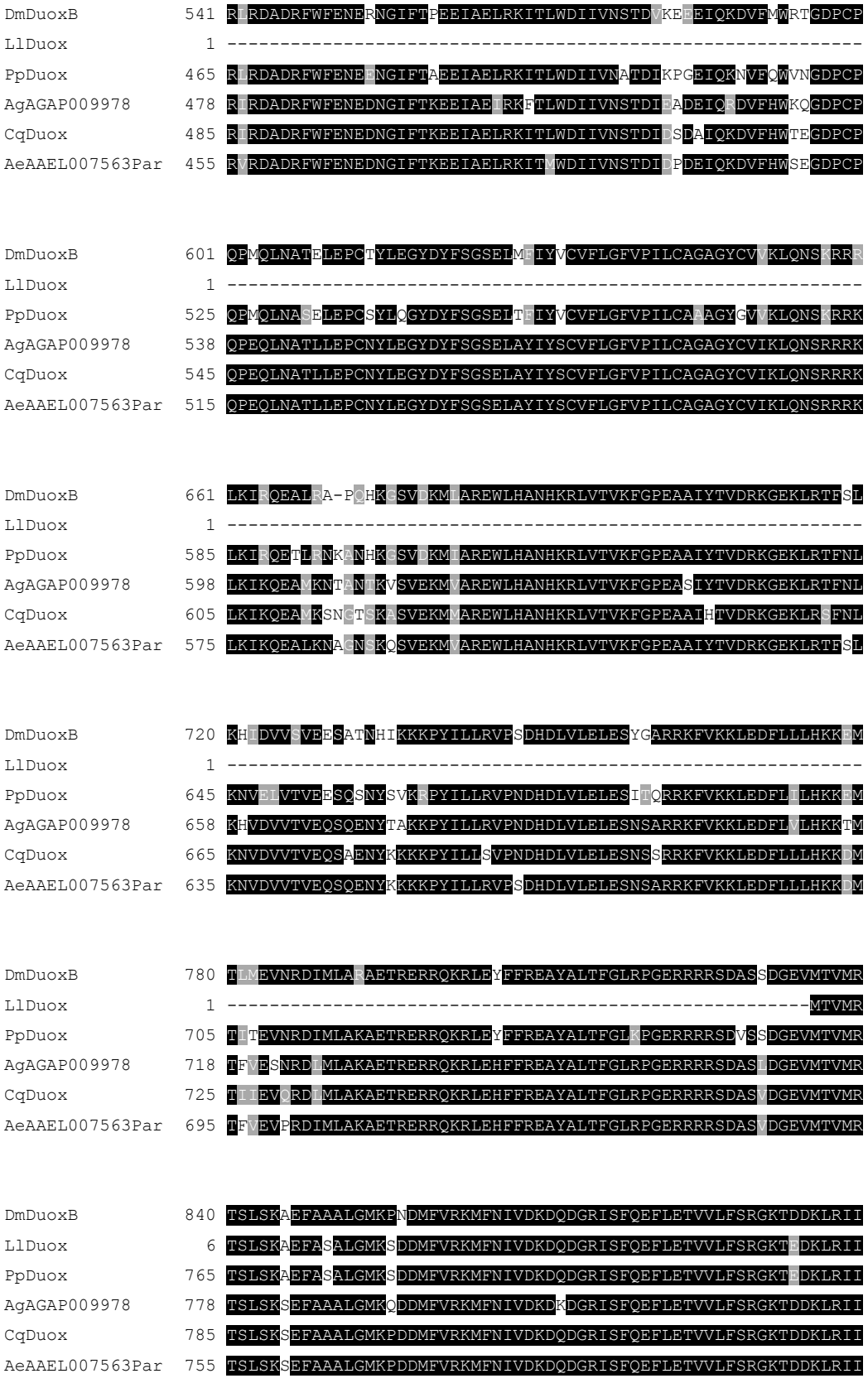
DmDuoxB 541 RIRDADRFWFENERNGIFTPEEIAELRKITLWDIIVNSTDVKEEEIQKDVFMWRTGDPCP
LlDuox 1 ----------
PpDuox 465 RIRDADRFWFENEENGIFTAEEIAELRKITLWDIIVNATDIKPGEIQKNVFQWVNGDPCP
AgAGAP009978 478 RIRDADRFWFENEDNGIFTKEEIAELRKFTLWDIIVNSTDIEADEIQRDVFHWKQGDPCP
CqDuox 485 RIRDADRFWFENEDNGIFTKEEIAELRKITLWDIIVNSTDIISDAIQKDVFHWTEGDPCP
AeAAEL007563Par 455 RVRDADRFWFENEDNGIFTKEEIAELRKITVWDIIVNSTDIIPDEIQKDVFHWSEGDPCP
DmDuoxB 601 QPMQLNATELEPCTYLEGYDYFSGSELMSIYVCVFLGFVPILCAGAGYCVVKLQNSKRRR
LlDuox 1 ----------
PpDuox 525 QPMQLNASELEPCSYLQGYDYFSGSELTSIYVCVFLGFVPILCAAAGYGVVKLQNSKRRK
AgAGAP009978 538 QPEQLNATLLEPCNYLEGYDYFSGSELAYIYSCVFLGFVPILCAGAGYCVIKLQNSRRRK
CqDuox 545 QPEQLNATLLEPCNYLEGYDYFSGSELAYIYSCVFLGFVPILCAGAGYCVIKLQNSRRRK
AeAAEL007563Par 515 QPEQLNATLLEPCNYLEGYDYFSGSELAYIYSCVFLGFVPILCAGAGYCVIKLQNSRRRK
DmDuoxB 661 LKIRQEALRA-PQHKGSVDKMLAREWLHANHKRLVTVKFGPEAAIYTVDRKGEKLRTFSL
LlDuox 1 ----------
PpDuox 585 LKIKQETLRNKANHKGSVDKMIAREWLHANHKRLVTVKFGPEAAIYTVDRKGEKLRTFNL
AgAGAP009978 598 LKIKQEAMKNTANTKVSVEKMVAREWLHANHKRLVTVKFGPEASIYTVDRKGEKLRTFNL
CqDuox 605 LKIKQEAMKSNGTSKASVEKMMAREWLHANHKRLVTVKFGPEAAIHTVDRKGEKLRSFNL
AeAAEL007563Par 575 LKIKQEALKNAGNSKQSVEKMVAREWLHANHKRLVTVKFGPEAAIYTVDRKGEKLRTFSL
DmDuoxB 720 KHIDVVSVEESATNHIKKKPYILLRVPSDHDLVLELESYGARRKFVKKLEDFLLLHKKEM
LlDuox 1 ----------
PpDuox 645 KNVEIVTVEESQSNYSVKPPYILLRVPNDHDLVLELESIIQRRKFVKKLEDFLILHKKEM
AgAGAP009978 658 KHVDVVTVEQSQENYTAKKPYILLRVPNDHDLVLELESNSARRKFVKKLEDFLVLHKKTM
CqDuox 665 KNVDVVTVEQSAENYKKKKPYILLSVPNDHDLVLELESNSSRRKFVKKLEDFLLLHKKDM
AeAAEL007563Par 635 KNVDVVTVEQSQENYKKKKPYILLRVPSDHDLVLELESNSARRKFVKKLEDFLLLHKKDM
DmDuoxB 780 TLMEVNRDIMLARAETRERRQKRLEYFFREAYALTFGLRPGERRRRSDASSDGEVMTVMR
LlDuox 1 ----------MTVMR
PpDuox 705 TITEVNRDIMLAKAETRERRQKRLEYFFREAYALTFGLKPGERRRRSDVSSDGEVMTVMR
AgAGAP009978 718 TFVESNRDLMLAKAETRERRQKRLEHFFREAYALTFGLRPGERRRRSDASLDGEVMTVMR
CqDuox 725 TIIEVQRDLMLAKAETRERRQKRLEHFFREAYALTFGLRPGERRRRSDASVDGEVMTVMR
AeAAEL007563Par 695 TFVEVPRDIMLAKAETRERRQKRLEHFFREAYALTFGLRPGERRRRSDASVDGEVMTVMR
DmDuoxB 840 TSLSKAEFAAALGMKPNDMFVRKMFNIVDKDQDGRISFQEFLETVVLFSRGKTDDKLRII
LlDuox 6 TSLSKAEFASALGMKSDDMFVRKMFNIVDKDQDGRISFQEFLETVVLFSRGKTEDKLRII
PpDuox 765 TSLSKAEFASALGMKSDDMFVRKMFNIVDKDQDGRISFQEFLETVVLFSRGKTEDKLRII
AgAGAP009978 778 TSLSKSEFAAALGMKQDDMFVRKMFNIVDKDKDGRISFQEFLETVVLFSRGKTDDKLRII
CqDuox 785 TSLSKSEFAAALGMKPDDMFVRKMFNIVDKDQDGRISFQEFLETVVLFSRGKTDDKLRII
AeAAEL007563Par 755 TSLSKSEFAAALGMKPDDMFVRKMFNIVDKDQDGRISFQEFLETVVLFSRGKTDDKLRII

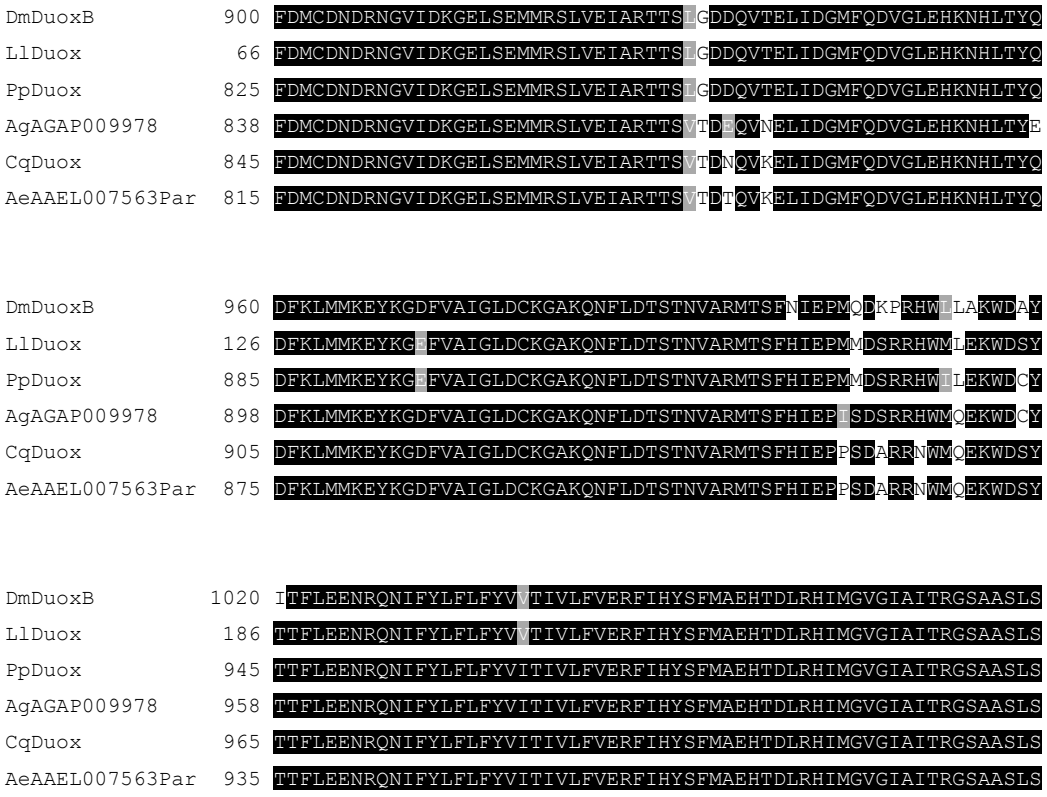
DmDuoxB 900 FDMCDNDRNGVIDKGELSEMMRSLVEIARTTSLGDDQVTELIDGMFQDVGLEHKNHLTYQ
LlDuox 66 FDMCDNDRNGVIDKGELSEMMRSLVEIARTTSLGDDQVTELIDGMFQDVGLEHKNHLTYQ
PpDuox 825 FDMCDNDRNGVIDKGELSEMMRSLVEIARTTSLGDDQVTELIDGMFQDVGLEHKNHLTYQ
AgAGAP009978 838 FDMCDNDRNGVIDKGELSEMMRSLVEIARTTSVTDEQVNELIDGMFQDVGLEHKNHLTYE
CqDuox 845 FDMCDNDRNGVIDKGELSEMMRSLVEIARTTSVTDNQVKELIDGMFQDVGLEHKNHLTYQ
AeAAEL007563Par 815 FDMCDNDRNGVIDKGELSEMMRSLVEIARTTSVTDTQVKELIDGMFQDVGLEHKNHLTYQ
DmDuoxB 960 DFKLMMKEYKGDFVAIGLDCKGAKQNFLDTSTNVARMTSFNIEPMQDKPRHWLLAKWDAY
LlDuox 126 DFKLMMKEYKGEFVAIGLDCKGAKQNFLDTSTNVARMTSFHIEPMMDSRRHWMLEKWDSY
PpDuox 885 DFKLMMKEYKGEFVAIGLDCKGAKQNFLDTSTNVARMTSFHIEPMMDSRRHWILEKWDCY
AgAGAP009978 898 DFKLMMKEYKGDFVAIGLDCKGAKQNFLDTSTNVARMTSFHIEPISDSRRHWMQEKWDCY
CqDuox 905 DFKLMMKEYKGDFVAIGLDCKGAKQNFLDTSTNVARMTSFHIEPPSDARRNWMQEKWDSY
AeAAEL007563Par 875 DFKLMMKEYKGDFVAIGLDCKGAKQNFLDTSTNVARMTSFHIEPPSDARRNWMQEKWDSY
DmDuoxB 1020 ITFLEENRQNIFYLFLFYVVTIVLFVERFIHYSFMAEHTDLRHIMGVGIAITRGSAASLS
LlDuox 186 TTFLEENRQNIFYLFLFYVVTIVLFVERFIHYSFMAEHTDLRHIMGVGIAITRGSAASLS
PpDuox 945 TTFLEENRQNIFYLFLFYVITIVLFVERFIHYSFMAEHTDLRHIMGVGIAITRGSAASLS
AgAGAP009978 958 TTFLEENRQNIFYLFLFYVITIVLFVERFIHYSFMAEHTDLRHIMGVGIAITRGSAASLS
CqDuox 965 TTFLEENRQNIFYLFLFYVITIVLFVERFIHYSFMAEHTDLRHIMGVGIAITRGSAASLS
AeAAEL007563Par 935 TTFLEENRQNIFYLFLFYVITIVLFVERFIHYSFMAEHTDLRHIMGVGIAITRGSAASLS

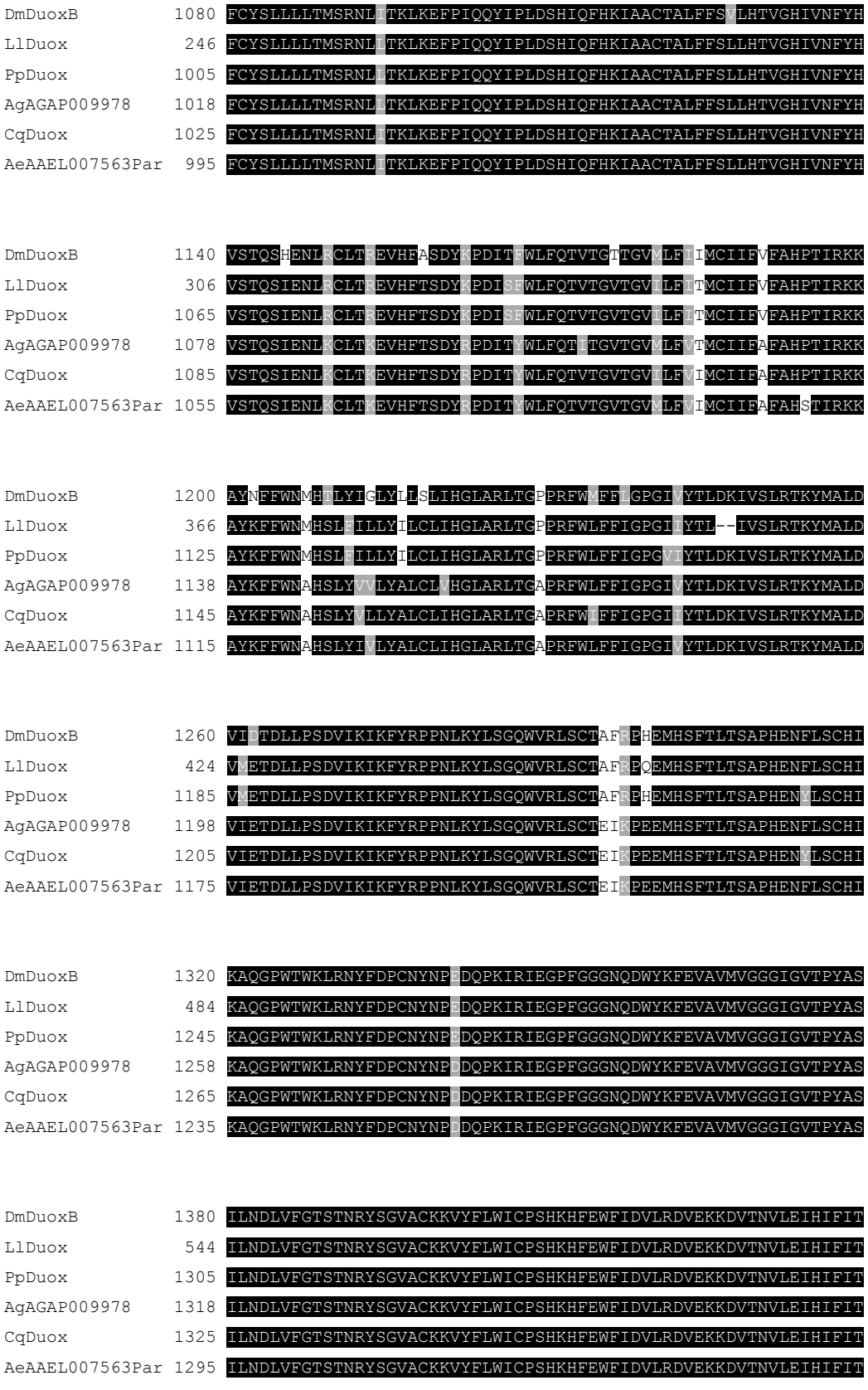
DmDuoxB 1080 FCYSLLLLTMSRNLITKLKEFPIQQYIPLDSHIQFHKIAACTALFFSVLHTVGHIVNFYH
LlDuox 246 FCYSLLLLTMSRNLLTKLKEFPIQQYIPLDSHIQFHKIAACTALFFSLLHTVGHIVNFYH
PpDuox 1005 FCYSLLLLTMSRNLLTKLKEFPIQQYIPLDSHIQFHKIAACTALFFSLLHTVGHIVNFYH
AgAGAP009978 1018 FCYSLLLLTMSRNLLTKLKEFPIQQYIPLDSHIQFHKIAACTALFFSLLHTVGHIVNFYH
CqDuox 1025 FCYSLLLLTMSRNLLTKLKEFPIQQYIPLDSHIQFHKIAACTALFFSLLHTVGHIVNFYH
AeAAEL007563Par 995 FCYSLLLLTMSRNLLTKLKEFPIQQYIPLDSHIQFHKIAACTALFFSLLHTVGHIVNFYH
DmDuoxB 1140 VSTQSHENLRCLTREVHEASDYKPDITFWLFQTVTGTTGVVLFIIMCIIFVFAHPTIRKK
LlDuox 306 VSTQSIENLRCLTREVHFTSDYKPDISFWLFQTVTGVTGVTLFITMCIIFVFAHPTIRKK
PpDuox 1065 VSTQSIENLRCLTREVHFTSDYKPDISFWLFQTVTGVTGVTLFITMCIIFVFAHPTIRKK
AgAGAP009978 1078 VSTQSIENLKCLTKEVHFTSDYRPDITYWLFQTITGVTGVVLFVTMCIIFAFAHPTIRKK
CqDuox 1085 VSTQSIENLKCLTKEVHFTSDYRPDITYWLFQTVTGVTGVTLFVIMCIIFAFAHPTIRKK
AeAAEL007563Par 1055 VSTQSIENLKCLTKEVHFTSDYRPDITYWLFQTVTGVTGVVLFVIMCIIFAFAHSTIRKK
DmDuoxB 1200 AYNFFWNMHTLYIGLYLLSLIHGLARLTGPPRFWMFFLGPGIVYTLDKIVSLRTKYMALD
LlDuox 366 AYKFFWNMHSLFILLYILCLIHGLARLTGPPRFWLFFIGPGIIYTL--IVSLRTKYMALD
PpDuox 1125 AYKFFWNMHSLFILLYILCLIHGLARLTGPPRFWLFFIGPGVIYTLDKIVSLRTKYMALD
AgAGAP009978 1138 AYKFFWNAHSLYVVLYALCLVHGLARLTGAPRFWLFFIGPGIVYTLDKIVSLRTKYMALD
CqDuox 1145 AYKFFWNAHSLYVLLYALCLIHGLARLTGAPRFWIFFIGPGIIYTLDKIVSLRTKYMALD
AeAAEL007563Par 1115 AYKFFWNAHSLYIVLYALCLIHGLARLTGAPRFWLFFIGPGIVYTLDKIVSLRTKYMALD
DmDuoxB 1260 VIDTDLLPSDVIKIKFYRPPNLKYLSGQWVRLSCTAFRPHEMHSFTLTSAPHENFLSCHI
LlDuox 424 VVETDLLPSDVIKIKFYRPPNLKYLSGQWVRLSCTAFRPQEMHSFTLTSAPHENFLSCHI
PpDuox 1185 VVETDLLPSDVIKIKFYRPPNLKYLSGQWVRLSCTAFRPHEMHSFTLTSAPHENYLSCHI
AgAGAP009978 1198 VIETDLLPSDVIKIKFYRPPNLKYLSGQWVRLSCTEIKPEEMHSFTLTSAPHENFLSCHI
CqDuox 1205 VIETDLLPSDVIKIKFYRPPNLKYLSGQWVRLSCTEIKPEEMHSFTLTSAPHENYLSCHI
AeAAEL007563Par 1175 VIETDLLPSDVIKIKFYRPPNLKYLSGQWVRLSCTEIKPEEMHSFTLTSAPHENFLSCHI
DmDuoxB 1320 KAQGPWTWKLRNYFDPCNYNPEDQPKIRIEGPFGGGNQDWYKFEVAVMVGGGIGVTPYAS
LlDuox 484 KAQGPWTWKLRNYFDPCNYNPEDQPKIRIEGPFGGGNQDWYKFEVAVMVGGGIGVTPYAS
PpDuox 1245 KAQGPWTWKLRNYFDPCNYNPEDQPKIRIEGPFGGGNQDWYKFEVAVMVGGGIGVTPYAS
AgAGAP009978 1258 KAQGPWTWKLRNYFDPCNYNPDDQPKIRIEGPFGGGNQDWYKFEVAVMVGGGIGVTPYAS
CqDuox 1265 KAQGPWTWKLRNYFDPCNYNPDDQPKIRIEGPFGGGNQDWYKFEVAVMVGGGIGVTPYAS
AeAAEL007563Par 1235 KAQGPWTWKLRNYFDPCNYNPDDQPKIRIEGPFGGGNQDWYKFEVAVMVGGGIGVTPYAS
DmDuoxB 1380 ILNDLVFGTSTNRYSGVACKKVYFLWICPSHKHFEWFIDVLRDVEKKDVTNVLEIHIFIT
LlDuox 544 ILNDLVFGTSTNRYSGVACKKVYFLWICPSHKHFEWFIDVLRDVEKKDVTNVLEIHIFIT
PpDuox 1305 ILNDLVFGTSTNRYSGVACKKVYFLWICPSHKHFEWFIDVLRDVEKKDVTNVLEIHIFIT
AgAGAP009978 1318 ILNDLVFGTSTNRYSGVACKKVYFLWICPSHKHFEWFIDVLRDVEKKDVTNVLEIHIFIT
CqDuox 1325 ILNDLVFGTSTNRYSGVACKKVYFLWICPSHKHFEWFIDVLRDVEKKDVTNVLEIHIFIT
AeAAEL007563Par 1295 ILNDLVFGTSTNRYSGVACKKVYFLWICPSHKHFEWFIDVLRDVEKKDVTNVLEIHIFIT

Figure A.13. Clustal Omega protein alignment of Duox sequences from *L. longipalpis*, *P. papatasi*, *D. melanogaster*, *A. gambiae*, *A. aegyti*, and *C. quinquefasciatus*.

>USP36

ATGGTGTGCGACATCGTCAGTGCGGCACTCCGCGAGTCACTTTCATCCGCCAAGGCG
GCGGAACGGGCTGACCGTAATCTCCAGACGCAGCTCGTTAGTACGACAAAGCGAAT
TTTTCTCACAAAAATTGAATACGAAGACGTGGACAGTACCCACAGCACTTGTGACGC
CCTCAAATCCAAATATATTGTCTTCAAACCAACTTCCGGCATTATTTCCGGTACCACT
GCTGAGGATAAAATGCCTGGTGTGTCAGCAGCCGGCTCCTGCTCGACACAGAATGG
CACAACTGCAGTGAATGGCAGCAGCAGCAAGGATGCTCAGTTGCCAGCACCCAAAC
GTGTCCTTTTTTCCCGCGACAGCGTGCAGGTGGGCTGGCGGGCGAGTGGACGAAAAT
GGCAGGTGGGCGCCGGGTTGATAAACATGGGTAACACGTGCTACCTCAATTCGACG
CTGCAGGCTCTCTTCCACGTGCCCGCCATTGCAAATTGGCTCATGGCCGACGATGCG
CACCGGGAATCATGCGAAGATTCCGGCGGTGGGCAGGGTGGTTGTATAAATTGCGC
AATGGCACGTACACTCATCTCGTCGCAAACAAACCAATCCCCCATTAAGCCGTGGCT
GATTCACTCAAAACTCCGGCTGGTGTGTAAGCACTTCTTCCCGGGGCGTCAGGAGGA
TGCGCATGAGTTCCTGCGGTACCTCGTGGAGGCCATGGAGAAGGCATACCTGGCAC
GCGTGAAGAATAGCCGTGATTTGGATCAGTACAGCAAGGAGACGACGCCTCTCAAT
CAAATTCTCGGTGGCTACCTACGGTCCACTGTGCGCTGCCTGGCGTGTGGGCACGTC
TCGACGACGTTCCAGCACTTTGAGGATCTCCTGTTGGACATTAGGAAAGCCAATACG
GTGGAAGAGGCCCTCGGGGGGTACTTCGCGCGTGAACGTCTCGAGGATATGGGCTA
CAAATGTGAGGCGTGCAAGAAGAAAACGTCCGCTACGAAGCAATTTAGCCTCGAAC
GTGCCCCCGTGGCGTTGTGTATTCAACTAAAACGCTTCTCCATGGCGGGTACGAAGC
TCAATAAACACGTGGCTATACGATCAAAGCTCGATCTTACCCCCTACGCGTCTGGGC
GTGCGTCTGGAGCGCCTCTTGTTTACCGTCTCGTTGCAATGGTGACGCATTTGGGTGC
TTCGCAGAATTGTGGGCACTACACGGCTATTGGGCTGACGGAAACGGGCAATTACT
ACCACTTTGACGATAGCACGGTACGACCAATTAGTGTGCAGAATGTCCTCCAGACAA
ATGCCTACATTATCTTCTACGAACTGGAAGATGGTGCCCCTGCAAAAGCCCATCAAC
CACCACCCCCAAGTACAGCTACGAGCGCCAGTGCACGCGAAGAGCTTCGCAGCAAT
GGGGAGATGTCAAATGGAATCACAACAAATGGGGCAAAAGACACGTCATCCCCAAT
GCGACACATTGAGCATCAGCCAGAGACAAAATCACCCTTCATTGGACCCCTTTTGCC
GGCTGAAGAGAAGACGCCGGAGAAGAAGGTAACCCTCAATGGGGATGCAAATCAG
AAGATTACCTTCAGCATTACACCACCGAGTAGTAGGGCGGCAGTCCTTCAGGCACA
GAGCACCAGCCCCGTAGCACGTCCCATTTCCTCCAGTAAACTCGTCACAGTGGCAAA

GAAGATGACCTTCAATGGTAGCTCAAATGGTGTTGCAGCAGCCCCAAAGAGATTCA
CCCCACTTATCCTCACGAATAAGAGCAACAATTCAGCGGATAAGGGCGCAGAGGGA
AAGTCCGTGGAGCAGGCAATGATACCACCAGCGGCGAAAAAGATGAAACTGCCGCC
ATCGCTTCAGCCCAAACCCAAAAGTCTCGTCCCCTATGAATCGGACGATGAGTCGAA
TCCATCGGAAAATGATGAACCAGTCATACTGAAGACACCAACAGGTGTGTGGCAGG
TTACACCAATGGATGATCCAAATGTAGTCAAGAACAGCATCCCAACATCGTCGTCCA
ATGGGGCTGCAGCAGCTGCTACACCAGCGCGGAAAGCAGCTCTCCCAGCACCTGAG
AATGGGGGAGGAAATGAAATTATACGTAACACTGCCACAGTTAATCATTTGCTCAA
GACAGGTGGGCATCGAGGCTATGGGGCATCGAATGTCTACTCGTGGAATGGCCAAA
AGACATCCCTCGACAGAGAGGTGCAAGAGGACAAGAAGGAAGAGCGGAAGCGTGA
ATTGGAGCATCAAATGGAGAATGGTGACATGGACAGAGGGAGGACGAAAAAGGTG
AAGGTGCACCATCCACCGGGGAAGGACAATCCGGGCTATAATCCCTTCCAGGAGTA
CCAGATGCGCAATTGGACGTGGCTCAATAATGGTCGTCAGGGCTACCAGGGGCACA
TCTACCGCCAAAAGTCCTACAGCAACAATCACTACAACAACTACCGGGGCCAAGGA
GGGGGTGGTGGTGGTGGCTTCCGGGGGCGCCATCGGGGTGTCTTTAATAGCAATTTC
CGTTCCCACCATGGCTACCGACGTGACAAATGA

Figure A.14. Putative CDS for mRNA encoding *L. longipalpis* USP36.

Full length predicted mRNA is depicted in black, while the primers used for RT-qPCR amplicon measurement are shown in pink. Sequences in blue denote agreement between prediction and sequenced amplicons, while nucleotides in red depict a difference at that base pair.

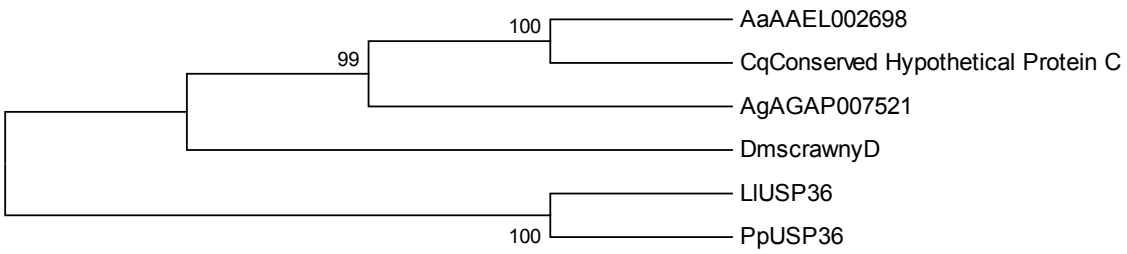

Figure A.15. Neighbor-joining tree to infer the evolutionary relationship of USP36 sequences.

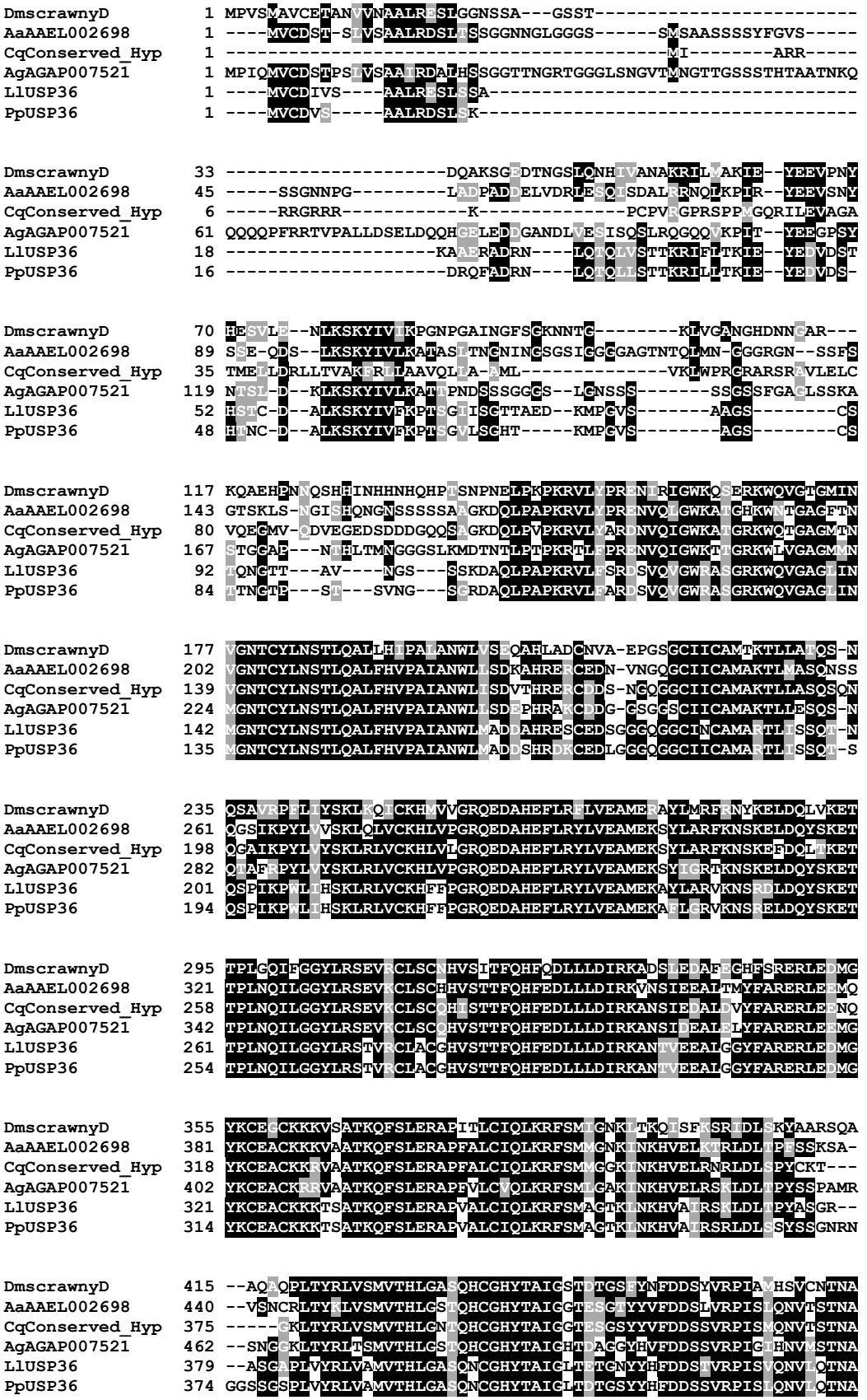

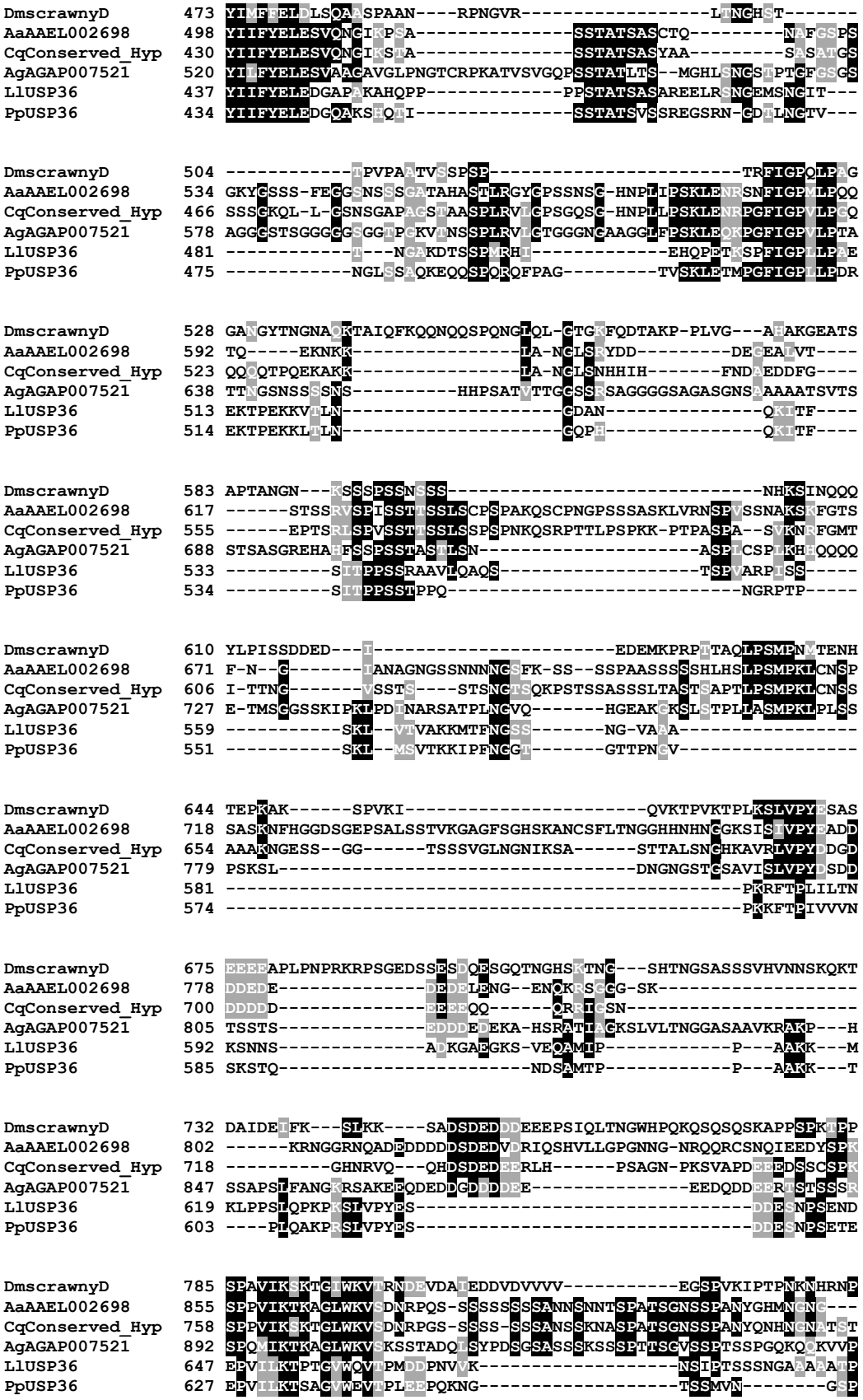
DmscrawnyD 473 YIMFTELDLSQAASPAAN----RPNGVR-----------------LTNGHST-------
AaAAEL002698 498 YIIFYELESVQNGIKPSA---------------SSTATSASCTQ---------NAFGSPS
CqConserved_Hyp 430 YIIFYELESVQNGIKSSA---------------SSTATSASYAA---------SASATGS
AgAGAP007521 520 YILFYELESVAAGAVGLPNGTCRPKATVSVGQPSSTATLTS--MGHLSNGSIPTGFGSGS
LlUSP36 437 YIIFYELEDGAPAKAHQPP-------------PPSTATSASAREELRSNGEMSNGIT---
PpUSP36 434 YIIFYELEDGQAKSHQII---------------SSTATSVSSREGSRN-GDILNGTV---
DmscrawnyD 504 ------------TPVPATTVSSPSP-------------------------TRFIGPQLPAG
AaAAEL002698 534 GKYGSSS-FEGGSNSSSGATAHASTLRGYGPSSNSG-HNPIIPSKLENRSNFIGPMLPQQ
CqConserved_Hyp 466 SSSGKQL-L-GSNSGAPAGSTAASPLRVLGPSGQSG-HNPLLPSKLENRPGFIGPVLPGQ
AgAGAP007521 578 AGGGSTSGGGGGSGGTPGKVLNSSPLRVLGTGGGNGAAGGLFPSKLEQKPGFIGPVLPTA
LlUSP36 481 ------------T---NGAKDTSSPMRHI-------------EHQPETKSPFIGPLLPAE
PpUSP36 475 ------------NGLSSAQKEQQSPQRQFPAG---------TVSKLETMPGFIGPLLPDR
DmscrawnyD 528 GANGYTNGNAQKTAIQFKQQNQQSPQNGTQL-GTGKFQDTAKP-PLVG---APAKGEATS
AaAAEL002698 592 TQ-----EKNKK----------------LA-NGLSRYDD---------DEGEAIVT----
CqConserved_Hyp 523 QQQQTPQEKAKK----------------LA-NGLSNHHIH-------FNDAEDDFG----
AgAGAP007521 638 TTNGSNSSSSNS----------HHPSATVTTGGSSRSAGGGGSAGASGNSPAAAATSVTS
LlUSP36 513 EKTPEKKVTLN----------------------GDAN---------------QKITF----
PpUSP36 514 EKTPEKKLTLN----------------------GQPH---------------QKITF----
DmscrawnyD 583 APTANGN---KSSSPSSNSSS-----------------------------NHKSINQQQ
AaAAEL002698 617 ------STSSRVSPISSTTSSLSCPSPAKQSCPNGPSSSASKLVRNSPVSSNAKSKFGTS
CqConserved_Hyp 555 ------EPTSRLSPVSSTTSSLSSPSPNKQSRPTTLPSPKK-PTPASPA--SVKNRFGMT
AgAGAP007521 688 STSASGREHAHFSSPSSTASILSN----------------------ASPLCSPLKHEQQQQ
LlUSP36 533 ----------SITPPSSRAAVLQAQS-------------------TSPVARPLSS-----
PpUSP36 534 ----------SITPPSSTPPQ-----------------------------NGRPTP-----
DmscrawnyD 610 YLPISSDDED---I----------------------EDEMKPRPTTAQLPSMPNMTENH
AaAAEL002698 671 F-N--G-------TANAGNGSSNNNNGSFK-SS--SSPAASSSSSHLHSLPSMPKLCNSP
CqConserved_Hyp 606 I-TTNG-------VSSTS-----STSNGTSQKPSTSSASSSLTASTSAPTLPSMPKLCNSS
AgAGAP007521 727 E-TMSGGSSKIPKLPDTNARSATPLNGVQ-------HGEAKGKSLSTPLLASMPKLPLSS
LlUSP36 559 -----------SKL--VTVAKKMTFNGSS-------NG-VAPA----------------
PpUSP36 551 -----------SKL--MSVTKKIPFNGGT-------GTTPNGV----------------
DmscrawnyD 644 TEPKAK------SPVKI----------------------QVKTPVKTPLKSLVPYESAS
AaAAEL002698 718 SASKNFHGGDSGEPSALSSTVKGAGFSGHSKANCSFLTNGGHHNHNGGKSISIVPYEADD
CqConserved_Hyp 654 AAAKNGESS--GG------TSSSVGLNGNIKSA------STTALSNGHKAVRLVPYDDGD
AgAGAP007521 779 PSKSL----------------------------------DNGNGSTGSAVISLVPYDSDD
LlUSP36 581 --PKRFTPLILTN
PpUSP36 574 --PKKFTPIVVVN
DmscrawnyD 675 EEEEAPLPNPRKRPSGEDSSESDQESGQTNGHSKTNG---SHTNGSASSSVHVNNSKQKT
AaAAEL002698 778 DDEDE--------------DEDELENG--ENQKRSGGG-SK--------------------
CqConserved_Hyp 700 DDDDD--------------EEEEQQ------QRRIGSN----------------------
AgAGAP007521 805 TSSTS--------------EDDDEDEKA-HSRATIAGKSLVLTNGGASAAVKRAKP---H
LlUSP36 592 KSNNS--------------ADKGAEGKS-VEQAMIP------------P---AAKK---M
PpUSP36 585 SKSTQ----------------------NDSAMTP------------P---AAKK---T
DmscrawnyD 732 DAIDEIFK---SIKK----SADSDEDDDEEEPSIQLTNGWHPQKQSQSQSKAPPSPKTPP
AaAAEL002698 802 ------KRNGGRNQADEDDDDDSDEDVDRIQSHVLLGPGNNG-NRQQRCSNQIEEDYSPK
CqConserved_Hyp 718 ----------GHNRVQ---QHDSDEDEERLH------PSAGN-PKSVAPDEEEDSSCSPK
AgAGAP007521 847 SSAPSIFANGKRSAKEEQDEDDGDDDDEE---------------EEDQDDEERRTSTSSSR
LlUSP36 619 KLPPSIQPKPKSLVPYES-------------------------------DDESNPSEND
PpUSP36 603 ----PIQAKPRSLVPYES-------------------------------DDESNPSETE
DmscrawnyD 785 SPAVIKSKTGIWKVTRNDEVDAIEDDVDVVVV-----------EGSPVKIPTPNKNHRNP
AaAAEL002698 855 SPPVIKTKAGLWKVSDNRPQS-SSSSSSSSANNSNNTSPATSGNSSPANYGHMNGNG---
CqConserved_Hyp 758 SPPVIKSKTGLWKVSDNRPGS-SSSS-SSSANSSKNASPATSGNSSPANYQNHNGNATST
AgAGAP007521 892 SPQIIKTKAGLWKVSKSSTADQLSYPDSGSASSSKSSSPTTSGVSSPTSSPGQKQCKVVP
LlUSP36 647 EPVIIKTPTGVWQVTPMDDPNVVK-------------------NSIPTSSSNGADAAATP
PpUSP36 627 EPVIIKTSAGVWEVTPLEEPQKNG-------------------TSSMVN--------GSP

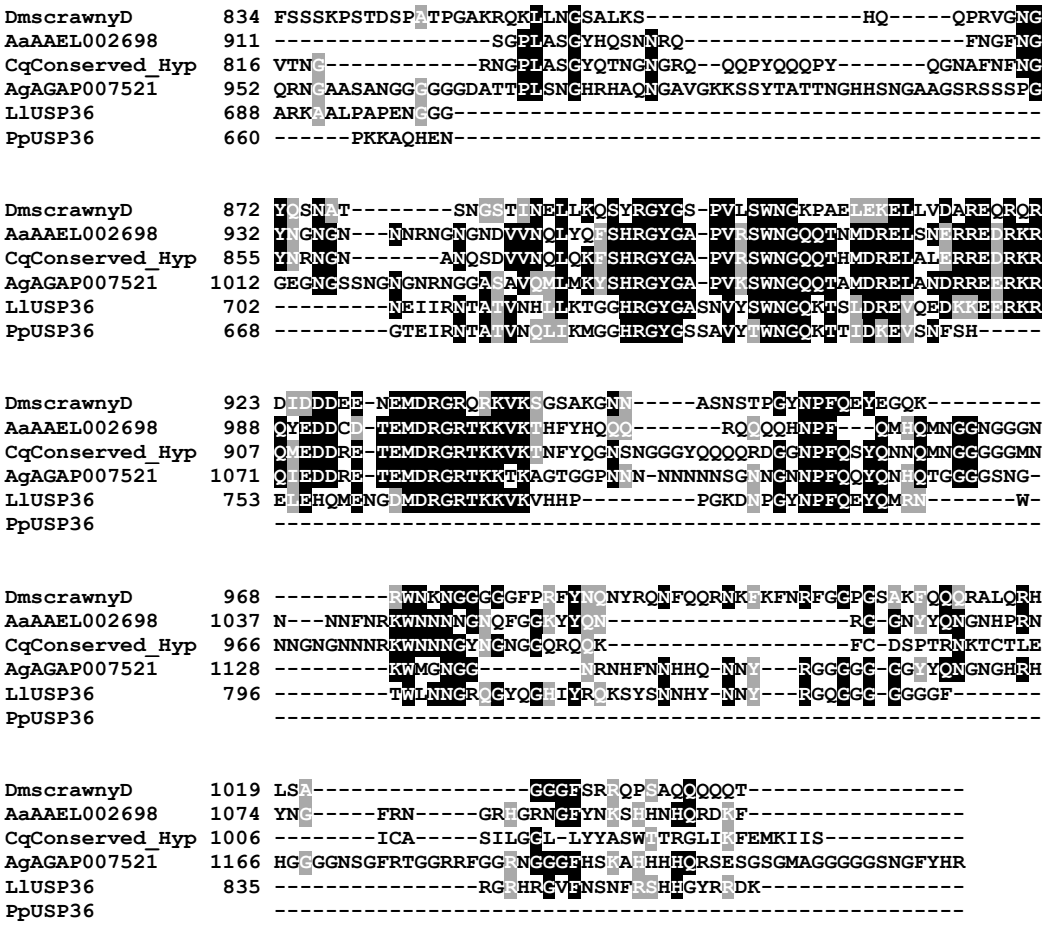

Figure A.16. Clustal Omega protein alignment of USP36 sequences from *L. longipalpis*, *P. papatasi*, *D. melanogaster*, *A. gambiae*, *A. aegyti*, and *C. quinquefasciatus*.

>IMD

ATGAAAGTCGTGAAAGTACCGGAAGAAGTGCGAATTTCAGTGAAAAATTCTCCAGAAAAAATGTCCAAAGTCTCAGA

GATTTTCTCAAATATCTTCACACGAACTGCCAAATCGGGCACCGGAAGTAGCTCCAAGAGTACTCAGGGGGTACTCA

AAACAGATGCTGGTCCCATTGCACCGAGAACAGATGAAGAAATCGAGGAAGCTGTGCTGGAAGAGCGAAATAATTCT

GAGACATCCTTCCCTTCCATCCCTCCCACACCGATTCCATCACTTGAGATCGCACGGCAAGAATCACAGATCAGTGT

CCCAGAGACACCATCACCTCTCCTGCCCATTCCTGGGGGTTCGGGAATGGATCATGGCAGAAGGAAGGATCAGTTGG

GATTGGCTCA**GGTGAACAACACTCAAGCAT**GCAATGTCTTCCAATTCACGAATGTCAATAATCTGCACATTGGATCA

GTTTTCAACATTACCACAGAGGCAGGAGGAGCTGAGGG**AGGAAGGAGAACC**TCTCCCAGACCCAGAGTAACGGAGAA

TGGTGAGAGAATCTTTAGGAAGACACCTTCAATTGATGCAATGATGAAGAGTCAGGAGAGGCTGGAGCATGAGCATA

TTGAAATTATTGCTACTCACCTTGGAGAAGACTGGAGGAATGTGGCACGAGATCTGGGATATTCTCAGGGACAGATT

GATCAACTCCTGGAGGATAATCACATCAATGGCATCAAAGAAGTGATTTATCAGATGATCCTCGGATGGACCCAAGA

CGACACAACTGCCACCCTTGGGAGGATTACGGAGATCTTATGGCGGAGACGACCACACCAGGAGGTTGTCTACTATC

TCAAGGAGTACTGGAAGCGAAATAATAAAACCAAAGCTCGCCGACAATCTGAAGTGAGTGCCGAATCAACCGAATAA

Figure A.17. Putative CDS for mRNA encoding *L. longipalpis* IMD.

Full length predicted mRNA is depicted in black, while the primers used for RT-qPCR amplicon measurement are shown in pink. Sequences in blue denote agreement between prediction and sequenced amplicons, while nucleotides in red depict a difference at that base pair.

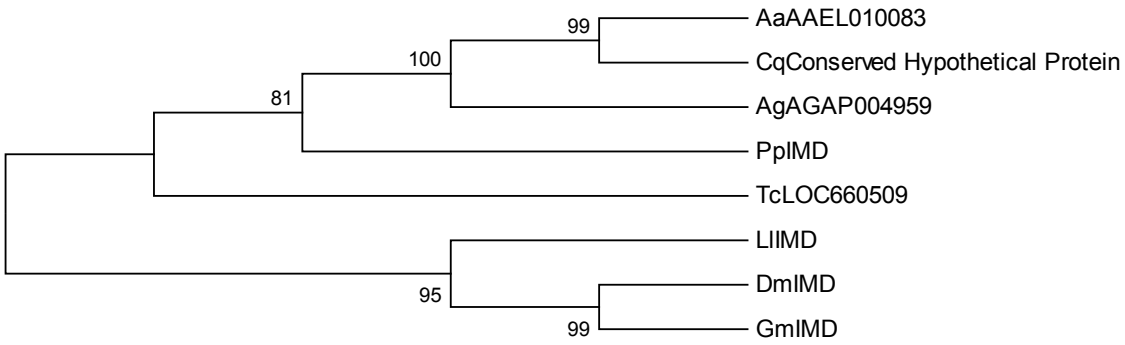

Figure A.18. Neighbor-joining tree to infer the evolutionary relationship of IMD sequences.

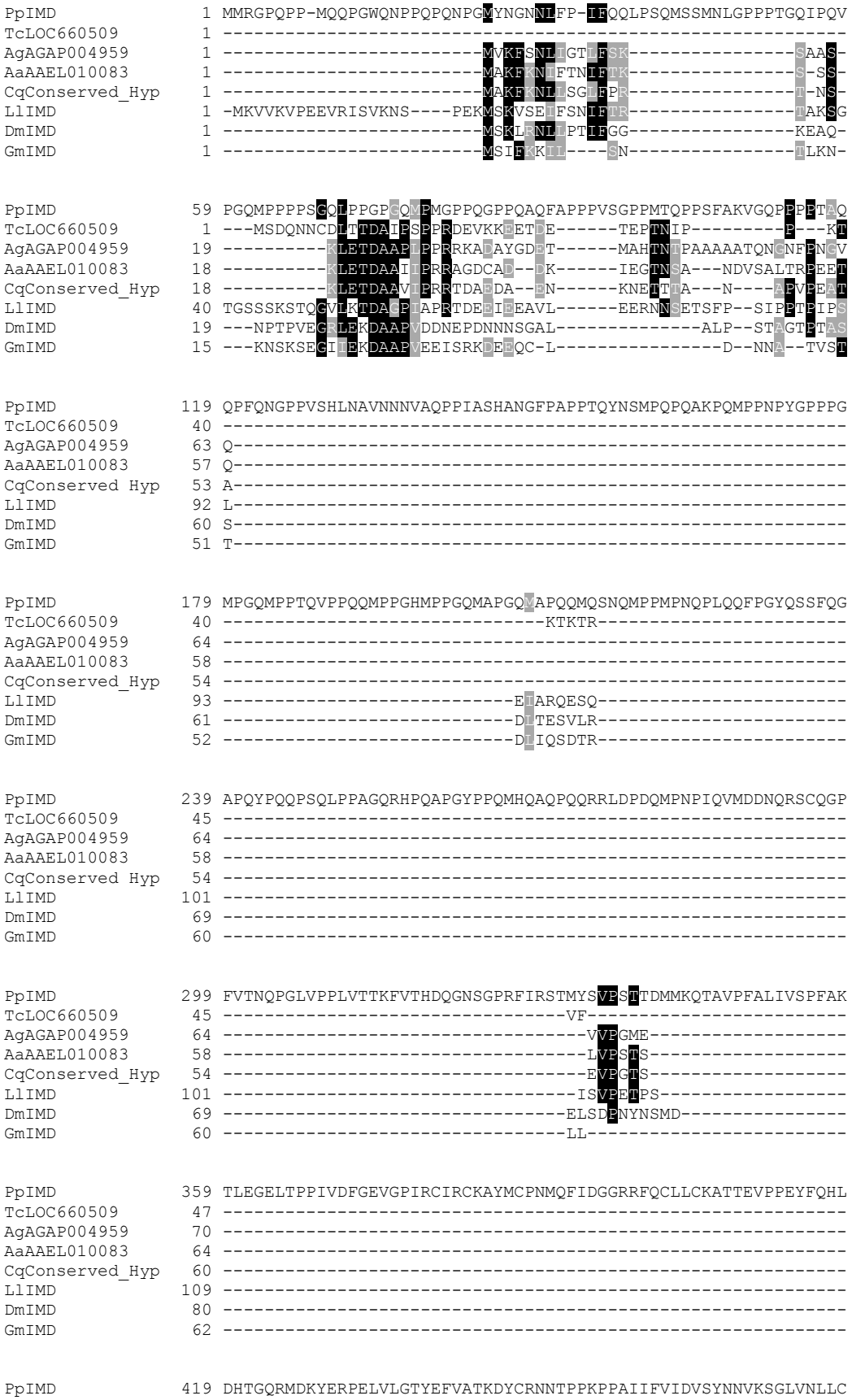
PpIMD 1 MMRGPQPP-MQQPGWQNPPQPQNPGMYNGNNLFP-IFQQLPSQMSSMNLGPPPTGQIPQV
TcLOC660509 1
AgAGAP004959 1 MVKFSNLIGTLFSK SAAS
AaAAEL010083 1 MAKFTNLFTNIFTK S-SS
CqConserved_Hyp 1 MAKFTNLLSGLFPR T-NS
LlIMD 1 -MKVVKVPEEVRISVKNS----PEKMSKVSEIFSNIFTR TAKSG
DmIMD 1 MSKLFNLLPTIFGG KEAQ
GmIMD 1 MSIFKKLL----SN TLKN
PpIMD 59 PGQMPPPPSGQLPPGPCQVPMGPPQGPPQAQFAPPPVSGPPMTQPPSFAKVGQPPPPTAQ
TcLOC660509 1 ---MSDQNNCDLTTDAIPSPPRDEVKKHETIE------TEPTNIP---------P---KT
AgAGAP004959 19 ----------KLETDAAPIPPRRKALAYGDET------MAHTNIPAAAAATQNCNFPNGV
AaAAEL010083 18 ----------KLETDAAIIPRRAGDCAS--LK------IEGTNSA---NDVSALTRPEET
CqConserved_Hyp 18 ----------KLETDAAVIPRRTDAHDA--EN------KNETTTA---N----APVPEAT
LlIMD 40 TGSSSKSTQGVLKTDAIPIAPRTDEEIHEAVL------EERNNSETSFP--SIPETPIPS
DmIMD 19 ---NPTPVEGRLEKDAAPVDDNEPDNNNSGAL--------------ALP--STAGTPTAS
GmIMD 15 ---KNSKSEGITEKDAAPVEEISRKDEHQC-L----------------D--NNA--TVST
PpIMD 119 QPFQNGPPVSHLNAVNNNVAQPPIASHANGFPAPPTQYNSMPQPQAKPQMPPNPYGPPPG
TcLOC660509 40
AgAGAP004959 63 Q
AaAAEL010083 57 Q
CqConserved Hyp 53 A
LlIMD 92 L
DmIMD 60 S
GmIMD 51 T
PpIMD 179 MPGQMPPTQVPPQQMPPGHMPPGQMAPGQLAPQQMQSNQMPPMPNQPLQQFPGYQSSFQG
TcLOC660509 40 KTKTR
AgAGAP004959 64
AaAAEL010083 58
CqConserved_Hyp 54
LlIMD 93 EIARQESQ
DmIMD 61 DITESVLR
GmIMD 52 DIIQSDTR
PpIMD 239 APQYPQQPSQLPPAGQRHPQAPGYPPQMHQAQPQQRRLDPDQMPNPIQVMDDNQRSCQGP
TcLOC660509 45
AgAGAP004959 64
AaAAEL010083 58
CqConserved Hyp 54
LlIMD 101
DmIMD 69
GmIMD 60
PpIMD 299 FVTNQPGLVPPLVTTKFVTHDQGNSGPRFIRSTMYSVPSTTDMMKQTAVPFALIVSPFAK
TcLOC660509 45 VF
AgAGAP004959 64 VVPGME
AaAAEL010083 58 LVPSTS
CqConserved_Hyp 54 EVPGTS
LlIMD 101 ISVPETPS
DmIMD 69 ELSDPNYNSMD
GmIMD 60 LL
PpIMD 359 TLEGELTPPIVDFGEVGPIRCIRCKAYMCPNMQFIDGGRRFQCLLCKATTEVPPEYFQHL
TcLOC660509 47
AgAGAP004959 70
AaAAEL010083 64
CqConserved_Hyp 60
LlIMD 109
DmIMD 80
GmIMD 62
PpIMD 419 DHTGQRMDKYERPELVLGTYEFVATKDYCRNNTPPKPPAIIFVIDVSYNNVKSGLVNLLC

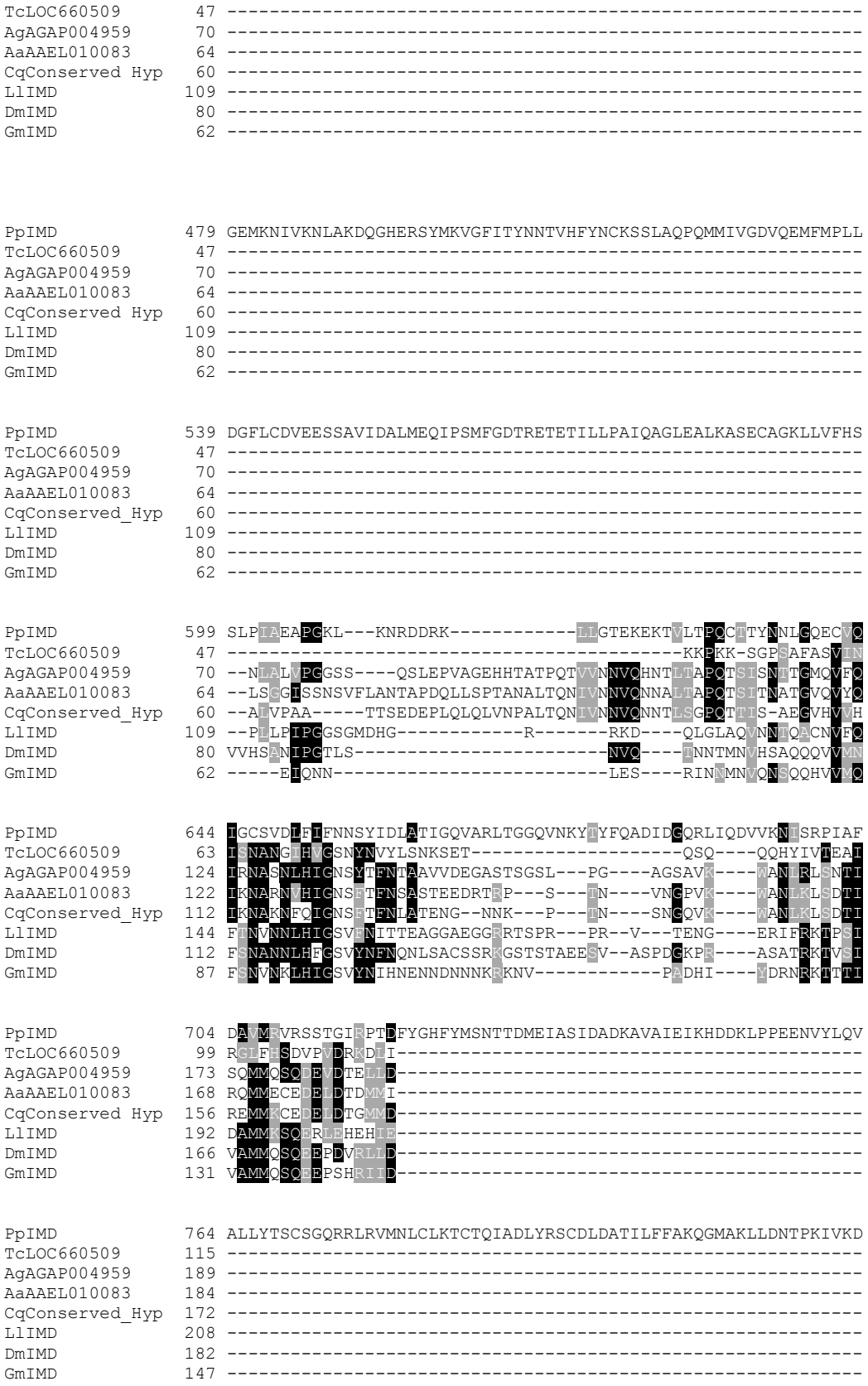
TcLOC660509 47
AgAGAP004959 70
AaAAEL010083 64
CqConserved Hyp 60
LlIMD 109
DmIMD 80
GmIMD 62
PpIMD 479 GEMKNIVKNLAKDQGHERSYMKVGFITYNNTVHFYNCKSSLAQPQMMIVGDVQEMFMPLL
PpIMD 539 DGFLCDVEESSAVIDALMEQIPSMFGDTRETETILLPAIQAGLEALKASECAGKLLVFHS
CqConserved_Hyp 60
PpIMD 599 SLPIAEAPGKL---KNRDDRK
AgAGAP004959 70 --NLALVPGGSS----QSLEPVAGEHHTATPQTVVNNVQHNTLTAPQTSISNNTGMQVFQ
AaAAEL010083 64 --LSCGISSNSVFLANTAPDQLLSPTANALTQNIVNNVQNNALTAPQTSITNATGVQVYQ
CqConserved_Hyp 60 --ATVPAA-----TTSEDEPLQLQLVNPALTQNIVNNVQNNTLSGPQTTIS-AEGVHVVH
LlIMD 109 --PLLPIPGGSGMDHG
DmIMD 80 VVHSANIPGTLS
GmIMD 62 -----EIQNN
PpIMD 644 IGCSVDLFIFNNSYIDLATIGQVARLTGGQVNKYTYFQADIDGQRLIQDVVKNISRPIAF
TcLOC660509 63 ISNANGIHVGSNYNVYLSNKSET
AgAGAP004959 124 IRNASNLHIGNSYTFNTAAVVDEGASTSGSL---PG----AGSAVK----TANTRLSNTI
AaAAEL010083 122 IKNARNVHIGNSFTFNSASTEEDRTRP---S---TN----VNGPVK----TANLKLSDTI
CqConserved_Hyp 112 IKNAKNFQIGNSFTFNLATENG--NNK---P---TN----SNGQVK----TANLKLSDTI
LlIMD 144 FTNVNNLHIGSVTNITTEAGGAEGGRRTSPR---PR--V---TENG----ERIFRKTPSI
DmIMD 112 FSNANNLHFGSVYNFNQNLSACSSRKGSTSTAEESV--ASPDGKPR----ASATRKTVSI
GmIMD 87 FSNVNKLHIGSVYNIHNENNDNNNKRKNV-----PADHI----MDRNRKTTTI
PpIMD 704 DAVMRVRSSTGIRPTDFYGHFYMSNTTDMEIASIDADKAVAIEIKHDDKLPPEENVYLQV
TcLOC660509 99 RGLFHSDVPVDRKDLI
AgAGAP004959 173 SQMMQSQEEVDTELLD
AaAAEL010083 168 RQMMECEEELDTDMMI
CqConserved Hyp 156 REMMKCEEELDTGMMD
LlIMD 192 DAMMTSQERLEHEHIE
DmIMD 166 VAMMQSQEEPDVRLLD
GmIMD 131 VAMMQSQEEPSHRIID
PpIMD 764 ALLYTSCSGQRRLRVMNLCLKTCTQIADLYRSCDLDATILFFAKQGMAKLLDNTPKIVKD
TcLOC660509 115
AgAGAP004959 189
AaAAEL010083 184
CqConserved_Hyp 172
LlIMD 208
DmIMD 182
GmIMD 147

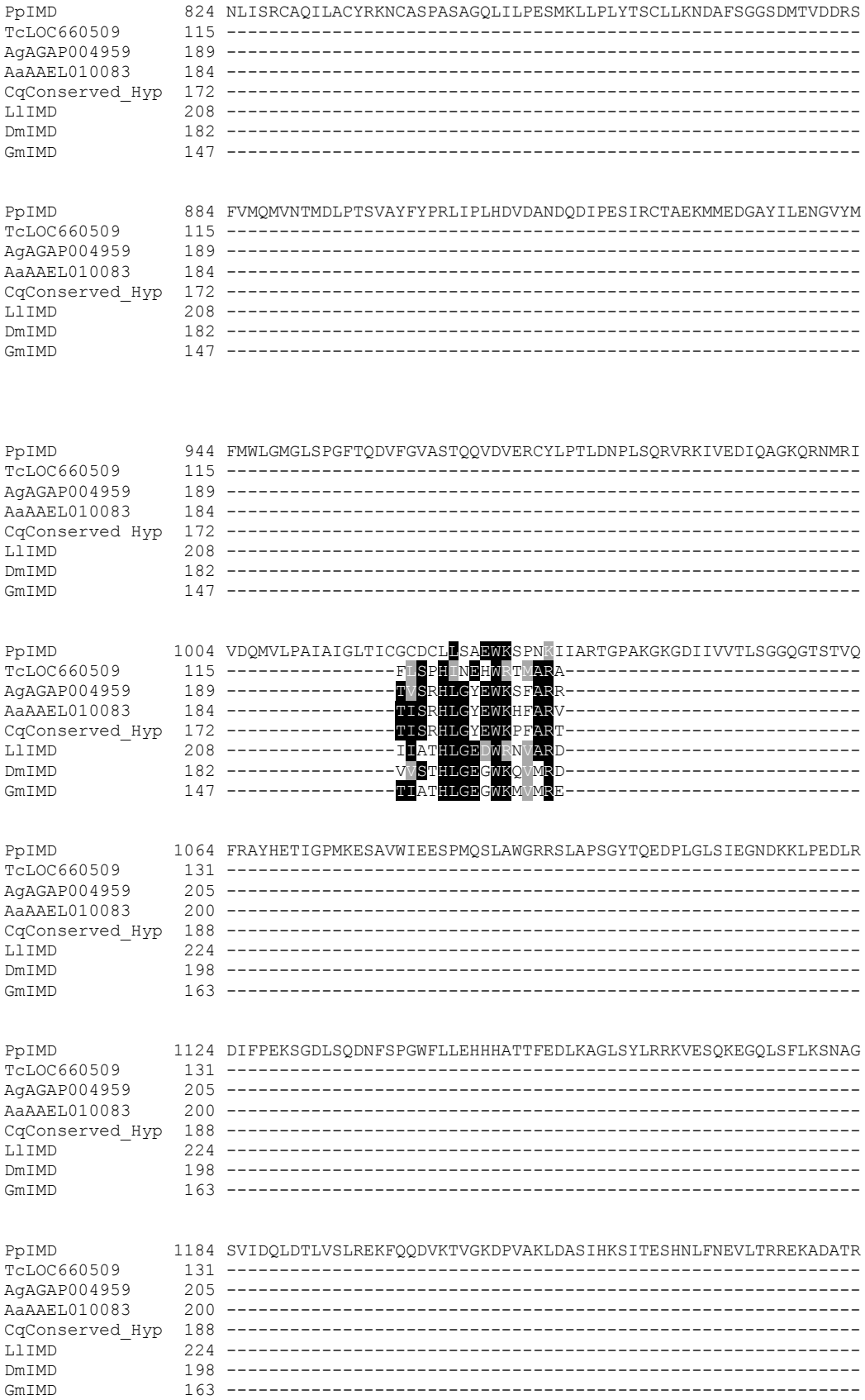
PpIMD 824 NLISRCAQILACYRKNCASPASAGQLILPESMKLLPLYTSCLLKNDAFSGGSDMTVDDRS
TcLOC660509 115
AgAGAP004959 189
AaAAEL010083 184
CqConserved_Hyp 172
LlIMD 208
DmIMD 182
GmIMD 147
PpIMD 884 FVMQMVNTMDLPTSVAYFYPRLIPLHDVDANDQDIPESIRCTAEKMMEDGAYILENGVYM
TcLOC660509 115
AgAGAP004959 189
AaAAEL010083 184
CqConserved_Hyp 172
LlIMD 208
DmIMD 182
GmIMD 147
PpIMD 944 FMWLGMGLSPGFTQDVFGVASTQQVDVERCYLPTLDNPLSQRVRKIVEDIQAGKQRNMRI
TcLOC660509 115
AgAGAP004959 189
AaAAEL010083 184
CqConserved Hyp 172
LlIMD 208
DmIMD 182
GmIMD 147
PpIMD 1004 VDQMVLPAIAIGLTICGCDCLLSAEWKSPNWIIARTGPAKGKGDIIVVTLSGGQGTSTVQ
TcLOC660509 115
AgAGAP004959 189
AaAAEL010083 184
CqConserved_Hyp 172
LlIMD 208
DmIMD 182
GmIMD 147
PpIMD 1064 FRAYHETIGPMKESAVWIEESPMQSLAWGRRSLAPSGYTQEDPLGLSIEGNDKKLPEDLR
TcLOC660509 131
AgAGAP004959 205
AaAAEL010083 200
CqConserved_Hyp 188
LlIMD 224
DmIMD 198
GmIMD 163
PpIMD 1124 DIFPEKSGDLSQDNFSPGWFLLEHHHATTFEDLKAGLSYLRRKVESQKEGQLSFLKSNAG
TcLOC660509 131
AgAGAP004959 205
AaAAEL010083 200
CqConserved_Hyp 188
LlIMD 224
DmIMD 198
GmIMD 163
PpIMD 1184 SVIDQLDTLVSLREKFQQDVKTVGKDPVAKLDASIHKSITESHNLFNEVLTRREKADATR
TcLOC660509 131
AgAGAP004959 205
AaAAEL010083 200
CqConserved_Hyp 188
LlIMD 224
DmIMD 198
GmIMD 163

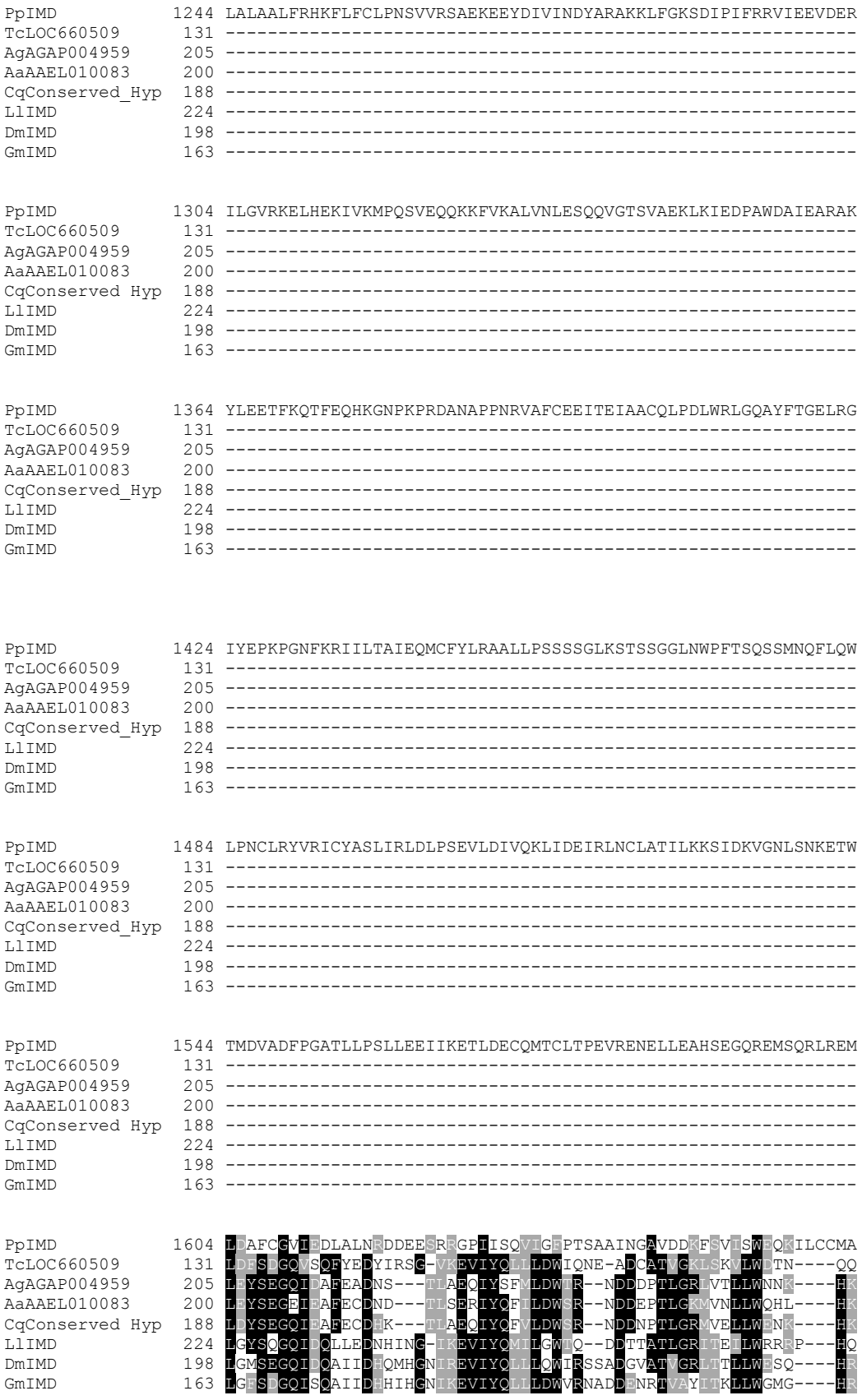
PpIMD 1244 LALAALFRHKFLFCLPNSVVRSAEKEEYDIVINDYARAKKLFGKSDIPIFRRVIEEVDER
TcLOC660509 131
AgAGAP004959 205
AaAAEL010083 200
CqConserved_Hyp 188
LlIMD 224
DmIMD 198
GmIMD 163
PpIMD 1304 ILGVRKELHEKIVKMPQSVEQQKKFVKALVNLESQQVGTSVAEKLKIEDPAWDAIEARAK
TcLOC660509 131
AgAGAP004959 205
AaAAEL010083 200
CqConserved Hyp 188
LlIMD 224
DmIMD 198
GmIMD 163
PpIMD 1364 YLEETFKQTFEQHKGNPKPRDANAPPNRVAFCEEITEIAACQLPDLWRLGQAYFTGELRG
TcLOC660509 131
AgAGAP004959 205
AaAAEL010083 200
CqConserved_Hyp 188
LlIMD 224
DmIMD 198
GmIMD 163
PpIMD 1424 IYEPKPGNFKRIILTAIEQMCFYLRAALLPSSSSGLKSTSSGGLNWPFTSQSSMNQFLQW
TcLOC660509 131
AgAGAP004959 205
AaAAEL010083 200
CqConserved_Hyp 188
LlIMD 224
DmIMD 198
GmIMD 163
PpIMD 1484 LPNCLRYVRICYASLIRLDLPSEVLDIVQKLIDEIRLNCLATILKKSIDKVGNLSNKETW
TcLOC660509 131
AgAGAP004959 205
AaAAEL010083 200
CqConserved_Hyp 188
LlIMD 224
DmIMD 198
GmIMD 163
PpIMD 1544 TMDVADFPGATLLPSLLEEIIKETLDECQMTCLTPEVRENELLEAHSEGQREMSQRLREM
TcLOC660509 131
AgAGAP004959 205
AaAAEL010083 200
CqConserved Hyp 188
LlIMD 224
DmIMD 198
GmIMD 163
PpIMD 1604
TcLOC660509 131
AgAGAP004959 205
AaAAEL010083 200
CqConserved Hyp 188
LlIMD 224
DmIMD 198
GmIMD 163

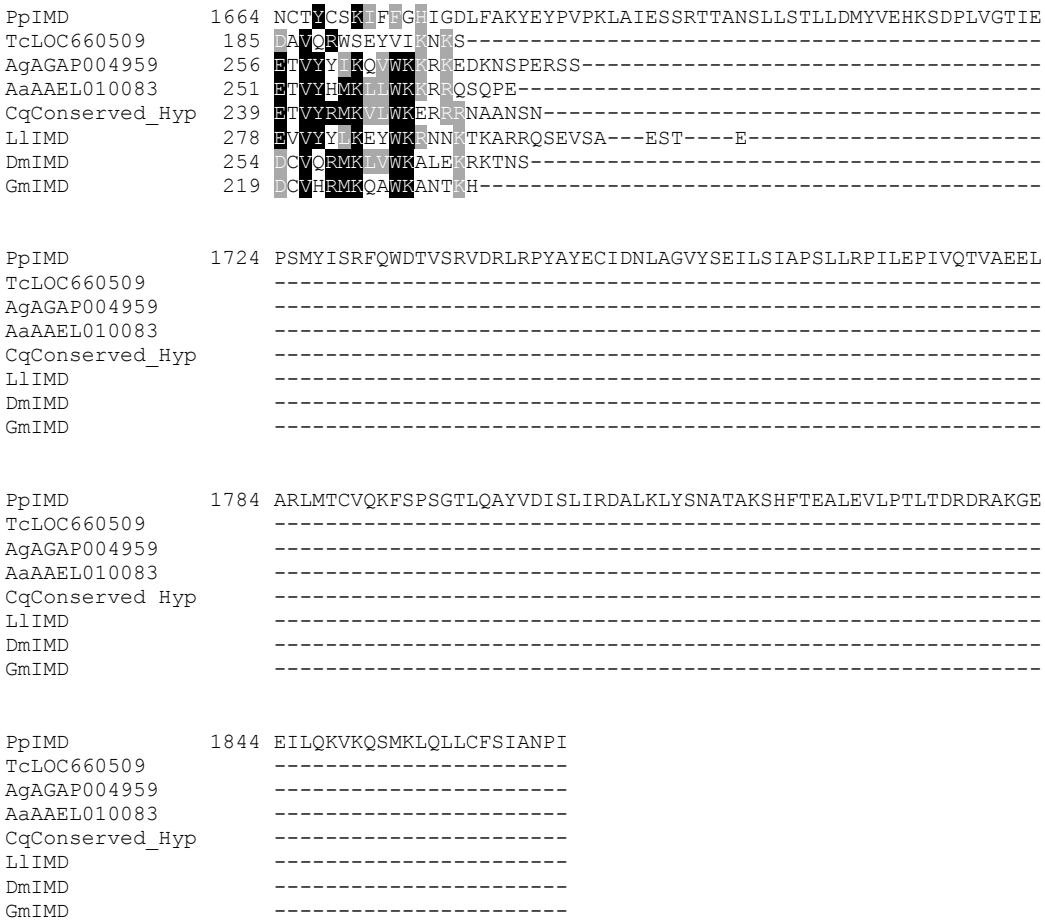

Figure A.19. Clustal Omega protein alignment of IMD sequences from *L. longipalpis*, *P. papatasi*, *D. melanogaster*, *A. gambiae*, *A. aegyti*, *C. quinquefasciatus*, *T. Castaneum*, and *G. morsitans*.

>Nos

ATGCAATGCAAGCCAGATTGTTGCTATGGGAGTGTCATGTTTCCGGCAGTTGTTGGC
ACTGAGCCCAGGAAGCCGGAAGTTATTTTGGAGCATGCCAAGGATTTTATGGAGCA
ATACTTTACCTCAATTCGCCGGTACAAATCACCGGCTCATGAGGCACGTTGGCAACA
GGTGCAGAAAGAAATTGAGACAAGTGGGAAATATCATTTGACGGAAACTGAGTTAA
TTTTCGGCGCCAAATTGGCCTGGAGGAATGCAAATCGGTGCATTGGTCGCATTCAAT
GGTCCAAATTGCAGGTGTTCGACTGCCGATATGTAACAACTACGAGCCAAATGTTCG
AGGCAATTTGCAATCACATCAAATATGCCACAAACAAGGGCAATATTCGGTCCGCC
ATCACTATTTTCCCCCAACGTACGGATGGGAAGCACGACTATCGTGTATGGAATAGT
CAGCTTATCCTCTATGCTGGCTACCGTGAACCCGATGGACGCATAATCGGTGACCCT
GCTAATGTGGAATTTACAGAATTTTGCATTAAATTAGGTTGGAAGGCACCACGTGGC
GAATGGGATATACTCCCAATGGTACTTTCAGCCAATGGACACGACCCCGAGTACTTT
GAGTACCCACCAGATCTAATCCTCGAAGTACCCATTACACATCCCACTTACAAGTGG
TTTGCGGACTTTGGGCTTAGGTGGTATGCTGTTCCGGCGGTATCGGGAATGCTATTT
GACTGCGGTGGAATCCAATTTACGGGGGTACCATTCAATGGTTGGTACATGTCCACT
GAAATTGGCTGTCGCAATTTGTGTGACACAAATCGTCGCAATATGTTGGAGCCGATT
GCAACAAAATTGGGTCTAAATACACGAAATCCAGCATCCCTGTGGAAGGATAAGAC
ACTGGTTGAGGTGAACATTGCGGTTTTGCATTCCTTCCACACGCACGGGGTGACGAT
TGTGGATCATCACACGGCCAGTGATAGCTTCATCAAGCACCTGGAAAATGAATCGC
GACTACGGAATGGATGTCCTGCAGATTGGGTGTGGATTGTACCACCAATGGCCAGTT
CAACGACACAGGTGTTCCATCAGGAGATGGCCAACTACTACCTGAAGCCCTCCTTTG
AGTACCAAGACTCCCCGATGAAGACGCACGTGTGGAAGAAGGGACGTGAACAGTCG
AAGAATAAGAAGCCCAAAAGGAAGTTCCACTTTAAACAAATTGCC

Figure A.20. Putative CDS for mRNA encoding *L. longipalpis* Nos.

Full length predicted mRNA is depicted in black, while the primers used for RT-qPCR amplicon measurement are shown in pink. Sequences in blue denote agreement between prediction and sequenced amplicons, while nucleotides in red depict a difference at that base pair.

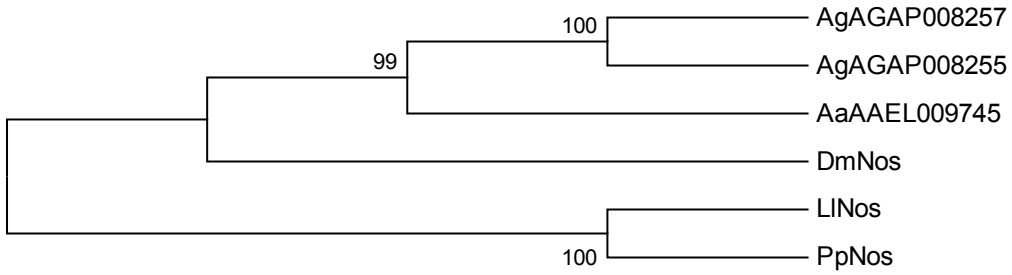

Figure A.21. Neighbor-joining tree to infer the evolutionary relationship of Nos sequences.

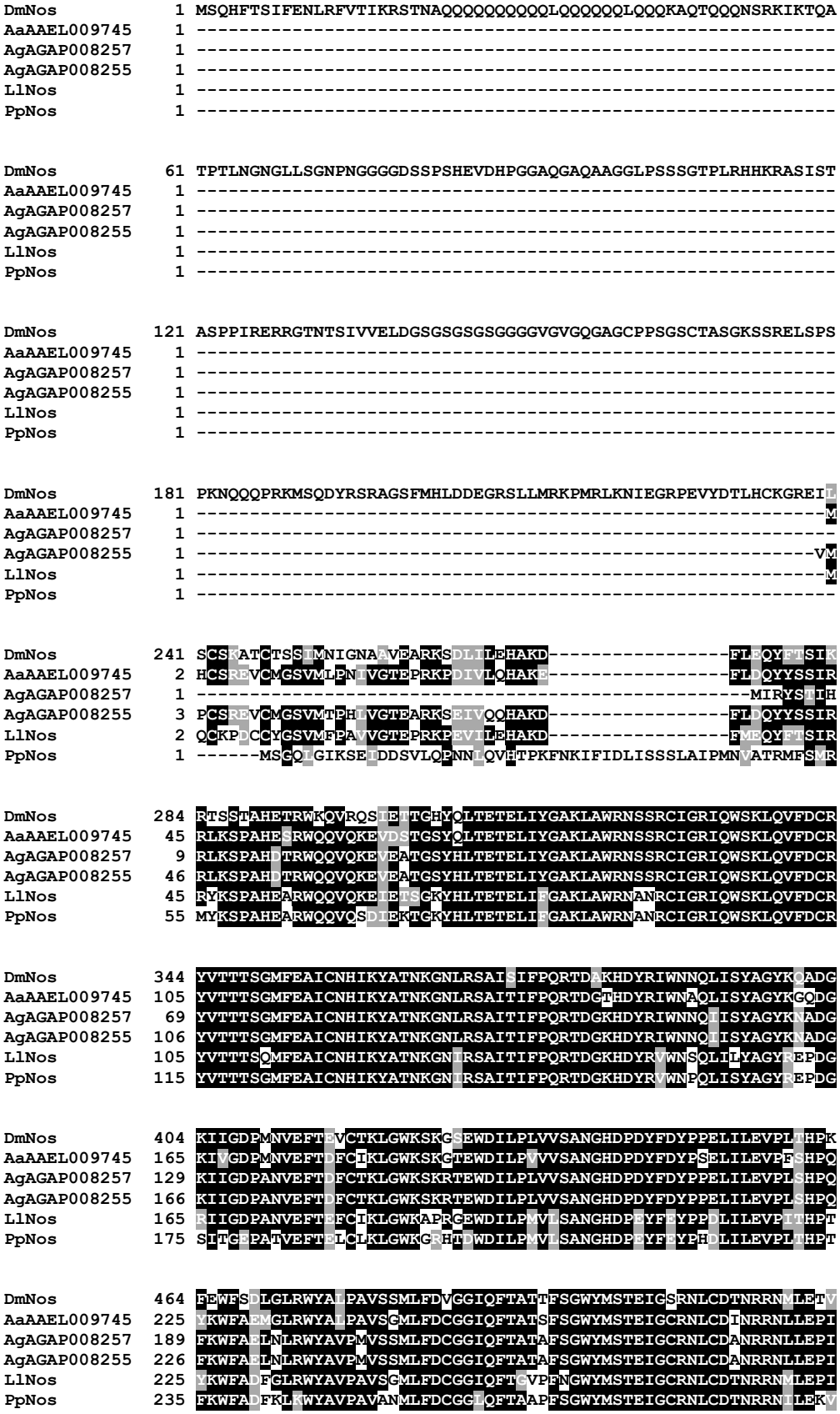
DmNos 1 MSQHFTSIFENLRFVTIKRSTNAQQQQQQQQQQLQQQQQQLQQQKAQTQQQNSRKIKTQA
AaAAEL009745 1
AgAGAP008257 1
AgAGAP008255 1
LlNos 1
PpNos 1
DmNos 61 TPTLNGNGLLSGNPNGGGGDSSPSHEVDHPGGAQGAQAAGGLPSSSGTPLRHHKRASIST
AaAAEL009745 1
AgAGAP008257 1
AgAGAP008255 1
LlNos 1
PpNos 1
DmNos 121 ASPPIRERRGTNTSIVVELDGSGSGSGSGGGGVGVGQGAGCPPSGSCTASGKSSRELSPS
AaAAEL009745 1
AgAGAP008257 1
AgAGAP008255 1
LlNos 1
PpNos 1
DmNos 181 PKNQQQPRKMSQDYRSRAGSFMHLDDEGRSLLMRKPMRLKNIEGRPEVYDTLHCKGREIL
AaAAEL009745 1
AgAGAP008257 1
AgAGAP008255 1
LlNos 1
PpNos 1
DmNos 241 SCSKATCTSSIMNIGNAAVEARKSDLILEHAKD FLEQYFTSIK
AaAAEL009745 2 HCSREVCMGSVMLPNIVGTEPRKPDIVLQHAKE FLDQYYSSIR
AgAGAP008257 1 MIRYSIIH
AgAGAP008255 3 PCSREVCMGSVMTPHIVGTEARKSEIVQQHAKD FLDQYYSSIR
LlNos 2 QCKPDCCYGSVMFPAVVGTEPRKPEVILEHAKD FMEQYFTSIR
PpNos 1 ------MSCQIGIKSETDDSVLQPNNLQVHTPKFNKIFIDLISSSLAIPMNVATRMFSMR
DmNos 284 RTSSTAHETRWKQVRQSTETTCHYQLTETELIYGAKLAWRNSSRCIGRIQWSKLQVFDCR
AaAAEL009745 45 RLKSPAHESRWQQVQKEVDSTGSYQLTETELIYGAKLAWRNSSRCIGRIQWSKLQVFDCR
AgAGAP008257 9 RLKSPAHDTRWQQVQKEVEATGSYHLTETELIYGAKLAWRNSSRCIGRIQWSKLQVFDCR
AgAGAP008255 46 RLKSPAHDTRWQQVQKEVEATGSYHLTETELIYGAKLAWRNSSRCIGRIQWSKLQVFDCR
LlNos 45 RYKSPAHEARWQQVQKEIETSGKYHLTETELIFGAKLAWRNANRCIGRIQWSKLQVFDCR
PpNos 55 MYKSPAHEARWQQVQSDIEKTGKYHLTETELIFGAKLAWRNANRCIGRIQWSKLQVFDCR
DmNos 344 YVTTTSGMFEAICNHIKYATNKGNLRSAISIFPQRTDAKHDYRIWNNQLISYAGYKQADG
AaAAEL009745 105 YVTTTSGMFEAICNHIKYATNKGNLRSAITIFPQRTDGTHDYRIWNAQLISYAGYKGQDG
AgAGAP008257 69 YVTTTSGMFEAICNHIKYATNKGNLRSAITIFPQRTDGKHDYRIWNNQIISYAGYKNADG
AgAGAP008255 106 YVTTTSGMFEAICNHIKYATNKGNLRSAITIFPQRTDGKHDYRIWNNQIISYAGYKNADG
LlNos 105 YVTTTSQMFEAICNHIKYATNKGNIRSAITIFPQRTDGKHDYRVWNSQLILYAGYREPDG
PpNos 115 YVTTTSGMFEAICNHIKYATNKGNIRSAITIFPQRTDGKHDYRVWNPQLISYAGYREPDG
DmNos 404 KIIGDPMNVEFTEVCTKLGWKSKGSEWDILPLVVSANGHDPDYFDYPPELILEVPLIHPK
AaAAEL009745 165 KIVGDPMNVEFTDFCIKLGWKSKGTEWDILPVVVSANGHDPDYFDYPSELILEVPFSHPQ
AgAGAP008257 129 KIIGDPANVEFTDFCTKLGWKSKRTEWDILPLVVSANGHDPDYFDYPPELILEVPLSHPQ
AgAGAP008255 166 KIIGDPANVEFTDFCTKLGWKSKRTEWDILPLVVSANGHDPDYFDYPPELILEVPLSHPQ
LlNos 165 RIIGDPANVEFTEFCIKLGWKAPRGEWDILPMVISANGHDPEYFEYPPDLILEVPITHPT
PpNos 175 SITGEPATVEFTELCLKLGWKGRHTDWDILPMVTSANGHDPEYFEYPHDLILEVPLTHPT
DmNos 464 EEWFSDLGLRWYALPAVSSMLFDVGGIQFTATTFSGWYMSTEIGSRNLCDTNRRNMLETV
AaAAEL009745 225 YKWFAEMGLRWYALPAVSGMLFDCGGIQFTATSFSGWYMSTEIGCRNLCDINRRNLLEPI
AgAGAP008257 189 FKWFAELNLRWYAVPMVSSMLFDCGGIQFTATAFSGWYMSTEIGCRNLCDANRRNLLEPI
AgAGAP008255 226 FKWFAELNLRWYAVPMVSSMLFDCGGIQFTATAFSGWYMSTEIGCRNLCDANRRNLLEPI
LlNos 225 YKWFADFGLRWYAVPAVSGMLFDCGGIQFTCVPFNGWYMSTEIGCRNLCDTNRRNMLEPI
PpNos 235 FKWFADFKLRWYAVPAVANMLFDCGGLQFTAAPFSGWYMSTEIGCRNLCDTNRRNILEKV

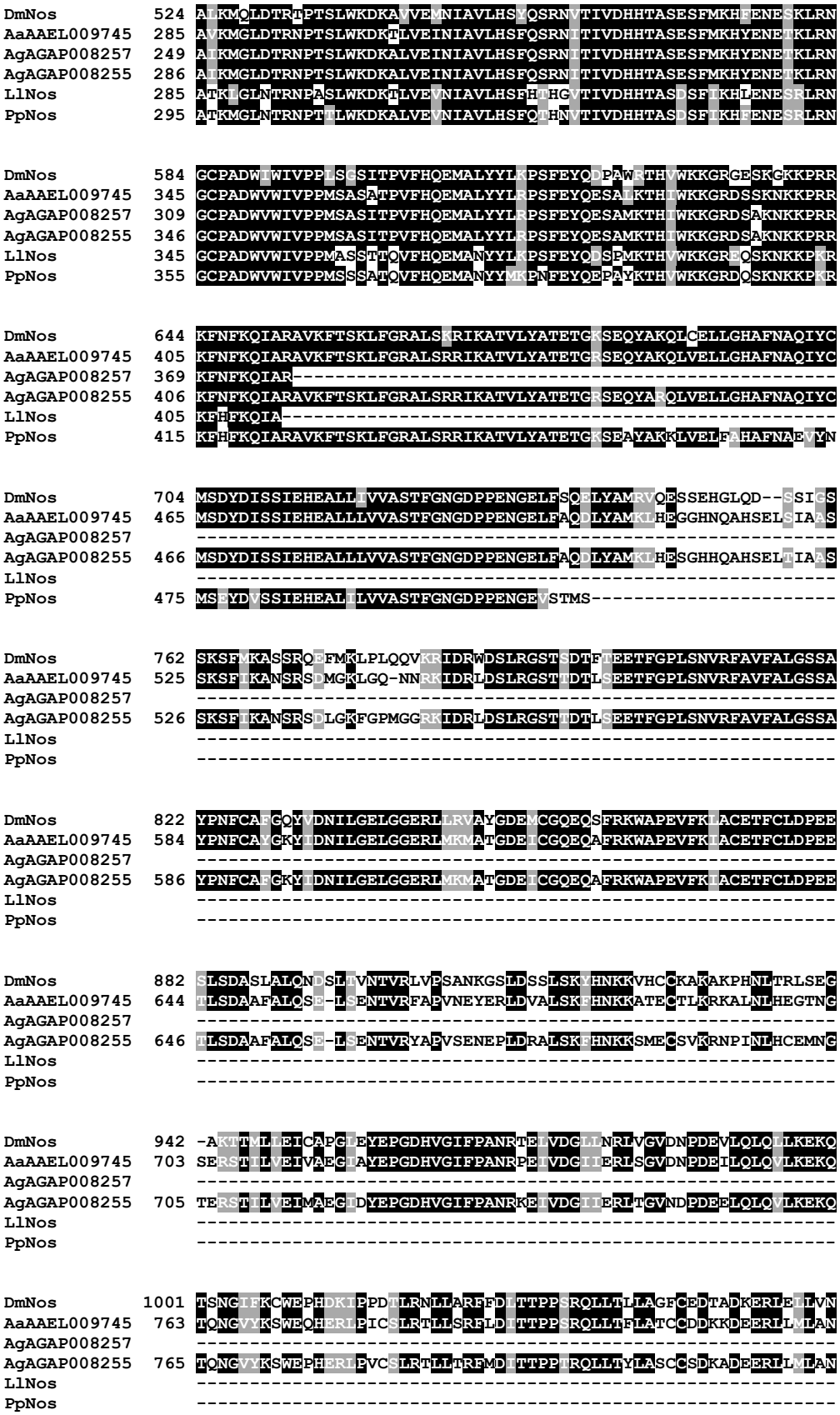
DmNos 524 ALKMQLDTRTPTSLWKDKAVEMNIAVLHSYQSRNVTIVDHHTASESFMKHFENESKLRN
AaAAEL009745 285 AVKMGLDTRNPTSLWKDKTLVEINIAVLHSFQSRNITIVDHHTASESFMKHYENEIKLRN
AgAGAP008257 249 AIKMGLDTRNPTSLWKDKALVEINIAVLHSFQSRNITIVDHHTASESFMKHYENETKLRN
AgAGAP008255 286 AIKMGLDTRNPTSLWKDKALVEINIAVLHSFQSRNITIVDHHTASESFMKHYENETKLRN
LlNos 285 ATKLGLNTRNPASLWKDKTLVEVNIAVLHSFHQHGVTIVDHHTASDSFIKHLENESRLRN
PpNos 295 ATKMGLNTRNPTTLWKDKALVEVNIAVLHSFQLHNVTIVDHHTASDSFIKHFENESRLRN
DmNos 584 GCPADWIWIVPPLSGSITPVFHQEMALYYLKPSFEYQDPAWRTHVWKKGRGESKGKKPRR
AaAAEL009745 345 GCPADWVWIVPPMSASATPVFHQEMALYYLRPSFEYQESALKTHIWKKGRDSSKNKKPRR
AgAGAP008257 309 GCPADWVWIVPPMSASITPVFHQEMALYYLRPSFEYQESAMKTHIWKKGRDSAKNKKPRR
AgAGAP008255 346 GCPADWVWIVPPMSASITPVFHQEMALYYLRPSFEYQESAMKTHIWKKGRDSAKNKKPRR
LlNos 345 GCPADWVWIVPPMASSTTQVFHQEMANYYLKPSFEYQDSPMKTHVWKKGREQSKNKKPKR
PpNos 355 GCPADWVWIVPPMSSSATQVFHQEMANYYMKPNFEYQEPAYKTHVWKKGRDQSKNKKPKR
DmNos 644 KFNFKQIARAVKFTSKLFGRALSKRIKATVLYATETGKSEQYAKQLCELLGHAFNAQIYC
AaAAEL009745 405 KFNFKQIARAVKFTSKLFGRALSRRIKATVLYATETGRSEQYAKQLVELLGHAFNAQIYC
AgAGAP008257 369 KFNFKQIAR----------
AgAGAP008255 406 KFNFKQIARAVKFTSKLFGRALSRRIKATVLYATETGRSEQYAKQLVELLGHAFNAQIYC
LlNos 405 KFHFKQIA----------
PpNos 415 KFHFKQIARAVKFTSKLFGRALSRRIKATVLYATETGKSEAYAKKLVELFAHAFNAEVYN
DmNos 704 MSDYDISSIEHEALLIVVASTFGNGDPPENGELFSQELYAMRVQESSEHGLQD--SSIGS
AaAAEL009745 465 MSDYDISSIEHEALLLVVASTFGNGDPPENGELFAQDLYAMKLHEGGHNQAHSELSIAAS
AgAGAP008257 ----------
AgAGAP008255 466 MSDYDISSIEHEALLLVVASTFGNGDPPENGELFAQDLYAMKLHESGHHQAHSELLIAAS
LlNos ----------
PpNos 475 MSEYDVSSIEHEALILVVASTFGNGDPPENGEVSTMS----------
DmNos 762 SKSFMKASSRQEFMKLPLQQVKRIDRWDSLRGSTSDTFTEETFGPLSNVRFAVFALGSSA
AaAAEL009745 525 SKSFIKANSRSDMGKLGQ-NNRKIDRLDSLRGSTTDTLSEETFGPLSNVRFAVFALGSSA
AgAGAP008257 ----------
AgAGAP008255 526 SKSFTKANSRSDLGKFGPMGGRKIDRLDSLRGSTTDTLSEETFGPLSNVRFAVFALGSSA
LlNos ----------
PpNos ----------
DmNos 822 YPNFCAFGQYVDNILGELGGERLLRVAYGDEMCGQEQSFRKWAPEVFKLACETFCLDPEE
AaAAEL009745 584 YPNFCAYGKYIDNILGELGGERLMKMATGDEICGQEQAFRKWAPEVFKIACETFCLDPEE
AgAGAP008257 ----------
AgAGAP008255 586 YPNFCAFGKYTDNILGELGGERLMKMATGDETCGQEQAFRKWAPEVFKIACETFCLDPEE
LlNos ----------
PpNos ----------
DmNos 882 SLSDASLALQNDSLTVNTVRLVPSANKGSLDSSLSKYHNKKVHCCKAKAKPHNLTRLSEG
AaAAEL009745 644 TLSDAAFALQSE-LSENTVRFAPVNEYERLDVALSKFHNKKATECTLKRKALNLHEGTNG
AgAGAP008257 ----------
AgAGAP008255 646 TLSDAAFALQSE-LSENTVRYAPVSENEPLDRALSKFHNKKSMECSVKRNPINLHCEMNG
LlNos ----------
PpNos ----------
DmNos 942 -AKTTMLLEICAPGLEYEPGDHVGIFPANRTELVDGLLNRLVGVDNPDEVLQLQLLKEKQ
AaAAEL009745 703 SERSTTLVEIVAEGIAYEPGDHVGIFPANRPELVDGIIERLSGVDNPDEILQLQVLKEKQ
AgAGAP008257 ----------
AgAGAP008255 705 TERSTTLVEIMAEGIDYEPGDHVGIFPANRKELVDGIIERLTGVNDPDEELQLQVLKEKQ
LlNos ----------
PpNos ----------
DmNos 1001 TSNGIFKCWEPHDKIPPDILRNLLARFFDLTTPPSRQLLTLLAGFCEDTADKERLEIIVN
AaAAEL009745 763 TQNGVYKSWEQHERLPICSLRTLLSRFLDITTPPSRQLLTFLATCCDDKKDEERLLVLAN
AgAGAP008257 ----------
AgAGAP008255 765 TQNGVYKSWEPHERLPVCSLRTLLTRFMDITTPPTRQLLTYLASCCSDKADEERLLVLAN
LlNos ----------
PpNos ----------

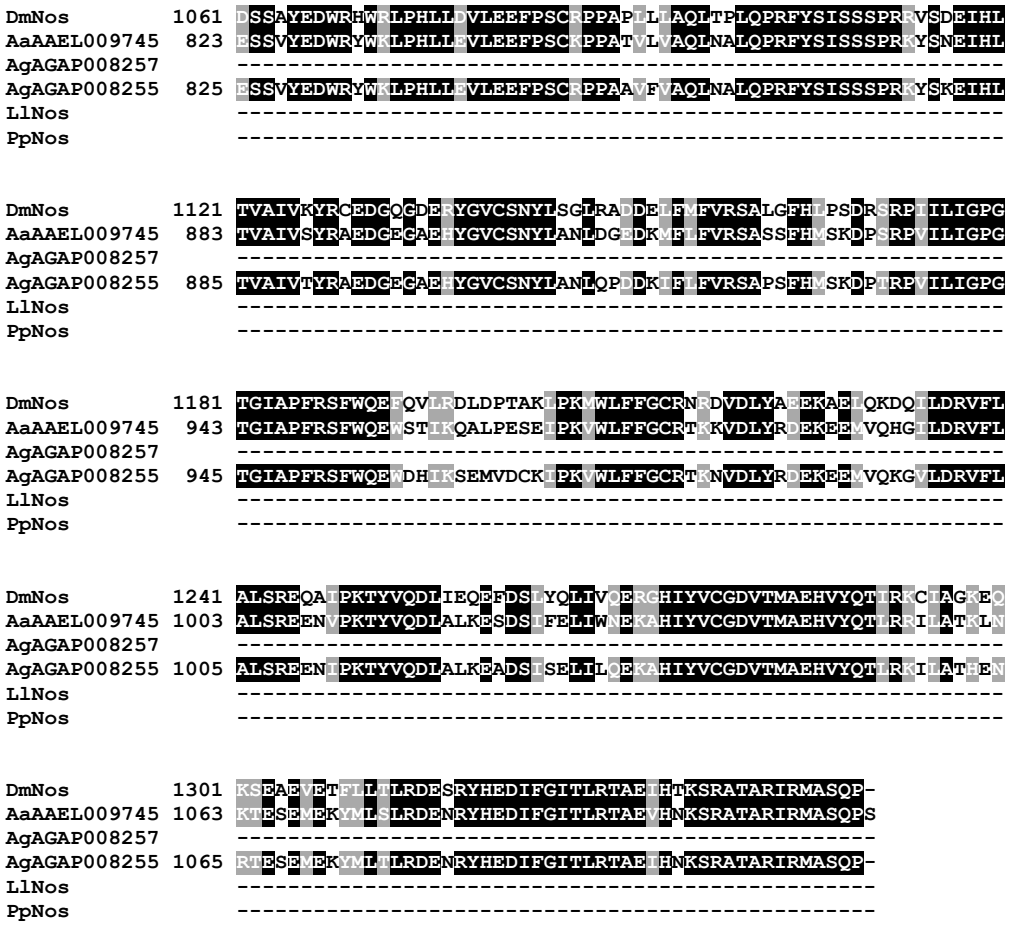

Figure A.22. Clustal Omega protein alignment of Nos sequences from *L. longipalpis*, *P. papatasi*, *D. melanogaster*, *A. gambiae*, and *A. aegyti*.

>Domeless

ATGGAAGAAATTCACAGGAATCTCACGAGAGTCTTTAGACTACAAATGTGGCTTCTCATTTGCTGCATTTTATTCTT
CGTAACGGCATCATCAAATGTAGAATTGGGAGTTGTCCATCCGGGTGAGGTAAACATTGCTGTTGGGACCCCGTTGA
ATTTGACTTGCAATATAAATTGGTCAGTAGCTGAACTACTCCCAACGCCGTACAGAGAGGAAGATGGTGATCTTGAT
TATTTGAGTTTTAACGTCAATAAAACTCAAGTAGAAAAAAAATTTATCACGATACTTAATAGTTCAGCCATTGAATT
GTACATCCCTGAGATGAAGGAGCCGACTTTTGTGAAGTATGTTTGCGTTCTATTGAATAAGCATAAGAAAAGTAAAA
AGGACAATGATATTGGGGTCAGCTATTCTGATGTTCATGTTGGCTATGCCCCGAAGAAAGTAAGGAACTTCCGATGC
ATCTCCTACAATTGGGAAACACTCAATTGTACCTTTGACAAGGATGTAAATTATATTTTTACAAATTATCAAGTTAC
TATTGGTCCAGTTCTAACAACACGAAGGCATCAATTGGAAATTAATCCAAATGACAACAATACATCCTTTACGTTTC
AAATGCCGGAATATACGGCAGTTTATGAGATATATTCATTTGATTTTGATATTAGCAATATTATTGGGCATGTGTCA
CAGAGTATTTATGTTAATACGTTTGAATGCATCAAACCTGATCCACCGCTATCAATGAATGTAACCCTCAGAGAGCC
AAAACGTGTGACAATTACGTGGAAATTGCACTATCATATGAAGGCCTTTGAGAGGGGTTTCATTCATGAAGGTGAAA
TTTTTCAATCGCCAAATTCACACGGGCAGTCGCTTGATATGTCCAAATTGAAGAATACAACACGTGTGGATTATTCA
TTGACCATCGATGGATTGTACGCTCATACATGGTATGACATTCGGATTCGTGTGCGAGTACCAAATGCCGATCGCGA
AGAACTCTGGTCAAATTACACTGATTTCCAATT**TCAAACACACCCCAAAATAC****CCGATCGTCCCCCAAGAGTGGATA**
TTGGGAGTTTCTACGTGAATGATCACAATGATATAGTGTTGTATTGGGAACAGCTACCGCTTGAGGAGCAAAATGGC
AATAATTCGCATTATGTTGTGAGTGAAGTACGGAATGCACATAATATGGTGATTGAGAGGCGTCCAACTGAGATTAA
TAACATCATGGCGAAATTTGTGAATATGCCATCGGGAAATTTAACATTTACAATTCATAGTGCAAATTCCCAGGGGC
AATCAATTGGGGGGAGCACAATTCATGTACCGGCACGAAATAAGCGCTTCCCACCGCCGACACAGCTCAAGAAGTAC
AGTATTGATTCGAAGTATAAGCTGACGTGGGCCCCGCCAACAAGACGACAAAATGAACTTGTCAGCTACACCGTATT
CTGGTGTGAATCCAAAACGAATTATCCCAGTGAATGTGATGGTCCCATGTCCTTTACAACAGTCGACAGTACACAGC
ATGAGTATGAATTGAATAATACAAAGGGATTTAATATTGCGCTCTCGGCAAATTCATGGGATTCCAGTTCTGGATTA
ATTTGGTCCATGTGCACAGCATCCAAGAGTGACGAAATTGGCAAACTCAATCCTGTTTGGGTGTCAAAAATGGATGC
CACTTATATGGAAATTCAGTGGCGACTGGAGTGTATGGATACCCCCATTGTTGTGGGTTACACCCTCACATATTGCC
CCATAACTGCCCCGAAGAATCTCACGTGTAAGCCCGGTATGGAGGTTGTGAAGAATATTACGGGAACAACGCAGTAC
AACATCACAGGATTGACACCCTATACGACCTATAAAACAACAATTGCGATGTTCTCAAAGACAAGAACAGGCGTACC
GAGTGATCCACTTGTCAACACAACCCTCGAAGCAGCTCCAACTCCACCGAGAGATATCCGAATAACACACGTGAGCA
ATACATCGGTGACAATCACGTGGAAAGCCCCAGAGAGGATTAATGGCTTTTTGAAGAATTACATTGTTTGGTGCAAT
AGTTCGAGCTTTCAAGTCTTTGATGGGATCAAAGAGAACACAACGCTGCAGTATAAAATAGAAAAGCTCCAGACTTA
CAGCTACTATGAGATTGTCGTTGTGGCATGCACCATCAGCTGTTCAAATAAGAGTGAAACCCTCACGGTGCGAACGG
AAATGGGAGTTCCTGATCAAGTAACTTCAATGCTAAAAGTACGTCATGGTGACTACACTCTCTTCTCGTGGGATCGT
CCCCGACATGTTGGTGGTAATTTGGATTACTACGAAGTCTTCGTGAAGATCACTGAGACGGGCAATATAACCGTCAA
TCGGACAATTCTCCTCAATGGGACACAATGTTGGATAAATCGAGCATGTGACAAGAACTGGGCGGAGATAGAGCTAC
TTCTGAGTGCTGTGAATGTCGTCCGGAGTCCCCATGAGCGCCTCGAAGAGGGTAGTGGTGAGAGGGATGTGCTAAAT
ATCTCCGATGGGCCGCGTGCACTGACTTTCCACAATGATGACCTTCCGGCGGAAATTCGGATGTACCCATCGTGTAC
GCGTGAGAGTTTTGAGCACTATCAATTGGTGAAGTGGAAGAAGTCCGATGAGCATTCAACATTCCTCAAAAGTAGCT
CAATTCCACTCTTCAACAATAACTGCGGACTAAGCTCTAGCAGTCCACTTCTCTACATTTTTATCATCTTCGTGGGA
CTCATTGGAATGGTGACGGCTGTACTGTTTCTGTACAAGAAGTGCAAGACAATGAGTGACATCAAAGTGGTACTTCC

GGATGCATTGAATGACATTAATAAAGATTCAAAATGCCCCAAAATGGGTGAAATGATCGATGGGGGTGTACTGCGGA
ATGTTCAGATACATCGTGGGGAGATGCGTGTGCAGCAGGATGAGCAGGAGAGGAGTCTCCTGAGGAATCATATGGAG
TCAAGTAGTAGTAGTACAACGAGTAGTACGGCAAATGTGGACAACCAGAGTCAGTGTGAATCTCACGATGGACCTCC
GGAGGAGATGATGGACTCCATGGAGGAGCATCAGCATCATCAACCCGAGGAGGATGAGGATAAGCATTCAGTTGAAT
CTCAACCGGAGGATCCGGCTCAGGAGATCTCCTTTGATGTGCTGCAGCCAGAAAAATTGGACGAAATTATGATTCGT
CCACAAATTGAGCCACAGCAAACGCATCAAGTTGCTCTCTGTCCGGGAGTCAATCAATACGTCCACTTTGCTAAGCC
CTCACAGGGTTATACACAACTGGCATCCCTTAAGGTGCCCATTAAAACGCCCATGGCGGCTGAGACTGATGAAACGG
GAATTTCAGGATACGTTACACGAAAACAACTTGCTGATTTTGGGCAACGTATGTAA

Figure A.23. Putative CDS for mRNA encoding *L. longipalpis* Domeless.

Full length predicted mRNA is depicted in black, while the primers used for RT-qPCR amplicon measurement are shown in pink. Sequences in blue denote agreement between prediction and sequenced amplicons, while nucleotides in red depict a difference at that base pair.

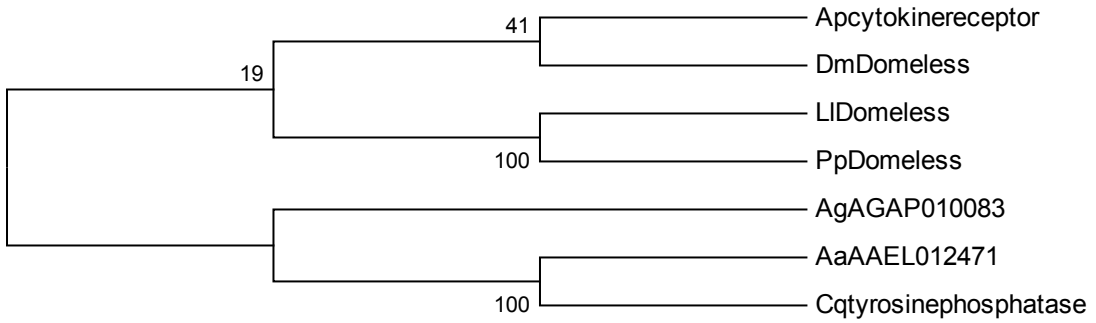

Figure A.24. Neighbor-joining tree to infer the evolutionary relationship of Domeless sequences.

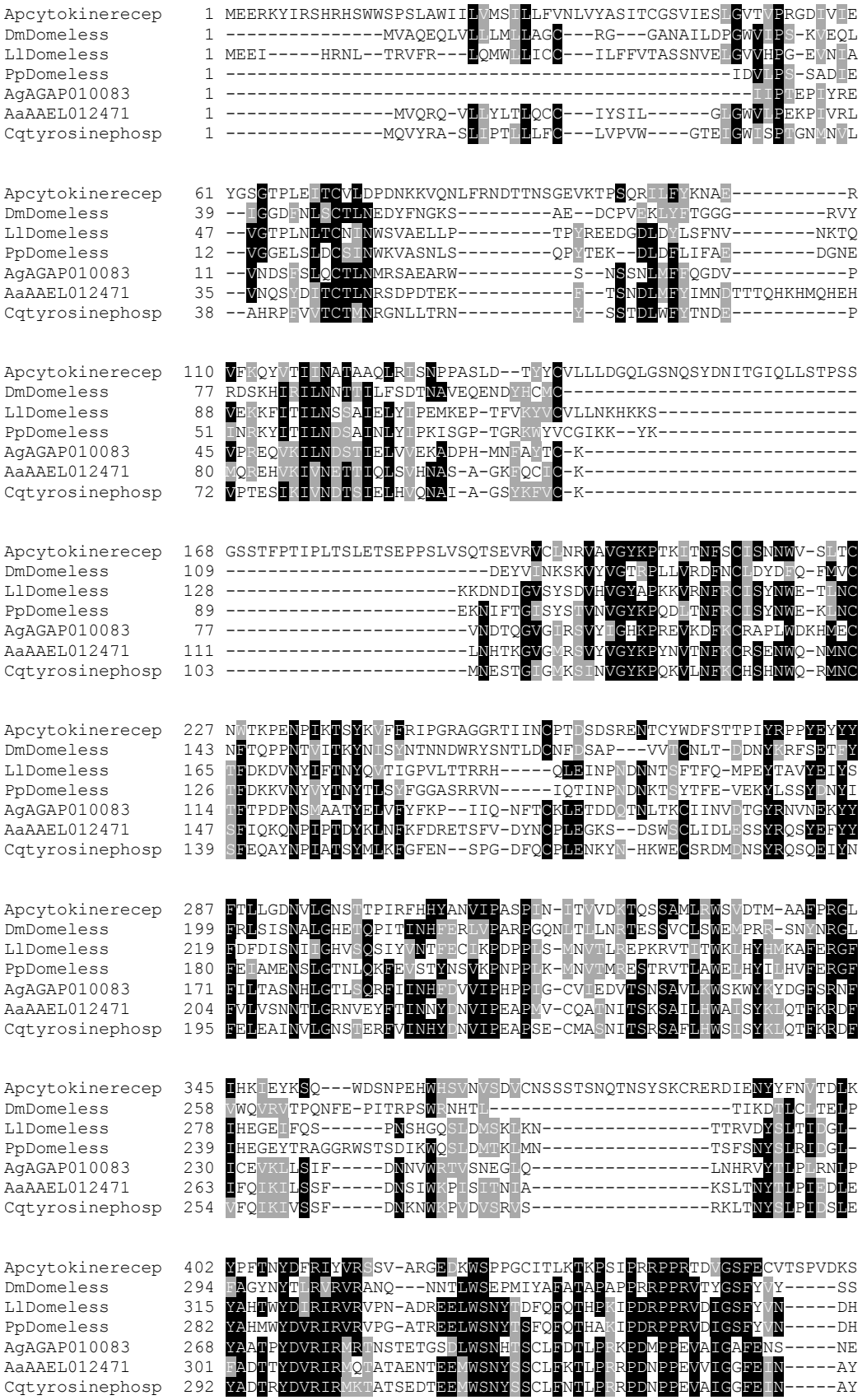

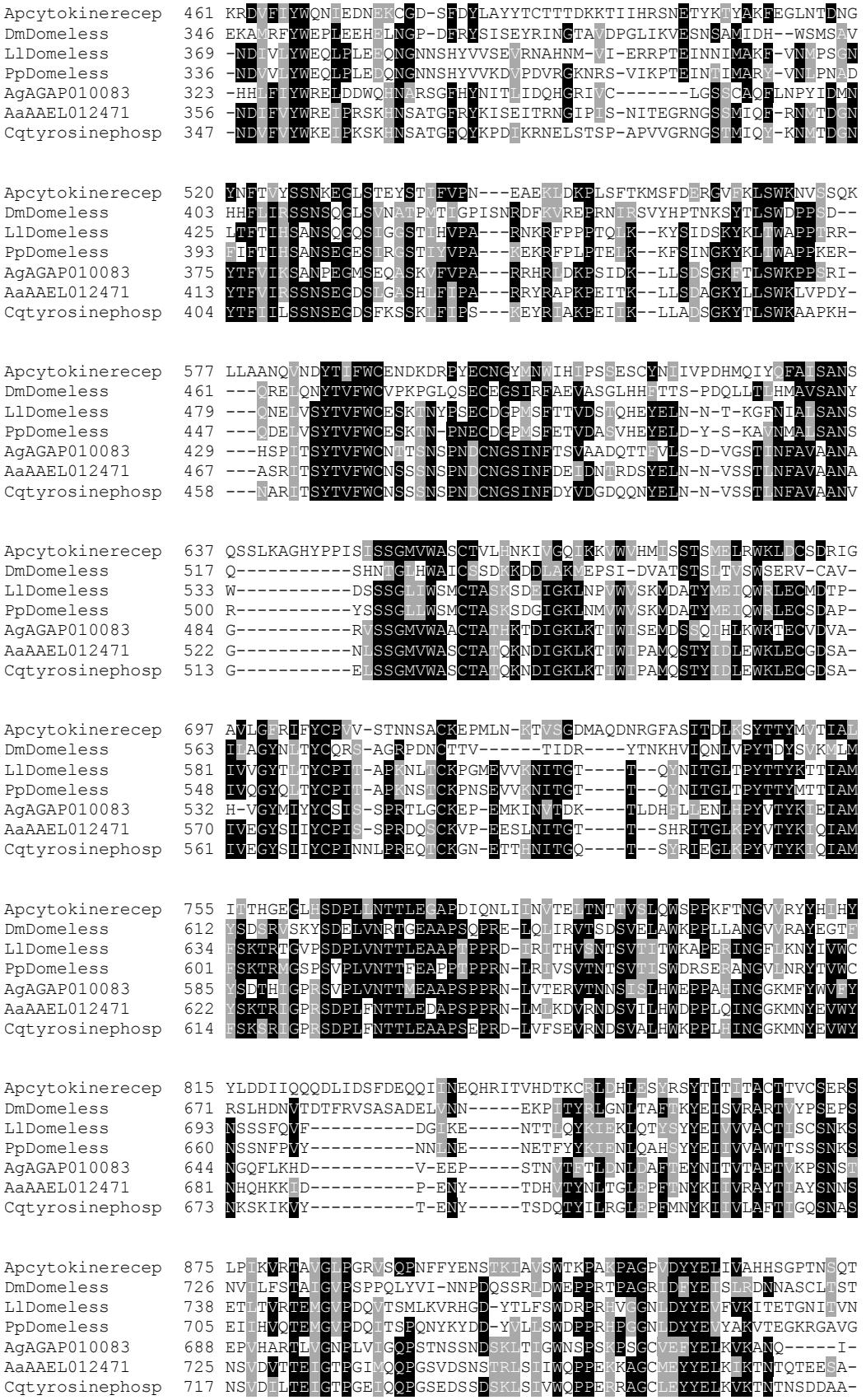

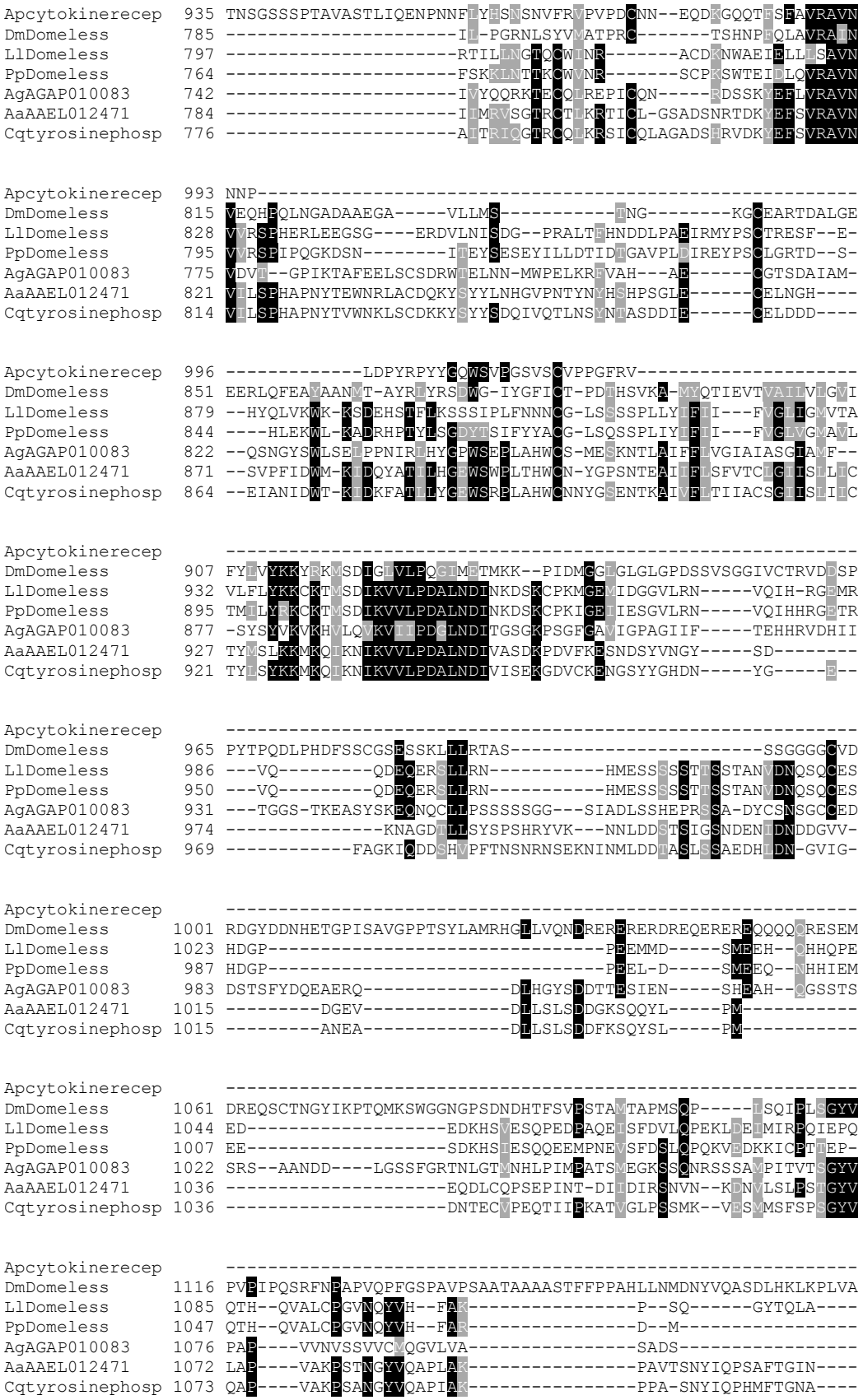

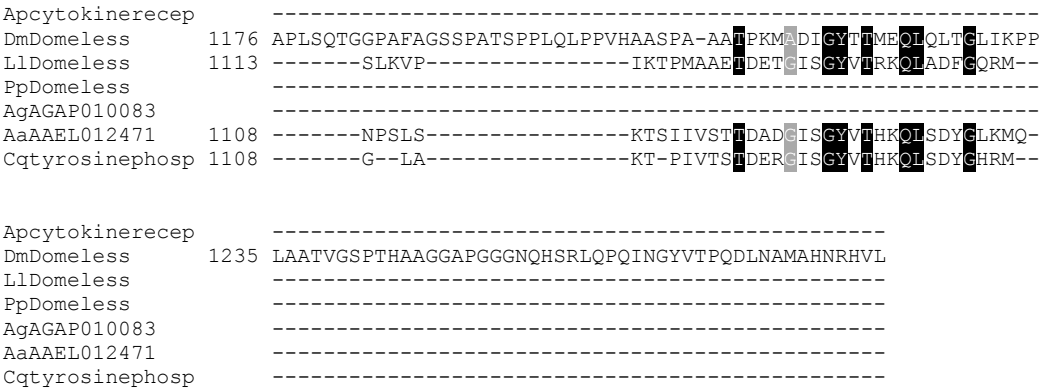

Figure A.25. Clustal Omega protein alignment of Domeless sequences from *L. longipalpis*, *P. papatasi*, *D. melanogaster*, *A. gambiae*, *A. aegyti*, and *C. quinquefasciatus*.

>IMPer

ATGGCCTTTGCAGAGGCATCCAAGGAAATTGATGCAGCCATTAATCAAACAGTGGCGTCCCTCTTTTCGCCTACAGC
GCCAAGTACGCATGACTACGCGGATAAATTCCGAATCTTCCGTTTCCCCAATGAACCAGCACGGGAATTAGCCAGAG
CAGCGGAAGTCTATGAGAGAACTCTCGTTAATATTCGTCGGCACATTGATAGTGGTCACACAATGATGGCCAATAAG
ACGGACTTCAACTACACGGAAATTCTCTCTCCGGAACACTTGGAGCTCATTGCAAGCCTTTCGGGATGCATGGCTCA
TCGACAGAAGCCCAATTGTACTGATATGTGCTTCCATGGGAAGTACAGAACCGTTGATGGGACGTGCAATAACTTGG
GGAATCCAACCTGGGGTGCTTCCTTGACGGGATTCCGAAGGATTCTGCCTCCGGTGTATGAGAATGAATTTAGTATG
CCCGTTGGATGGACAAAGGGACGTCTCTACAATGGATTCCAACTCCCAAGTGCACGTCTCGTGTCAAGTCGAATGAT
TGCCACGGAAGAGATTACTCCGGATAGTCGAATCACGCACATGGTGATGCAATGGGGTCAATTCCTCGATCACGATC
TTGATCATGCCATTCCATCAGTTAGCTCCGAAAGCTGGGATGGTGTGGATTGCAAGAAAACGTGTGACTATGCAGCT
CCTTGCTATCCCATTGAAGTACCTCCAGACGATGTGAGGGTGAACAATAGACGATGCTTGGACTTTGTTCGATCCAG
TGCAATCTGTGGTTCTGGTCAAACATCAATTCTCTTTGGGCAGGTGCAACCACGGGAGCAGATCAATCAGCTAACAT
CCTACCTCGATGCTTCCCAAGTTTATGGGTATTCCAAACAATTTGCCAATGATTTGCGCAATTTAACAGCAGATGAG
GGTAGATTGAGAATTGGGCTGCATTTCCCGGGGCAGAAACCTCTGCTTCCCTTTGCCTCCCCAACGGATGGTATTGA
TTGCCGGCGGGAGATTGGTGAGAGCAATGTTAATTGCTTCACAGCCGGTGATATTCGTGTCAATGAGCAGGTTGGAC
TCCTGGCAATGCATACAATTTGGTTCCGGGAGCACAATCGCATTGCCGACACTCTGCGATTGTACAATCCACACTGG
GATGGGGAGACACTCTACCATGAAGCAAGGAAGATTGTTGGGGCTCAGATGCAGCACATTACATACTCCAAGTGGCT
CCCATTGATCCTCGGTGAGGAAGGAATGAAGATGCTGGGAGAATATCGTGGCTACAATCCAACGGTTAATCCATCGA
TCTCCAATGAGTTTGCCACAGCAGCCCTGCGTTTTGGGCATAGTCTCATCAATCCAATTCTCCATCGGTACGATGCA
AATTACAAGGAGATCCCTCAGGGGCATTTGCCTCTTCATCGGGCATTCTTTGCACCCTGGCGGCTTGTCTACGAGGG
TGGTGTTGATCCTCTAATGCGGGGCTTGTTCCTCACACCAGCTAAGCTGAAGAAACCCCTTGAGAATCTCAATACTG
AACTCACGGAAAAGCTCTTCCATTCTGCACATGCTGTTGCCCTCGATCTGGCTGCCATCAACATTCAACGATCACGA
GATCATGCCATACCCTCGTACAATGACTACCGCCGTGTGTGCAATCTCACCGTTGCAAAAACCTTTGATGATTTTAC
TGAAATCTCCAATAAGCAGGTGCGGAAGCGACTGCAAGACATCTACGGGCATCCCAATAATGTCGACATCTGGGTTG
GGGGAATTCTGGAGGATCAAGTGGACGGTGGGAAAGTTGGTCCACTCTTCCGTTGCCTCCTTGTGGAACAATTCCAA
CGTCTTCGCGATGGTGATAGGTTTTGGTATGAAAACCCATCAATCTTCAAACCTGATCAACTTGTGCAGATCAAGCA
ATCCTCCCTAGCACGCGTCTTGTGCGACAATGGGGATAATATTACAGAAATCAGCGAAGATGTCTTTATGCTGTCTC
ACCTGCAGGATGGATTGAGGGCATGTGAAAAGCTCCCAGAGATGGATTTGCGTTTCTGGATGGATTGCAGTGGGTGC
ACACCACGTCCCCATCAGGGAGGTGAACTGATTCGACGTCGAAGATCCCTCAATACCACCTTCGTGGAGAAGGAGCA
CGAGGAGGATGACAGCAACTGGGTGGATATGAATGAGGAGCGCATTGAGGGGCTTGAGACAACGCTGGAATCCTTCC
AGAAGACCCTAAAGCAGATGCGGAGGAAATTGAAAAGTTGGAGGCATCGTGCCAAGCTGGTGGTGGGAAGATACAGA
AGCCACATGGGCACTGTACCGACTGGAGTGGAATACGACGTCTCAACAATGAGGTCTGGAAGGAAGATCCGTGCACG
CAGTGTGAGTGCAAGCATCGTGAAGTTCA**CTGTGTGCGTGATAAATGTC**CAGAGGTTGAGAAATGCCCTGATGGTGC
TATACCCACGAAATCACCCACCAGCTGCTGTCCAACATGCCCACCAGCTGCAACCCCATCAACTTCACCAGCACCTA
CCACATCGACATCCGTTCCTGCGGCATAAGCTGTTGGATAAACTCTTTTGGACATCCTGCACTGCAAGGAGGTGGAG
ATTTCCAACTGCCTCCGCAACCTATGAATTGAACCATCTCCTTGTTGAACTACATGATACATTTAAAAAAAATCTCA
TTCTTCGGAGGAAAAATTGTTCATTTTTTATGGAATTTTATGAGCAACACGAAAGCAAAAACGATGTTAATTCCCCT
CTAGATAGTGGATTAAACACACTGAAAATACTTACCTACCCTCTACCATTCATTATATATTCATAA

Figure A.26. Putative CDS for mRNA encoding *L. longipalpis* IMPer.

Full length predicted mRNA is depicted in black, while the primers used for RT-qPCR amplicon measurement are shown in pink. Sequences in blue denote agreement between prediction and sequenced amplicons, while nucleotides in red depict a difference at that base pair.

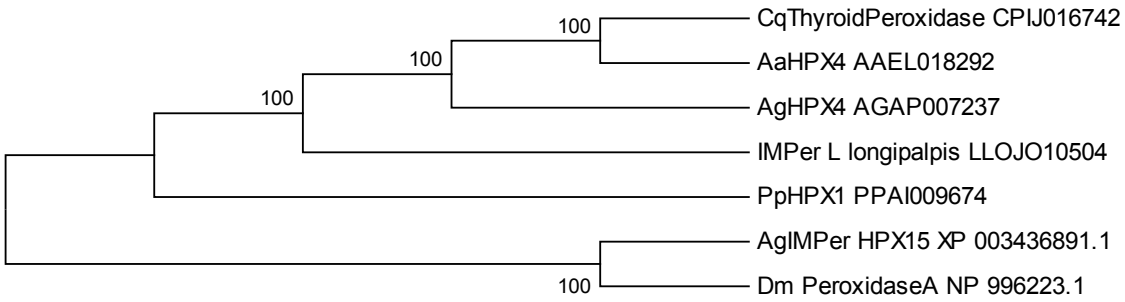

Figure A.27. Neighbor-joining tree to infer the evolutionary relationship of IMPer sequences.

```
PpHPX1_PPAI0096    1 ---------------------------------MEQIHQTG-------AAACE---AER
IMPer_L_longipa    1 ------------------------------------------------------------
AgHPX4_AGAP0072    1 MGHGHVLRDRVWLISGNNGRLLLIATIVALVAGLAEGLGCPQKCSCQQRTVRCVKQQLDK
CqThyroidPeroxi    1 ------------------------------------------------------------
AaHPX4_AAEL0182    1 ------------------------------------------------------------
AgIMPer_HPX15_X    1 ------------------------------------------------------------
Dm_PeroxidaseA_    1 ------------------------------------------------------------

PpHPX1_PPAI0096   17 PPPCPPSK----------FRSPTGECNNINHRD-------------WGA-----------
IMPer_L_longipa    1 ------------------------------------------------------------
AgHPX4_AGAP0072   61 VPEMPPDTSIIDLRYNHIREVPTGAFDGLQHLHTIFLNENQLTKIHSGAFRDLPSLKYLY
CqThyroidPeroxi    1 ------------------------------------------------------------
AaHPX4_AAEL0182    1 ------------------------------------------------------------
AgIMPer_HPX15_X    1 ------------------------------------------------------------
Dm_PeroxidaseA_    1 ------------------------------------------------------------

PpHPX1_PPAI0096   43 -----------RGDILLRLFEANYADGRSTPRNSQSSHALPAPEGIVAEL----------
IMPer_L_longipa    1 ------------------------------------------------------------
AgHPX4_AGAP0072  121 LNRNRIGTIAADAFISLSRLHSIYLHGNQI---------KTIPEGSFERLPSLRRLRLDD
CqThyroidPeroxi    1 ------------------------------------------------------------
AaHPX4_AAEL0182    1 ------------------------------------------------------------
AgIMPer_HPX15_X    1 ------------------------------------------------------------
Dm_PeroxidaseA_    1 ------------------------------------------------------------

PpHPX1_PPAI0096   82 -------------QTTTDPNRE-----------------------------HPHIT---
IMPer_L_longipa    1 ------------------------------------------------------------
AgHPX4_AGAP0072  172 NALECDCSLLWFVRTMQQPNRKSLVAGATCATPPALEGQPISSITEEDFHCAKPEIVVQP
CqThyroidPeroxi    1 ------------------------------------------------------------
AaHPX4_AAEL0182    1 ---------------------------------------------MDSDFHCTKPEIVTEP
AgIMPer_HPX15_X    1 ------------------------------------------------------------
Dm_PeroxidaseA_    1 ------------------------------------------------------------

PpHPX1_PPAI0096   96 -AMLPAWGQLLAYDLVDTVTPSLSCCQAINGNRTQEQVALCYVPSSTECQREQMNSVSGY
IMPer_L_longipa    1 ------------------------------------------------------------
AgHPX4_AGAP0072  232 RDIEISYGQTAVF-----------SCKASGDPRPE----IVWLQEGSPIRSESDGRITLL
CqThyroidPeroxi    1 ------------------------------------------------------------
AaHPX4_AAEL0182   17 RDIEISYGQTAVF-----------SCKAVGDPRPE----IVWMLNANEIHS-DDTRINVL
AgIMPer_HPX15_X    1 ------------------------------------------------------------
Dm_PeroxidaseA_    1 ------------------------------------------------------------

PpHPX1_PPAI0096  155 IDGSGLYGATERDFLNLRTLKGGLVNITACARCNEQGAVGALHTILLKEHNRIAKVLSKM
IMPer_L_longipa    1 ------------------------------------------------------------
AgHPX4_AGAP0072  277 PDGS----------LRIDEIVPADAGQYACIARNSLGESRSRTASLAVNNEVVE-S----
CqThyroidPeroxi    1 ------------------------------------------------------------
AaHPX4_AAEL0182   61 PDGS----------LRIDEVTAIDAGHYECMAKNNMGEVHSRQAQMIVNNEVIE-T----
AgIMPer_HPX15_X    1 ------------------------------------------------------------
Dm_PeroxidaseA_    1 ------------------------------------------------------------

PpHPX1_PPAI0096  215 NPVWTDTTLFLEARRAITAQIQHITYNEFLPVVLGQQITA----------------KDEL
IMPer_L_longipa    1 ------------------------------------------------------------
AgHPX4_AGAP0072  322 ---EAEAPKFLRT------PADPLELLEGEPIVLDCVVTGAPTPSILWKFNNENIQNGRI
CqThyroidPeroxi    1 ------------------------------------------------------------
AaHPX4_AAEL0182  106 ---EAEAPKFIQT------PPAEVDLLEGQPLVLHCVVSGAPTPSILWKFNNQNIQNGRI
AgIMPer_HPX15_X    1 ------------------------------------------------------------
Dm_PeroxidaseA_    1 ------------------------------------------------------------

PpHPX1_PPAI0096  259 R-LETSKHFTQYSSINRGGVFNEVAVAALPAFLTMLPAAMMDDSASAEILIRTPALMKTF
IMPer_L_longipa    1 ------------------------------------------------------------
AgHPX4_AGAP0072  373 KLFGNGSLILPTSTLDDGGIYTCCAGNALGNISVNVTVL-V-----N-------------
CqThyroidPeroxi    1 ------------------------------------------------------------
AaHPX4_AAEL0182  157 KLFGNGSLILPVASLDNGGVYSCYAGNAIGNVSVNATVH-V-----NEIL---PSTTTTT
AgIMPer_HPX15_X    1 ------------------------------------------------------------
Dm_PeroxidaseA_    1 ------------------------------------------------------------
```

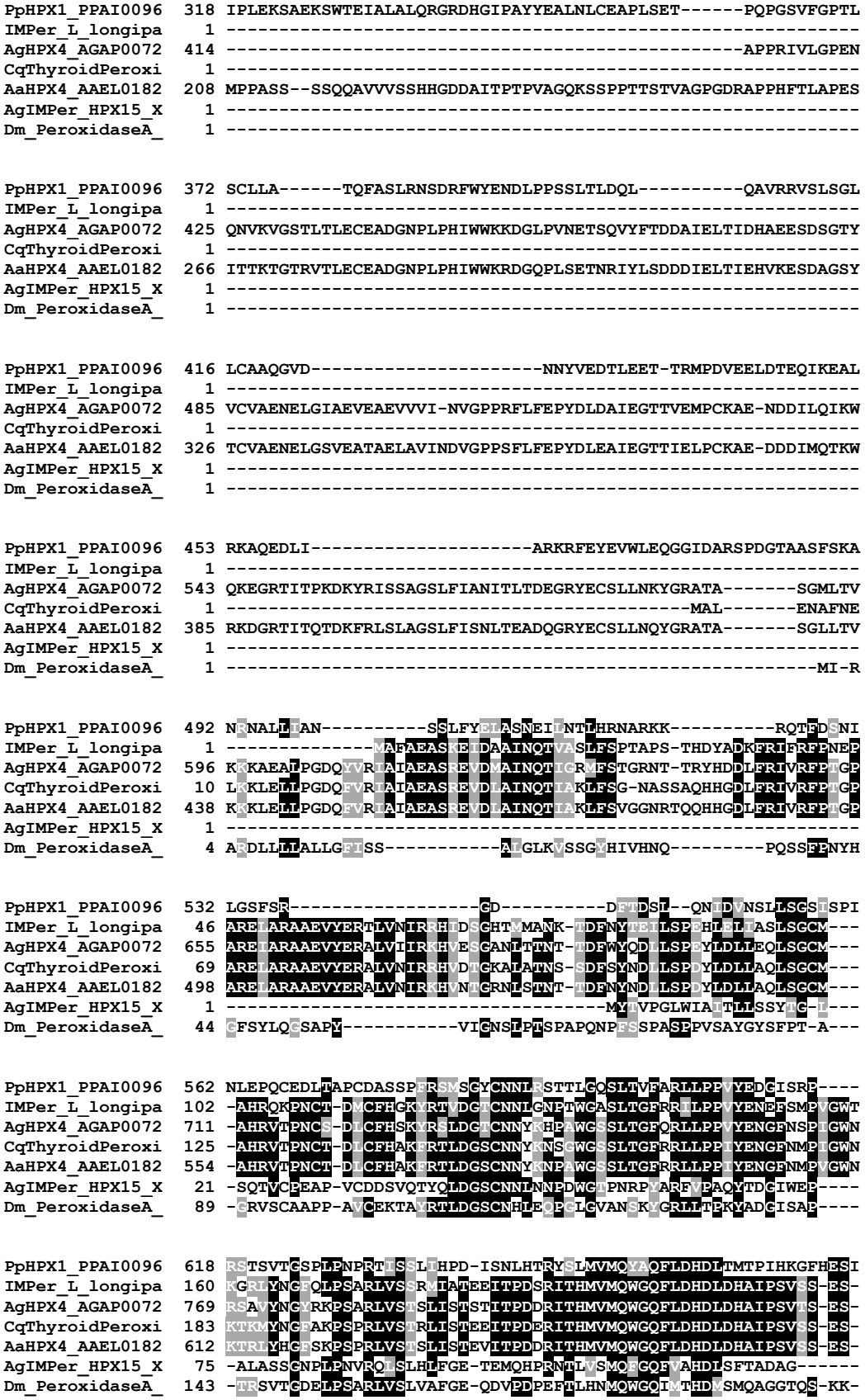
PpHPX1_PPAI0096 318 IPLEKSAEKSWTEIALALQRGRDHGIPAYYEALNLCEAPLSET------PQPGSVFGPTL
IMPer_L_longipa 1 ----------
AgHPX4_AGAP0072 414 ----------APPRIVLGPEN
CqThyroidPeroxi 1 ----------
AaHPX4_AAEL0182 208 MPPASS--SSQQAVVVSSHHGDDAITPTPVAGQKSSPPTTSTVAGPGDRAPPHFTLAPES
AgIMPer_HPX15_X 1 ----------
Dm_PeroxidaseA_ 1 ----------
PpHPX1_PPAI0096 372 SCLLA------TQFASLRNSDRFWYENDLPPSSLTLDQL----------QAVRRVSLSGL
IMPer_L_longipa 1 ----------
AgHPX4_AGAP0072 425 QNVKVGSTLTLECEADGNPLPHIWWKKDGLPVNETSQVYFTDDAIELTIDHAEESDSGTY
CqThyroidPeroxi 1 ----------
AaHPX4_AAEL0182 266 ITTKTGTRVTLECEADGNPLPHIWWKRDGQPLSETNRIYLSDDDIELTIEHVKESDAGSY
AgIMPer_HPX15_X 1 ----------
Dm_PeroxidaseA_ 1 ----------
PpHPX1_PPAI0096 416 LCAAQGVD----------NNYVEDTLEET-TRMPDVEELDTEQIKEAL
IMPer_L_longipa 1 ----------
AgHPX4_AGAP0072 485 VCVAENELGIAEVEAEVVVI-NVGPPRFLFEPYDLDAIEGTTVEMPCKAE-NDDILQIKW
CqThyroidPeroxi 1 ----------
AaHPX4_AAEL0182 326 TCVAENELGSVEATAELAVINDVGPPSFLFEPYDLEAIEGTTIELPCKAE-DDDIMQTKW
AgIMPer_HPX15_X 1 ----------
Dm_PeroxidaseA_ 1 ----------
PpHPX1_PPAI0096 453 RKAQEDLI----------ARKRFEYEVWLEQGGIDARSPDGTAASFSKA
IMPer_L_longipa 1 ----------
AgHPX4_AGAP0072 543 QKEGRTITPKDKYRISSAGSLFIANITLTDEGRYECSLLNKYGRATA-------SGMLTV
CqThyroidPeroxi 1 ----------MAL-------ENAFNE
AaHPX4_AAEL0182 385 RKDGRTITQTDKFRLSLAGSLFISNLTEADQGRYECSLLNQYGRATA-------SGLLTV
AgIMPer_HPX15_X 1 ----------
Dm_PeroxidaseA_ 1 ----------MI-R
PpHPX1_PPAI0096 492 NRNALLLAN----------SSLFYELASNEIDNTLHRNARKK----------RQTFDSNI
IMPer_L_longipa 1 ----------MAEAEASKEIDAAINQTVASLFSPTAPS-THDYADKFRIERFPNEP
AgHPX4_AGAP0072 596 KKKAEAPGDQYVRLAIAEASREVDMAINQTTGRMFSTGRNT-TRYHDDLFRIVRFPTGP
CqThyroidPeroxi 10 LKKLELLPGDQFVRLAIAEASREVDLAINQTIAKLFSG-NASSAQHHGDLFRIVRFPTGP
AaHPX4_AAEL0182 438 KKKLELLPGDQFVRLAIAEASREVDLAINQTIAKLFSVGGNRTQQHHGDLFRIVRFPTGP
AgIMPer_HPX15_X 1 ----------
Dm_PeroxidaseA_ 4 ARDLLLLALLGFTSS----------AIGLKVSSGYHIVHNQ---------PQSSFPNYH
PpHPX1_PPAI0096 532 LGSFSR----------GD----------DFTDSD--QNIDVNSLLSGSISPI
IMPer_L_longipa 46 ARELARAAEVYERTLVNIRRHIDSGHTVMANK-TDFNYTEILSPEHLFLLTASLSGCM---
AgHPX4_AGAP0072 655 ARELARAAEVYERALVIIRKHVESGANLTTNT-TDFWYQDLLSPEYLDLLEQLSGCM---
CqThyroidPeroxi 69 ARELARAAEVYERALVNIRRHVDTGKALATNS-SDFSYNDLLSPDYLDLLAQLSGCM---
AaHPX4_AAEL0182 498 ARELARAAEVYERALVNIRKHVNTGRNLSTNT-TDFNYNDLLSPDYLDLLAQLSGCM---
AgIMPer_HPX15_X 1 ----------MYTVPGLWIAITLLSSYTGCLL---
Dm_PeroxidaseA_ 44 GFSYLQCSAPY----------VIGNSLPTSPAPQNPFSSPASEPVSAYGYSFPT-A---
PpHPX1_PPAI0096 562 NLEPQCEDLTAPCDASSPTRSMSGYCNNLSSTTLGQSLTVFARLLPPVYEDGISRP----
IMPer_L_longipa 102 -AHRQKPNCT-DMCFHGKRTVDGTCNNLGNETWGASLTGFRRILPPVYENEFSMPVGWT
AgHPX4_AGAP0072 711 -AHRVTPNCS-DLCFHSKRSLDGTCNNYKHPAWGSSLTGFQRLLPPVYENGFNSPIGWN
CqThyroidPeroxi 125 -AHRVTPNCT-DLCFHAKRTLDGSCNNYKNSGWGSSLTGFRRLLPPTYENGFNMPIGWN
AaHPX4_AAEL0182 554 -AHRVTPNCT-DLCFHAKRTLDGSCNNYKNPAWGSSLTGFRRLLPPIYENGFNMPVGWN
AgIMPer_HPX15_X 21 -SQTVCPEAP-VCDDSVQTYQLDGSCNNLNNEDWGTPNRPLARFVPAQYTDGIWEP----
Dm_PeroxidaseA_ 89 -GRVSCAAPP-AVCEKTAVRTLDGSCNHIEQPGLGVANGKYGRLLTPKYADGISAP----
PpHPX1_PPAI0096 618 RSTSVTGSPLPNPRTASSLTHPD-ISNLHTRYSLMVMQYAQFLDHDLTMTPIHKGFHESI
IMPer_L_longipa 160 KGRLYNGEQLPSARLVSSRMIATEEITPDSRITHMVMQWGQFLDHDLDHAIPSVSS-ES-
AgHPX4_AGAP0072 769 RSAVYNGVRKPSARLVSTSLISTSTITPDDRITHMVMQWGQFLDHDLDHAIPSVTS-ES-
CqThyroidPeroxi 183 KTKNYNGEAKPSPRLVSTRLISTEEITPDERITHMVMQWGQFLDHDLDHAIPSVSS-ES-
AaHPX4_AAEL0182 612 KTRLYHGESKPSPRLVSTSLISTEVITPDDRITHMVMQWGQFLDHDLDHAIPSVSS-ES-
AgIMPer_HPX15_X 75 -ALASSGNPLPNVRQASLHLFGE-TEMQHPRNTLVSMQFGQFVAHDLSFTADAG------
Dm_PeroxidaseA_ 143 -TRSVTGDELPSARLVSLVAFGE-QDVPDPEFTLHNMQWGQIMTHDMSMQAGGTQS-KK-

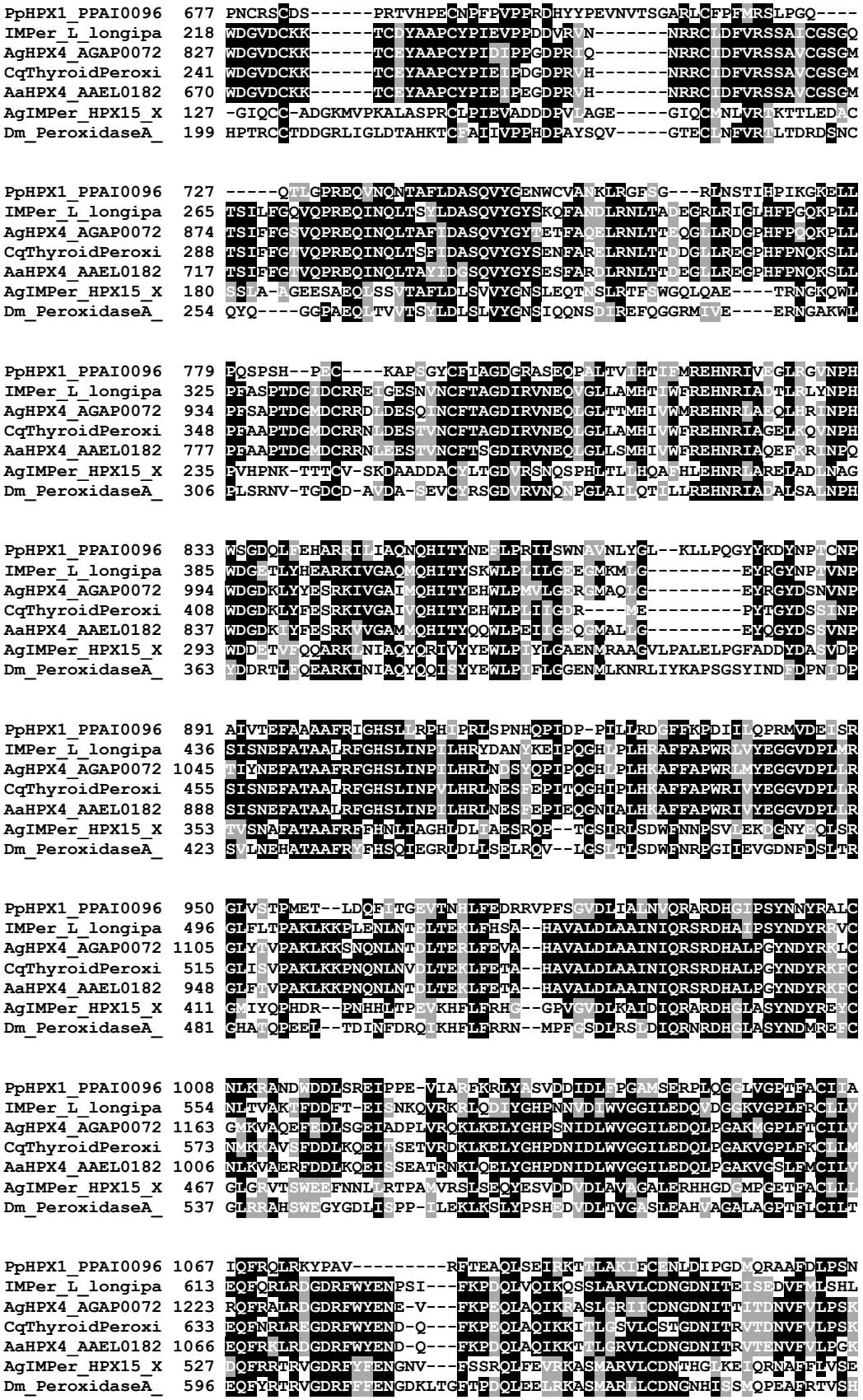

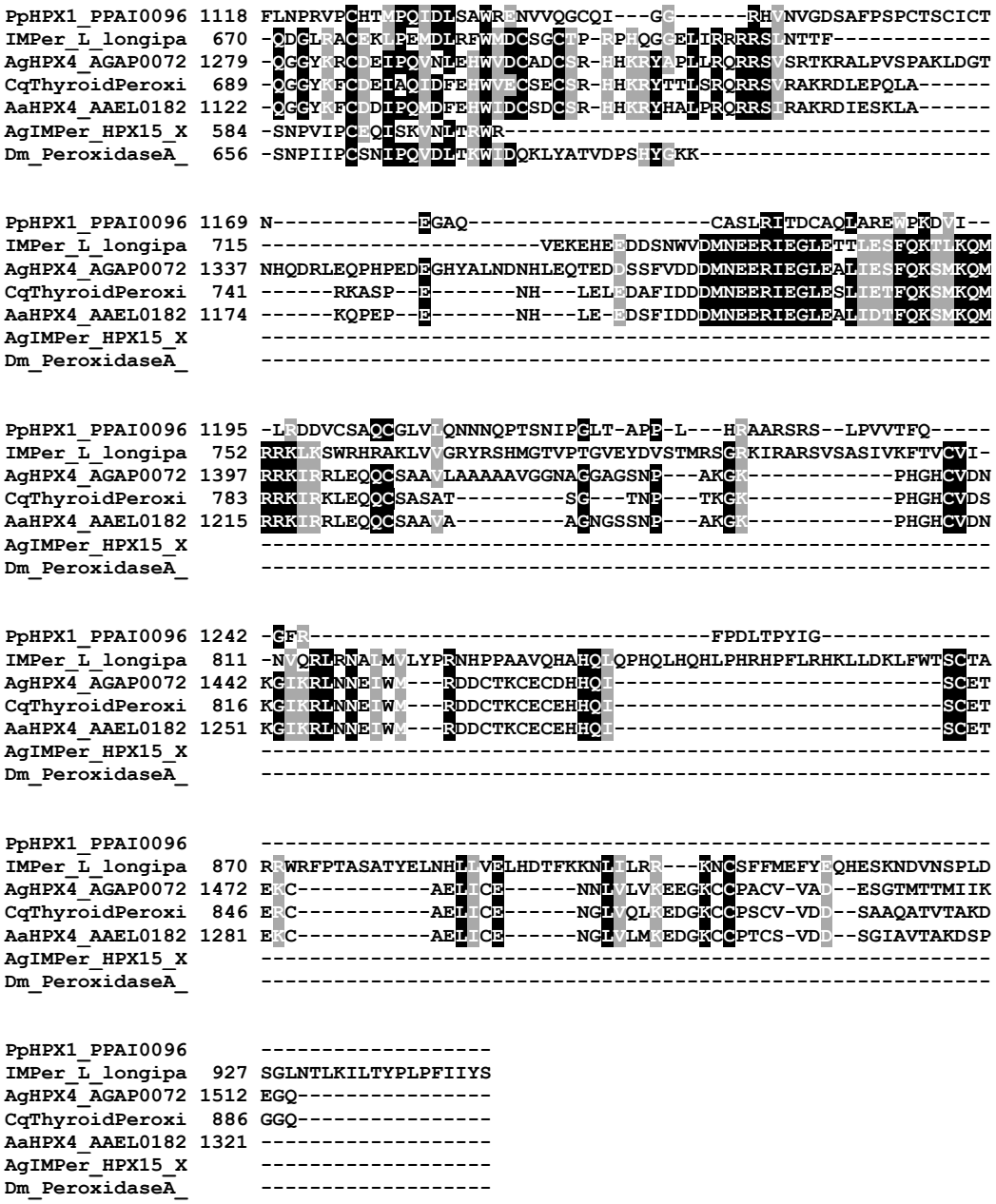

Figure A.28. Clustal Omega protein alignment of IMPer sequences from *L. longipalpis*, *P. papatasi*, *D. melanogaster*, *A. gambiae*, *A. aegyti*, and *C. quinquefasciatus*.